

**EVOLUTION OF DEPOSITIONAL AND SLOPE INSTABILITY PROCESSES
ON BRYANT CANYON AREA, NORTHWEST GULF OF MEXICO**

A Dissertation

by

EFTHYMIOS TRIPSANAS

Submitted to the Office of Graduate Studies of
Texas A&M University
in partial fulfillment of the requirements for the degree of

DOCTOR OF PHILOSOPHY

December 2003

Major Subject: Oceanography

**EVOLUTION OF DEPOSITIONAL AND SLOPE INSTABILITY PROCESSES
ON BRYANT CANYON AREA, NORTHWEST GULF OF MEXICO**

A Dissertation

by

EFTHYMIOS TRIPSANAS

Submitted to Texas A&M University
in partial fulfillment of the requirements
for the degree of

DOCTOR OF PHILOSOPHY

Approved as to style and content by:

William R. Bryant
(Chair of Committee)

David B. Prior
(Member)

Arnold H. Bouma
(Member)

Niall C. Slowey
(Member)

Wayne A. Dunlap
(Member)

Wilford D. Gardner
(Member)

Wilford D. Gardner
(Head of Department)

December 2003

Major Subject: Oceanography

ABSTRACT

Evolution of Depositional and Slope Instability Processes on Bryant Canyon Area, Northwest Gulf of Mexico. (December 2003)

Efthymios Tripsanas, B.S., University of Patras, Greece

Chair of Advisory Committee: Dr. William R. Bryant

Bryant and Eastern Canyon systems are located on the northwest Gulf of Mexico, and they are characterized by a very complex sedimentological history related to glacioeustatic cycles, river discharges, and interactions of depositional and halokinetic processes. Both canyon systems were active during the low sea-level stand of Oxygen Isotope Stage 6, and provided the pathways for the transport of enormous amounts of sediments on the continental slope and abyssal plain of the northwest Gulf of Mexico. Right after their abandonment, at the beginning of Stage 5, salt diapirs encroached into the canyons, and resulted in their transformation into a network of intraslope basins. The transformation of the canyons resulted in the generation of massive sediment failures.

The mid-shelf (Stages 4 and 3) to shelf edge (Stage 2) lowering of the sea-level during the last glacial episode resulted in: 1) extensive river-sourced deposits on the outer shelf and/or upper continental slope that contributed in a seaward mobilization of the underlying salt masses, and 2) the generation of numerous gravity flows and turbidity currents on the outer shelf/upper continental slope. The seaward mobilization of the salt masses resulted in the oversteepening of the flanks of the basins, and consequently in the generation of numerous and massive sediment failures. The turbidity currents were confined on the intraslope basins of the upper continental slope, depositing their coarsest material. However, their most diluted upper and end members were able to continue their downslope propagation depositing characteristic fine-grained turbidites. The frequency of the turbidity currents was highly increased during the last glacial maximum (Stage 2), and three short melt-water pulses centered at 30.5, 36, and 52 ky B.P.

The last deglaciation event is characterized by the development of a major melt water event that resulted in the deposition of distinct organic rich sediments, similar to the sapropels of the Eastern Mediterranean. At about 11 ky B.P. the melt water discharges of the North America

switched from Mississippi River to St Lawrence Seaway, causing the domination of hemipelagic sedimentation on the continental slope of the northwest Gulf of Mexico.

**This dissertation is dedicated to my parents,
Hristos and Vassiliki Tripsanas**

ACKNOWLEDGMENTS

I am sincerely grateful to the chair of my committee, William Bryant, who with his trust, encouragement, and scientific knowledge helped me to fulfill the writing of this dissertation. I also want to acknowledge the rest of the members of my committee, Arnold Bouma, David Prior, Wilford Gardner, Hans Nelson, Niall Slowey and Wayne Dunlap, for their scientific contribution and constructive reviews.

I also owe a big thanks to my co-students, Dan Bean, Debora Berti, and Brett Phaneuf for their help during the last five years, Eddy Lee who had the patience to teach me how to produce and develop X-ray radiographs, and Jin Wook Kim for the SEM analysis of the sediments. Special acknowledgments are dedicated to Mrs. Sandy Drews, the secretary of our department, for her help, support, and understanding.

The fulfillment of this dissertation is largely due to the support that my family provided to me, economically and psychologically. At this point, I also want to thank Marie des Neiges Leonard for standing by my side.

This project was sponsored by a National Science Foundation grant to Texas A&M (No. BES-9530370) with supplemental support from Chevron, Mobil, Texaco, Phillips, Marathon, and MARSCO Inc. The SSF Institution of the Greek Republic funded my studies in Texas A&M University during the first three and a half years.

Finally, I want to acknowledge all scientists, independently of the magnitude of their contribution. It is due to their sacrifices and efforts that I was able to transcend all the difficulties and fulfill the writing of my Ph.D. dissertation.

TABLE OF CONTENTS

	Page
ABSTRACT.....	iii
DEDICATION.....	v
ACKNOWLEDGMENTS.....	vi
TABLE OF CONTENTS.....	vii
LIST OF FIGURES.....	x
LIST OF TABLES.....	xvi
CHAPTER	
I INTRODUCTION.....	1
II SEDIMENTOLOGICAL HISTORY OF BRYANT CANYON AREA.....	4
Introduction.....	4
Methodology.....	6
Sedimentology.....	8
Sedimentological Unit F.....	11
Characteristics.....	11
Interpretation.....	13
Sedimentological Unit E.....	13
Characteristics.....	13
Interpretation.....	15
Sedimentological Units C and D.....	18
Characteristics of Sedimentological Unit D.....	19
Characteristics of Sedimentological Unit C.....	21
Sedimentological Subunit Ca.....	22
Sedimentological Subunit Cb.....	24
Sedimentological Subunit Cc.....	26
Interpretation.....	28
Silty-Clay Facies.....	28
Depositional Time Framework and Paleomorphology..	29
Sedimentological Processes.....	30
Sedimentological History of the Last Glacial Episode..	35
Sedimentological Unit B.....	39
Characteristics.....	39
Interpretation.....	41

CHAPTER	Page
Sedimentological Unit A.....	43
Characteristics.....	43
Interpretation.....	43
Bulk Density Profiles and Seismic Characterization.....	44
Conclusions.....	47
 III OXYGEN ISOTOPE STAGE 6 TURBIDITY CURRENT DEPOSITS.....	 50
Introduction.....	50
Geological Setting.....	50
Data and Methods.....	52
Sedimentary Facies.....	54
Mud Turbidite Facies/Units.....	55
Grain-Size Analysis of Mud Turbidite Facies.....	61
Interpretation.....	62
Coarse-Grained Turbidite Facies/Units.....	67
Interpretation.....	69
Spatial and Vertical Distribution of the Turbidite Facies.....	71
Intracanyon Environments.....	71
Flow Properties.....	73
Areas Subjected to Overflowing Processes.....	77
Flow Properties.....	80
Conclusions.....	83
 IV SLOPE INSTABILITY PROCESSES CAUSED BY SALT MOVEMENTS....	 85
Introduction.....	85
Geology of Bryant Canyon Area.....	87
Sediment Stratigraphy of Bryant Canyon Area.....	88
Methods.....	90
Beaumont Basin.....	92
Geomorphology.....	92
Core Descriptions.....	99
Reveille Basin.....	101
Geomorphology.....	101
Core Descriptions.....	105
Calcasieu Basin.....	106
Geomorphology.....	106
Core Descriptions.....	115
Discussion.....	118
Basin Flanks.....	118
Basin Floors.....	122

CHAPTER	Page
V UNIFORM MUD DEPOSITS (UNIFITES).....	125
Introduction.....	125
Geology of the Area.....	126
Sediment Stratigraphy of Bryant Canyon Area.....	128
Data and Methods.....	130
Geomorphology, Sedimentology, and Seismic Interpretation.....	131
Unifites.....	137
Discussion and Conclusions.....	140
VI CONCLUSIONS.....	146
Sedimentological History.....	146
Slope Stability.....	149
Unifites.....	150
REFERENCES.....	151
VITA.....	164

LIST OF FIGURES

FIGURE	Page
I-1	Morphological maps of the northwest continental slope of the Gulf of Mexico and Bryant Canyon area..... 2
II-1	Morphological map of the northwest Gulf of Mexico displaying the locations of Oxygen Isotope Stage 6 thalwegs of Bryant and Eastern Canyon systems..... 5
II-2	Morphological map of Bryant Canyon area displaying the locations of the Jumbo Piston Cores (JPC), and the tracks of the seismic information..... 7
II-3	Image displaying the $\delta^{18}\text{O}$ and bulk density profiles, and sedimentological descriptions of core JPC-31..... 9
II-4	Image displaying the sedimentological descriptions of the twelve cores, on which this study is based. SL: slumped sediments..... 10
II-5	Photographs (left) and X-ray radiographs (right) (negatives) of: A) sandy and silty turbidites (T_d to T_{b-e} Bouma Sequences) capped by mud turbidites ($T_{3/4-7}$ to $T_{4/5-7}$ sequences of Stow and Shanmugam, 1980) (intracanyon deposits), B) silt-mud turbidites (T_{0-7} to $T_{4/5-7}$ sequences of Stow and Shanmugam, 1980) located on overbank areas adjacent to the canyons (JPC-09), and C) base-cut-out mud turbidites ($T_{4/5-7}$ sequences of Stow and Shanmugam, 1980) located on distal overbank areas (JPC-31)..... 12
II-6	Mud turbidite facies model..... 12
II-7	Photographs (left) and X-ray radiographs (right) (negatives) displaying: A) typical hemipelagic sediments of unit E interbedded by the Y-8 ash layer (note the thick mixing zone on the top of the layer produced by bioturbation activities), B) silt to mud turbidites interbedded in hemipelagic sediments (JPC-37), and C) mud turbidites interbedded in hemipelagic sediments (JPC-26)..... 14
II-8	Image showing X-ray radiographs (negatives) and weight % grain-size curves, from successive samples, of: a) laminated silty-clay facies, b) normally graded silty-clay facies, and c) mottled silty-clay facies..... 17
II-9	Typical X-ray radiographs (negatives) of lenticularly interlayered silty-clay facies with normal grading (A), inverse grading (B), and normal grading characterized by very silty and erosional bases (C)..... 18
II-10	Photographs (left) and X-ray radiographs (right) (negatives) of

FIGURE	Page
chronostratigraphic horizon III from four cores from the upper to lower continental slope.....	20
II-11 Photographs (left) and X-ray radiographs (right) (negatives) of sedimentological subunit Ca from four cores from the upper to lower continental slope	23
II-12 X-ray radiographs (negatives) of subunit Cb from nine cores from the upper to lower continental slope.....	25
II-13 Typical photographs (left) and X-ray radiographs (right) (negatives) of the upper part of sedimentological subunit Cc, focusing in chronostratigraphic horizon II.....	27
II-14 Histogram displaying the sedimentation rates of sedimentological unit D and subunits Ca, Cb, and Cc.....	31
II-15 Morphological map of Bryant Canyon area displaying the routes of the major bottom-riding sediment flows during the last Glacial Episode.....	32
II-16 Typical photographs (left) and X-ray radiographs (right) (negatives) of chronostratigraphic horizon I from the upper to middle continental slope (A) (JPC-26), and lower continental slope (B) (JPC-33) of the northwest Gulf of Mexico.....	40
II-17 Image displaying the seismic (3.5 kHz subbottom profiles) and bulk density characterization of the six sedimentological units.....	46
III-1 Morphological map of the northwest Gulf of Mexico displaying the locations of Oxygen Isotope Stage 6 Bryant and Eastern canyon systems (adopted from Lee et al., 1996; from Twichell et al., 2000), along with an ancient lowstand fluvial system on the shelf and an ancestral Mississippi River delta (adopted from Sutter and Berryhill, 1985).....	51
III-2 Morphological map of Bryant Canyon area displaying the locations of the Jumbo Piston Cores (JPC), and the tracks of the high-resolution geophysical information.....	53
III-3 Fine-grained turbidite facies model.....	54
III-4 Negative photograph of X-ray radiograph (top) and environmental scanning electron microscope (ESEM) images (bottom) of facies M1 deposits.....	55
III-5 Image displaying X-ray radiographs (negatives) of two typical M2 mud turbidite facies.....	56

FIGURE	Page
III-6 X-ray radiographs (negatives) showing two typical M3 mud turbidite facies.....	56
III-7 X-ray radiographs (negatives) displaying typical M4a (A and B), and M4b (C) mud turbidite facies.....	58
III-8 Image displaying X-ray radiographs (negatives) of typical M5a (A), M5b (B and C), and M5c (D) mud turbidite facies.....	59
III-9 Image representing weight % grain-size curves from successive samples (~ 5 mm thick) of three discrete mud turbidite facies.....	60
III-10 Image showing weight % grain-size curves from successive samples (~ 1 mm thick) of two discrete M1 mud turbidite facies.....	62
III-11 Image displaying the two depositional stages of silt and mud laminae deposition: A) the shear in the boundary layer leads to the breakage of the settling flocs and allows for the deposition of the silt fraction only, B) since the amount of clays re-entraining in the overlying flow is less than the settling aggregated clays, their concentration is continuously increased leading to shear reduction within the boundary layer (thickening of the boundary layer, and reduction of the bursting frequency), C) the clay (cohesive sediments) concentration in the boundary layer exceeds a critical value, under which the shear in the boundary layer can not sustain the cohesive sediments disaggregated, leading to their massive deposition, and D) the boundary layer is depleted of cohesive sediments (restoration of its initial thickness, bursting frequency, and shear), after their massive deposition, and a new depositional cycle is developed (modified from Stow and Bowen, 1980).....	64
III-12 Photograph and X-ray radiograph (negative) of a typical S1 turbidite facies.....	68
III-13 Photograph, X-ray radiograph (negative), and weight % grain-size curves, from successive samples, of a characteristic S2 turbidite facies.....	69
III-14 Photograph, X-ray radiograph (negative), and weight % grain-size curves of successive samples of two S3 turbidite facies.....	70
III-15 Morphologic map of the Bryant Canyon area displaying the spatial distribution of the main sedimentological environments, during Oxygen Isotope Stage 6.....	72
III-16 X-ray radiographs (negatives) of: 1) waning and waxing-waning coarse (high-energy) mud-rich turbidite facies sequences (A), and 2) waning (B) and waxing-waning (C) fine-grained (low-energy) mud turbidite	

FIGURE	Page
facies sequences.....	79
III-17 Diagram displaying the velocity fields of the four flow regime stages under which the mud turbidite facies were deposited.....	81
IV-1 Bathymetric/morphological map of Bryant Canyon area, focusing on the three studied intraslope-interlobal basins.....	86
IV-2 Image displaying the bulk density profiles, and associated sedimentological units (Chapter II) of two typical sediment cores from the Bryant Canyon area, along with their corresponding 3.5 kHz subbottom profiles.....	89
IV-3 Bathymetric and geomorphological maps of Beaumont Basin.....	91
IV-4 Schematic illustration of three seismic lines from Beaumont Basin.....	93
IV-5 Image displaying 3.5 kHz subbottom profiles and side-scan sonar images from the northern flank of Beaumont Basin.....	94
IV-6 Image displaying 3.5 kHz subbottom profile and side-scan sonar image of the complex geomorphology of the canyon-like landslide troughs.....	95
IV-7 Image displaying 3.5 kHz subbottom profile and side-scan sonar images from the (a) upper and (b) lower parts of the inter-trough areas on the southern flank of Beaumont Basin.....	96
IV-8 Typical 3.5 kHz profiles and side-scan sonar images from the three geomorphological areas occurring on the floor of Beaumont Basin.....	97
IV-9 Bulk density profiles and associated sedimentological units (Chapter II) of five Jumbo Piston cores (JPC) from Beaumont Basin.....	99
IV-10 Sedimentological descriptions and bulk density profiles of sediment core JPC-07.....	101
IV-11 Morphological map of Reveille Basin displaying core locations (circles: USGS-cores; squares: JPC-cores) and deep-tow line.....	102
IV-12 Image showing 3.5 kHz profile and side-scan sonar imagery across Reveille Basin.....	103
IV-13 Sedimentological descriptions and bulk density profile of sediment core JPC-39 located on Reveille Basin.....	104

FIGURE	Page
IV-14 Bathymetric and geomorphological maps of Calcasieu Basin.....	107
IV-15 Schematic illustrations of the three seismic lines crossing Calcasieu Basin.....	108
IV-16 Image showing a 3.5 kHz subbottom profile from the western flanks of Calcasieu Basin.....	109
IV-17 Image showing 3.5 kHz subbottom profiles and side-scan sonar image from the western flanks of Calcasieu Basin.....	109
IV-18 Image showing 3.5 kHz profiles and side-scan sonar image from the apron at the foot of the western flank of Calcasieu Basin.....	110
IV-19 Image showing a 3.5 kHz profile and side-scan sonar imagery from the northern flank of Calcasieu Basin.....	111
IV-20 Image displaying 3.5 kHz profile of the southern ridge, Calcasieu Basin.....	113
IV-21 Image showing 3.5 kHz profile and side-scan sonar imagery of the concentric mud flow deposits at the southeast floor of the basin.....	113
IV-22 Bulk density profiles and associated sedimentological units (Chapter II) of four sediment cores from Calcasieu Basin.....	115
IV-23 Sedimentological descriptions and bulk density profiles of sediment cores JPC-15, and LGC-13.....	117
IV-24 Cartoon of the evolution of the basins during the second episode of high salt-tectonic activity.....	121
V-1 Morphologic map of the northwest Gulf of Mexico (upper image) and Hedberg Basin (lower image), showing core locations and seismic lines.....	127
V-2 A) bulk-density profile, associated sedimentological units, and corresponding 3.5 kHz subbottom profile of a typical sediment core located south-southwest of Hedberg Basin, and B) photograph and X-ray radiograph of chronostratigraphic horizon II (H-II).....	129
V-3 3.5 kHz profiles and side-scan sonar images from the western-southwestern flanks of Hedberg Basin.....	132
V-4 Sedimentological descriptions and bulk density profiles of three Jumbo Piston cores from Hedberg Basin.....	133
V-5 3.5 kHz profiles and side-scan sonar images from the (A) central-northern	

FIGURE	Page
flanks of Hedberg Basin displaying buried (smoothed) parallel lineations and possible flute marks, revealing the passage of debris flows and turbidity currents, and (B) eastern flanks of Hedberg Basin characterized by abundant sediment blocks and their glide tracks.....	134
V-6 3.5 kHz profiles and side-scan sonar images of the floor of Hedberg Basin.....	136
V-7 X-ray radiographs displaying the entire unfite sequence, which is observed in core JPC-29.....	139

LIST OF TABLES

TABLE	Page
II-1 Sedimentation rates of each sedimentological unit and subunit.....	16
III-1 Waning spectrums of flow regimes resulting in the deposition of each mud turbidite facies.....	67
III-2 Results of the funneled turbidity current velocities and sediment concentrations, based on the two methods described in the paper.....	76

CHAPTER I

INTRODUCTION

Sedimentological processes on continental slopes have been long time neglected, assuming that they simply represent a pathway for density currents to transport sediments onto the deep abyssal plains of world's oceans. This was mainly due to the focussed interest of petroleum industries on the deep-sea fans, which are excellent oil reservoirs. However, during the last two decades, the reduction of oil reservoirs, combined with the concomitant increasing need for energy around the world, has forced industry to expand its activities into the deep ocean environment, and search for additional environments that could act as oil reservoirs. However, in order to achieve this goal, we must first increase our limited knowledge on continental slope environments.

The northwest continental slope of the Gulf of Mexico is famous for both its critical economic importance and its complicated geomorphology and sedimentological history. Its economic importance is concentrated on the abundant oil reservoirs existing in its vicinity. Its sedimentological history depends on interactions between sedimentological and halokinetic processes due to the underlying, thick, allocthonous salt masses. This infers that the geomorphology of the northwest Gulf of Mexico is in constant mobility, in an effort for the underlying salt masses to equilibrate the differential loading of the newly deposited sediments. Consequently, sedimentological processes depend not only on sea-level fluctuations and river discharges, but also on the existing morphology of the slope that could have been very different than the present one.

This dissertation is focused on the sedimentological study of a large set of long sediment cores (up to 20 m long) and high-resolution seismic information (3.5 kHz acoustic subbottom profiles and side-scan sonar imageries) from Bryant Canyon area located on the northwest continental slope of the Gulf of Mexico (Fig. I-1). Bryant Canyon area is characterized by the presence of Bryant and Eastern Canyons, which have been transformed into a network of intraslope basins by halokinetic processes.

This dissertation follows the style and format of the journal, *Marine Geology*.

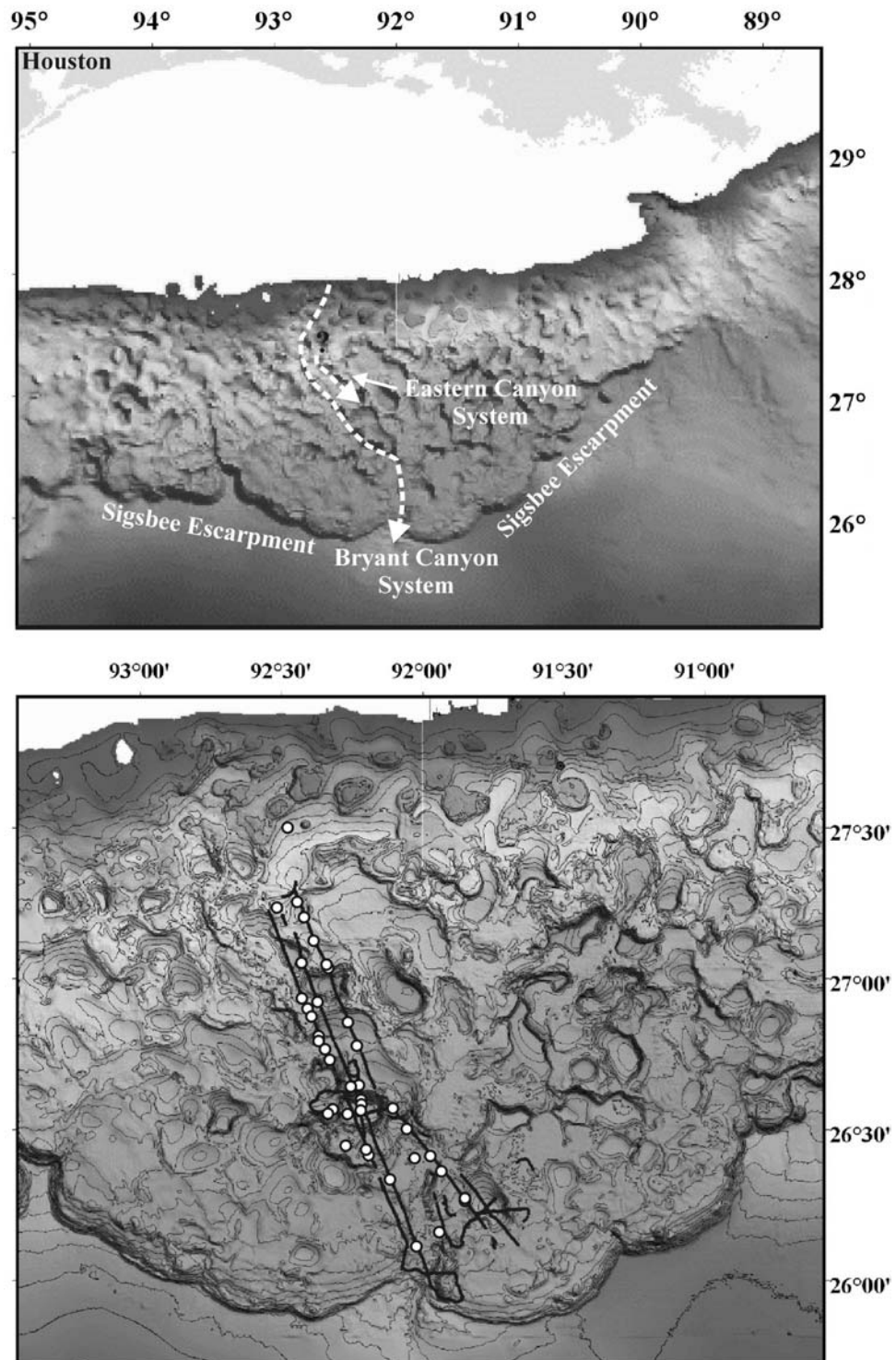


Fig. I-1. Morphological maps of the northwest continental slope of the Gulf of Mexico and Bryant Canyon area. White circles and black lines represent the location of the sediment cores and seismic survey lines, respectively.

This dissertation consists of four chapters, which deal with different sedimentological issues and perspectives of the Bryant Canyon area. After this brief introductory chapter, Chapter II focuses on the determination of the sedimentological history of Bryant Canyon area, and the establishment of a sedimentary/chronostratigraphic/seismic time framework, which will be used extensively in the following chapters for dating purposes. In that chapter, it is attempted to: a) assess the time period of the formation and destruction of the Bryant and Eastern Canyon systems, b) determine the spatial and time evolution of the sedimentological processes acting in the Bryant Canyon area, c) determine the relation of the existing sedimentological processes to glacio-eustatic cycles and short melt-water events, d) discuss the influence of the canyons (prior and after their destruction by halokinetic processes) on the sedimentological processes, and e) discuss the influence of bottom currents on the sedimentation of the northwest Gulf of Mexico.

The third chapter is focused on the determination of flow properties of turbidity currents acting during the active period of the Bryant and Eastern Canyon systems. This study will present a discussion on: a) the sedimentary turbiditic facies observed in and around the canyons, b) the properties of the sediment flows that resulted in their deposition, and c) the influence of turbidity currents on the sedimentation not only of the intracanyon areas but also of the surrounding areas as well.

The fourth chapter concentrates on the identification and characterization of sediment failures on the Bryant Canyon area through 3.5 kHz subbottom profiles, side-scan sonar imageries and long sediment cores. The ultimate goal of that chapter is to assess the triggering mechanisms of Bryant Canyon area slope instability processes, and to determine their relation to the acting halokinetic processes.

The fifth chapter deals with the study of a mysterious sedimentary unit, the unifites, which drapes the seafloor of the intraslope basins and consists of uniform mud that exceeds 20 m in thickness. Similar uniform mud deposits have been documented in intraslope basins from the Eastern Mediterranean and northwest Gulf of Mexico (Blanpied and Stanley, 1981; Behrens, 1984). Their origin is mysterious and there is much contradiction, whether they represent mud-flow deposits, or deposits of mud turbidites. This issue will be discussed and a depositional model is proposed for the development of the uniform mud deposits.

CHAPTER II

SEDIMENTOLOGICAL HISTORY OF BRYANT CANYON AREA

Introduction

The Northwest Gulf of Mexico is an area of geologic and bathymetric complexity due to salt tectonism (Fig. II-1). It is characterized by a hummocky morphology, consisting of numerous intraslope basins, surrounded by shallow tabular salt (Bryant et al., 1990; Lee et al., 1996). Despite the highly deformed morphology of the northwest continental slope of the Gulf of Mexico, remnants of two major erosional/depositional systems are still observed. They are those of Bryant and Eastern Canyon systems. Both canyons are represented by a network of intraslope basins, separated from each other by sills/plateaus (shallow salt structures). Bryant Canyon can be traced from the shelf margin to the lower continental slope, whereas, on the continental rise, it is succeeded by the well-developed Bryant deep-sea fan. Inversely, Eastern Canyon is confined to the upper continental slope, and terminates in a prominent intraslope basin (Lee et al., 1996; Twichell et al., 2000).

The formation and destruction of the canyons have been discussed extensively by Lee et al. (1996) and Twichell et al. (2000). However, the timeframe of their formation and destruction still remains to be determined. Their formation was initiated at some point during the last or pre-last glacial episode by the development of an ancestral Mississippi River Delta on the shelf edge/upper continental slope (Suter and Berryhill, 1985). This led to the generation of numerous gravity flows triggered either by sediment failures on the delta front, or directly from hyperpycnal river plumes (Hampton, 1972; Bornhold et al., 1994; Mulder and Syvitski, 1995). The gravity flows advanced downslope, and were eventually confined/ponded in the intraslope basins of the upper continental slope, developing sheet sands and channel-levee complexes. When the intraslope basins were filled up to a certain level, the gravity flows spilled and propagated into the adjacent, downdip intraslope basin, resulting in a downslope shift of the ponded fan facies (Bouma, 1981; Bouma and Roberts, 1990; Lee et al., 1996). Repetition of this gravity flow infilling-bypassing process led to the peculiar structure of Bryant and Eastern Canyon systems, which in the infilled intraslope basins had the form of well-developed channel-levee systems, and on the sills/plateaus, separating the basins, had the form of typical

V-shaped erosional canyons (Lee, 1990; Satterfield and Behrens, 1990; Twichell et al., 2000). The well-developed deep-sea fan system at the mouth of Bryant Canyon indicates that, at some point, it extended itself throughout the entire continental slope, and evolved into an unconfined river-sourced system.

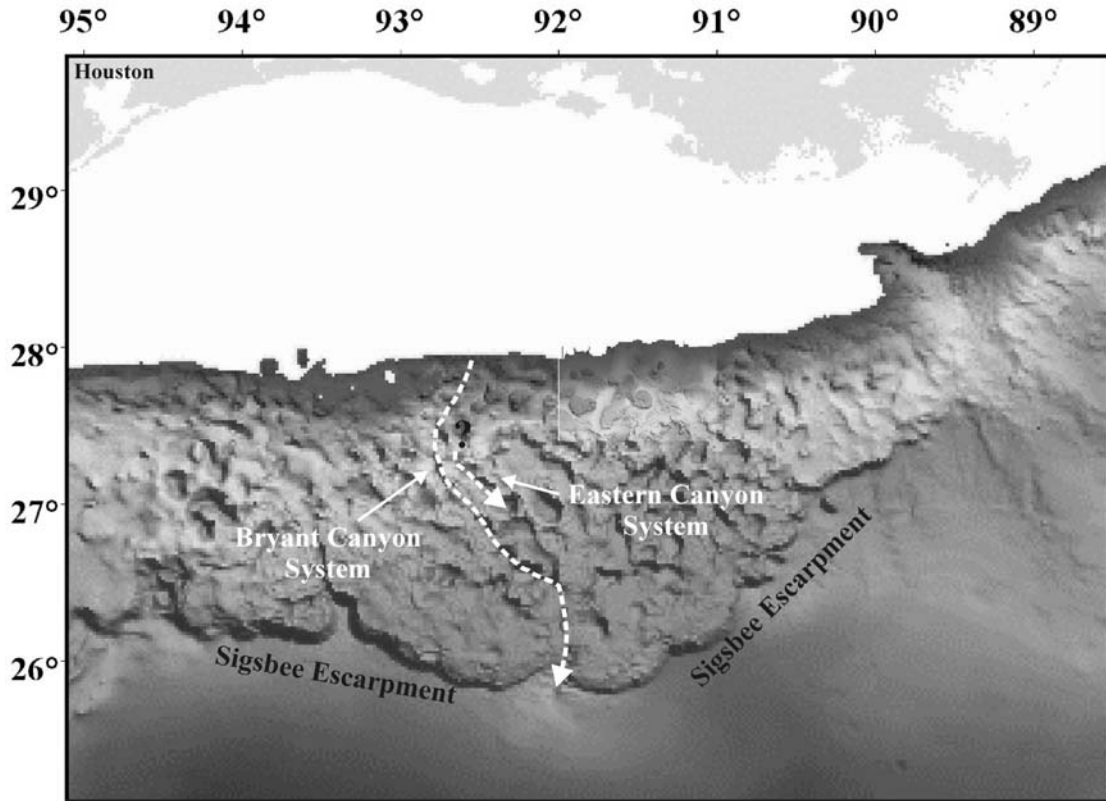


Fig. II-1. Morphological map of the northwest Gulf of Mexico displaying the locations of Oxygen Isotope Stage 6 thalwegs of Bryant and Eastern Canyon systems (adopted from Lee et al., 1996, and Twichell et al., 2000).

The existence of such erosional/depositional environments certainly disturbed the stability of the underlying salt masses, which, through differential sediment loading, tended to obliterate and restore the seafloor morphology on the erosional parts of the canyons, and to retreat and collapse on the canyons depocenters (Lee, 1990; Lee et al., 1996; Twichell et al., 2000). However, coupled erosional-depositional processes of the gravity flows were able to balance

the salt movements during the active low-level stand of the canyon systems. The destruction of Bryant and Eastern Canyons occurred at the beginning of the subsequent high sea-level stand (interglacial period), due to the confinement of the majority of the alluvial sediments on the widespread continental shelf of the northwest Gulf of Mexico that ceased the production of turbidity currents on the shelf margin/upper continental slope (Morton and Price, 1987; Suter et al., 1987).

It is revealed from the above information that, even though many questions have been answered, many remain unresolved about the sedimentological history of Bryant Canyon area. This study is focused on the detailed sedimentological and geochronological investigation of forty-eight long (up to 20 m) sediment cores, acquired from this area, in order to answer two crucial, but yet unresolved issues. The first concerns the assessment of the formation and destruction time framework of Bryant and Eastern Canyon systems. The second issue deals with the determination of the sedimentological history of Bryant Canyon area (spatial and time evolution of the acting sedimentological processes, and their interactions with salt tectonics).

Methodology

This study is based on a large set of data, consisting of high-resolution acoustic information, and forty-eight long sediment cores (up to 20 m long). The acoustic information was collected during the R/V *Gyre* 1998 cruise, using the Texas A&M Deep-tow system equipped with a 3.5 kHz subbottom profiler, and a 100 kHz side-scan sonar towed thirty meters above the seafloor (Fig. II-2). The determination of the core locations was based on the preliminary analysis of the above seismic information. The sediment cores were acquired during a cruise in 1998 with the R/V *Knorr*, using the WHOI Jumbo Piston Corer.

The bulk densities and P-wave velocities of the sediments were acquired by the use of a GEOTEK Multi-Sensor Core Logger, at 2 cm intervals. Sixteen sediment cores were split lengthwise: one half was archived, and the other half was described at the millimeter-level scale, and photographed on high-resolution film. X-radiographs were also taken from the entire length of the cores by cutting 1-cm-thick sediment slabs, to detect sedimentary structures not visible to the naked eye. The sedimentological analysis of the rest of the cores was based on their density profiles. Based on the above observations, successive samples from strategic sedimentary units were retrieved for grain-size analysis. The analyses of the silt and clay fractions were performed by the use of a Sedigraph and Coulter Counter. The sand fraction was

removed from the samples by wet sieving, and the distribution of its population was calculated by dry sieving. Nineteen total samples were also obtained from the cores, and sent to TDI-BI for the determination of the sediment organic carbon content.

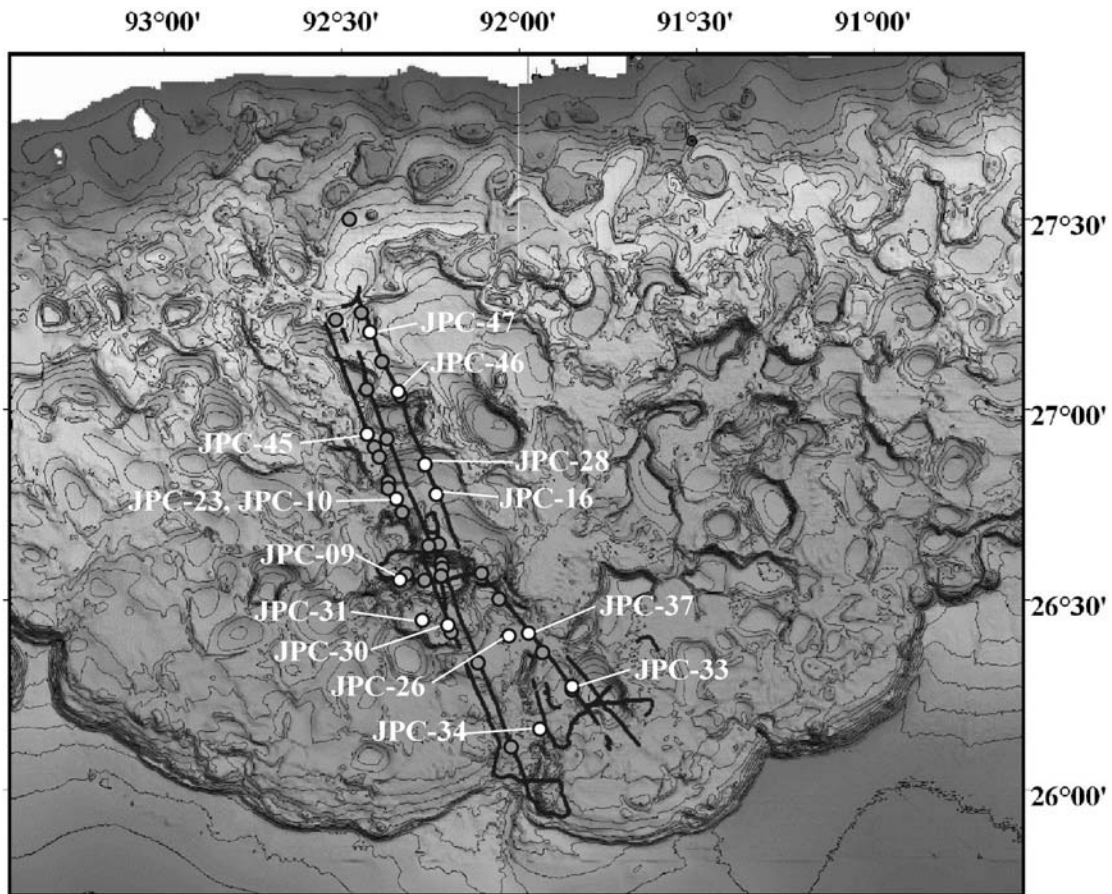


Fig. II-2. Morphological map of Bryant Canyon area displaying the locations of the Jumbo Piston Cores (JPC), and the tracks of the seismic information. White circles represent the locations of the cores displayed in this paper, whereas gray circles the rest of the cores.

The $\delta^{18}\text{O}$ of numerous samples from cores JPC-31 (lower continental slope) and JPC-46 (upper continental slope) were analyzed. Sediment was taken from the cores at intervals of 10 cm and washed through a sieve with distilled water. Shells of the planktonic foraminifera *Globigerinoides ruber* (white variety) were hand picked from the 212 to 250 μm fraction of sediment, cleaned in an ultrasonic bath, dried, and stored under vacuum prior to isotopic

analysis. The oxygen composition of the foraminifera were measured using a Finnigan/MAT 251 isotope ratio mass spectrometer with a Keil II automated sample acidification system. The $\delta^{18}\text{O}$ values are referred to the PDB standard through intercalibration of our reference gas with the NBS-19 standard. From 10 to 14 shells were used for each sample.

After examination of all of the above data, six samples were picked from JPC-31 for ^{14}C AMS dating. Despite the great similarity of the $\delta^{18}\text{O}$ profiles of cores JPC-31 and JPC-46, JPC-31 was considered as the most representative for the dating of sediments. Six samples were acquired for radiocarbon dating. Approximately 1,200 foraminifera shells (*G. ruber*) were hand picked for each one of these radiocarbon dates. The shells were cleaned in an ultrasonic bath, dried, then they were further cleaned, converted to graphite, and the ratio of the radioactive ^{14}C to stable ^{12}C in each sample was measured by FN tandem accelerator mass spectrometer following standard methods. The resultant absolute AMS- ^{14}C ages were converted to calendar years before 1950 B.P. To do this, a correction of 400 years was made for the surface ocean reservoir age effect, and a correction was made for temporal variation in the production of radiocarbon upon a data set of paired radiocarbon and U/Th dates (Shakleton and Opdyke, 1973; Stuiver and Reimer, 1993; Stuiver et al., 1998). Radiocarbon dating is generally effective for the samples in the age ~ 0 to 40,000 years. The dating for sediments older than 40 ky B.P. was based on the comparison of the $\delta^{18}\text{O}$ profiles of cores JPC-31 and JPC-46 with those provided by Martinson et al. (1987).

Sedimentology

The sedimentology of four out of the sixteen split cores (20 out of the forty-eight total cores) had been so extensively disturbed by sediment failures, that the remolded sediments could not allow the drawing of any conclusions on the sedimentological history of Bryant Canyon (the slope stability evolution of Bryant Canyon area based on these cores is discussed in Chapter IV). This led to the restriction of the present study on the 12 remaining cores, located on the most tranquil environments (sills and plateaus) of Bryant Canyon area. All of these cores consist of 6 distinct sedimentological units, which have a widespread occurrence, and they are tightly related to Oxygen Isotope Stages 1 through 6 (Figs. II-3 and II-4). Starting from the oldest sedimentological unit, they are:

JPC-31

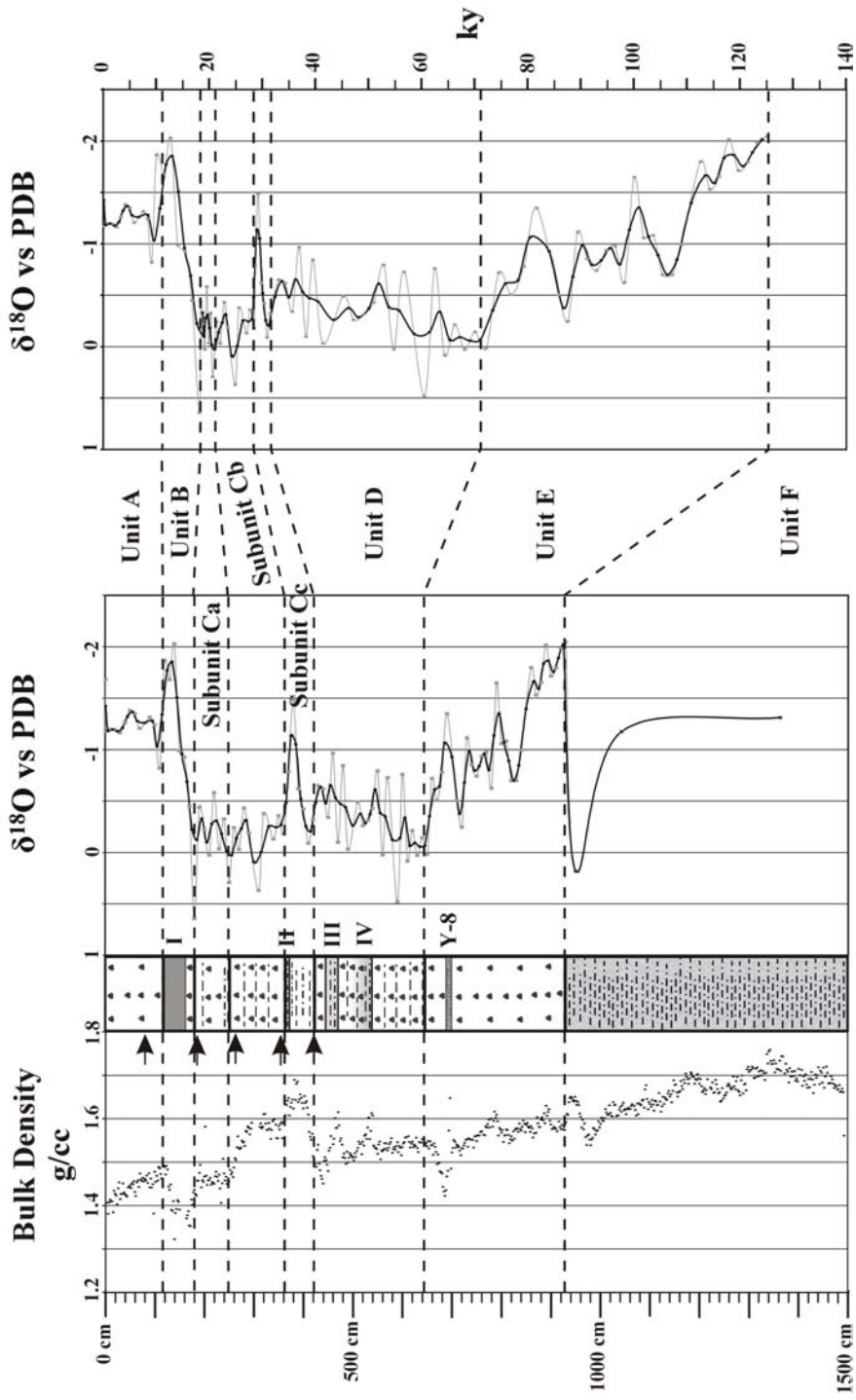


Fig. II-3. Image displaying the $\delta^{18}\text{O}$ and bulk density profiles, and sedimentological descriptions of core JPC-31. The arrows indicate the location of the samples used for ^{14}C AMS dating. The Latin numbers indicate the locations of horizons I, II, III, and IV, and Y-8 ash layer in the core. Information on the symbols of the sedimentological descriptions is presented in Figure II-4. The light gray lines represent the real $\delta^{18}\text{O}$ data, whereas the heavy black line the running average of two.

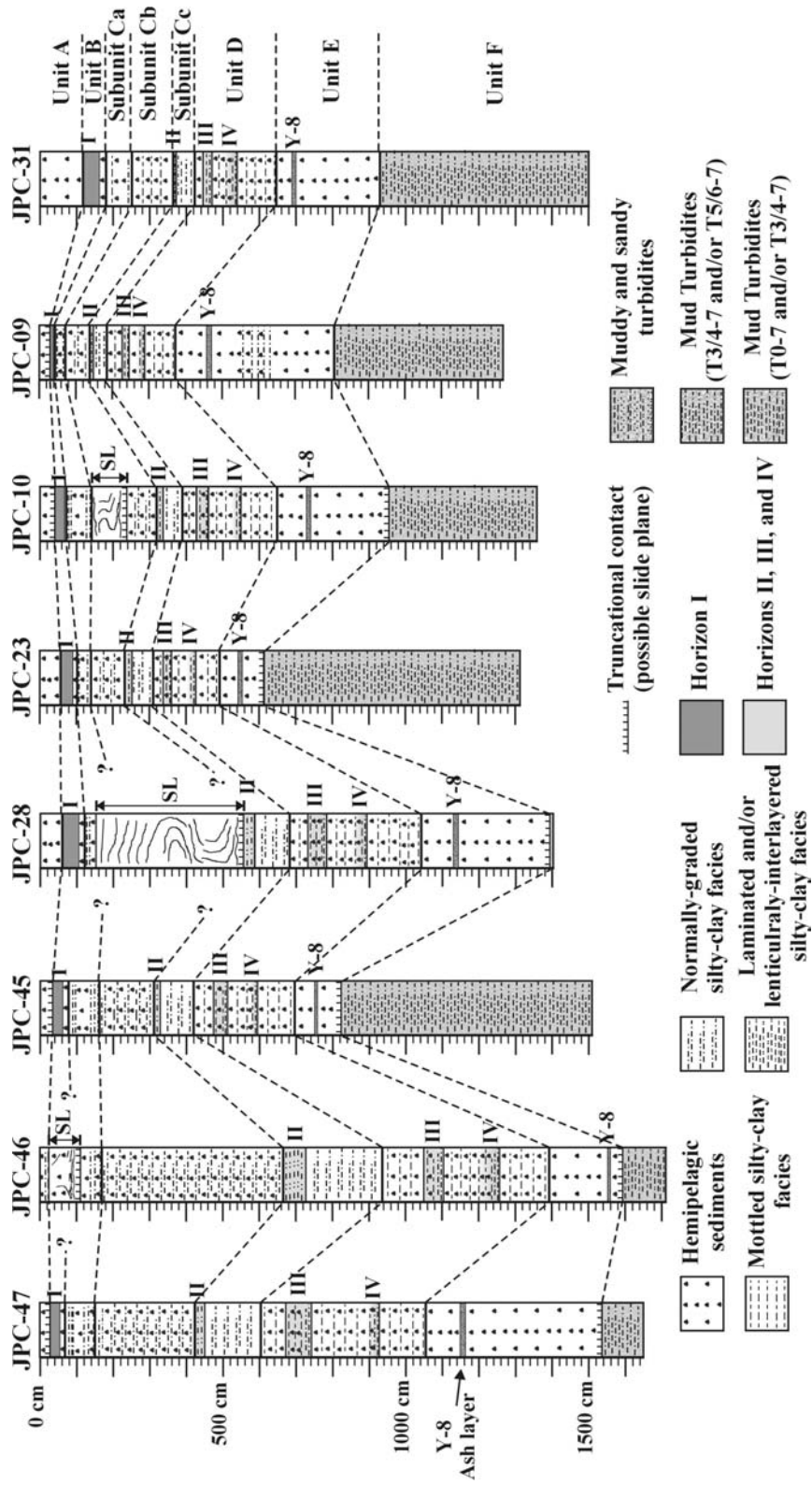


Fig. II-4. Image displaying the sedimentological descriptions of the twelve cores, on which this study is based. SL: slumped sediments.

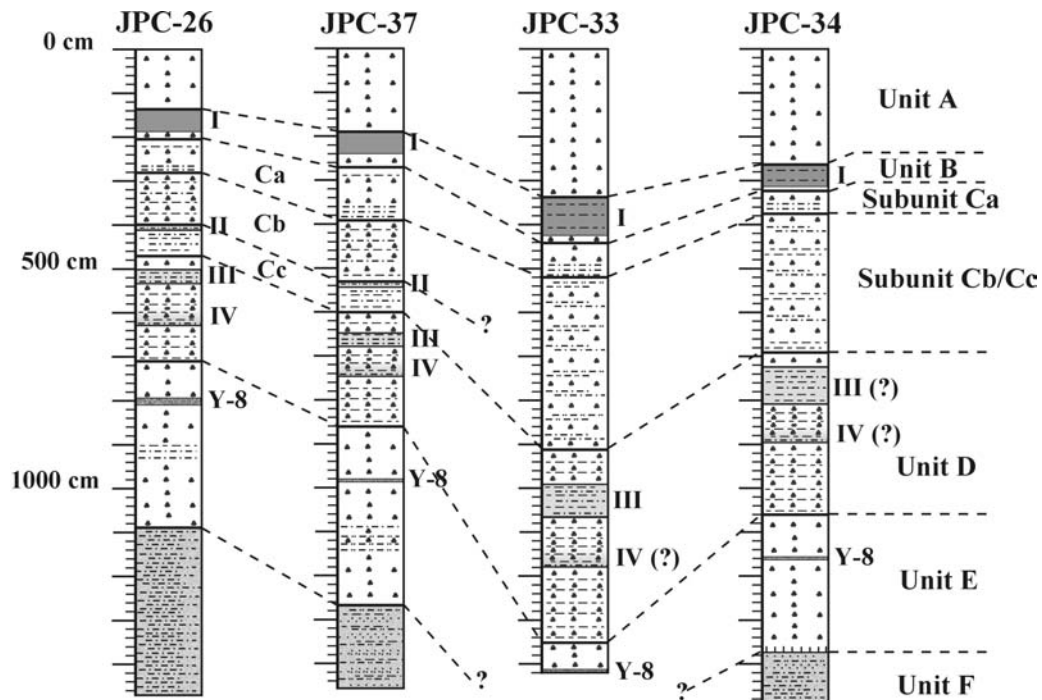


Fig. II-4. Continued.

Sedimentological Unit F

Characteristics

Sedimentological unit F consists exclusively of turbidites, and is characterized by the total absence of hemipelagic sediments and bioturbation structures. The sedimentology of this unit has been studied in great detail in Chapter III, and, for this reason, it will be only briefly discussed in this chapter. Depending on the location of the sediment cores and the nature of turbidite facies, sedimentological unit F is divided into two types (Fig. II-5). The first type (unit Fa) is observed to occur along the pathway of the canyons (JPC-37 and JPC-34), and consists of silt- and sand-rich turbidites (T_{b-c} to T_{d-e} Bouma Sequences) interbedded in successions of fine-grained (mud) turbidites (Figs. II-5 and II-6). The second type (unit Fb) is developed in all of the cores around the canyons. It consists entirely of mud turbidites that reveal a strong fining pattern moving away from the canyons. Adjacent to the canyons, they are represented by T0-7/8 mud turbidites, whereas, with increasing the distance from the canyons, they rapidly grade into T3/4-7/8 and T6-7/8 mud turbidites.

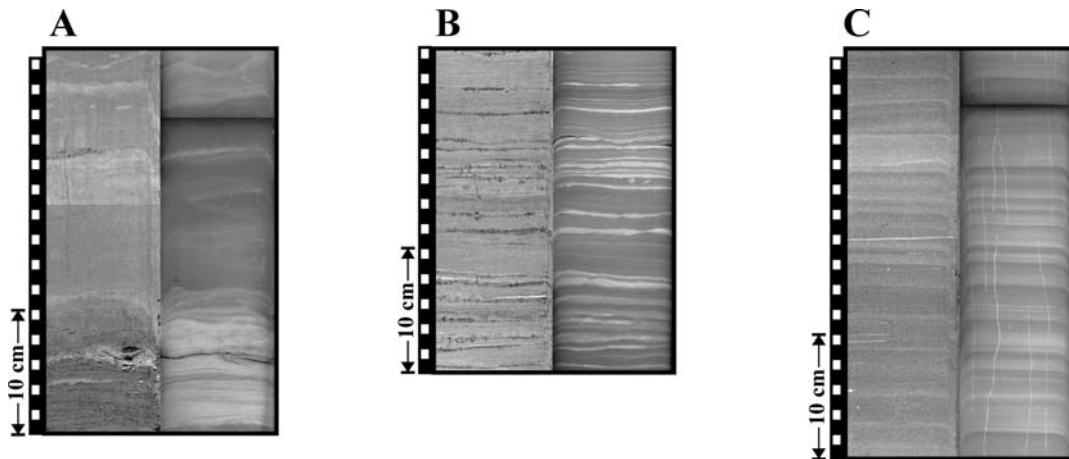


Fig. II-5. Photographs (left) and X-ray radiographs (right) (negatives) of: A) sandy and silty turbidites (T_d to T_{b-c} Bouma Sequences) capped by mud turbidites ($T_{3/4-7}$ to $T_{4/5-7}$ sequences of Stow and Shanmugam, 1980) (intracanyon deposits), B) silt-mud turbidites (T_{0-7} to $T_{4/5-7}$ sequences of Stow and Shanmugam, 1980) located on overbank areas adjacent to the canyons (JPC-09), and C) base-cut-out mud turbidites ($T_{4/5-7}$ sequences of Stow and Shanmugam, 1980) located on distal overbank areas (JPC-31).

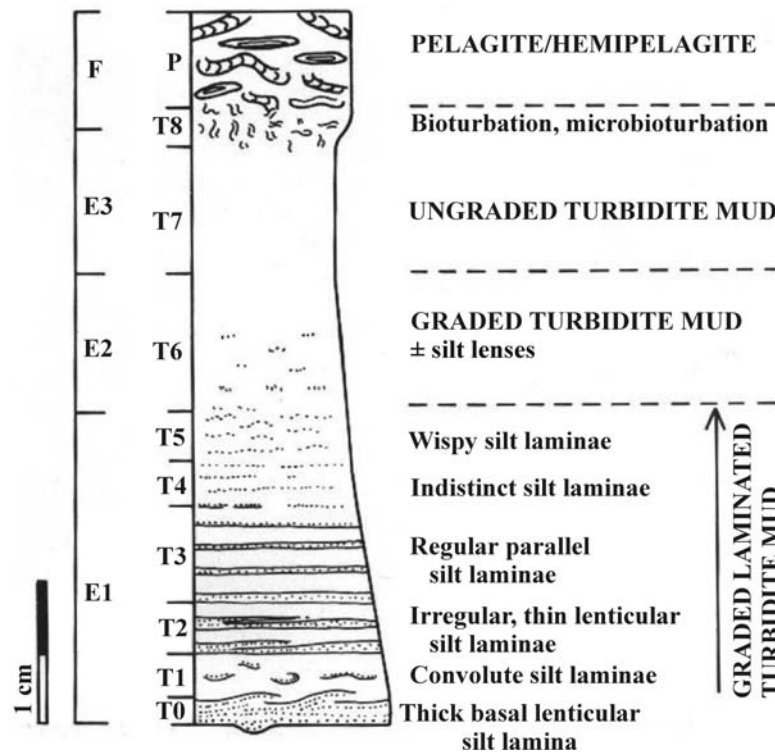


Fig. II-6. Mud turbidite facies model. Structural divisions after (E1, E2, E3, F) Piper (1978) and (T0-T8, P) Stow and Shanmugam (1980) (from Stow and Piper, 1984).

Interpretation

The age determination of sedimentological unit F meets two untranscendent difficulties. The first is that due to the total absence of hemipelagic sediments, no reliable $\delta^{18}\text{O}$ measurements could be performed on these sediments. The second difficulty is focused on the fact that the sediments are older than 40 ky, and consequently no ^{14}C AMS dating could be applied. However, Figure II-3 clearly reveals that unit F is placed below Oxygen Isotope Stage 5 sediments. This, in combination with the turbidite successions of unit F that could have been deposited only during a glacial episode (low sea-level stand), infers that unit F represents Oxygen Isotope Stage 6 deposits.

The presence of the thick turbidite successions in and around the canyons implies that Bryant and Eastern Canyons were active during Stage 6, and they were probably supplied with sediments from an ancestral Mississippi River (Suter and Berryhill, 1985; Suter et al., 1987). Unit Fa is interpreted to represent intracanyon turbidity current deposits. In more detail, mud turbidites are interpreted as deposits of the most diluted, end-members of the passing over turbidity currents, whereas the coarse (sand/silt) turbidites as deposits from the main bodies of the turbidity currents. Unit Fb is interpreted to represent overbank turbidity current deposits. The fining of the mud turbidites with increasing distance from the canyons indicates the waning and depletive character of the spilled-over turbidity currents.

Sedimentological Unit E

Characteristics

Sedimentological Unit E consists of light greenish gray to pale green, intensely bioturbated, muddy foraminifera ooze (hemipelagic sediments). The Y-8 ash layer, dated at 84 ky B.P. (Rabek et al., 1985), is interbedded in this unit. The determination of the ash layer was based on its chemical composition and location on the $\delta^{18}\text{O}$ curve of core JPC-31 (Fig. II-7a). The transition from unit F to unit E sediments is sharp and bioturbated in most cases, and gradational only in cores JPC-09, JPC-31, JPC-26, and JPC-37.

In cores JPC-09, JPC-26, and JPC-37, sedimentological unit E is interbedded, below the Y-8 ash layer, by a 31-79 cm thick interval (Figs. II-7b and c) that is characterized by the presence of: 1) sharp based layers of silt and clayey-silt alternated laminae, covered by a normally-

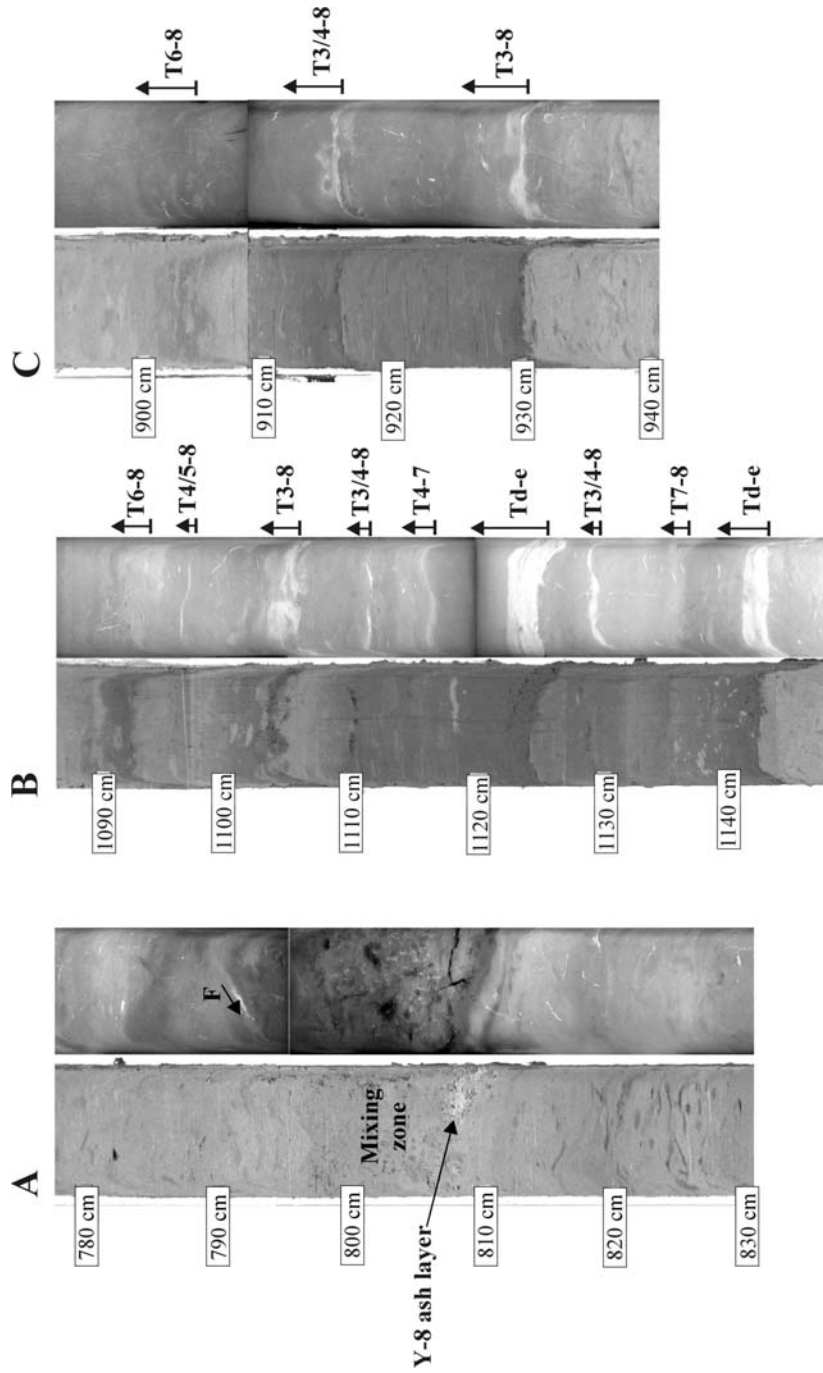


Fig. II-7. Photographs (left) and X-ray radiographs (right) (negatives) displaying: A) typical hemipelagic sediments of unit E interbedded by the Y-8 ash layer (note the thick mixing zone on the top of the layer produced by bioturbation activities), B) silt to mud turbidites interbedded in hemipelagic sediments (JPC-37), and C) mud turbidites interbedded in hemipelagic sediments (JPC-26). Note that the coarser and more abundant turbidites are developed in core JPC-37, located on the Bryant Canyon pathway, indicating that the turbidity currents were channelized with only the largest of them to be able to spillover and print their records in core JPC-26. According to the thickness of the interbedded hemipelagic sediments (2 – 7 cm), a periodicity of about 200 – 700 years is implied for the production of the turbidity currents. The darker hue of the Y-8 ash layer in the X-ray radiographs is due to smaller density of the bubble-structured volcanic glass. The core locations are displayed in Figure II-2. F: micro-fault.

graded to uniform mud layer (~ 2 - 4 cm thick) (T_{d-e} Bouma Sequences), and/or 2) sharp based, normally-graded or uniform, mud layers that in some cases display silty basal laminae (< 3 mm thick) (T3/4-8 Stow and Shanmugam's sequences). The tops of these turbidites are bioturbated, whereas the finest-grained turbidite facies display bioturbation structures throughout their entire thickness. The coarsest facies occur in core JPC-37, located on the pathway of Bryant Canyon, whereas the finest facies in cores JPC-09 and JPC-26 located on the banks of Bryant Canyon.

Interpretation

The $\delta^{18}O$ profile of core JPC-31 (Fig. II-3) indicates that sedimentological unit E represents deposits of the interglacial Isotope Stage 5 (high sea-level stand). The dominance of the hemipelagic sediments infers that the majority of the river-sourced sediments were trapped on the widespread northwest continental shelf of Gulf of Mexico. That led to the cessation of turbidity currents, and consequently to the abandonment of Bryant and Eastern Canyon systems.

The presence of the Y-8 ash layer, in sedimentological unit E, is of great importance, since it allows the assessment of the sedimentation rates prior and after its deposition (Table II-1). The sedimentation rates after the deposition of the Y-8 ash layer (71-84 ky B.P.) range between 4.23 and 9.92 cm/ky. It is interesting that, in every core, the sedimentation rates prior to the deposition of the Y-8 ash layer (84-125 ky), are lower (1.46-8.68 cm/ky) than the sedimentation rates for the time interval 71-84 ky B.P. The only exception is observed in cores JPC-09 and JPC-31, where the sedimentation rates of the time interval 84-125 ky are slightly higher.

A possible explanation for this discrepancy in the sedimentation rates may be hidden in the presence of undetected unconformities, originating from the development/passage of sediment failures, in the hemipelagic sediments deposited prior to the Y-8 ash layer. This assumption is in agreement with Lee et al. (1996) and Twichell et al. (2000), which stated that the destruction of the canyons, right after their abandonment, led to the triggering of numerous sediment failures. Proof of the above interpretation is provided through the following two observations.

The first observation is the sharp contact between sedimentological units F and E observed in most of the cores, which most probably represent slide planes of passing over slumps/gravity

flows. The very small thickness of unit E below the Y-8 ash layer in cores JPC-45 and JPC-23 provide extra support to the above theory.

Table II-1. Sedimentation rates of each sedimentological unit and subunit.

Location	Upper continental slope			Middle continental slope				Lower continental slope				
	Upper part					Middle and lower part						
JPC-Core	47	46	45	28	23	10	09	31	26	37	33	34
Unit A (0-11.16 ky) (cm/ky)	?	?	?	5.38	5.20	?	?	10.66	12.46	17.29	30.29	23.52
Unit B (11.16-18.17 ky) (cm/ky)	?	?	?	8.84	6.28	?	?	8.70	9.42	10.84	14.84	8.77
Unit Ca (18-21 ky) (cm/ky)	26.86	20.06	26.54	?	?	22.01	9.06	26.67	24.60	39.48	22.33	16.18
Unit Cb (21-28.23 ky) (cm/ky)	39.10	70.44	21.52	?	13.63	?	9.33	14.20	17.36	20.09	37.68	30.03
Unit Cc (28.23-31.85 ky) (cm/ky)	49.65	75.80	30.29	29.18	21.58	?	13.42	17.70	19.64	19.64	37.68	30.03
Unit D (31.85-71 ky) (cm/ky)	11.54	11.67	7.06	9.18	4.60	?	4.80	5.72	6.07	6.64	11.39	9.45
Unit E (71-84 ky) (cm/ky)	9.92	5.00	4.77	7.85	4.92	7.08	7.50	4.23	7.65	9.77	5.38	7.92
Unit E (84-125 ky) (cm/ky)	8.68	3.29	1.61	6.20	1.46	5.32	8.16	5.61	6.83	6.80	?	5.12

The questionmarks indicate that the sedimentation rates were impossible to be estimated, due to disturbances of the sediment either by sediment failures, or by extensive micro faulting. The micro-faulting of the sediments is not indicated on the descriptions because it is not known if it is real or artificial that could lead us to the wrong conclusions.

The second observation is focused on the presence of fine-grained turbidites in cores JPC-09, JPC-26, and JPC-37, located on the middle/lower continental slope. It is interesting that in all three cores the turbidites were deposited during the same time interval (~ 94 to 100 or 105 ky

B.P.). These turbidity currents are probably related to the triggering of a series of sediment failures, which resulted from the diapiric blockage of Bryant Canyon. The absence of the turbidite series in the cores upslope of core JPC-09 infers that the sediment source of the turbidity currents was located between cores JPC-09 and JPC-10. The absence of this interval in core JPC-34, on the lower continental slope, indicates that the diapiric blockage of Bryant Canyon was significantly advanced, prohibiting the downslope propagation of the turbidity currents.

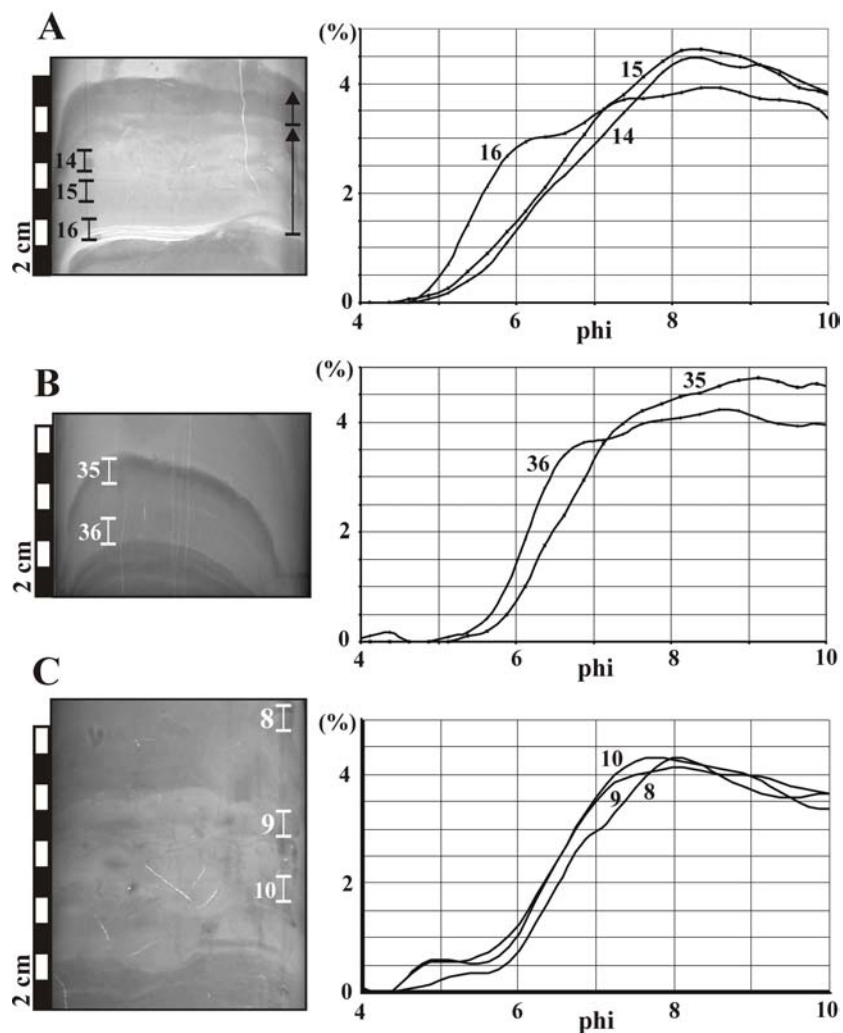


Fig. II-8. Image showing X-ray radiographs (negatives) and weight % grain-size curves, from successive samples, of: a) laminated silty-clay facies, b) normally graded silty-clay facies, and c) mottled silty-clay facies. The exact location of the samples is displayed in the X-ray radiographs.

Sedimentological Units C and D

The most intriguing similarity of units C and D is that both are interbedded by brown to greenish gray silty-clay facies, which are characterized by a scarcity or total absence in forams. The brown facies are characterized by an organic carbon content (C_{org}) less than 0.95 %, whereas in the greenish gray facies the organic carbon ranges between 1.1–1.7 %. According to their sedimentary structures, they are distinguished into four types:

Laminated silty-clay facies (2-10 cm thick): It consists of a normally-graded, sharp-based, basal zone of silty-clay (silt/clay: 30/70-55/45), which is characterized by a thin (1–3 mm), basal, silt/clayey-silt lamina, and thin (< 1 mm) fading upwards, indistinct to wispy, silty laminae (Fig. II-8a). In some cases, two or three parallel, silty laminae may be developed at its base. The normally-graded zone is usually capped by a homogeneous zone of silty-clay/clay (silt/clay: 20/80 - 35/65), which is bioturbated on its upper reaches. These silty-clay facies resemble T3/4-8 sequences of Stow and Shanmugam (1980), and turbiditic facies M2 and M3 (Chapter III). In some cases, isolated burrows are observed to develop in these facies.

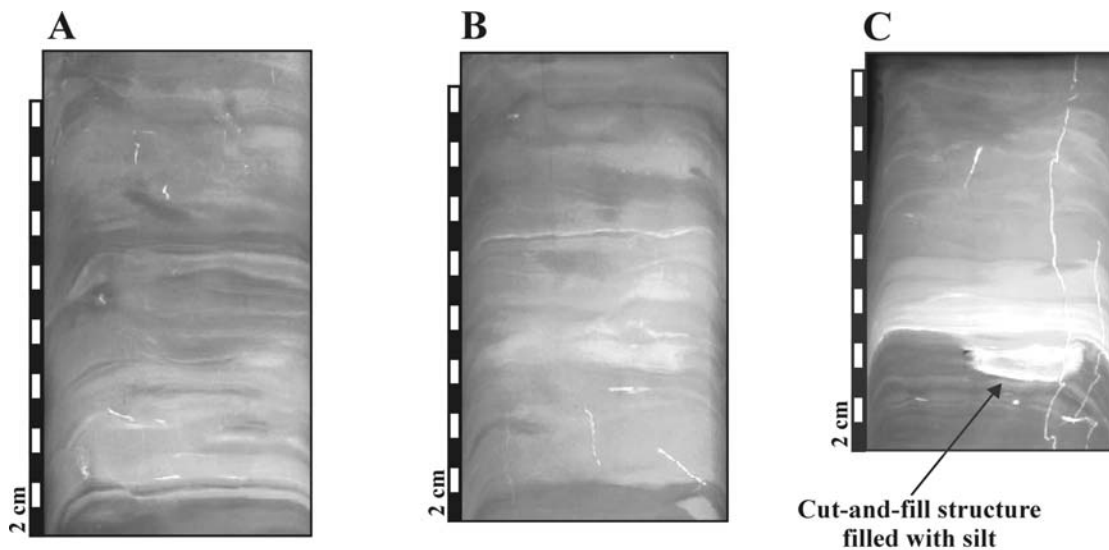


Fig. II-9. Typical X-ray radiographs (negatives) of lenticularly interlayered silty-clay facies with normal grading (A), inverse grading (B), and normal grading characterized by very silty and erosional bases (C). Note that the inverse grading could be interpreted as a less silty normally-graded silty-clay facies preceding the base of a normally-graded, lenticularly-interlayered silty-clay facies.

Normally-graded silty-clay facies (0.2-3 cm, or even up to 5 cm thick): It consists of a normally-graded, sharp-based, basal zone of silty-clay (silt/clay: 25/75-40/60), which is bioturbated on its upper reaches (Fig. II-8b). In some cases, these facies may be characterized by a siltier basal lamina (1–3 mm), and/or the presence of fading upwards, indistinct to wispy laminae of siltier silty-clay. These sedimentary facies resemble to T5/6-8 sequences of Stow and Shanmugam (1980), and turbiditic facies M1 (Chapter III). In some cases, these facies may be minor to medium bioturbated.

Mottled silty-clay facies (3–20 cm thick): Mottled silty-clay facies are recognized in the X-ray radiographs as nebulous zones/layers of silty-clay (silt/clay: 25/75-35/65), capped by mottled and ghost layered hemipelagic sediments (Fig. II-8c). They are heavily bioturbated, obscuring most of their primary syn-sedimentary structures. However, a ghost layering is usually observed. Usually, they appear to be either ungraded, or weakly normally graded. In some cases, a faint inverse grading is observed adjacent to their bases. Their bases grade from bioturbated to sharp and bioturbated, whereas their tops are gradational and bioturbated.

Lenticularly-interlayered silty-clay facies: It consists of sharp-based, normally-graded, mottled silty-clay, with wavy thin lenses to discontinuous layers/laminae of siltier silty-clay/clayey-silt (Fig. II-9). In some cases, it is characterized by an inverse grading adjacent to its base. Bioturbation structures are observed throughout the entire thickness of these facies. In some extreme cases, the bases of the lenticularly interlayered silty-clay facies may be very silty with erosional features filled with almost clear silt (e.g. cut and fill structures). Similarly to the mottled silty-clay facies, they are capped by mottled and/or ghost layered hemipelagic sediments.

Similar sedimentary facies already have been recognized in units F and E, and they have been interpreted as fine-grained turbidites. However, since a turbiditic origin is not apparent for the above facies (no sand or silt turbidites occur in units C and D), they are examined independently.

Characteristics of Sedimentological Unit D

Sedimentological unit D consists of pink to pinkish gray to light greenish gray (locally), bioturbated clayey sand to sandy silty-clay, where the sand fraction is entirely of biogenic origin (foraminifera). These hemipelagic sediments are interbedded by several, irregularly and widely-spaced, normally-graded and mottled silty-clay facies, with the later to be dominant.

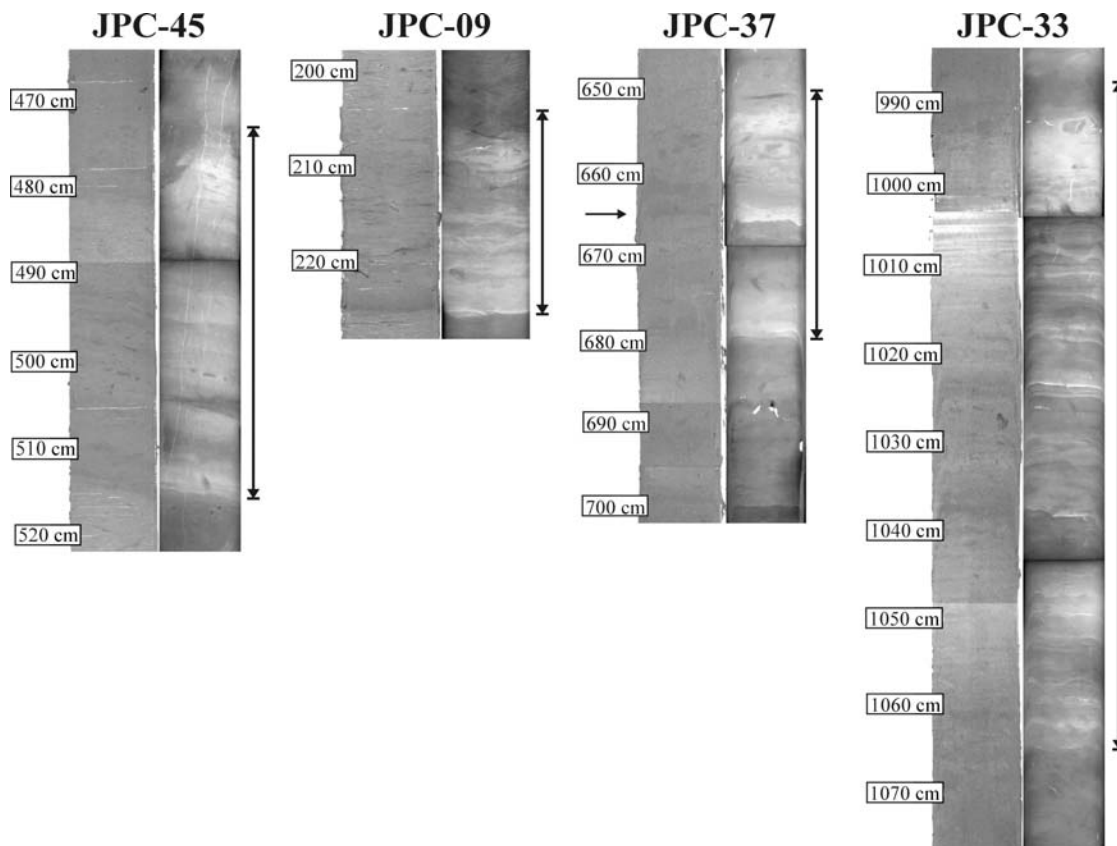


Fig. II-10. Photographs (left) and X-ray radiographs (right) (negatives) of chronostratigraphic horizon III from four cores from the upper to lower continental slope. Observe the very different sedimentological nature of horizon III on the lower continental slope (JPC-33 in this figure). Also note that horizon III is surrounded by less silty mottled silty-clay facies in core JPC-37. The arrow indicates a normally-graded silty-clay facies that does not fit the sedimentological pattern of horizon III on the upper to middle continental slope (JPC-45 and JPC-09 on this figure). The occurrence of this silty-clay facies only in cores JPC-37 and JPC-26 reveals that it has been probably resulted from a local-scale depositional event as low-density sediment flows originating from the sediment clouds of an adjacent sediment failure. The core locations are displayed in Figure II-2.

The thickness of sedimentological unit D ranges from 457 to 180 cm (Fig. II-4), and it follows a general dowdip thinning trend. The same pattern is also observed in the nature of the silty-clay facies. They are better developed and siltier on the upper continental slope, whereas downslope they become finer-grained and higher bioturbated, tending to lose their identity and vanish. However, on the middle and lower parts of the lower continental slope (JPC-33 and JPC-34), unit D sediments do not follow the same trend. Inversely, they reveal significantly increased thickness than in the cores on the middle/lower continental slope, exhibiting their

largest thickness in core JPC-33. Unit D is also thicker in cores JPC-31, JPC-26, and JPC-37 than in their adjacent upslope cores, but not as much as in cores JPC-33 and JPC-34.

The tracing of the individual silty-clay facies on the continental slope is very difficult to impossible due to the downslope disintegration of the sedimentological events. However, there are two intervals characterized by siltier and closely-spaced, silty-clay facies that can be traced in all of the studied cores. These two intervals are also traceable in the bulk density profiles of the cores, and they are represented by high-density values (Figs. II-3 and II-17).

The upper zone is named chronostratigraphic horizon III, is the most easily identifiable, and its thickness ranges from 79 to 18 cm (Fig. II-10). On the upper continental slope, horizon III is represented by closely-spaced, normally-graded silty-clay facies that upwards become finer grained, more bioturbated, and grade either into mottled silty-clay facies or straight into mottled hemipelagic sediments. At the top of horizon III, a siltier mottled silty-clay facies occurs. Horizon III is thickest and most silty in the cores of the upper continental slope, revealing a downdip thinning and fining trend. However, in cores JPC-33 and JPC-34, horizon III exhibits a very different sedimentological character. It has a much greater thickness (79 and 49 cm, respectively), and it consists of several series of upwards fining, normally-graded silty-clay facies. The silty-clay facies are best developed in core JPC-33, where horizon III exhibits its largest thickness on the lower slope. Horizon III is also thicker in cores JPC-31, JPC-26, and JPC-37, compared to their most adjacent upslope cores. However, the upper slope sedimentological identity of horizon III is still preserved in these cores, with the only discrepancy that it is surrounded by finer-grained, mottled silty-clay facies.

The lower zone of closely-spaced, silty-clay facies (chronostratigraphic horizon IV) is not as distinct as horizon III, and it is represented by two successive, normally-graded silty-clay facies that upwards are succeeded by a series of mottled silty-clay facies. On the middle and lower continental slope, only one basal, normally-graded silty-clay facies is observed to develop. The presence of horizon IV is uncertain in cores JPC-34 and JPC-33.

Characteristics of Sedimentological Unit C

As it was previously mentioned, sedimentological unit C is similar to unit D with the only discrepancy being that the silty-clay facies are siltier, better developed, and more closely spaced. Depending on the organization and nature of the silty-clay facies, three subunits are distinguished in unit C. Starting from the uppermost subunit, they are:

Sedimentological Subunit Ca

Sedimentological subunit Ca is represented by light greenish gray to pale yellow, bioturbated muddy foraminifera ooze, which is interbedded by two characteristic series of silty-clay facies named as the upper, and lower facies series (Fig. II-11). The hemipelagic sediments may reveal a faint ghost layering in some of the cores. This is most apparent in cores JPC-47, JPC-46, JPC-45, located on the upper continental slope, and cores JPC-37, JPC-33, and JPC-34 placed on the lower continental slope. The thickness of subunit Ca ranges from 28 to 83 cm.

The upper facies series are characterized by a distinct reddish brown shade. On the upper continental slope, they are represented by three normally-graded silty-clay facies that downslope become finer grained, bioturbated and gradually tend to lose their identity. In cores JPC-37, JPC-26, and JPC-31 (upper part of lower continental slope) the reddish brown facies are recognized only as faint lenses or mottled silty-clay facies of a reddish hue. The upper facies series are not observed in cores JPC-33, and JPC-34 from the lower continental slope. On the bulk-density profiles of the cores, the upper facies series are represented by high values (apex) (Figs. II-3 and II-17).

The lower facies series is characterized by three dark olive green to greenish gray, organic-rich (up to 2.02 % Corg) silty-clay facies, and it determines the lower boundary of subunit Ca. This silty-clay facies series has a different sedimentological character on the upper to middle continental slope than on the lower continental slope. On the upper continental slope, they are represented as very clayey, normally-graded silty-clay facies that are separated from each other by a 3–10 cm thick layer of ghost-layered to typical hemipelagic sediments. The dark olive green to greenish gray zone represents only the upper uniform part of the facies, whereas their siltier bases are almost indistinguishable from the surrounding hemipelagic sediments on the optical descriptions/photographs. These facies are best developed in core JPC-10.

On the lower continental slope (JPC-31, JPC-26, JPC-37, JPC-33, JPC-34), the lower facies series are represented by three successive very clayey, normally graded silty-clay facies, that are best developed and coarser in core JCP-33, and they become finer grained and thinner with increasing distance from the location of core JPC-33. The bioturbated tops of the above three facies indicate that their deposition did not occur at once, but they were deposited by three discrete depositional events separated from each other by a short, calm period of hemipelagic sedimentation (couple of years).

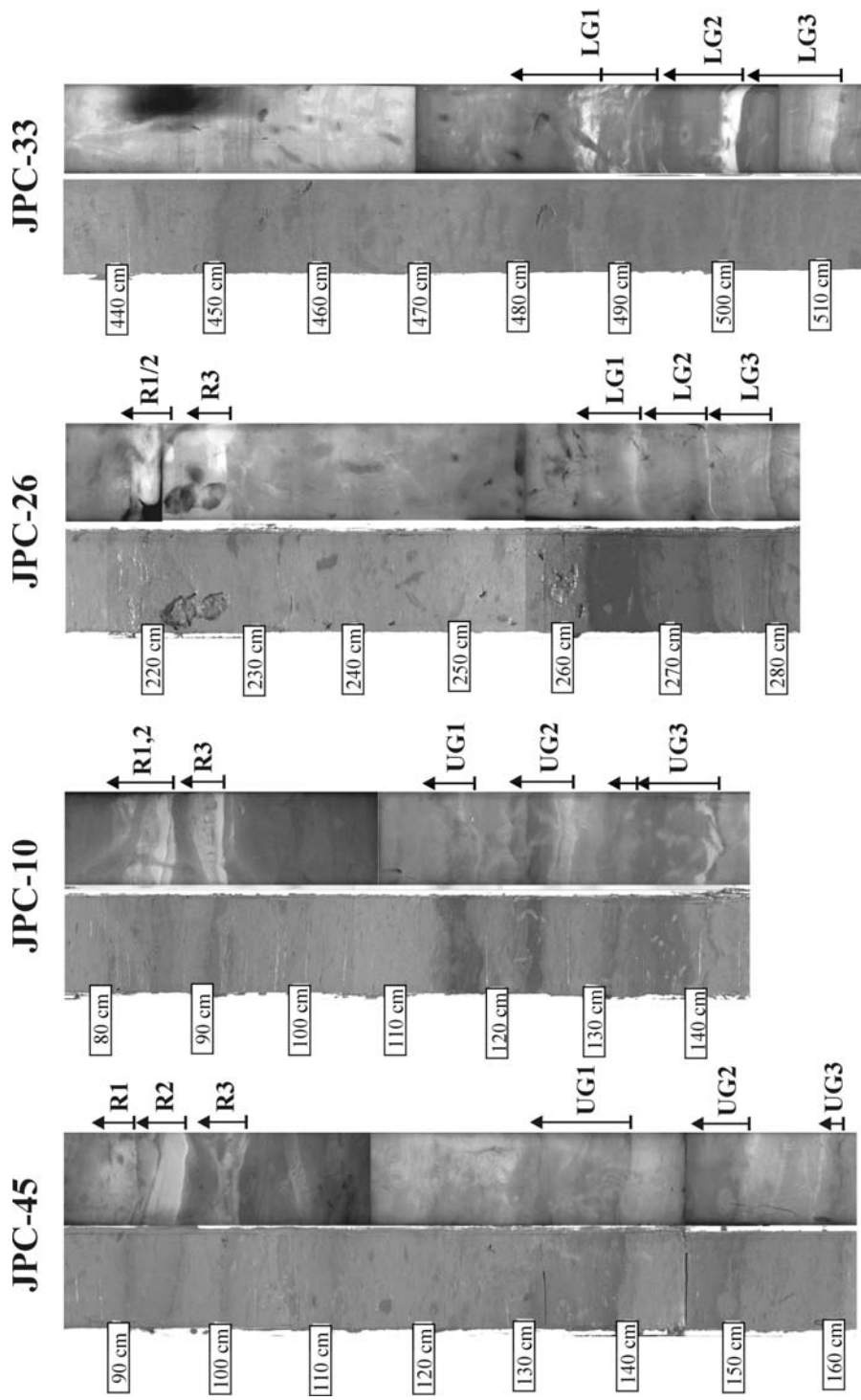


Fig. II-11. Photographs (left) and X-ray radiographs (right) (negatives) of sedimentological subunit Ca from four cores from the upper to lower continental slope. Note the different nature of the upper to middle (UG) (JPC-45 and JPC-10), and lower (LG) (JPC-26 and JPC-33) continental slope greenish gray silty-clay facies (lower facies series), indicating their different origin. Note that the greenish gray facies are less subtle in core JPC-45 (upper continental slope) than in core JPC-10 (middle continental slope). For further discussion see text (interpretation). The core locations are displayed in Figure II-2.

Sedimentological Subunit Cb

Sedimentological subunit Cb consists of closely spaced silty-clay facies separated from each other by a thin layer (mm to 5 cm, or even up to 10 cm in some rare cases) of light greenish gray to pale yellow, bioturbated foraminifera ooze (hemipelagic sediments) (Fig. II-12). The thickness of subunit Cb ranges from 65–491 cm, and reveals a general downdip thinning pattern. As in Subunit Ca, the silty-clay facies do not retain their sedimentary character all over the continental slope, but their appearance mainly depends on their proximity to the shelf margin.

On the upper continental slope (JPC-47, JPC-46, and JPC-45), they are represented almost solely by well-developed, normally-graded silty-clay facies. The normally-graded silty-clay facies are organized into sequences, in which they grade upwards to finer-grained, thinner, and bioturbated, normally-graded silty-clay facies and eventually into mottled/ghost-layered hemipelagic sediments. In some cases, a few finer-grained, normally-graded silty-clay facies may precede the above facies sequences. On the middle continental slope (JPC-23, and JPC-10), the silty-clay facies gradually become finer grained, thinner, and bioturbated, which makes harder the identification of the silty-clay facies as individual depositional events. In some cases, the facies sequences may resemble sharp-based, normally-graded, ghost-layered, silty-clay facies. On the middle to lower continental slope (JPC-09, JPC-31, JPC-26, and JPC-37), mottled silty-clay facies become dominant in subunit Cb, whereas just a few normally-graded silty-clay facies are observed to develop.

In cores JPC-46 and JPC-37, subunit Cb deviates from the norm, representing a larger thickness, and siltier and better-developed silty-clay facies than their adjacent upslope cores. It is puzzling that, even though subunit Cb is finer grained in core JPC-31, consisting almost entirely of mottled silty-clay facies, it is thicker than in the upslope cores JPC-09 and JPC-23.

Sedimentological subunit Cb reveals a very different sedimentological character on the middle and lower part of the continental slope (JPC-33 and JPC-34). It is almost twice as thick than in the most adjacent upslope cores, and consists of lenticularly-interlayered silty-clay facies, mottled silty-clay facies, and normally-graded silty-clay facies sequences. Subunit Cb is thicker in core JPC-33, where the silty-clay facies also reveal their siltier nature.

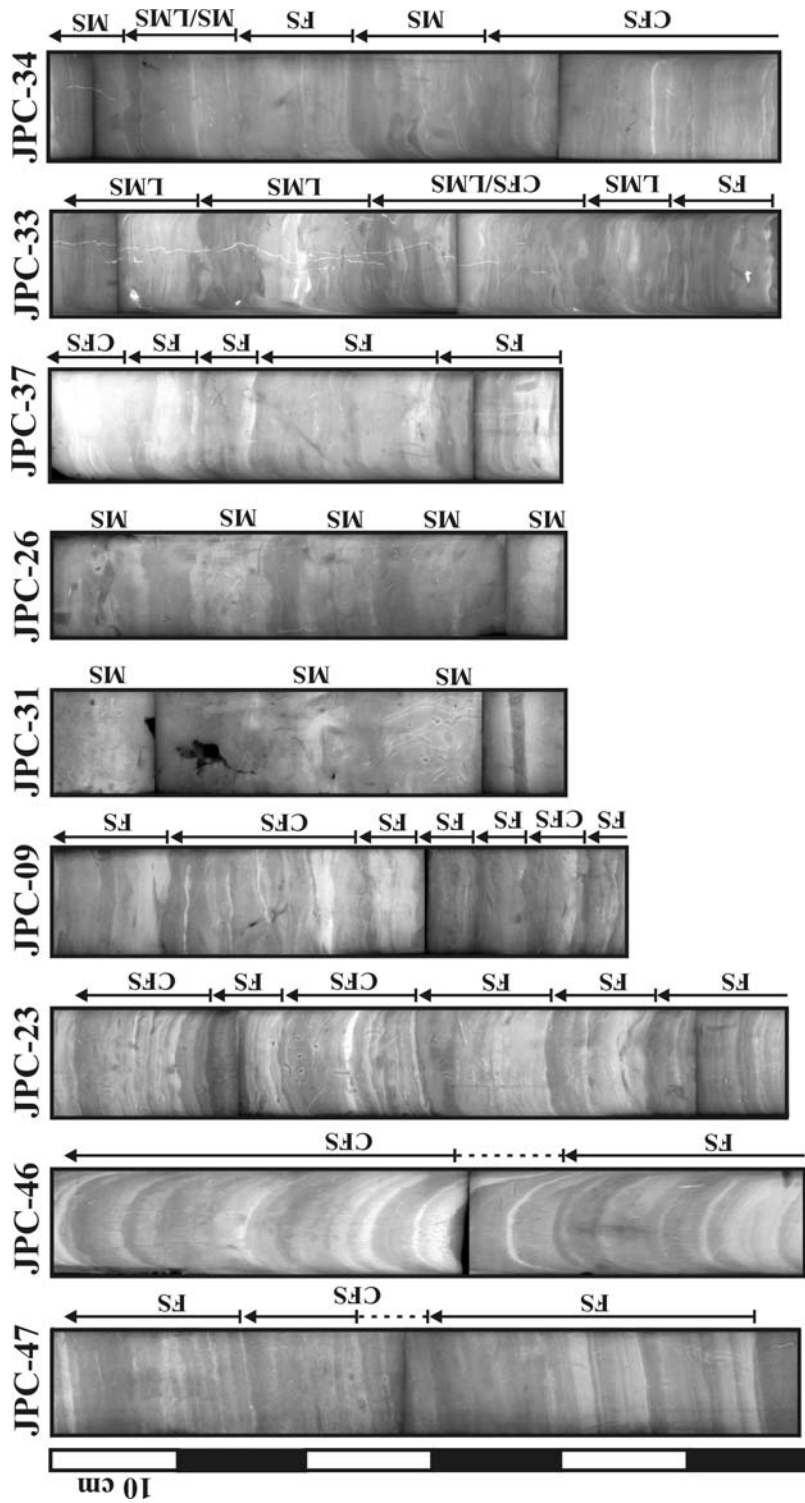


Fig. II-12. X-ray radiographs (negatives) of subunit Cb from nine cores from the upper to lower continental slope. Observe the organization of the silty-clay facies into sequences (arrows), and watch how they grade from abundant and well-developed normally-graded silty-clay facies on the upper continental slope (JPC-47, JPC-46) to indistinct mottled silty-clay facies on the lower continental slope (JPC-31, JPC-26, JPC-37). The smaller number of silty-clay facies, consisting the facies sequences on middle to lower continental slope, reveals that not all depositional events extended to the lower parts of the slope, but only the most powerful. Also note the very different nature of the silty-clay facies on the middle and lower part of the lower continental slope (JPC-33 and JPC-34). The core locations are displayed in Figure II-2. FS: fining upwards sequences of normally-graded silty-clay facies, CFS: coarsening-fining upwards sequences of normally-graded silty-clay facies, LMS: lenticularly-interlayered silty-clay facies, MS: mottled silty-clay facies.

Sedimentological Subunit Cc

Sedimentological subunit Cc consists almost exclusively of successive normally-graded silty-clay facies, separated from each other by a thin layer/lamina (mm to 0.5 cm, or even up to 2 cm thick) of hemipelagic sediments (Fig. II-13). Similarly to subunit Cb, the silt-clay facies are organized in fining upwards sequences, whereas in some cases a few, finer-grained, silty-clay facies may develop at their bases. Subunit Cc exists in all cores, except from cores JPC-33 and JPC-34. On the upper continental slope, the normally-graded silty-clay facies are well-developed and preserved, whereas they gradually become thinner, partially bioturbated, and fewer in the downslope direction. However, in contrast to subunit Cb, the normally-graded silty-clay facies retain their identity all over the slope, without changing into mottled silty-clay facies. The thickness of subunit Cc ranges between 49–274 cm, and reveals a general downdip thinning trend.

Due to the similar appearance of the normally-graded silty-clay facies, the tracing of the individual depositional events along the slope is impossible. However, there is a zone at the top of subunit Cc that is very distinct and can be traced in all cores. This zone is named as chronostratigraphic horizon II. On the upper continental slope (JPC-47, JPC-46, and JPC-45), horizon II is represented by two dark greenish gray series of successive, normally-graded and/or laminated, silty-clay facies, and a distinct reddish brown laminated silty-clay facies at its base (Fig. II-13). Bioturbation structures are limited only on the upper silty-clay facies, of the dark greenish gray facies series, and brown facies. The rest of silty-clay facies in the facies series are characterized by a missing top. Despite the top-cut-out nature of the silty-clay facies their contacts are sharp and not erosional. The characteristic color identity of horizon II is preserved all along the slope. The silty-clay facies grade, in the downslope direction, to finer-grained and partially-bioturbated, silty-clay facies. Downslope of core JPC-28, the dark greenish gray series are condensed into a single, normally-graded silty-clay facies.

Cores JPC-46, JPC-31, JPC-26, and JPC-37 deviate from the norm of the other cores, revealing a thicker subunit Cc compared to that of the immediate upslope cores. Cores JPC-46 and JPC-37 are also characterized by siltier silty-clay facies.

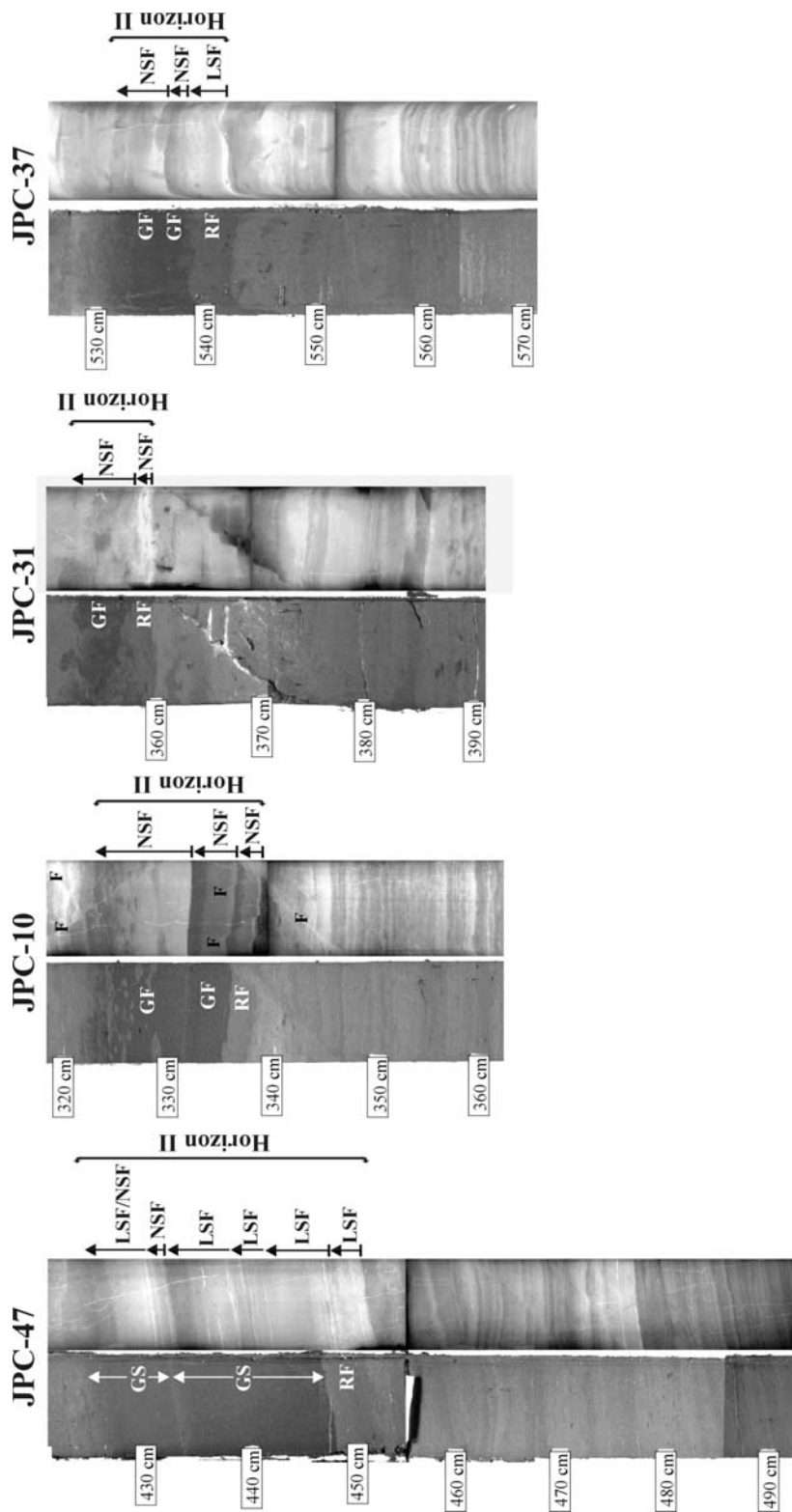


Fig. II-13. Typical photographs (left) and X-ray radiographs (right) (negatives) of the upper part of sedimentological subunit Cc, focusing in chronostratigraphic horizon II. Note that even though there is a strong downslope fining and thinning trend of the silty-clay facies, they are thicker and siltier in core JPC-37 than in its adjacent upslope core JPC-31. Also note that in core JPC-47 the greenish gray facies series (GS) consists of successive, laminated to normally-graded silty-clay facies, characterized by sharp but not erosional tops and bases, with bioturbation structures and hemipelagic sediments to occur only on the upper silty-clay facies of the facies series. This, in combination with the top-cut-out nature of the rest of the facies, indicates that each greenish gray facies series resulted from a single pulsating, low-density flow event, and not from multiple and discrete flow events. The core locations are displayed in Figure II-2. NSF: normally-graded silty-clay facies, LSF: laminated silty-clay facies, GF: greenish gray silty-clay facies, RF: reddish brown silty-clay facies, GFs: greenish gray facies series, F: micro-fault.

Interpretation

Silty-Clay Facies

Silty-clay facies are the most important deposits observed in sedimentological units C and D. The comprehension of the processes, resulting in their deposition, is vital to the determination of their origin, and in extension to the comprehension of Oxygen Isotope Stages 2, 3, and 4 sedimentological history.

Laminated silty-clay facies are characterized by normal grading, sharp bases, and upward fading silty laminae. The normal grading indicates that they represent suspension deposits, whereas the silty laminae infer the existence of flow activity during their deposition. There are two mechanisms that could have resulted in the development of the silty laminae: 1) fluctuations of the shear stress within the boundary layer of a bottom-riding, fine-grained sediment flow that is driven either by gravity or bottom currents, and 2) velocity fluctuations of a bottom-riding sediment flow driven by bottom currents alone (Stow and Bowen, 1980; Best and Leader, 1993) (chapter III).

Normally-graded silty-clay facies are interpreted to be suspension deposits, as well. In the few cases that indistinct to wispy, siltier silty-clay laminae occur at their bases, they may be interpreted as deposits of bottom-riding sediment clouds driven either by gravity, or bottom currents. However, in most cases, these facies are characterized only by a normal grading, which could have resulted from suspension deposition of either bottom-riding, fine-grained sediment flows, or intermediate/surficial nepheloid layers (Stanley, 1983; Hill, 1984; Ferentinos et al., 1985; Stow et al., 1996; Bahk et al., 2000; Klauke et al., 2000; O Cofaigh and Dowdeswell, 2001).

Typical concentrations of nepheloid layers range between 0.01-0.54 mg/l, whereas in some extreme situations may achieve values as high as 5 mg/l (McCave and Swift, 1976; Stow and Bowen, 1980; Gardner, 1989). However, nepheloid layers with concentrations ranging from 3–9 mg/l to 30–90 mg/l, or even higher would have been required for the deposition of the normally-graded silty-clay facies. These concentrations resemble more those of “suspension cascades” (downdip, bottom-riding, fine-grained sediment flows) (10-100 mg/l), than those of intermediate/surficial nepheloid layers, which would have required the development of a strong density interface within the water column (Wilson and Roberts, 1995).

In the determination of the sediment concentration of the nepheloid layers, it was assumed that deposition resulted from a stationary, 300 – 1000 m thick nepheloid layer. However, if deposition had resulted from the gradual settling of a continuously replenished nepheloid layer (e.g. related to long-lasting river plumes/storms), then much lower concentrations could have actually accounted for the deposition of at least the thinner, normally-graded silty-clay facies.

There are two possible interpretations for the deposition of the mottled silty-clay facies and lenticularly-interlayered silty-clay facies. The first is that they represent a series of normally-graded silty-clay facies, which have been disturbed by intense bioturbation activities, attributing to them a rather nebulous character, and concealing the identity of the individual depositional events. The second interpretation is that they represent deposits of bottom currents. This explanation holds especially for the lenticularly-interlayered silty-clay facies, which are observed exclusively on the lower continental slope.

Depositional Time Framework, and Paleomorphology

The dating of the boundaries of sedimentological subunits Ca, Cb, and Cc was based on ^{14}C AMS dating from core JPC-31, and they were confirmed for the cores of the upper continental slope by the intriguing similarity of the $\delta^{18}\text{O}$ profiles of cores JPC-31 and JPC-46. Dating of the lower boundary of unit D was based entirely on the $\delta^{18}\text{O}$ curves of the above two cores compared with the dates and $\delta^{18}\text{O}$ curve provided by Martinson et al. (1987). The above information revealed that unit D represents entirely Isotope Stages 3 and 4 deposits (31.85 – 71 ky B.P.), whereas unit C is more complicated with subunits Ca (18.17 – 21.26 ky B.P.) and Cb (21.26 – 28.57 ky B.P.) to represent Stage 2 deposits, and subunit Cc (28.57 – 31.85 ky B.P.) late (ending) deposits of Stage 3.

At this point, it has to be emphasized that the morphology of the northwest continental slope of the Gulf of Mexico is not static. It is continuously modified due to the activities of intense halokinetic processes. It was stated earlier that the modification of Bryant and Eastern Canyons into a series of successive intraslope basins was initiated right after their abandonment at the beginning of Isotope Stage 5. However, the question is whether this transformation had been completed or not by the beginning of Stage 4. This knowledge is vital to the understanding of the sedimentological processes and their evolution during the Last Glacial Episode.

Sedimentological descriptions of Unit E (Stage 5) reveal that early Stage 5 (94 – 125 ky B.P.) was characterized by the development of numerous sediment failures, whereas during late

Stage 5 (71 – 94 ky B.P.) no indication of sediment failures is observed in any of the cores. This, in combination with the fact that the main triggering mechanism for sediment failures was the oversteepening of the intraslope basins flanks by halokinetic processes, infers that the modification of the canyons had been fulfilled about 20 ky prior to the beginning of the last glacial episode.

One of the most important observations in units C and D is the total absence of sandy and silty turbidites. This is most apparent in cores JPC-37 and JPC-34, located in the thalweg of Bryant Canyon. However, it would be expected that numerous turbidity currents would have been generated on the self margin and/or upper continental shelf during the low sea-level stand of the Last Glacial Episode, and especially during the Last Glacial Maximum (Stage 2) (Suter et al., 1987). The most plausible interpretation for the above contradiction is that the intraslope basins were of sufficient relief to trap the turbidity currents on the upper continental slope, and prohibit their downslope propagation. This provides extra support to the completion of the canyon's destruction prior to the beginning of the Last Glacial Episode.

The above information infers that the major sediment depocenter during the Last Glacial Episode was located on the outer continental shelf and/or upper part of the upper continental slope. This implies that no extreme sedimentation changes occurred on the rest of the Bryant Canyon area, which would have resulted in the destruction of the continental slope morphology by halokinetic processes. Consequently, it would be safe to assume that the morphology of Bryant Canyon area, during the Last Glacial Episode, was very similar to the present one. Support for this assumption is provided by Tripsanas et al. (2003a) (chapter IV), who concluded that the thick sediment deposits on the outer shelf and upper continental slope contributed in a seaward mobilization of the underlying salt masses that resulted only in the oversteepening of the intraslope basins flanks, and not in their destruction.

Sedimentological Processes

The sedimentation rates of unit D, and subunits Ca, Cb, and Cc have been estimated based on the ages presented in a previous section (Fig. II-14 and Table 1). According to these sedimentation rates and the sedimentological descriptions, two sedimentary provinces have been distinguished on Bryant Canyon area.

The first province extends from the upper continental slope to the upper part of the lower continental slope (Fig. II-15). The sedimentation rates, of each unit and subunit (except for

subunit Ca), reveal a strong downslope decreasing trend in this province. A similar pattern is also observed in the nature of the silty-clay facies, which reveal a strong downslope fining and thinning trend. This information indicates that, in this upper province, the deposition of the silty-clay facies came from fine-grained, low-density sediment clouds derived from the outer shelf and/or upper continental slope. It was stated earlier that laminated silty-clay facies have been deposited by waning, low-density, bottom-riding sediment flows, whereas the normally-graded silty-clay facies could have also been produced by the deposition of intermediate and/or surficial, high-density nepheloid layers.

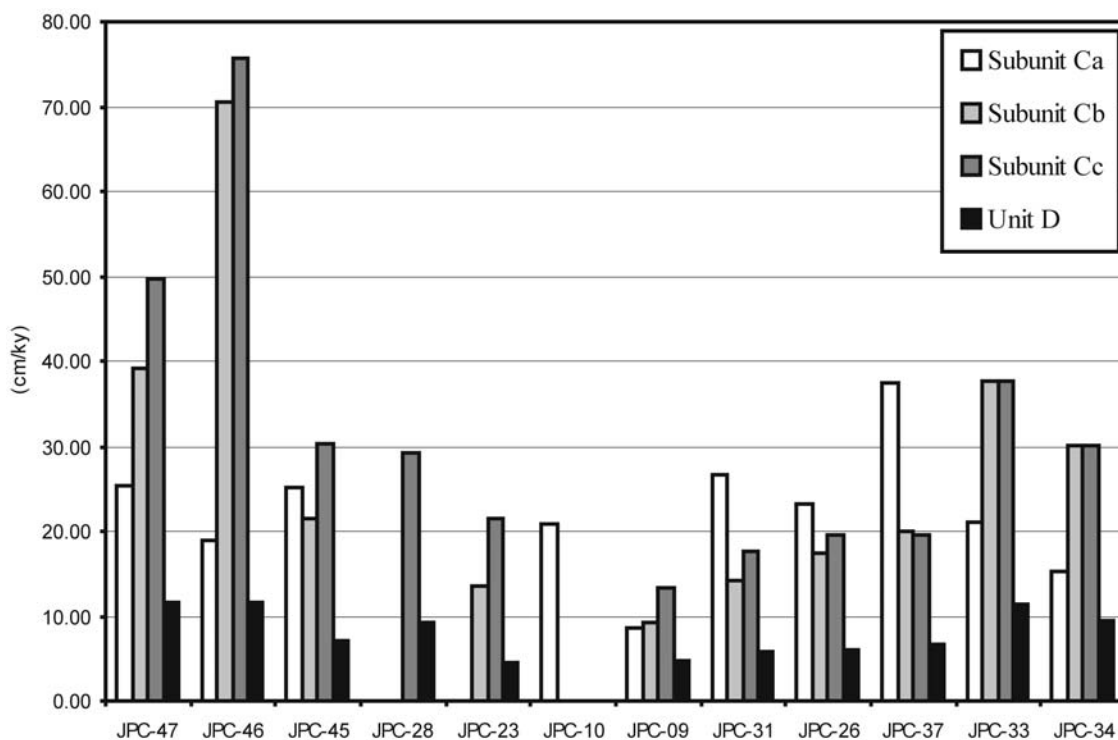


Fig. II-14. Histogram displaying the sedimentation rates of sedimentological unit D and subunits Ca, Cb, and Cc.

However, when studying in more detail the distribution of the sedimentation rates and nature of the silty-clay facies, it is observed that cores JPC-46 and JPC-37 reveal higher sedimentation rates, and coarser and thicker silty-clay facies compared to their adjacent upslope cores. It is

interesting that cores JPC-46 and JPC-37 are located very close to and on a sill, respectively, separating two successive intraslope basins. The above information excludes deposition from nepheloid layers as a possible interpretation for the development of the silty-clay facies, since if it would have been the case, it would be expected that these sediment clouds would have spread out seaward in a radial mode, resulting in a similar blanketing sedimentation pattern independently of the existing topography. Consequently, the majority, if not all, of the silty-clay facies on the upper province have been resulted from the gradual deposition of waning and depletive, bottom-riding, low-density sediment clouds driven by gravity.

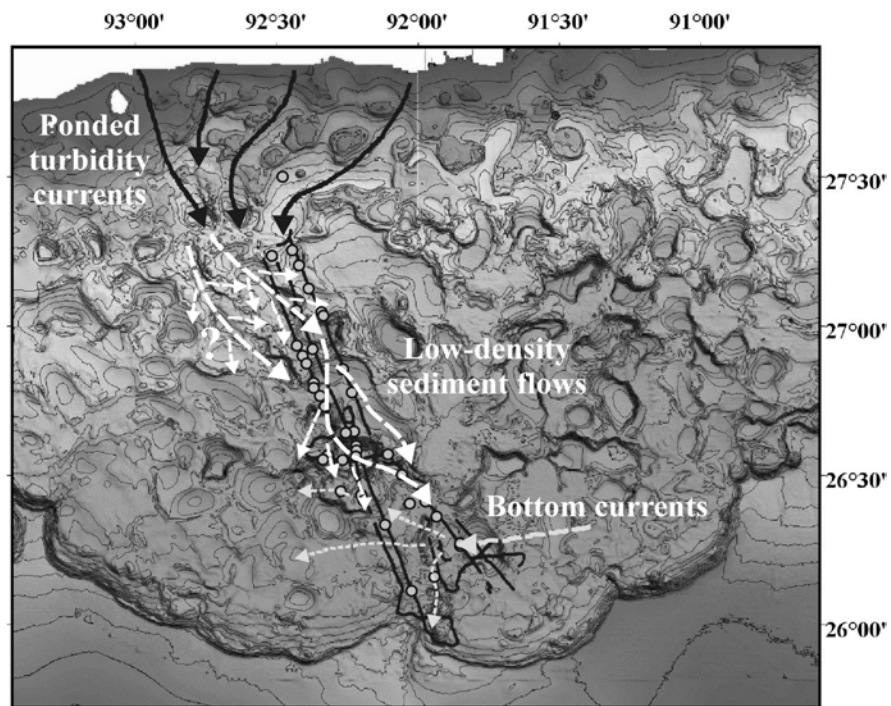


Fig. II-15. Morphological map of Bryant Canyon area displaying the routes of the major bottom-riding sediment flows during the last Glacial Episode.

The most possible interpretation for the origin of the bottom-riding, low-density, fine-grained sediment flows is through turbidity currents generated on the outer shelf and/or upper continental slope by sediment failures and/or hyperpycnal river plumes. These turbidity currents propagated downslope, and they were eventually trapped in the intraslope basins of the

upper continental slope, where they deposited their coarsest material. Turbidity current experiments have revealed that a density flow can cross an obstacle, if the height of the obstacle is not higher than 1.5 times the height of the head of the current (Muck and Underwood, 1990; Kneller and Buckee, 2000). In addition, the main body of a turbidity current is accompanied at its top by an overlying, fine-grained, low-density cloud (wash load), the thickness of which can be very big (even up to 1000 m thick) (Stow and Bowen, 1980). Consequently, in the cases that the turbidity currents were sufficiently thick, it would have been possible, at least for their most diluted upper parts, to spillover the sills and continue their downslope propagation, resulting in the generation of the bottom-riding sediment flows that led to the deposition of the silty-clay facies.

It is amazing that these low-density, fine-grained sediment flows were able to travel over a distance exceeding 200 km, without being trapped in the successive intraslope basins (200 – 700 m deep) of the northwest continental slope of Gulf of Mexico. Assuming that the depth of the intraslope basins did not change significantly during the last 71 ky, it is concluded that these flows were characterized by a minimum thickness of 750 m (based on the depth of the floor of the basins and the depth of the core locations on the adjacent plateaus). This thickness is in agreement with previous studies on low-density, fine-grained turbidity currents, which concluded that these flows are characterized by a thickness of 100 – 1000 m, velocities of 10 – 20 cm/s, and concentrations of 26 – 2500 mg/l (Normark et al., 1980; Stow and Bowen, 1980) (chapter III). However, even though these low-density sediment flows were sufficiently thicker than the intraslope basins, their downslope propagation was not independent from the morphology of Bryant Canyon area. Indeed, a part of these flows was probably confined to the intraslope basins, and they were propagating downslope, in the most adjacent intraslope basins by their spilling-over through the easiest pathways. In most cases, these pathways are represented by the sills separating the basins, which are of lower relief compared to the rest of the basin flanks (Fig. II-15). This interpretation justifies the siltier nature of the silty-clay facies in cores JPC-46 and JPC-37.

The second province occupies the middle and lower part of the lower continental slope. The sedimentation rates in this region are much higher than on the middle continental slope, and they are largest in core JPC-33. The same pattern is also observed in the nature of the silty-clay facies, exhibiting an eastward thickening and coarsening trend. This information, combined with the rheological interpretation of the lenticularly-interlayered silty-clay facies observed

exclusively on the lower continental slope, infers that the silty-clay facies of the lower province have resulted from the gradational deposition of bottom-riding, low-density, and fine-grained sediment flows that were driven not by gravity but by eastward flowing bottom currents (Fig. II-15). This is supported by the presence of well-developed furrows adjacent to the location of JPC-33. Furrows are erosional, almost linear structures produced by the helical flow of bottom currents (Allen, 1985). Additional support to the above theory is provided by the extensive furrow field that is developed on the continental rise of the northwest Gulf of Mexico, combined with current meter data, which indicate a western net of bottom mass-water transportation (W. R. Bryant, 2003, personal communication).

The remaining question to be answered is the origin of the sediment clouds. The most logical explanation would be that it is from the erosion and suspension of the silty sediments of the Mississippi Fan by bottom currents. In this case, another question is generated. Why are Isotope Stage 5 and 1 (unit A, see later section) deposits characterized by the absence of silty-clay facies? A possible answer could be a dissipation of the bottom currents during high sea-level stands. However, preliminary studies of W. R. Bryant and D. Bean (unpublished data) have revealed that the bottom currents are of larger intensity during high sea-level stands, whereas, during low sea-level stands, there is at least a 50 % decrease in their magnitude. This is because the bottom currents are driven by the Loop Current, which, during low sea-level stands, is considerably weakened due to the shallower depths of the Yucatan Straits.

The above argument brings us back to the first question. It is common knowledge that during the Last Glacial Episode, numerous turbidity currents flowed down the Mississippi Canyon and developed the Mississippi Fan (Bouma et al., 1985; Bouma and Coleman, 1985; Kolla and Perlmutter, 1993; Stow et al., 1996). According to the above information, it is proposed that the westward-flowing sediment clouds resulted from pirating of the most diluted and fine-grained, upper- and end-members of turbidity currents from Mississippi Canyon and Fan. Pirating of turbidity currents by bottom currents has been frequently proposed for the formation of fan drifts (e.g., Lewis, 1994; McCave and Carter, 1997; Massé et al., 1998; Weaver et al., 2000; Rasmussen et al., 2003).

It is interesting to note that in cores JPC-31, JPC-26, and JPC-37, located on the middle to lower continental slope, the Last Glacial Episode deposits display characteristics of both provinces. This infers that there is no abrupt boundary between the two provinces, but the transition from the one province to the other is through a transitional mixing zone.

Sedimentological History of the Last Glacial Episode

The most extreme hydrological change that occurred during the Last Glacial Episode was the eastward switch of the major Mississippi River discharges from Bryant and Eastern Canyon to Mississippi Canyon (Coleman et al., 1983; Bouma et al., 1985a, 1985b; Lee et al., 1996). This definitely led to the reduction of sediment supply in Bryant Canyon area, but not to the total cease of turbidity current generation. This is supported by Suter et al. (1987), which recorded Last Glacial Episode deltaic formations on the mid shelf and shelf margin updip of Bryant Canyon. This indicates that, even though significantly reduced, the sediment supply in Bryant Canyon area continued to be directly related to river discharges.

Sedimentological unit D was deposited during Oxygen Isotope Stages 3 and 4 (31.85–71 ky B.P.). During this period, even though the sea-level stand dropped to 20-70 m below the present sea-level stand, it never reached the shelf edge (Suter et al., 1987; Camoin et al., 2001; Lea et al., 2002.). This led to the trapping of the majority of the river-sourced sediments on the continental shelf, with the seaward propagation of their finest fractions (clay and fine silt) to occur mainly as nepheloid layers, contributing to the pinkish hue of the hemipelagic sediments of unit D. However, the presence of the widely spaced and isolated silty-clay facies in unit D infers the development of several turbidity currents during this period. These turbidity currents were probably related to: 1) slope instabilities on the shelf margin/upper continental slope due to halokinetic processes, 2) sediment resuspension during strong storms, and 3) periods of exceptionally large river discharges.

It is interesting that chronostratigraphic horizons III and IV, characterized by closely-spaced and siltier silty-clay facies, coincide in the $\delta^{18}\text{O}$ profiles with two intervals of high $\delta^{18}\text{O}$ values centered at 36 and 52 ky B.P (Fig. II-3). These intervals are interpreted to represent periods of very high river discharges, related to short deglaciation events (melt-water pulses), that resulted in the production of frequent turbidity currents. The generation of turbidity currents could have been resulted from: 1) hyperpycnal river plumes, 2) the rapid deposition of unconsolidated sediments on the outer continental shelf that resulted in the development of massive sediment failures, and 3) the formation of seaward moving fluid mud by the action of waves and currents that, when they reach the shelf margin, begin to cascade and evolve into turbidity currents (Bornhold et al., 1994; Mulder et al., 1998a, 1998b; Piper et al., 1999; Klaucke et al., 2000; Wright et al., 2001; Puig et al., 2003). The development of horizons III and IV in the sediment

records of both provinces indicates that the high river discharges were not centered just above Bryant Canyon area, but it was a widespread phenomenon.

In a similar manner, subunit Cc (28.57 – 31.85 ky B.P.), characterized by very well-preserved and closely-spaced, normally-graded silty-clay facies, is interpreted to represent another deglaciation event (melt-water pulse). However, the very high $\delta^{18}\text{O}$ values infer that the magnitude of this melt-water pulse was much larger than the previous two (horizons III and IV). A similar, large melt-water event, centered at 31 ky B.P., has also been documented on the $\delta^{18}\text{O}$ records of Lea et al. (2002) from sediment cores from Cocos Ridge. The siltier and thicker nature of the abundant silty-clay facies of subunit Cc, compared to the silty-clay facies of horizons III and IV, indicates that they have resulted from larger and more frequent turbidity currents. A periodicity ranging from a few decades to 200 years is estimated for the occurrence of the turbidity currents. The calculation of the turbidity currents periodicity was based on the thickness of the hemipelagic sediments (mm to 2 cm), separating the silty-clay facies, and by assuming a sedimentation rate of 10 cm/ky for the deposition of the hemipelagic sediments.

Chronostratigraphic horizon II is developed at the top of subunit Cc, and it consists of successive, laminated and/or normally-graded silty-clay facies. The very silty, interlaminated (in many cases), and thick nature of the silty-clay facies of horizon II clearly reveals that their deposition resulted from the development of exceptionally large turbidity currents. This, combined with the development of horizon II at the end of the melt-water event, infers a different origin for the above turbidity currents, which have probably resulted from the development of a series of enormous and massive sediment failures on the shelf margin and/or upper continental slope. The development of such failures is probably due to: 1) the rapid deposition of undrained sediments on the outer shelf and/or upper continental slope, through the exceptionally large river discharges (hypopycnal and hyperpycnal river plumes), and 2) mobilization of the underlying salt masses due to their sudden and large sediment loading (Prior et al., 1984; Bornhold et al., 1994; Klauke et al., 2000; Tripsanas et al., 2003a). The later interpretation is favored because the expected time lag of the mobilization of the underlying salt masses fits the development of horizon II at the end of this enormous melt-water event.

On the upper continental slope, horizon II is represented by two series of successive, dark greenish gray, top-cut-out (T3/4-6/7 sequences) laminated silty-clay facies, and a single, basal, reddish brown laminated silty-clay facies. Bioturbation structures and hemipelagic sediments

are restricted only at the top of the upper facies of the greenish gray facies series, and at the top of the lower reddish brown silty-clay facies (Fig. II-13). On the middle and lower continental slope, the series are expressed as single, laminated to normally-graded, silty-clay facies (Fig. II-13). This information infers that the deposition of horizon II occurred by three discrete and large low-density turbidity-currents, of which the last two were characterized by a strong pulsating nature (showing internal surges). The loss of the pulsating identity of the low-density turbidity currents on the middle and lower continental slope is probably due to: 1) the catching up of the earlier surges by the later surges, 2) the loss of the identity of the surges by their multiple hydraulic jumps and partial deposition in the successive intraslope basins, and 3) the downslope fining trend of the pulsating, low-density turbidity currents. The successive surges of a very fine-grained (clay and fine silt), pulsating, low-density turbidity current will result in the deposition of successive ungraded mud layers (E2 division of Piper, 1978) that will be unidentifiable from each other. The pulsating nature of the low-density turbidity currents is probably due to: 1) the nature of the large turbidity currents, from which the low density flows have been resulted (e.g. retrogressive failures cause the generation of pulsating turbidity currents of long duration), 2) the development of internal waves on the top of the original turbidity currents, leading to pulsating spill-over flows, 3) reflections of the original turbidity currents on the basin walls, resulting in a pulsating spill-over mechanism, and 4) a combination of the above mechanisms.

Subunit Cc is not observed in the cores of the lower province. However, this does not mean that it is absent, but probably that it is indistinguishable from subunit Cb. This is probably due to the fact that the silty-clay facies, on the lower province, do not represent deposits directly related to turbidity currents, but deposits of low-density, turbiditic sediment clouds that have been entrained into westward flowing bottom currents. Consequently, the character of the silty-clay facies on the lower province does not depend only on the magnitude and nature of the turbidity currents but also on the magnitude and nature of the bottom currents.

Subunits Cb (21.26 – 28.57 ky B.P.), and Ca (18.17 – 21.26 ky B.P.) are both representing deposits of the Last Glacial Maximum (Stage 2). However, even though both units have evolved under the same sea-level stand (about – 120 m), their sedimentological character is different. Subunit Cb is characterized by many series of fining upwards, silty-clay facies, that on the upper continental slope are expressed as well-preserved, normally-graded, silty-clay facies, which degrade rapidly into indistinct, mottled silty-clay facies in the downslope

direction. This information reveals that, due to the almost direct river discharges on the upper continental slope, abundant turbidity currents were generated during this period (21.26 – 28.57 ky B.P.). However, due to the more arid climatic conditions of the last Glacial Maximum, the produced turbidity currents were of lower magnitude, as it is indicated by their faster downdip dissipation. The organization of the silty-clay facies into fining upwards sequences reveals the existence of several short, more humid periods (small melt-water pulses), alternated with colder and drier periods (glacier formation). According to cores JPC-47 and JPC-46, located on the upper continental slope, at least 11 warm-cold climatic cycles developed during the period 21.26 – 28.56 ky B.P. The periodicity of the produced turbidity currents ranges from a few decades to 500 ky, or even up to 1000 ky in a few cases.

Subunit Ca (18.17 – 21.26 ky B.P.) consists of ghost-layered hemipelagic sediment interbedded by two series of normally graded silty-clay facies on its upper and lower part. The domination of hemipelagic sediment, in subunit Ca, infers a possible transition into more arid and cold climatic conditions, which may be related to the Heinrich Event H2 (Piper and Skene, 1998; Boessenkool et al., 2001; Pérez-Folgado et al., 2002). The higher $\delta^{18}\text{O}$ values of this interval (Fig. II-3) do not contradict the above theory, but they are probably due to the partial melting of the glaciers and iceberg formation on the North Atlantic (Zaragosi et al., 2001; Rashid et al., 2003). The upper facies sequence consists of three distinct, reddish brown, normally-graded silty-clay facies, it was deposited around 19 ky B.P., and it occurs only on the upper sedimentological province. This indicates that the reddish brown silty-clay facies did not originate from a period of high river discharges, but most probably from a series of sediment failures on the shelf edge and/or upper continental slope.

The lower facies series consists of three dark olive green to greenish gray, silt-clay facies dated at 19.9 – 21.26 ky B.P. The very clayey and organic-rich (1.7-2 % Corg) nature of their upper parts, combined with their occurrence in both provinces, infers that these facies are possibly related to high river discharges (hyperpycnal river plumes) that may be connected to a short melt water event, preceding the following arid period. The very different nature of the greenish facies in the upper and lower province is probably due to the geological differences of their sediment sources. For example on the upper province, only the lower silty-clay facies may respond to high river discharges, whereas the upper two facies could have actually originate from the development of sediment failures involving the slumping of organic-rich sediments on the shelf margin. However, despite the differences of the greenish facies on the lower and

upper province, the similar oxygen profiles of cores JPC-46 and JPC-31, combined with the development of this facies sequence just above subunit Cb, indicates that the greenish gray facies series are concomitant in both provinces.

Sedimentological Unit B

Characteristics

Sedimentological unit C is divided into two intervals. The lower interval (10 - 28 cm thick) consists of light greenish gray to very pale yellow, heavily bioturbated muddy foraminifera ooze. The upper interval is represented by distinct organic-rich clayey sediments, which will be referred as chronostratigraphic horizon I in the rest of the text. On the density profiles horizon I is recognized as an interval of very low density values (Fig. II-3 and II-17).

Horizon I reveals different sedimentary characteristics on the upper to middle continental slope (JPC-47 to JPC-37), and lower continental slope (JPC-33 and JPC-34) (Fig. II-2). On the upper to middle continental slope, horizon I (34 – 48 cm thick) consists of four discrete zones, which are characterized by gradational boundaries (Fig. II-16a). Starting from the lower zone, they are:

Zone 1 (2–6 cm thick): Dark olive green, bioturbated, lenticular, organic-rich clay (Corg: 1.316 – 2.133 %). This zone is best preserved on the middle continental slope, whereas on the upper continental slope is very subtle.

Zone 2 (up to 4 cm thick): Greenish to light greenish gray, bioturbated clay with abundant forams. Zone 2 is very subtle, and not easily distinguished in some of the cores.

Zone 3 (12–25 cm thick): Olive green to greenish gray, medium to minor bioturbated, organic-rich clay (Corg: 1.195 – 2.083 %), with common to rare forams.

Zone 4 (10–14 cm thick): Pink to pale yellow clay with abundant to common forams that is characterized by a very dense network of thin, interconnected bioturbation structures (sponge-like).

Zones 3 and 4 are truncated to totally removed in cores JPC-47, JPC-45, and JPC-09, whereas in cores JPC-10, and JPC-45 a thin debris flow deposit is developed just above horizon I. In core JPC-46, horizon I has been totally removed by the development/passage of a slump.

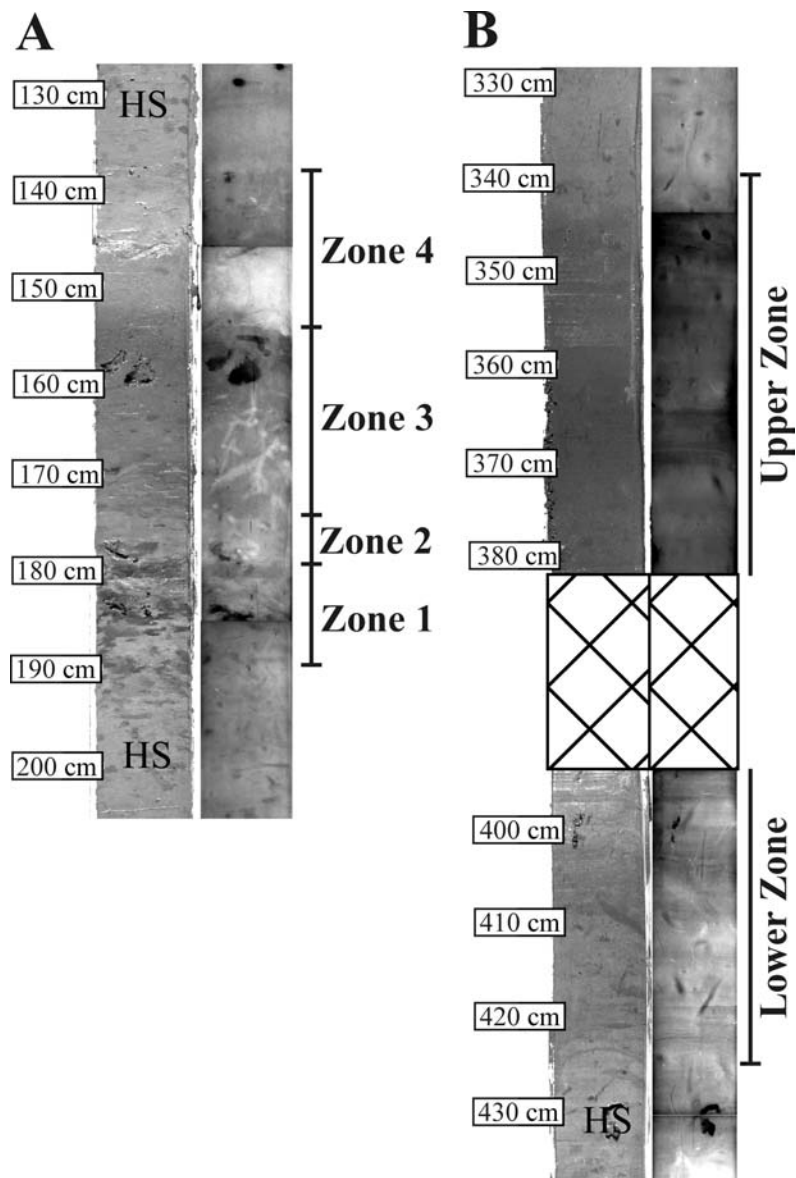


Fig. II-16. Typical photographs (left) and X-ray radiographs (right) (negatives) of chronostratigraphic horizon I from the upper to middle continental slope (A) (JPC-26), and lower continental slope (B) (JPC-33) of the northwest Gulf of Mexico. The gap in image B is due to sampling for consolidation tests. Note the fading upwards burrows in zone 3 (A), which indicates that zone 3 did not result from a violent bottom-riding sediment cloud, but from gradual suspension deposition (hemipelagic sedimentation). The upward elimination of bioturbation structures in zone 3 is probably due to the development of partially anoxic conditions. On the lower continental slope (B), horizon I consists of two ghost-layered, organic-rich zones, with the upper zone to be more clayey and organic-rich than the lower zone. This indicates, similarly to the upper and middle continental slope of the northwest Gulf of Mexico, the gradual development of partially anoxic conditions (a few bioturbation structures are still present) on the lower continental slope. However, the much greater thickness of horizon I and the ghost-layered nature of the upper and lower zones indicate that, similarly to subunits Ca, Cb, and Cc, horizon I was deposited from bottom-riding, clayey, sediment clouds driven by bottom currents.

On the middle and lower parts of the lower continental slope (JPC-33 and JPC-34), horizon I consists of only two zones (Fig. II-16b). The lower zone is represented by greenish gray, medium bioturbated clay with common forams, and it is interbedded by indistinct, slightly siltier (silty-clay to clay), pinkish layers/laminae. The pinkish layers, in some cases, resemble thin clayey silty-clay facies. This zone is succeeded upwards by a zone of dark greenish gray to greenish gray, minor bioturbated clay, with rare forams, characterized by a faint ghost layering. The top of this upper zone is characterized by a distinct reddish brown to pink hue.

Interpretation

Radiocarbon dating, combined with $\delta^{18}\text{O}$ profiles, indicate that sedimentological unit B represents deposits of the last deglaciation event (11.16–18.17 ky. B.P.). The sedimentation rates of this unit range from 6.28 to 14.84 cm/ky, and they are largest on the lower continental slope (Fig. II-4 and Table II-1). The first two thousand years of the deglaciation event (16.10 – 18.17 ky B.P.) are represented by the deposition of typical hemipelagic sediments. This probably indicates the existence of an initial arid period. The high $\delta^{18}\text{O}$ values occurring in chronostratigraphic horizon I clearly infer that these organic-rich sediments correspond to a large melt-water event, developed between 11.16 and 16.10 ky B.P.

The organic-rich sediments of horizon I are interpreted to have resulted from the development of partially anoxic conditions in the bottom waters of the northwest Gulf of Mexico (the existence of burrows in the organic-rich sediments indicates the survival of the most tolerant benthic organisms). There are two possible mechanisms for the development of anoxic conditions. The first is by the production of a low-salinity surficial layer in the water column produced by the highly increased river discharges. The existence of such a low-salinity layer would have led to the significant reduction of the re-oxygenation of the bottom waters, leading to the development of partially anoxic conditions. The second mechanism for the production of anoxic conditions is by the introduction of large amounts of organic matter in the deep-ocean environment. The large amounts of organic matter introduced in the deep-ocean environments could be of (a) terrigenous origin, directly related to high river discharges, and/or (b) marine origin, though the significant increase of primary productivity caused by the development of eutrophic conditions by the introduction of ample nutrients in the euphotic zone during high river discharges. The abundant organic matter will deposit on the ocean floor and, through its decomposition, will utilize most, if not all, of the dissolved oxygen of the

bottom waters, producing anoxic conditions. A combination of the above two mechanisms for the production of anoxic conditions, in the bottom water of the northwest Gulf of Mexico, is quite possible.

It is apparent, from the sedimentological descriptions of horizon I that the two sedimentological provinces of the Last Glacial Episode continued to exist even during the last deglaciation event. On the upper province, the gradational boundaries and bioturbated nature of the four zones, consisting horizon I, infers that they have resulted from hemipelagic sedimentation and/or deposition from intermediate or surficial nepheloid layers. Organic-rich sediments, similar to those of horizon I from the upper province, have been documented on the Eastern Mediterranean Sea. They are named as sapropels, and they are interpreted to result from the cessation of the bottom water re-oxygenation, due to the density stratification of the water column produced by the highly increased river discharges during melt-water pulses and/or very humid periods (Anastasakis and Stanley, 1984; Rohling, 1994).

Zone 1 sediments, of the upper province, are estimated to have been deposited between 15.18 and 16.10 ky B.P., and they probably correspond to a precursor melt-water event. The transition to typical hemipelagic sediments in zone 2 indicates the development of a short, arid period (reduced river discharges) between 14.61 and 15.18 ky B.P. During this period a partial re-oxygenation of the bottom waters occurred. Zones 3 and 4 have been deposited between 11.16 and 14.61 ky B.P., and they are probably linked to the major melt water pulse IA (mwp-IA) (Fairbanks, 1989; Kolla and Perlmutter, 1993). The pinkish shade and intense bioturbation of the sediments of zone 4 are interpreted to represent an oxidation zone, occurred right after the end of the melt water pulse, by the re-oxygenation of the bottom waters. The above interpretation of our data is supported by Geraga et al. (2000), Boessenkool et al. (2001), and Zaragosi et al. (2001) which reported the development of a precursor high sea surface temperature (SST) period, followed by a low SST period, right before the development of mwp-IA. They interpreted the low SST period to correspond to Heinrich event H1.

All of the above dates were based on the assumption that the sedimentation rates had been constant through out the entire deglaciation event. However, somebody would expect the sedimentation rates to have been higher during the deposition of horizon I, due to the higher sediment supply by the increased river discharges. This infers that the above dates may actually be older than the real ages of the horizon I zones.

On the lower sedimentary province (lower continental slope), the intense ghost layering of horizon I infers that the organic-rich sediments, in this region, have probably resulted from the gradational deposition of bottom-riding, low-density and fine-grained sediment clouds driven by westward flowing bottom-currents. The obscuring of the four discrete episodes, occurred during the deposition of the lower province horizon I, is probably due to the action of these bottom-riding flows. However, the two zones of the lower province horizon I indicate a precursor melt-water pulse (lower zone), followed by the major mwp-IA (dark greenish gray, upper zone).

Sedimentological Unit A

Characteristics

Sedimentological unit A consists of light greenish gray to pale yellow, heavily bioturbated muddy foraminifera ooze. A well-developed brown to reddish yellow oxidation zone (up to 30 cm thick) is usually occurred at the top of unit A. In cores JPC-47, JPC-46, JPC-45, JPC-10, and JPC-09, the oxidation zone is very thin (a few cm thick) and poorly developed. This is probably due to the disturbance of the Holocene sediments by the coring procedure (possible washout and compression of the upper sediments). In core JPC-46, three normally-graded silty-clay facies occur in the intervals 9 – 24 cm. Bellow 24 cm the hemipelagic sediments reveal a faint ghost layering and mottled character, ending at a highly remolded zone at 94-111 cm. The remolded basal zone probably indicates that the whole interval 24 – 111 cm represents a thin slide, in which the remolding of its sediments occurred only adjacent to its base.

Interpretation

The sea-level stand at 11 ky B.P. was placed at –50 to –60 m, and approached the present sea-level stand around 3 to 5 ky B.P. (Fairbanks, 1989). The domination of hemipelagic sediments in unit A indicates that the majority of the river-sourced sediments was trapped on the continental shelf of the northwest Gulf of Mexico. However, Fairbanks (1989) reported that at 9.5 ky B.P. another melt-water pulse occurred (mwp-IB). The absence of any indication of the mwp-IB, in the sedimentary records of our cores, is interpreted by the switch of the North America melt-water discharges from the Mississippi River to St. Lawrence Seaway around 11 – 12 ky B.P., which led to the significant reduction of the Mississippi River discharges.

The sedimentation rates of unit A range from 5.38 to 30.29 cm/ky (Table 1). The occurrence of the highest sedimentation rates on the lower continental slope infers that this area is supplied by extra sediments from westward flowing bottom currents.

In cores JPC-47, JPC-46, JPC-45, JPC-10, and JPC-09, the very small thickness of unit A (6–42 cm), in combination with the truncated top of horizon I, infers that a large to small part of unit A has slumped away. The triggering mechanism for these failures is probably the sediment loading of the low shear-strength, organic-rich sediments of horizon I. According to the sedimentation rates of unit A, from the undisturbed cores JPC-28 and JPC-23, the above sediment failures are dated around 1.1–8.1 ky B.P. The silty-clay facies in core JPC-46 are interpreted as low-density sediment flows originating from adjacent sediment failures.

Bulk Density Profiles and Seismic Characterization

Up to this point, the majority of our observations was based on the sedimentological study of 12 cores from the continental slope of the northwest Gulf of Mexico. However, it is obvious from Figure II-15 that all cores and the seismic information were used in order to define the continuity and spatial distribution of the sedimentological units. This was accomplished by the characteristic bulk density profiles of each sedimentary unit, and their seismic characterization in the 3.5 kHz subbottom profiles.

Unit A is characterized by low density values ($\sim 1.3 - 1.45 \text{ g/cm}^3$), and reveals a distinct downward increase in bulk density (Figs. II-3 and II-17). Unit B is represented by the sudden drop of its bulk density to $1.3 - 1.4 \text{ g/cm}^3$ (horizon I), and a consequent gradual increase up to 1.4 and 1.48 g/cm^3 . Subunit Ca is very distinct in the density profiles by its almost vertical density profile, and the very high (up to 1.8 g/cm^3) density values at its top, corresponding to the upper brown silty-clay facies series. The bulk density values of subunit Ca depend greatly on the location of the core, and they range in general from 1.4 to 1.55 g/cm^3 . Sedimentological units Cb and Cc are impossible to be distinguished from each other on the bulk density profiles, and they are represented as one interval with downward increased bulk density. Similarly to subunit Ca, density values of subunits Cb and Cc vary between cores, depending on their proximity to the sediment source of each province, and they range in general from 1.45 to 1.8 g/cm^3 .

Unit D is expressed by almost vertical lineated density profiles, characterized by two pinnacles (up to 1.75 g/cm^3) corresponding to horizons III and IV. In the sediment cores of the

upper continental slope a third density apex is also observed at the base of unit D. The upper boundary of unit D is represented by a sudden drop of the density values, as they transit from the silty-clay facies of subunit Cc to the hemipelagic sediments of unit D. Bulk densities of Unit D range from 1.5 to 1.7 g/cm³, depending on the location of the cores. The bulk density profile of unit E is represented by approximately constant values (~ 1.55 g/cm³), and characterized by a minimum (up to 1.38 g/cm³) occurring at the Y-8 ash layer. Finally, unit F is highly variable, depending on the location of the core. On the overflowing areas, density values range between 1.6 and 1.75 g/cm³, whereas, on the canyon pathways, they are expressed by a great variability, and density values exceeding 1.9 g/cm³. Sediment failure deposits are recognized in the core density profiles by the chaotic distribution of their bulk densities.

On the 3.5 kHz subbottom profiles, three discrete seismic zones are identified (Fig. II-17). Starting from the upper one they are:

Zone 1: It is characterized by two, strong, prolonged, and parallel reflectors occurring at its boundaries, and by a few weak, semi-prolong reflectors to develop in its interior. The strong reflectors at the boundaries of this zone represent the ocean floor, and the coarse silty-clay facies of subunit Cc. On the downslope direction (middle to lower continental slope), it is observed that the internal and basal reflectors become weaker, due to the downdip fining of the silty-clay facies. This zone corresponds to units A, B, and C.

Zone 2: This zone represents sedimentological units D and E. It is characterized by a set of strong to weak, relatively sharp reflectors that correspond to the density changes occurring in horizons III and IV, Y-8 ash layer, and the contacts of units E and D, and E and F. In the cases, that the transition from unit E to unit F is gradational, then only a very weak and indistinct reflector is observed at the base of this zone.

Zone 3: This zone represents sedimentological unit F, and its character depends on the location of the seismic line relatively to the pathways of the canyons. In the intracanyon areas (unit Fa), zone 3 is characterized by the development of a strong prolonged reflector at its top, and the absence of any further subbottom reflections (Fig. II-17b). This is due to the sandy nature of the intracanyon deposits. On the spillover areas, zone 3 (unit Fb) is represented by a semi-transparent seismic character with abundant weak to indistinct, discontinuous, parallel subbottom reflections. This is due to the incompetence of the sound waves to see the thin mud turbidites deposited in this area, recording only large-scale density differences related to thick sequences of fine-grained turbidites.

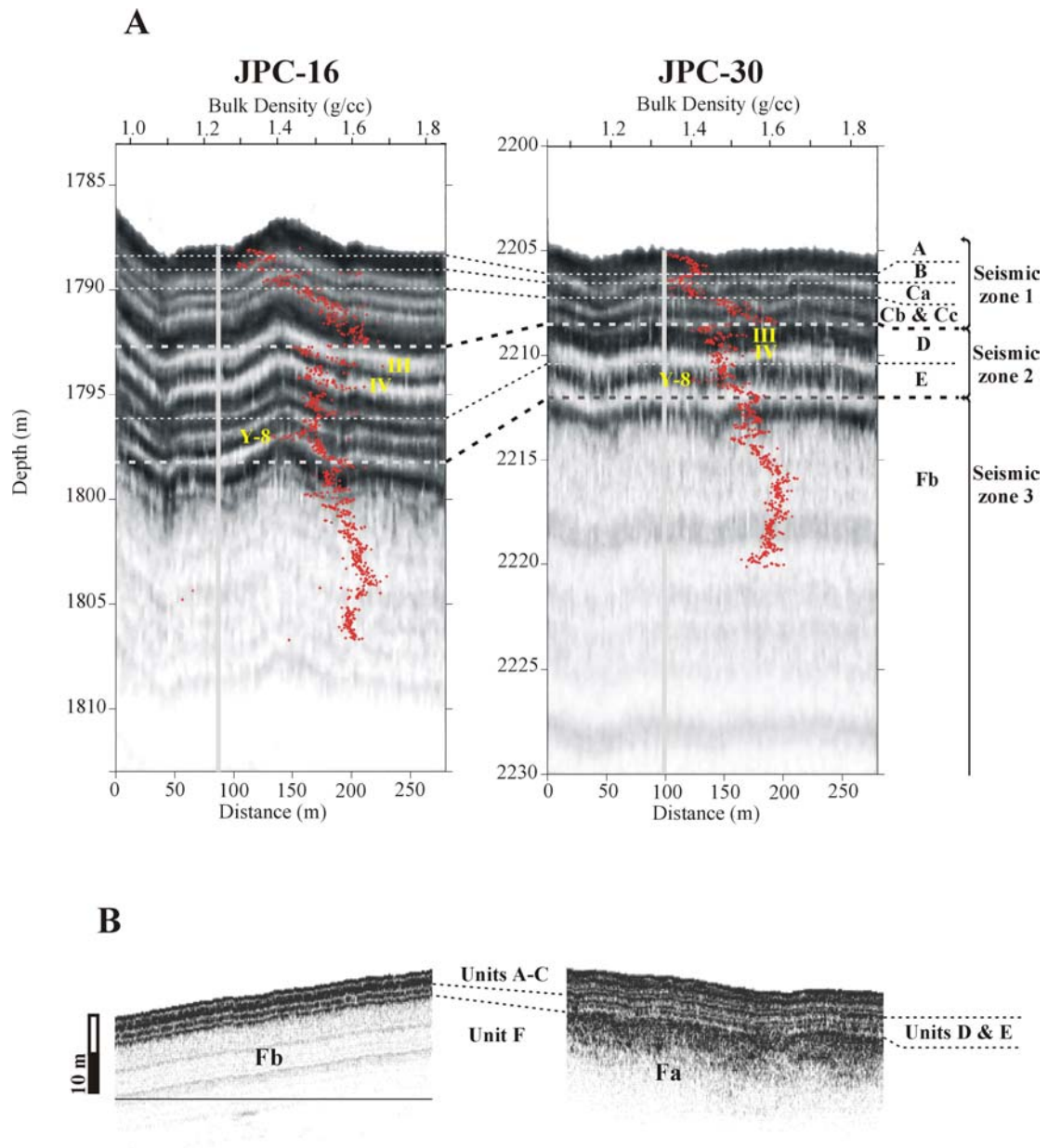


Fig. II-17. Image displaying the seismic (3.5 kHz subbottom profiles) and bulk density characterization of the six sedimentological units.

Conclusions

It is revealed, through this study, that the sedimentological history of Bryant Canyon area is very complex, and for each time period was mainly dependant on: 1) the sea-level stand, 2) the climatic conditions and magnitude of the river discharges, 3) location of the main river discharges, and 4) the morphology of Bryant Canyon area.

Bryant and Eastern Canyon systems were active during the low sea-level stand of Oxygen Isotope Stage 6, acting as conduits, through which gravity flows distributed enormous amounts of sediment on the continental slope and abyssal plain of the northwest Gulf of Mexico. The sediment source for these two canyons was likely from the discharges of an ancestral Mississippi River. The existence of such erosional/depositional environments certainly disturbed the stability of the underlying salt masses, which, through differential loading, tended to obliterate and restore the seafloor morphology on the erosional parts of the canyons, and to retreat and collapse on the canyons depocenters. However, coupled erosional-depositional processes of the gravity flows were able to balance the salt movements during the active low-level stand of the canyon systems.

During the high sea-level stand of Oxygen Isotope Stage 5, the majority of river-sourced sediments were trapped on the widespread continental shelf of the northwest Gulf of Mexico. That led to the cessation of the generation of turbidity currents on the shelf margin and/or upper continental slope, causing the abandonment of Bryant and Eastern Canyons. It was during the first 30 ky of Stage 5 that both canyons transformed by halokinetic processes into a series of basins and sills along their axis.

The low sea-level stand of the Last Glacial Episode (Stages 2, 3, and 4) was characterized by the eastward switch of the major discharges of the Mississippi River. However, river discharges, even though significantly reduced, were still occurring on the continental shelf updip of the Bryant Canyon area. Two sedimentological provinces coexisted on Bryant Canyon area during this time interval. The first was extended from the upper continental slope to the upper part of the lower continental slope, and it was supplied with sediments from the continental shelf, through low-density (mud) turbidity currents. The low-density turbidity currents originated from the depositional segregation of large turbidity currents generated on the shelf margin and/or upper slope, by the deposition of their coarsest material in the intraslope basins of the upper continental slope. The second province was located on the

middle and lower part of the lower continental slope, and was supplied with sediments by low-density, fine-grained, bottom-riding sediment clouds driven by westward flowing bottom currents. The sediment clouds originated from the pirating of Mississippi Canyon and Fan turbidity currents by bottom currents.

Five discrete sedimentological time periods occurred during the Last Glacial Episode:

1. The first period occurred during Oxygen Isotope Stages 4 and 3 (71-31.85 ky. B.P.). The sea-level stand of this period was ranging between -70 m (during Stage 4) and -20 to -40 m (during Stage 3), and consequently, it never reached the shelf edge (-120 m). This led to the confinement of the majority of the river-sourced sediments on the continental shelf, whereas the seaward sediment transportation was succeeded by the generation of infrequent turbidity currents related to either sediment failures, or exceptionally large river discharges (flooding episodes). Two melt water events, centered at 36 and 52 ky B.P., occurred during this first period, and they were characterized by the frequent initiation of turbidity currents.
2. The second period was developed at the end of Oxygen Isotope Stage 3 (-20 to 40 m) (31.85-28.57 ky B.P.). It represents a major melt-water pulse, which moved large amounts of sediments on the outer continental shelf and upper continental slope, resulting in the initiation of numerous sediment failures and gravity flows.
3. The third period occurred from 28.57 to 21.26 ky B.P. (Stage 2) (-120 m). During this period, the sea level dropped to the shelf edge, which led to the development of shelf margin deltas, which contributed to the development of numerous sediment failures and turbidity currents.
4. The fourth period represents the latest part of the Last Glacial Maximum (21.26-18.17 ky B.P.) (-120 m), and it is characterized by hemipelagic sedimentation (except for two series of turbidity currents occurring at 19 ky, and 19.9–21.6 ky B.P.) on the continental slope, indicating the development of colder and arid climatic conditions. This arid period is probably related to the Heinrich Event H2.
5. The fifth and last period represents the last deglaciation event (18.17-11.16 ky B.P.). It is characterized by the occurrence of a melt water pulse occurred at 16.10-11.16 ky B.P., which was interrupted at 15.18-14.61 ky B.P. by an arid period that probably corresponds to the Heinrich Event H1. During this melt-water pulse, the bottom waters of the northwest Gulf of Mexico became partially anoxic due to: 1) the development of a low salinity

surficial layer on the water column, and 2) the vast amounts of organic matter introduced in the ocean environment through the highly increased river discharges of this time interval, and 3) the highly increased primary production caused by the introduction of ample nutrients in the euphotic zone through the highly increased river discharges of this time interval.

At about 11-12 ky B.P. (-50 to -60 m), the North America melt-water discharges switched from the Mississippi River to St. Lawrence Seaway, leading to the significant reduction of the Mississippi River discharges. This led to the restriction of the river-sourced sediments on the continental shelf, and the domination of hemipelagic sedimentation of the continental slope, which continues to dominate up to the present time.

CHAPTER III

OXYGEN ISOTOPE STAGE 6 TURBIDITY CURRENT DEPOSITS

Introduction

Canyons are the most pervasive erosional structures on the continental slopes, through which turbidity currents are able to transfer enormous amounts of terrigenous sediments to the abyssal plains of the world's oceans (Damuth, 1977; Pratson et al., 1994; Bouma, 2000, 2001). The character and flow behavior of turbidity currents are of great importance, since they are one of the major factors contributing to the canyon and deepsea fan geometry, and through overflow processes to the sedimentology of the canyon and channel overbank areas (Stanley, 1983; Piper and Savoye, 1993; Hagen et al., 1994, 1996; Stow et al., 1996; Normark et al., 1998).

Overflowing of turbidity currents has been studied and reported from the interchannel areas of deepsea fans. Channel levees, overbank deposits, and mud waves represent typical formations of spillover flows (Piper and Normark, 1983; Savoye et al., 1993; Lewis, 1994; McHugh and Ryan, 2000; Migeon et al., 2001). Sediment cores of these areas consist mainly of low-density, fine-grained turbidites (Piper, 1978; Stow and Bowen, 1980; Stow and Piper, 1984; Stow et al., 1984).

This paper presents the results of a detailed sedimentological study of sediment cores (up to 20 m long), and high-resolution acoustic information from the Bryant and Eastern Canyon systems. The main purpose is to provide better insight into the flow characteristics and depositional processes of the channelized and spilled-over turbidity currents, and finding the connective link between the deposits of these two flow types.

Geological Setting

Bryant and Eastern Canyons are located on the hummocky continental slope of the northwest Gulf of Mexico (Fig. III-1). Severe halokinetic processes have contributed to the transformation of the initial morphology of the canyons into several basins and sills along their axis. Bryant Canyon extends itself all along the continental slope and terminates downslope at the Sigsbee Escarpment, where it grades into a fan valley/channel levee complex (Bryant et al.,

1990; Lee, 1990; Lee et al., 1996). Eastern Canyon is limited on the upper and upper/middle continental slope (Twichell et al., 2000).

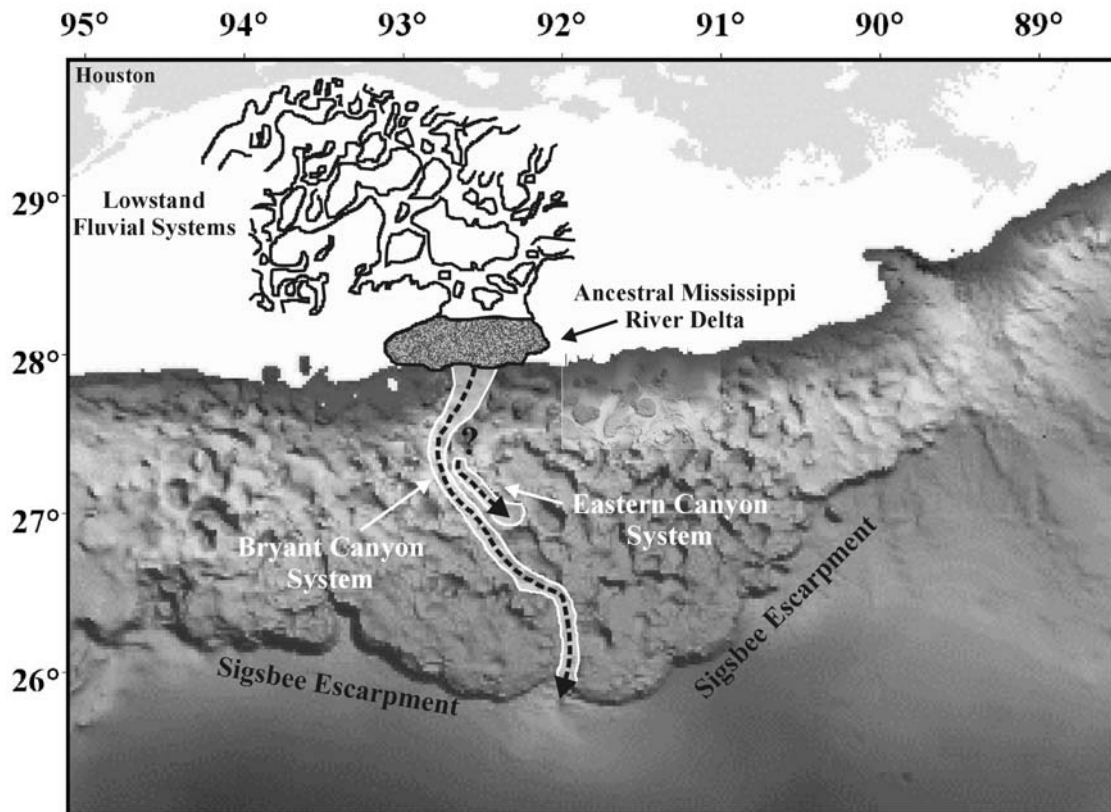


Fig. III-1. Morphological map of the northwest Gulf of Mexico displaying the locations of Oxygen Isotope Stage 6 Bryant and Eastern canyon systems (adopted from Lee et al., 1996; from Twichell et al., 2000), along with an ancient lowstand fluvial system on the shelf and an ancestral Mississippi River delta (adopted from Sutter and Berryhill, 1985). Even-though the fluvial system and its delta are dated as late Wisconsinian (Stage 4), the dependence of this assumption on deep-seismic information constitutes possible an underestimation of their age, which can be of Oxygen Isotope Stage 6. Such is more in accordance with the age of the well-developed Bryant Canyon Fan.

Lee et al. (1996), and Twichell et al. (2000) have discussed extensively the formation and destruction of Bryant and Eastern canyon systems. Their formation initiated at the beginning of the glacial Oxygen Isotope Stage 6, by the development of an ancestral Mississippi River Delta at the shelf edge and/or upper continental slope. That led to the generation of numerous gravity flows, either by sediment failures of the delta front, or directly from hyperpycnal river plumes

(Hampton, 1972; Sutter and Berryhill, 1985; Bornhold et al., 1994; Mulder and Syvitski, 1995) (Chapter II). In a first stage the gravity flows propagated downslope, developing a small erosional canyon on the upper continental slope, and were eventually confined in the most adjacent stage 6 prevalent intraslope basins, which led to the formation of ponded intraslope-intrabasinal fan systems (channel-levee complexes and sheet sands). As soon as an intraslope basin was sufficiently infilled, the gravity flows were propagating to the next downslope intraslope basin, cutting through the structural saddles (sills/plateaus) between them, and leading to the development of a new ponded fan system. Repetitions of this infilling-bypassing process led to the formation of the peculiar Bryant and Eastern Canyon systems, which in the infilled intraslope basins had the form of well-developed channel-levee systems, and on the sills/plateaus separating the basins, had the form of typical V-shaped erosional canyons (Lee, 1990; Satterfield and Behrens, 1990; Twichell et al., 2000). The well-developed deepsea fan system at the mouth of Bryant Canyon indicates that, at some point during Oxygen Isotope Stage 6, Bryant Canyon evolved into an unconfined river-sourced canyon system, acting as a conduit for Mississippi River sediments into the Sigsbee Abyssal Plain of the Gulf of Mexico (Chapter II).

The existence of such erosional/depositional environments certainly disturbed the sensitive balance of the underlying salt masses, which, through differential sediment loading, tended to obliterate and transform the canyon morphology (uplifting on the erosional parts of the canyons, and collapsing underneath the infilled intraslope basins) (Lee, 1990; Lee et al., 1996; Twichell et al., 2000). However, coupled erosional-depositional processes of the gravity flows were balancing the salt movements during the Oxygen Isotope Stage 6. The destruction of Bryant and Eastern Canyons occurred after their abandonment, during the beginning of the interglacial Oxygen Isotope Stage 5, due to the confinement of most of the alluvial sediments on the wide continental shelf of the northwest Gulf of Mexico (Chapter II).

Data and Methods

High-resolution acoustic subbottom information from the Bryant Canyon area was collected during the R/V *Gyre* 1998 cruise, using the Texas A&M Deep-tow system equipped with a 3.5 kHz subbottom profiler, and a 100 kHz side-scan sonar towed thirty meters above the seafloor (Fig. III-2). Forty-eight Jumbo Piston Cores (up to 20 m long) (JPC) were acquired from the

most interesting areas, using the WHOI Jumbo Piston Corer during a cruise in 1998 of the R/V *Knorr*.

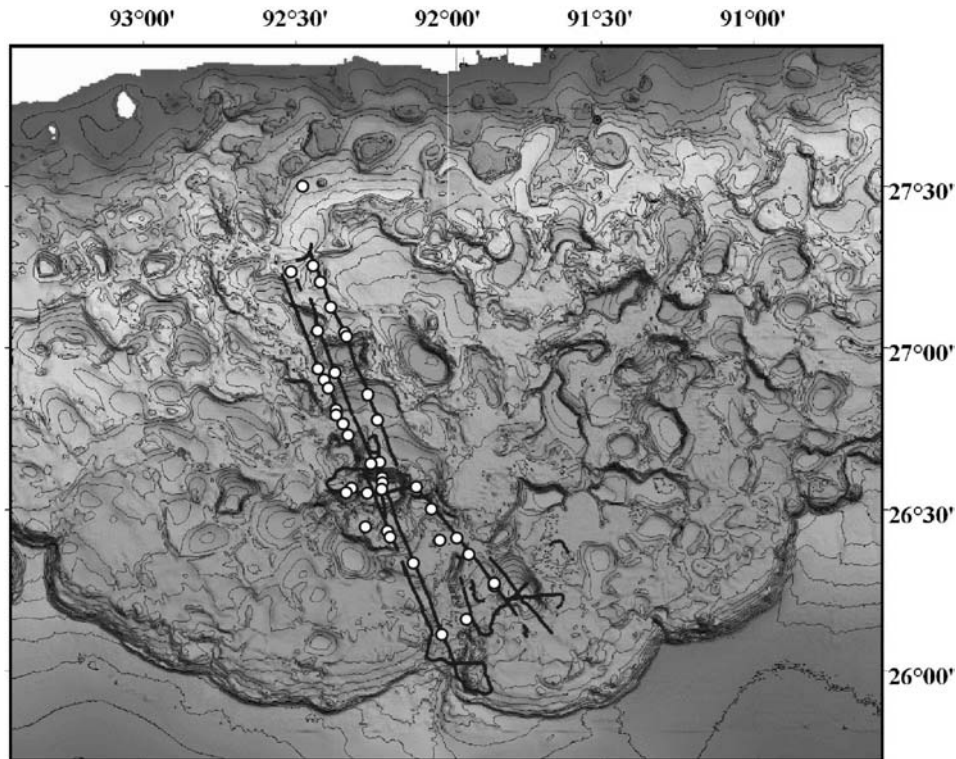


Fig. III-2. Morphological map of Bryant Canyon area displaying the locations of the Jumbo Piston Cores (JPC), and the tracks of the high-resolution geophysical information.

Bulk density and P-wave velocity profiles were derived from all cores with a GEOTEK Multi-Sensor Core Logger. Eighteen sediment cores were split lengthwise: one half was archived, and the other half was described at the millimeter-level scale, and photographed on high-resolution film. X-radiographs were also taken from the entire length of the cores by cutting 1-cm-thick sediment slabs, to detect sedimentary structures not visible to the naked eye. Based on the observations of this first stage, successive samples from strategic sedimentary units were retrieved for grain-size analysis. The analyses of the silt and clay fractions were performed by the use of a Sedigraph and Coulter Counter. The sand fraction was removed from the samples by wet sieving, and the distribution of its population was calculated by dry sieving.

Impregnated samples, thin sections, and numerous smear slides were also produced in order to study the microscopic structures and mineralogy of the sediments by SEM analysis and regular microscope observations. The sedimentological analysis of the remaining 30 cores was based on their physical sedimentary properties. The ages of the sediments were determined by radiocarbon dating on planktonic foraminefera shells (*Globigerinoides Ruber.*), and the obtainment of Oxygen Isotope curves from two characteristic cores (JPC-31 and JPC-46) (Chapter II).

Sedimentary Facies

The sedimentary facies, determined in this study, are organized into two groups, depending on their grain-size and structural characteristics. In Figure III-3 the Stow and Shanmugam (1980) silt-mud turbidite sequence is displayed, because it will be frequently referred to.

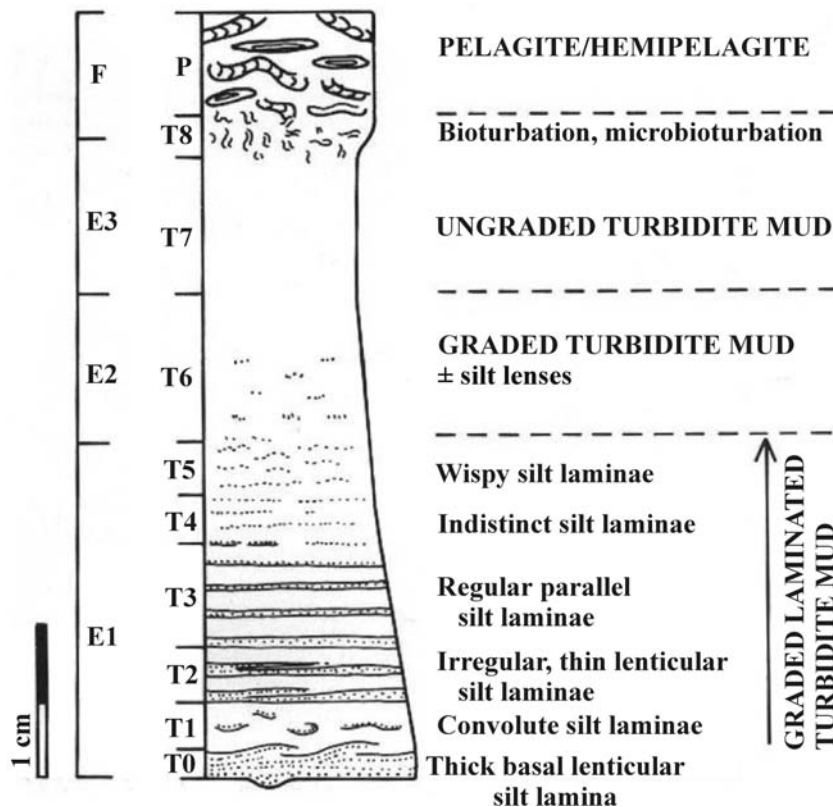


Fig. III-3. Fine-grained turbidite facies model. Structural divisions (E1, E2, E3, F) after Piper (1978), and (T0-T8, P) after Stow and Shanmugam (1980) (from Stow and Piper, 1984).

Mud Turbidite Facies/Units

The group of mud turbidites consists of five sedimentary facies, resembling the mud turbidite facies of Stow et al., (1984). Starting from the finest-grained, they are:

Facies M1: (a few mm up to 5 cm thick). This unit consists of a normally-graded, sharp-based, basal zone of silty-clay/clay that grades upwards into a uniform thin layer/lamina of silty-clay/clay (Fig. III-4). In many cases, this unit is characterized by a thin siltier basal lamina (~1-3 mm) and/or the presence of fading upwards planar to wispy, faint laminae of siltier silty-clay/clay. The silt to clay ratio of this unit ranges from 10/90 to 30/70 (considering 8 phi or 4 μm the limit between the silt and clay fraction). This unit is equivalent to the T5/6,7 partial sequence of Stow and Shanmugam (1980).

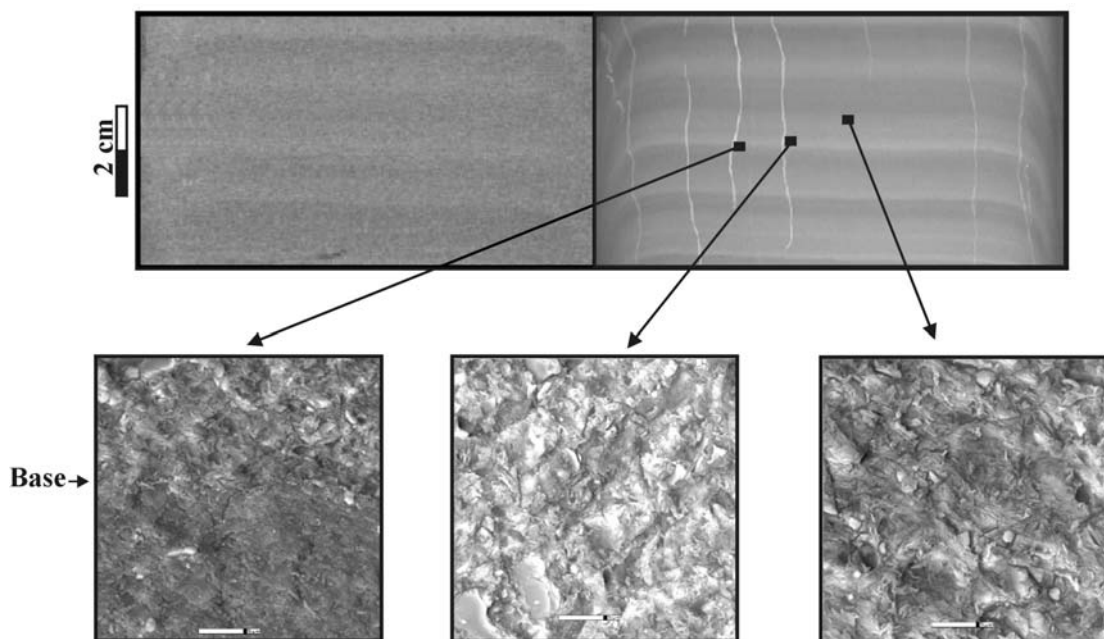


Fig. III-4. Negative photograph of X-ray radiograph (top) and environmental scanning electron microscope (ESEM) images (bottom) of facies M1 deposits. The sharp bases and normal micro-grading of the units is apparent on both X-ray radiographs and ESEM images, revealing that they represent discrete depositional events. Note that the silt grains are surrounded by clay flakes in all ESEM images, inferring that floc deposition was a dominant and nearly continuous process throughout the development of the entire unit. It is noted that these units in the optical descriptions (photographs) are represented as very vague color alternations. The white scale bar is 5 μm long.

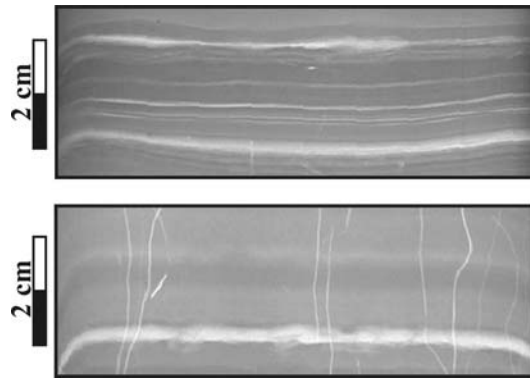


Fig. III-5. Image displaying X-ray radiographs (negatives) of two typical M2 mud turbidite facies.

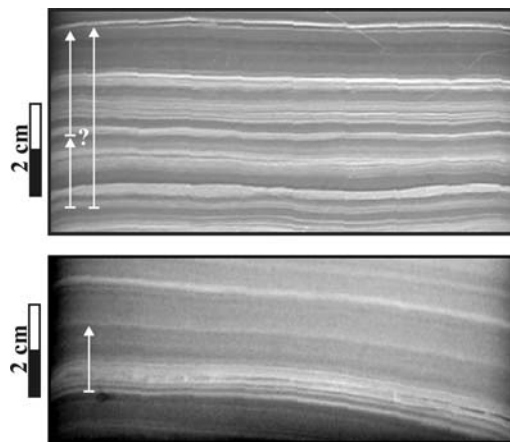


Fig. III-6. X-ray radiographs (negatives) showing two typical M3 mud turbidite facies. The upper picture may be the result of one or two successive surges. Note that in both cases a few weak silt laminae precede the sharp base of the M3 facies.

Facies M2: (0.5 to several cm thick). Normally-graded and sharp-based, silt-clay facies, which are characterized by a thin (1-3 mm) silt/clayey-silt basal lamina, and thin (<1mm), fading upwards, indistinct to wispy, silty laminae (Fig. III-5). In many cases they resemble facies M1 deposits, with the only discrepancy being the silt basal lamina. This unit is characterized by silt to clay ratios of 20/80 to 40/60, and is equivalent to the T3/4-7, or T3/4,6,7 partial sequences of Stow and Shanmugam (1980).

Facies M3: (1 to several cm thick). Sharp-based, silty-clay unit, characterized by thin (1-3 mm), parallel to wavy, silt/clayey-silt laminae, which become indistinct to wispy upwards and

gradually fade away (Fig. III-6). The basal silt/clayey-silt lamina is usually the thickest, and frequently may even display lenticular characteristics. In some cases, a few silt laminae may precede the sharp base of the units. The basal, planar laminated zone is characterized by silt to clay ratios of 40/60 to 55/45. This unit is equivalent to T3-7, or T3,5/6,7 partial sequences of Stow and Shanmugam (1980).

Facies M4: (1 to several cm thick):

- a) Sharp-based unit that is characterized by a basal zone of silty-clay with regular to thin (2-6 mm) planar to lenticular silt laminae, which may be micro-laminated or even display small ripples of low-altitude and long-wavelength, top fading ripples, and cross micro-laminations (Figs. III-7a and b). The silty-clay laminae between the lenticular silt laminae are usually structureless. However, in some cases they may be characterized by a few thin and small silt lenses, and/or silty micro-laminae. Upwards the silt laminae become thinner, discontinuous and obsolescent (resembling facies M3), or may pass sharply into a thin veneer of uniform silty-clay. The basal silt lamina is the thickest. In some cases, a few silt laminae may precede the sharp base of the units. The silt to clay ratio of the basal, lenticularly laminated zone ranges from 50/50 to 70/30. This unit is equivalent to T2-7, T2,3,6,7, or T2,2/3,6/7 partial sequences of Stow and Shanmugam (1980).
- b) Sharp-based and normally-graded unit, which is characterized by a thick basal zone (1-3 cm thick) of thin (1-3 mm), closely-spaced, planar silt laminae (Fig. III-7c). Isolated, small climbing ripples may be developed at its base. The laminated basal zone grades either sharply to a uniform, silty-clay, thin layer/lamina at the top, or more gradually through upward fading, silt to silty laminae. The basal zone is characterized by silt to clay ratios of 60/40 to 70/30.

Facies M5: (couple to several cm thick):

- a) Sharp- to gradational-based unit, characterized by a silty (clayey-silt to very silty silty-clay) basal zone (1-3.5 cm thick), with thick silt lenses (0.3-1.5 cm) and small isolated ripples of low-amplitude and long-wavelength (silt/clay: 60/40-75/25) (Fig. III-8a). Upwards the silty basal zone passes either sharply into a uniform mud layer (silt/clay: 55/45-35/65), or more gradually through fading upwards silt laminae (facies M4, M3, or M2). This unit is equivalent to the T1-7, or T1,2,6/7 partial sequences of Stow and Shanmugam (1980). Sand may be present in the silt lenses, but generally is of negligible importance (less than 5%).

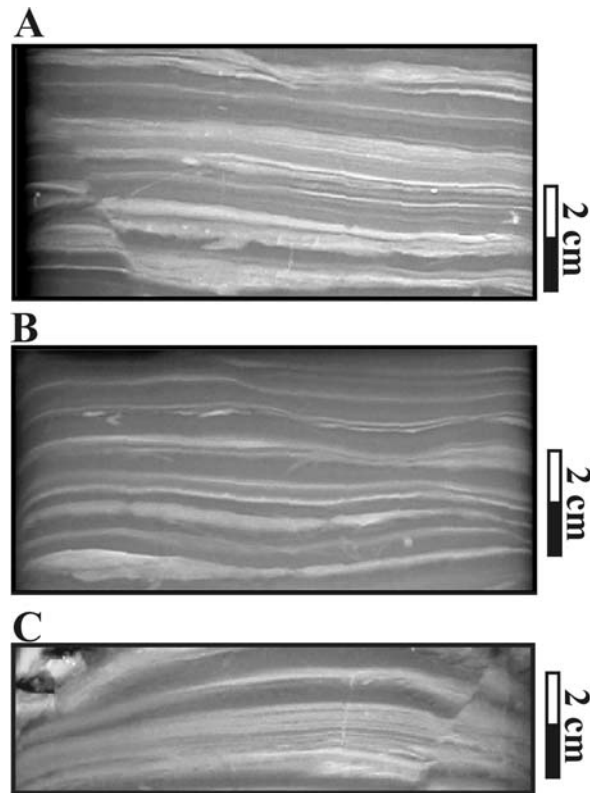


Fig. III-7. X-ray radiographs (negatives) displaying typical M4a (A and B), and M4b (C) mud turbidite facies.

- b) Unit characterized by a thick, basal, lenticular silt lamina/layer (1-2.5 cm), which is planar to cross micro-laminated, and may display immature lensoid ripples, low-amplitude long-wavelength climbing ripples, and top-fading ripples (silt/clay: 95/5-70/30) (Figs. III-8b and c). Its base is sharp with common scouring (e.g., cut and fill structures). It is generally ungraded, and only in a few cases may display a normal or even inverse grading. The sand fraction is negligible (less than 5%). In some cases, a few silt laminae may precede the sharp base of the units. The silt basal layer passes upwards either sharply to a structureless mud layer/lamina (0.5-2 cm thick; silt/clay: 55/45-35/65), or more gradually through upward fading silt laminae (facies M4, M3, or M2). This unit is equivalent to the T0-7, or T0,6/7 sequences of Stow and Shanmugam (1980). In a few cases, two or three repetitions of upwards weakening, thick to regular (1-0.3 cm) silt laminae alternated with uniform mud laminae (may display in cases small silty lenses and microlaminations) are observed.

The upper silt laminae are weaker, thinner, and characterized by sharp to gradational bases. These units are characterized as M5b/M4a transitional facies.

- c) Unit characterized by a thick, normally-graded, structureless, basal silt lamina/layer (0.5-1.5 cm; silt/clay: 90/10-70/30) (Fig. III-8d). At the top, it passes either sharply into a massive mud lamina/layer (0.5-2 cm thick; silt/clay: 55/45-35/65), or more gradually through upwards fading silt laminae (facies M4, M3, or M2). The sand fraction is almost negligible (less than 5%). Their bases are sharp with common scouring (e.g. cut and fill structures). This facies is equivalent to the T0-7, or T0,6/7 sequences of Stow and Shanmugam (1980).

Loading structures such as necking, boudinage, and distortion of the silt laminae, load clasts and small silt/silty pseudo-nodules are common in the mud-turbidite facies and most apparent in the M5 and M4 facies. A few dewatering structures are also observed in these units, but they are not common.

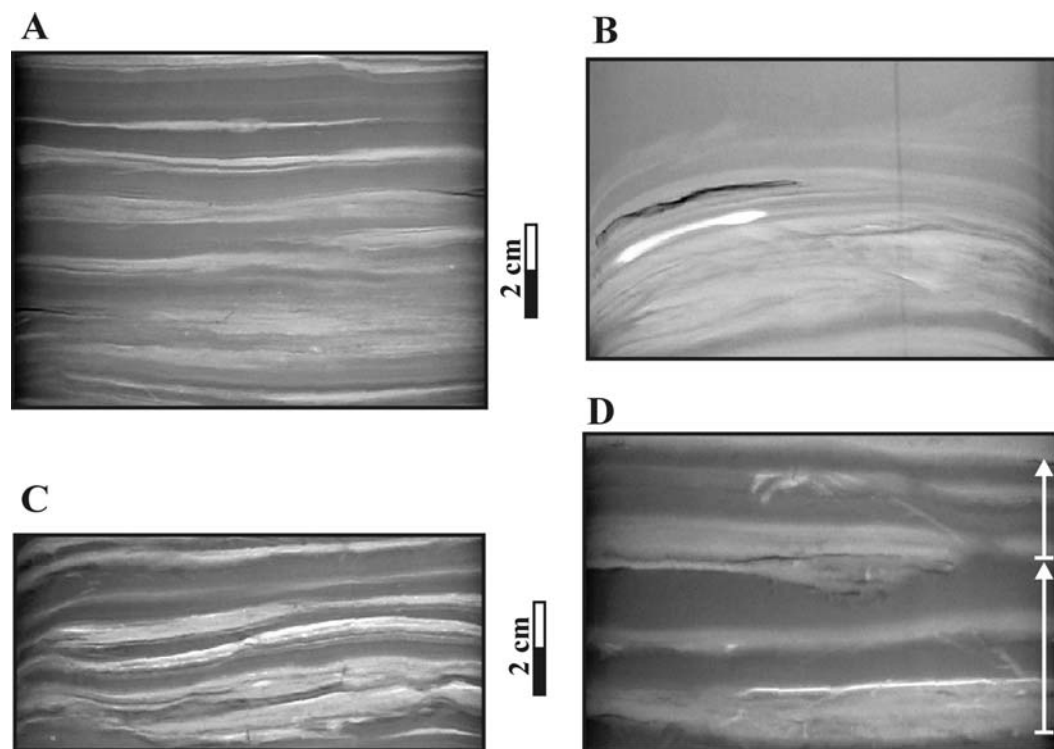


Fig. III-8. Image displaying X-ray radiographs (negatives) of typical M5a (A), M5b (B and C), and M5c (D) mud turbidite facies. In image D two successive M5c facies are represented with the upper unit being characterized by a truncational base.

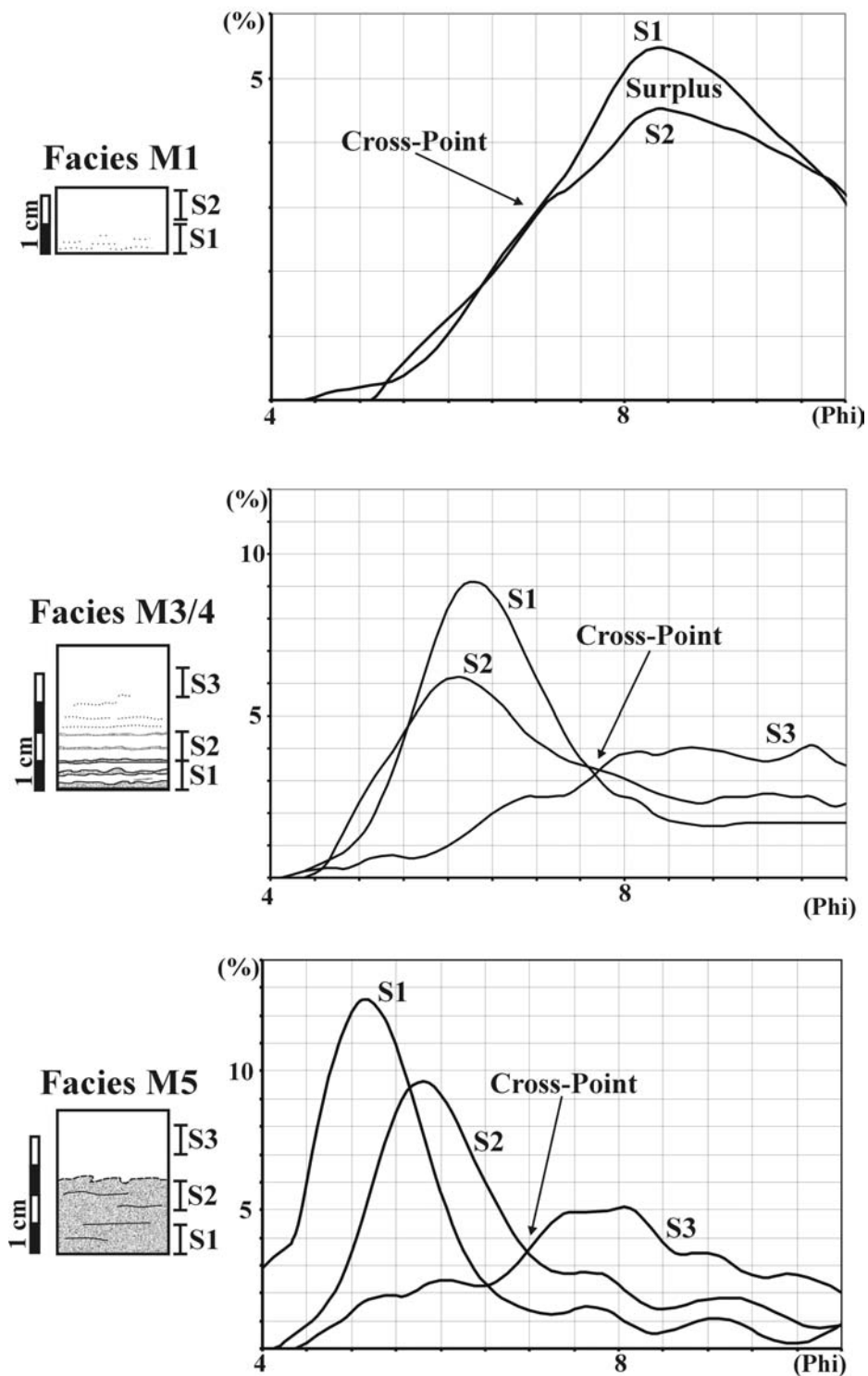


Fig. III-9. Image representing weight % grain-size curves from successive samples (~ 5 mm thick) of three discrete mud turbidite facies. The locations of the samples are shown in the drawings on the side of the diagrams.

Grain-Size Analysis of Mud Turbidite Facies

The results of grain-size analysis and sedimentological descriptions (Fig. III-9) clearly infer a depositional competition between the silt and clay fractions so much within the mud turbidite facies (normal grading), as between the facies as well (moving from higher to lower order facies). All five facies are not independent of each other, but they most probably represent a depositional continuum of a wide range of velocity, capacity of suspended sediment load, and silt to clay ratio low-density mud turbidity currents (Piper, 1978; Stow and Bowen, 1980; Stow and Piper, 1984; Nemeč, 1990; Hiscott, 1994; Kneller, 1995).

An interesting observation of the grain-size frequency curves of successive samples within a facies is the occurrence of a cross-point around 6.6-7.7 phi (10-5 μm). This tends to separate the modes of the coarser- and finer-grained deposits in the units. This cross-point also seems to coincide with the inflection point (change to marked upward trend) of the most clayey free parts (< 15% clay) of facies M5 basal silt zone (Fig. III-9). It is interpreted to represent a critical grain-diameter under which sediments can not be deposited as individual, incohesive particles, but only as aggregates (Stow and Bowen, 1980). The gradual, wave-like transition from the silt-dominated to the clay-dominated parts of the units (cross-point acts as stable reference point), reveals that incohesive (silt) and cohesive (clay) depositional modes are coexisting and competing with each other, rather than having independent occurrence.

Great interest was also focused on the rather peculiar results of the grain-size analysis from facies M1. In the Sedigraph results, all samples follow an almost identical trend, with the only exception being a surplus in the size range of 7 to 8 phi (7.8-1 μm) in the basal sample (Fig. III-9). Due to the relative large thickness (~0.5 cm) of the Sedigraph samples, 1-mm thick samples were acquired from six M1 facies for Coulter Counter analysis in order to provide a better insight in the grain-size evolution of these units. All of the results divide facies M1 units in three zones: 1) a very thin (1-3 mm), silty (but still silty-clay), basal lamina or zone (~0.5 cm) with wispy, silty laminae (<1mm), 2) a graded middle zone, in which upwards the samples reveal higher percentages of the size fraction between 6.8-7.2 phi (7-9 μm) and approximately 10 phi (1 μm) (judging from the trend of the curves and according to the Sedigraph results), and 3) an upper uniform silty-clay zone following a coarser trend similar to that of the basal sample of the graded zone. Frequently, the silty basal zone/lamina may be absent. The continuously increased surplus of the ~7-10 phi fraction, in the graded zone, infers an

intensification and domination of the flocculation processes during the deposition of the M1 facies. The upper uniform zone appears to be of lower bulk density in the X-ray radiographs (Fig. III-10), even though it is slightly coarser. This observation indicates that this final zone has been deposited under much higher sedimentation rates, leading to its loosely-packed nature.

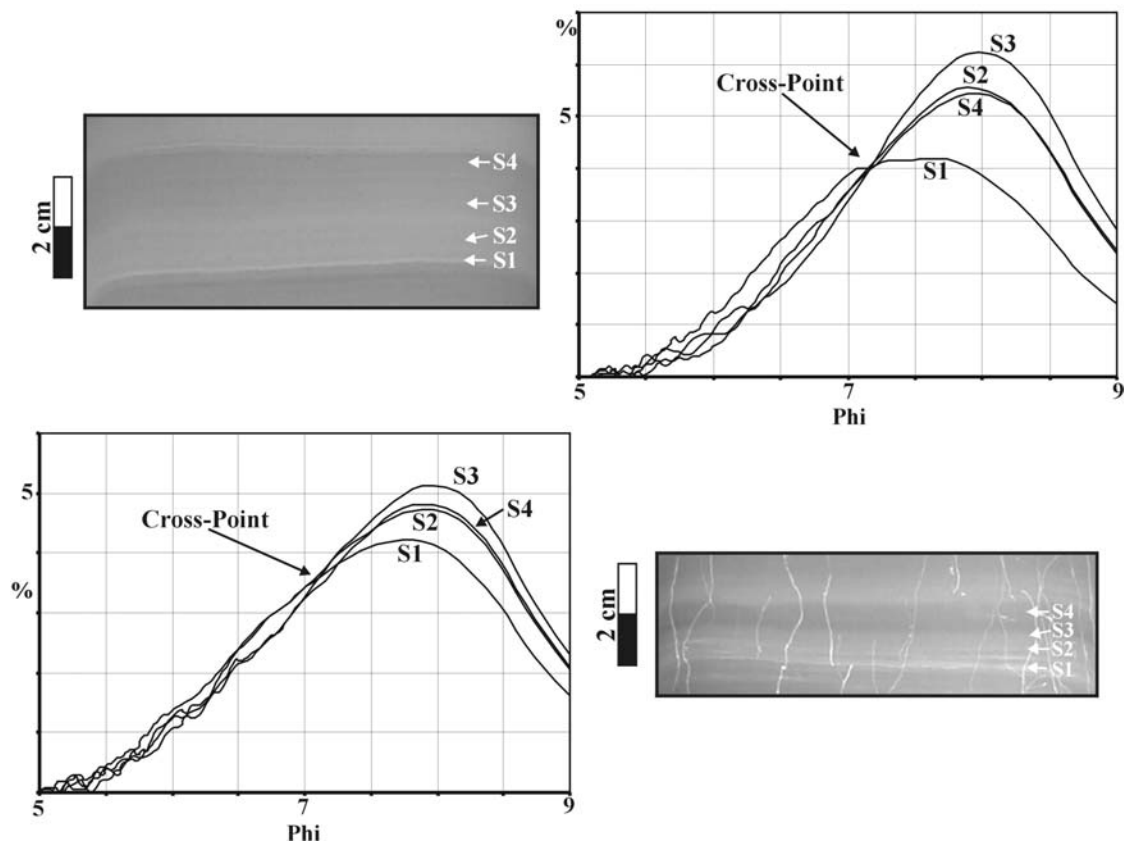


Fig. III-10. Image showing weight % grain-size curves from successive samples (~ 1 mm thick) of two discrete M1 mud turbidite facies. The exact locations of the samples are displayed on the X-ray radiographs (negatives) adjacent to the diagrams.

Interpretation

The previous information suggests that the deposition of a complete mud-turbidite sequence (T0-7) is developed under four distinct flow regime stages:

Stage 1: The velocity and turbulent energy of the flows is sufficient to maintain all of its sediments in suspension, and to even incorporate seafloor sediments into its body (Parker, 1982; Fukushima et al., 1985; Kneller, 1995). No deposition occurs at this flow regime, whereas scouring of the seafloor is common.

Stage 2: A reduction in the velocity and turbulent energy of the flows leads to a decrease in the amount of sediments that can be maintained in suspension (loss of capacity), resulting in sediment deposition. The settling sediments consist of silt particles and clay flocs of equivalent settling velocities. However, floc breakage occurs, due to the strong shear at the boundary layer of the flows, and the fine sediment particles are re-entrained into the main flows. This constitutes the silt-fraction as the main deposited material under these flow conditions (McCave and Swift, 1976; Stow and Bowen, 1980). The silty basal zones of facies M5b and M5c (T0 division) are deposited in this stage. The massive silty basal zones of M5c facies reveal that they have been deposited under high-sedimentation rates, constituting hindered settling and dispersive pressures to become dominant in the lower parts of the flows, and consequently to suppress the development of any traction-induced structures (Allen, 1991; Kneller and Branney, 1995; Baas et al., 2000). Inversely, the internal planar to lenticular to ripple laminations in the silt basal zone of the M5b facies infer that their deposition occurred under lower sedimentation rates and longer flow duration, allowing for the development of tractional structures (silt particles gradually pass from a suspension to a bed load transportation mode, and then they become deposited).

Stage 3: Low-speed streaks, characterized by increased concentrations of sediment particles, have long been recognized as ubiquitous structural elements within the boundary layers of turbulent flows (McCave and Swift, 1976; Allen, 1985). One of the most important characteristics of the low-speed zones is the cyclic development of turbulent bursts, through which low-momentum fluid parcels are ejected back into the main flow, playing an active role in the production of wall-region turbulence. Sediments settling in the boundary layer are re-entrained into the main flow through this cyclic streak-bursting mechanism. The frequency of the bursting events is directly related to the flow velocity, and inversely related to the boundary layer thickness (Allen, 1985). Best and Leeder (1993), and Li and Gust (2000) have shown, through laboratory experiments, that cohesive sediment suspensions in the flows result in the thickening of their boundary layers, the decrease of the occurrence time period of the bursting

events, and lead to the significant reduction of the bottom drag of the flows. The directly measured shear velocities in the viscous sublayer could be reduced as much as 70%.

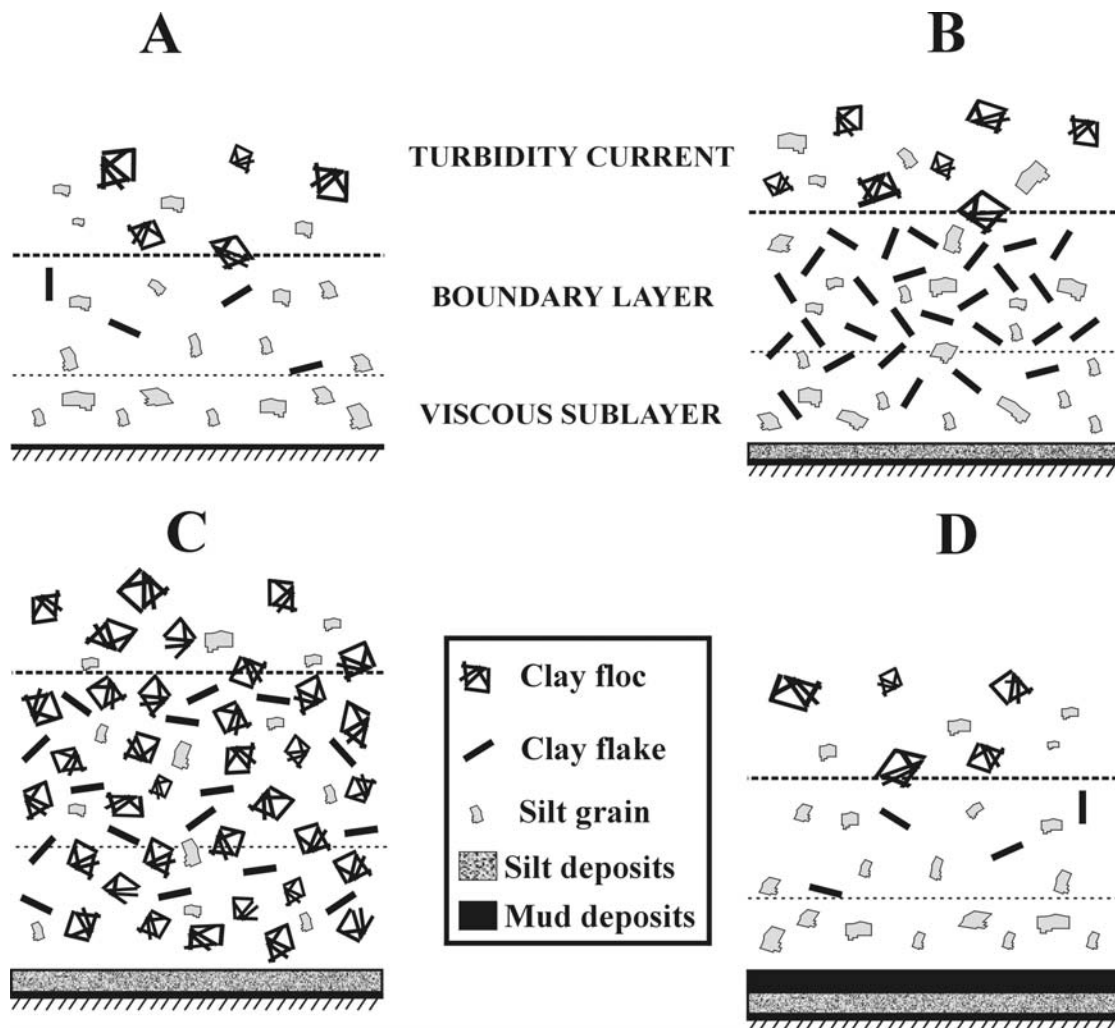


Fig. III-11. Image displaying the two depositional stages of silt and mud laminae deposition: A) the shear in the boundary layer leads to the breakage of the settling flocs and allows for the deposition of the silt fraction only, B) since the amount of clays re-entraining in the overlying flow is less than the settling aggregated clays, their concentration is continuously increased leading to shear reduction within the boundary layer (thickening of the boundary layer, and reduction of the bursting frequency), C) the clay (cohesive sediments) concentration in the boundary layer exceeds a critical value, under which the shear in the boundary layer can not sustain the cohesive sediments disaggregated, leading to their massive deposition, and D) the boundary layer is depleted of cohesive sediments (restoration of its initial thickness, bursting frequency, and shear), after their massive deposition, and a new depositional cycle is developed (modified from Stow and Bowen, 1980).

As a low-density turbidity current decelerates (concomitant reduction of the bursting frequency, and of the mixing and momentum exchange within the boundary layer), it will eventually achieve a critical flow velocity, below which the amount of the aggregated cohesive sediments settling into the boundary layer will exceed the amount of the disaggregated cohesive sediments re-entraining the main flow. A successive two step depositional model is proposed to occur, under flow velocities below this critical value, and for as long as the shear within the boundary layer is high enough to disaggregate the settling flocs (Fig. III-11). In the first step, the shear in the boundary layer causes floc disaggregation, prohibiting them from settling, and allowing only for the deposition of the silt fraction (coarser grains). However, since the amount of cohesive sediments entering the boundary layer is larger than that re-entraining into the main flow, a gradual increase of the cohesive sediment concentration into the boundary layer is inferred. That, in turn, leads to the extra: 1) thickening of the boundary layer, 2) reduction of the frequency of the bursting events, 3) enhancement of the cohesive sediment accumulation rate in the boundary layer, and 4) reduction of shear in the boundary layer. As soon as the cohesive suspended sediment concentration in the boundary layer achieves a critical value, above which the reduced shear is insufficient to maintain the cohesive sediments disaggregated, flocculation processes become dominant and result in the rapid deposition of the dispersed cohesive sediments trapped in the boundary layer. After the deposition of the dispersed cohesive sediments, their concentration in the boundary layer is significantly reduced (restoration of the initial boundary layer thickness, bursting frequency, and shear), and a new depositional cycle of silt and mud laminae occurs.

The lenticular, planar, indistinct, and wispy silt laminae of M4, M3, and M2 facies (T2, 3, 4, 5 divisions) are developed through these processes. The above theory is strongly supported by the studies of Stow and Bowen (1980), Stow and Piper (1984), and Best and Leeder (1993), which proposed a similar earlier model to explain the simultaneous development of the silt and mud laminae. The microlaminated character and the presence of low-amplitude long-wavelength and top-fading ripples in the regular to thick silt laminae of the M4 facies basal zones (T2 division), patently ascertain the development of tractional movements during the deposition of the silt grains. That combined with their relative large thickness (2-6 mm, or even up to 1 cm in some cases), reveals that their deposition occurred from flows characterized by: 1) high suspension loads, with high silt to clay ratios, accounting for the large thickness of the silt laminae, and 2) sufficiently large flow velocities that will be able to account for the

tractional movements of the silt-grains. The gradual thinning and fading of the silt laminae, moving either upwards within the facies or towards the lower order facies (M4 to M2), are interpreted as the result of: 1) the gradual silt depletion of the suspended load of the flows (lower silt accumulation rates on the seafloor), and 2) the gradual reduction of the flow velocity and consequently of the shear in the boundary layer. The latter results in the reduction of the silt and mud depositional time period, due to: 1) the reduced suspended load capacity of the flows, leading to increased accumulation rates of cohesive sediments in the boundary layer, and 2) the lower concentrations the cohesive sediments have to achieve in order to reduce sufficiently the already decreased shear of the boundary layer, in order to be deposited.

The silty basal zone of facies M5a is characterized by a rather peculiar sedimentological structure, displaying characteristics between M5b and M4 facies. M5a facies are interpreted to be deposited under transitional stage 2 to 3 flow conditions, yielding a cyclic silt and mud deposition under high depositional rates.

Stage 4: The graded M1 facies are developed in this last stage. Deposition occurs from a clay-rich flow ($\leq 30\%$ of medium to fine silt), characterized by velocities below a threshold value, which allows for the straight deposition of flocculated sediments. The normal grading in this unit is most probably due to the gradual domination of the settling aggregated sediments over the slowly accumulated silt grains on the seafloor. The effect of the cyclic reduction of the boundary layer shear is greatly diminished in this stage. It is expressed only by the development of siltier silty-clay (higher shearing-lower clay concentrations in the boundary layer), and more clayey silty-clay/clay (lower shearing-higher clay concentrations in the boundary layer) alternating laminae. The normally-graded zone of M1 facies is grading upwards into a thin veneer of uniform silty-clay, which has probably been developed by the massive deposition of a final very slowly moving (almost stationary) sediment cloud.

All of the above stages represent an ideal sequence of events of a depletive or waning, low-density turbidity current, as it evolves in time and space. The five mud turbidite facies, defined in this paper, have been deposited from flows that consisted of waning combinations of the above flow regime stages (Table III-1). This information reveals that the depositional low-density turbidity currents were of a waning nature, characterized by similar structural characteristics to those of typical surge-like turbidity currents: 1) a coarser, erosional/depositional head/body with higher suspended sediment concentrations, 2) a transitional zone (body) characterized by gradually declined velocities, suspended sediment

concentrations, and silt/clay ratios, and 3) a very diluted and slowly moving tail (almost stationary) (Middleton, 1993; Stow et al., 1996; Kneller and Buckee, 2000; Mulder and Alexander 2001). It is commonly observed that the silt/silty basal zones of M5 and M4 facies (T0, T1, T2 divisions) pass sharply into an upper layer/lamina of uniform silty-clay (T7 division). These units are interpreted as typical deposits of surge-type turbidity currents, characterized by the absence of a transitional zone, passing sharply into the deposits of their slowly moving, almost stationary tails.

Table III-1. Waning spectrums of flow regimes resulting in the deposition of each mud turbidite facies.

Mud turbidite facies	Waning stages of flow regime
M5	1, 2, 4 (final step, almost stationary sediment cloud) or 1 to 5
M4	3, 4 (final step, almost stationary sediment cloud) or 3 to 4
M3	3 (middle to low intensity) to 4
M2	3 (low intensity) to 4
M1	4

Stage 1 flow regime characterizes energetic flows that can retain their entire sediment load in suspension. Stage 2 flow regimes are characterized by fast running and rich in silt flows that allow for the deposition (loss of capacity) of the silt fraction only. Stage 3 is characterized by a vigorous silt vs clay depositional competition, leading to the development of the alternated silt and mud laminae of T2, T3, T4, and T5 divisions of Stow and Shanmugam (1980). The final stage 4 flow regime consists of two waning steps: 1) depleted in silt flows, where flocculation processes become dominant leading to the deposition of graded mud (T6), and 2) highly decelerated, almost stationary, sediment clouds (deposition of massive mud, T7). See text for further explanation on the flow regime spectrums.

Coarse-Grained Turbidite Facies/Units

The group of coarse-grained turbidites consists of the three following turbidite sedimentary facies:

Facies S1: (a few to several cm thick; 50-20% sand, 40-65% silt, 10-15 % clay) This sedimentary facies (Fig. III-12) is represented by a coarse basal zone, consisting of sand-silt/sandy-silt and clayey-silt/silty-clay, planar to more rarely lenticular, alternating laminae (T_d division of the Bouma Sequence). The base of the coarse basal zone is sharp with indications of scouring. Its top may be sharp with indications of scouring (capped by another depositional

event), or it may grade into finer-grained sediments resembling those of facies M4 or M3. This facies is equivalent to the $T_{d,e}$ partial Bouma Sequence.

Facies S2: (a few to several cm thick) This unit (Fig. III-13) is very similar to facies S1, with the only exception being that it is preceded at its base by a planar to lenticular to wavy laminated fine-sand layer (1 to a few cm thick; ~80% sand, ~15% silt, ~5% clay). This facies is equivalent to the $T_{b/c-e}$ partial Bouma Sequence.

Facies S3: (a few to several cm thick) This facies (Fig. III-14) consists of a structureless silt to clayey-silt zone (~70% silt) that is capped by a lenticular, wavy, rippled, and convolute laminated, better-sorted silt layer (80-90 silt). The sand fraction is negligible in these deposits and is always lower than 1%. The base of this unit is sharp with common scouring. Its top is either sharp and overlain by a new silt turbidite facies, or may gradually enter into finer-grained deposits, similar to those of facies M4 or M3. Dewatering structures are very common and pervasive (especially in the basal structureless silt zone).

Loading structures such as necking, distortion, load casts, and pseudo-nodules are evident in all three facies.

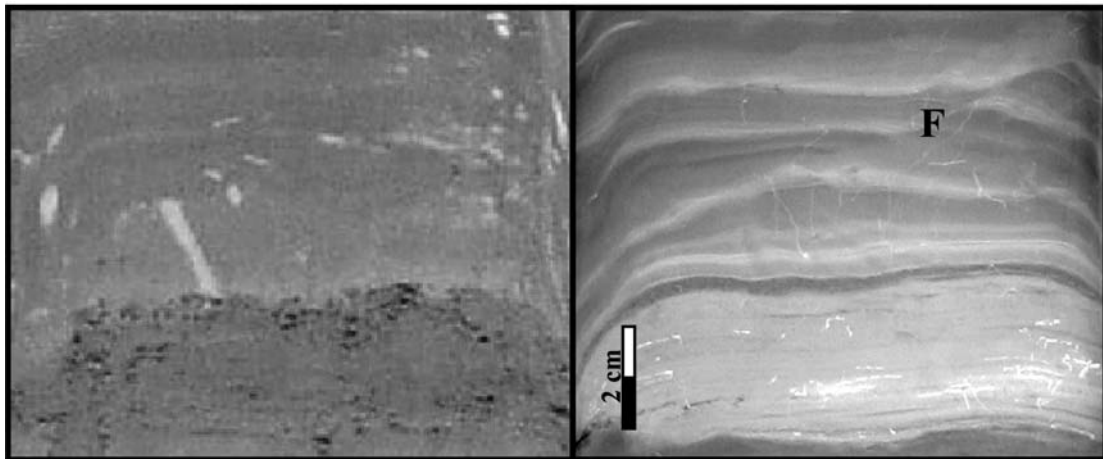


Fig. III-12. Photograph and X-ray radiograph (negative) of a typical S1 turbidite facies. Note that, in contrast to the silt laminae of the mud turbidite facies, the sand-silt/sandy-silt laminae are very closely spaced and dominant. This can be ascribed to the presence of the sand fraction (higher settling velocities) in the flows, which constitutes the accumulation of the incohesive sediments (sand-silt/sandy-silt laminae) on the seafloor to be more efficient and rapid, compared to the deposition of the aggregated sediments (mud laminae). F: fault.

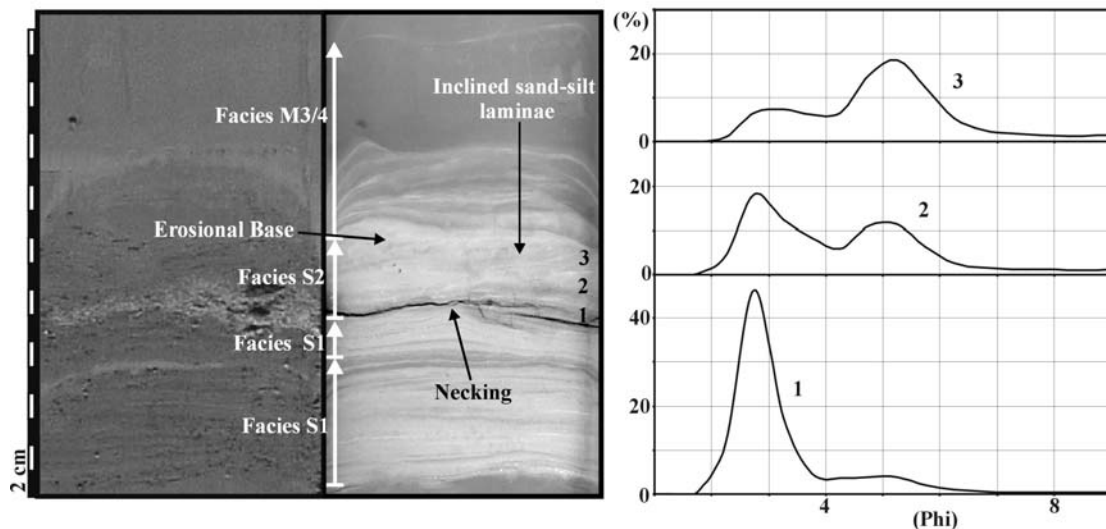


Fig. III-13. Photograph, X-ray radiograph (negative), and weight % grain-size curves, from successive samples, of a characteristic S2 turbidite facies. The S2 facies is preceded by two successive, top-cut-out S1 facies, and capped by a truncational M3/4 mud turbidite facies. All units are interpreted to result from four successive surges occurring in a single flow event (turbidity current). The grain-size distributions clearly reveal the normal graded nature of S2 turbidite facies, grading from sand-dominated sediments to sand-silt bimodal deposits. Note that the sand-silt laminae of the S2 facies are inclined (transitional $T_{c/d}$ Bouma division), indicating deposition under higher flow velocities, compared to the sand-silt laminae of S1 facies (T_d Bouma division). The three numbers on the X-ray radiograph represent the locations of the samples used for grain size analysis.

Interpretation

The laminated character of the facies S2 sand layer (upper stage plane bed formation) indicates that its deposition occurred under high flow velocities, under which deposition due to flocculation processes was diminished by the high shear within the boundary layer. The closely spaced sand-silt/sandy-silt laminae (T_d division) of S1 and S2 facies are interpreted to develop by cyclic depositional processes, similar to those that result in the deposition of the silt and mud laminae of the mud-turbidite facies. These processes are developed under much lower flow velocities than those of the sand layers, where the suspended cohesive sediments of the flows can produce substantial shear fluctuations within the boundary layers that will lead to the cyclic sand-silt and mud deposition.

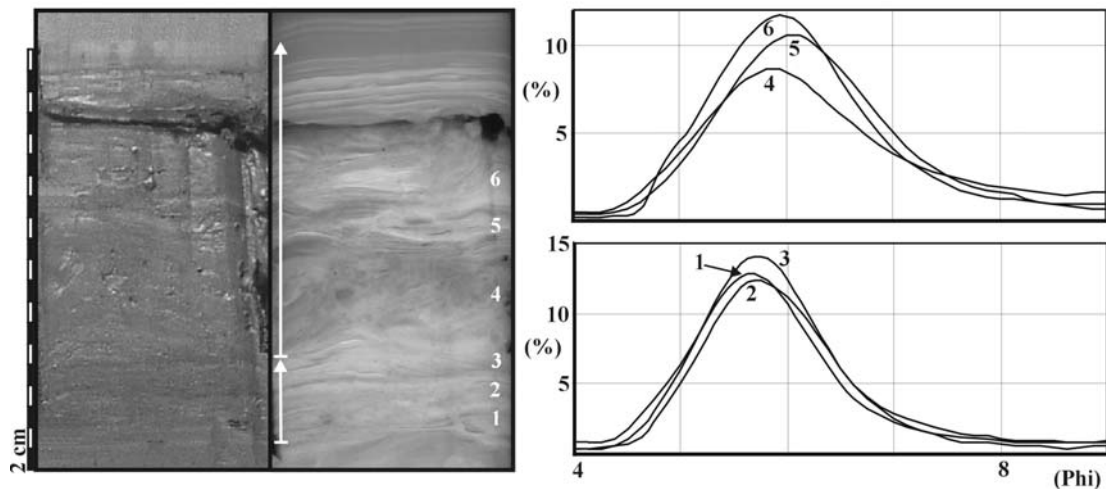


Fig. III-14. Photograph, X-ray radiograph (negative), and weight % grain-size curves of successive samples of two S3 turbidite facies. The successive character of the facies, in combination with the top-cut-out nature of the lower facies, suggests that their deposition resulted from two successive surges, occurring in a single flow event. Note that both facies grade from massive, poorly-sorted silt with abundant dewatering structures to lenticular, convolute, and/or ripple laminated, better sorted silt. The numbers on the X-ray radiographs indicate the locations of the samples used for grain-size analysis.

The silt deposits of facies S3 indicate that the turbidity currents, from which they resulted, were also silt dominated with very limited to negligible amounts of sand. The structureless basal silt zone of the S3 facies is interpreted to be deposited under exceptionally high sedimentation rates. High sedimentation rates would cause, in the lower portions of the flows, the domination of hindered settling and dispersive pressures over turbulence, and thus would lead to the suppression of any traction-induced structures (Kneller and Branney, 1995; Kneller and Buckee, 2000; Stow and Mayall, 2000; Migeon et al., 2001; Mulder and Alexander, 2001). The pervasive dewatering structures in this structureless silt zone are in agreement with the above interpretation. The presence of an overlying planar/lenticular to ripple laminated silt zone, with less common dewatering structures, clearly indicates the latter reduction of the sedimentation rates below a critical value, where turbulence becomes dominant again in the lower portions of the flows, and allows for the development of traction-induced structures.

It is apparent that S2 and S3 facies grade from incohesive sand and silt deposits of high flow velocities to cohesive deposits of low flow velocities. This strongly suggests that both facies have resulted from the deposition of fast flowing, waning (surge-like) turbidity currents. The same conclusion is also assumed for the S1 facies. However, the competing silt and mud

alternated laminae of their basal zones (T_d division) indicate that their deposition occurred either from slower moving flows, or almost exclusively from the slower moving and diluted end members of large turbidity currents (Allen, 1985, 1991).

Spatial and Vertical Distribution of the Turbidite Facies

The spatial distribution of the turbidite facies indicates the existence of two major sedimentological environments during the low sea-level stand of Oxygen Isotope Stage 6 (Fig. III-15): 1) The intracanyon areas of Bryant and Eastern Canyon systems, and 2) their surrounding areas subjected to overflowing and flow-stripping processes.

Intracanyon Environments

The sediments of most of the canyon floor cores were highly distorted by slope instability processes, initiated by the diapiric blockage of the canyons right after their abandonment (early Oxygen Isotope Stage 5). However, sediment cores JPC-37 (canyon floor) and JPC-34 (at the boundary of intracanyon and overflowing areas), located on the lower continental slope, display well-preserved and undisturbed Stage 6 deposits at their lower reaches.

Sediments of the intracanyon environments consist of successions of S1 and M5 to M1 turbidite facies, interbedded by coarse-grained (S2 and S3) turbidite facies. Interbedded and irregular spaced mass-transport deposits, from sediment failures on the canyon walls, are common. The S1 and M5 to M1 turbidite facies are interpreted as deposits from diluted and finer-grained end-members of turbidity currents. The silt and sand (S2 and S3) turbidite facies are interpreted as deposits of the main bodies of the funneled turbidity currents.

The resemblance of the Bryant Canyon floor sediments to levee deposits, and the absence of distinct and extensive erosional surfaces, indicates a depositional environment, which is in contradiction with the strongly erosional nature of most submarine canyons (Hagen et al., 1994, 1996; Pratson et al., 1994; Klauke et al., 2000; Babonneau et al., 2002). Two interpretations, or most probably a combination of them, can account for the depositional character of the Bryant Canyon floor. The first one implies that the erosional action of turbidity currents was not equally spread over the canyon floor, but was focused on a narrow zone (thalweg of the canyon), where the flows were exhibiting their highest sediment concentrations and velocities, developing on the surrounding canyon floor deposits similar to those of levee

and overbank formations. This interpretation is in perfect accordance with the channel/canyon nature of Bryant Canyon system (Satterfield and Behrens, 1990; Twichell et al. 2000).

Wonham et al. (2000) documented the existence of successive canyon-fill channel-levee formations in the Baliste-Crécérelle canyon, offshore Gabron. The fact that our observations are located at the ending of Oxygen Isotope Stage 6, and consequently at the final evolutionary stage (probably infilling stage) of Bryant Canyon, provides extra support to the above theory.

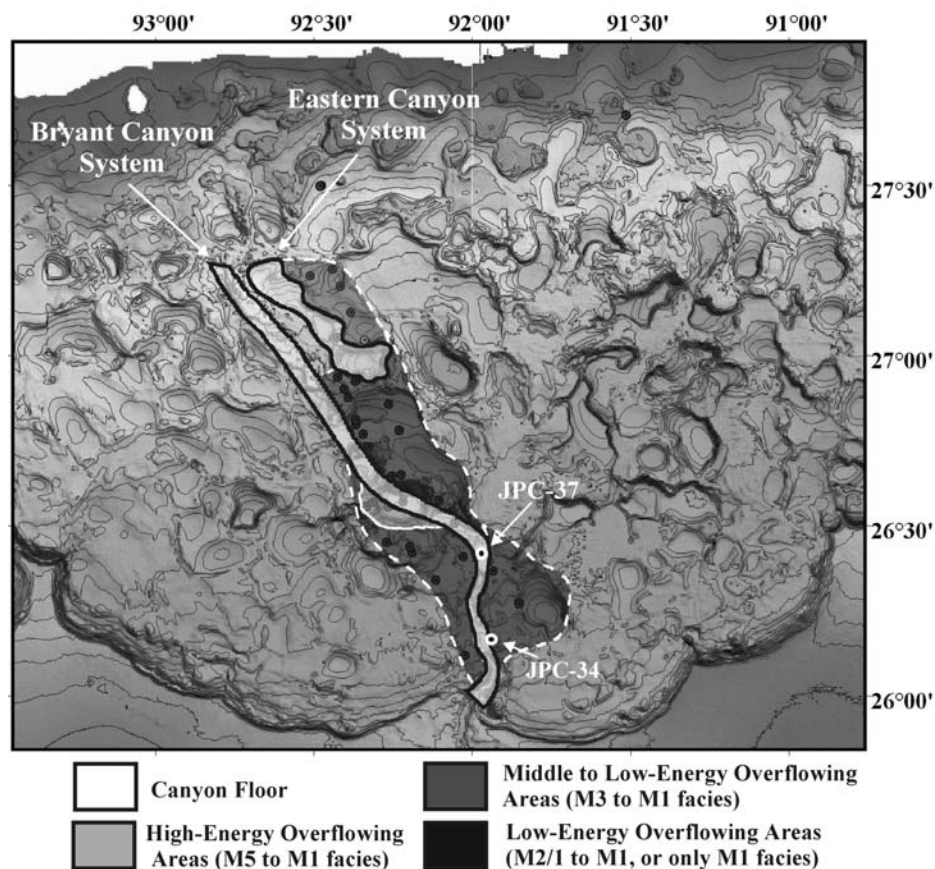


Fig. III-15. Morphologic map of the Bryant Canyon area displaying the spatial distribution of the main sedimentological environments, during Oxygen Isotope Stage 6. The dashed white lines represent uncertain borders. The dark dots represent the core locations, whereas the locations of cores JPC-37 and JPC-34 are represented as white and black circles. The intracanyon environments (canyon floors) plotted according to the studies by Lee et al. (1996) and Twichell et al. (2000). Note that spillover mechanisms are intensified at the turning points of the canyons (high-energy overflowing environments). Even though, overbank areas are observed to occur in specific areas (due to the clustering of our data), their actual boundaries are unknown, since stage 6 overflowing deposits were present in all of the cores from the surrounding to the canyon areas. This strongly suggests the much greater impact of the overbank processes on these areas, than the one presented in this figure.

The second interpretation of the depositional character of the Bryant Canyon floor implies that sedimentation is only of local extent, and it is due to: 1) the reduction of the turbidity currents capacity, and 2) flow instabilities of the currents caused by morphological irregularities. It was previously mentioned that sediment failures on the canyon walls, resulting in slumped masses and debris-flow deposits along the canyon floor, were common. These mass-transport deposits on the canyon floor could result in the generation of flow irregularities of the flow regime of the funneled turbidity currents, and cause sediment deposition upstream of their location (Kneller, 1995; Hagen et al., 1996; Kneller and Buckee, 2000; Babonneau et al., 2002). Figure III-15 shows that core JPC-37 is located adjacent (in the downstream direction) to a turning point of Bryant Canyon, where significant turbidity current flow-stripping occurred. The flow-stripping of the turbidity currents would have resulted in the reduction of their thickness, velocities and suspended sediment capacities, which in turn would have resulted in the partial deposition of the turbidity currents (sediment dumping), downstream from the turning point, in an effort to recover a new dynamic equilibrium (Piper and Normark, 1983; Bowen et al., 1984; Piper and Savoye, 1993; Hiscott, 1994). The frequent occurrence of S1 and M5 to M1 facies on the canyon floor indicates that the turbulent energy of many turbidity currents was sufficient to sustain their sediment load under suspension, with deposition occurring only from their slowly moving and diluted end members (no indication of flow capacity reduction). This strongly suggests that flow-stripping was a process that mainly occurred in the largest flows.

Flow Properties

A first approximation of the shear stresses and flow velocities of the sand-rich and silt-rich turbidity currents can be made through their structural characteristics. Laboratory experiments indicate that the upper stage plane bed structures, observed in the facies S2 basal sand deposits, are developed in non-dimensional shear stress (θ) values higher than 0.5. The ripples (ripple formations), and wavy to lenticular to ripple laminations (mixed ripple and upper stage plane bed formations) of the facies S3 silt deposits are developed in θ values ranging from 0.1 to 0.7, and 0.7 to 1.7 (or higher), respectively (Allen, 1982, 1985). The non-dimensional shear stress can be expressed as:

$$\theta = \tau / (\rho_s - \rho)gd \quad (1)$$

and

$$\tau = \rho U_*^2 = \rho C_f U^2 \quad (2)$$

Where τ is the shear stress of the flow, ρ_s and ρ are grain and fluid density, respectively, g is gravitational acceleration, d is grain-diameter (the modal grain diameters were used in our calculations), C_f is drag coefficient at the bed, and U_* and U are shear and flow velocities, respectively. Values for C_f range between 0.0029 and 0.01, with 0.004 the most commonly used (Bowen et al., 1984; Komar, 1985; Reynolds, 1987; Zeng et al., 1991; Piper and Savoye, 1993; Migeon et al., 2001). Ren et al. (1996), comparing real to parametric numerical data, concluded that a value of $C_f \approx 0.0029$ yields the most reasonable results. That value is used in this paper.

Solving equations 1 and 2 (Table III-2), it is concluded that the planar laminated sand layer of S2 facies was deposited under flow velocities higher than 63 cm/s (11.84 dynes/cm²), whereas the ripple, and wavy to lenticular to ripple laminated silt of S3 facies were developed under flow velocities of 10-27 cm/s (0.32-2.2 dynes/cm²) and 27-43 cm/s (2.2-5.4 dynes/cm²) or higher, respectively. Velocities of 27-43 cm/s, inferred for the silt-rich turbidity current by their upper plane/ripple bed formations, are assumed to be the most representative of the maximum intensity of these flows. The rippled silt formations are interpreted to result from a latter decelerating stage of the flows. Best and Leeder (1993) and Li and Gust (2000) pointed out that cohesive sediment concentrations of 0.1-8 g/l in turbidity flows resulted in a 30-70% reduction of shear velocity (U_*). This reveals that much higher velocities would be required in order for the observed sedimentary structures to develop. However, a clay concentration of 8 g/l seems extremely high, and close to the lower limit of the fluid mud clay concentrations (10 g/l). Consequently, a 30-50% reduction of the shear velocity (U_*), corresponding to clay-concentrations of 0.1-2 g/l, appear to be more reasonable. Adjusting the previously calculated velocities for the flow drag reduction, it is concluded that flow velocities higher than 90-126 cm/s, and 38.6-86 cm/s (or higher) account for the deposition of the sand and silt layers of S2 and S3 facies, respectively.

Another more accurate way of estimating the flow properties of the turbidity currents is by using the following semi-empirical equation (Bowen et al., 1984; Komar, 1985):

$$U = BW_{S(D)} / \sqrt{C_f} \quad (3)$$

Where $W_{s(D)}$ is the settling velocity of diameter (D) sediment particles, and B is a coefficient accounting for the mode of the sediment transportation (1-1.25: bed load, 1.25-7: suspension load, 7-30: wash load). In the present study, the grain-diameter of the coarsest 5% and 10% of the grain population was used for the calculation of $W_{s(D)}$ (Stoke's law) (Komar, 1985; Zeng et al., 1991; Ren et al., 1996).

Two types of turbidity currents occurred in Bryant Canyon during Oxygen Isotope Stage 6: 1) sand-rich turbidity flows, and 2) silt-rich turbidity flows. The sand deposits developed by the deposition of only a small portion of the suspended sediment load of the turbidity currents, and consequently a B value of 7 (suspended-load transportation) would probably yield the most reasonable estimation of their velocities. A similar approach is also adopted in the case of the silty turbidity currents. However, the extensive silt deposits on the overbank areas reveal that silt was also transported as wash-load, implying that a B value of 30 (wash-load transportation) would be the most reasonable. Solving equation 3, it is revealed that the sandy turbidity currents had velocities ranging from 331 to 414 cm/s, whereas the silty turbidity currents velocities of 27-61 cm/s, or even up to 162 cm/s (based on the over-banking silt deposits) (Table III-2). However, it must be kept in mind, that due to the fine-grained nature of the turbidity flows, and deposition due to loss of capacity (flow can not sustain in suspension all its sediment load, leading to sediment deposition independently of their grain-size) and not competence (flow can sustain in suspension only particles below a critical diameter), the above calculated flow velocities may be underestimated (Hiscott, 1994).

The sediment concentration of the turbidity currents can be estimated by the following modified chezy type equation (Komar, 1969, 1977):

$$U^2 = \frac{(\rho_s - \rho)}{\rho} C g h \frac{\sin \beta}{(1 + \alpha) C_f} \quad (4)$$

Where h is the thickness of the flow, β is the inclination of the canyon/channel, and α is a factor accounting for the drag at the upper surface of the flow (≈ 0.43). The remaining morphology of the canyon yields low gradients of $\sim 1^\circ$. The thickness of the turbidity currents is assumed to be equal or higher than the height of the canyon walls, due to their intense overflowing. However, the high transformation and distortion of the canyon initial morphology, by intense halokinetic processes, makes it almost impossible to determine the canyon wall height. A height of 200-400 m was assumed, which was based on the remaining

morphology of the canyon, and on other turbidity current studies involving intense overflowing and flow-stripping processes (Savoye et al., 1993; Hagen et al., 1994; Klaucke et al., 2000; McHugh and Ryan, 2000).

Solving equation 4 for the sediment concentration of the flows, it is concluded that the sandy turbidity currents were characterized by concentrations of $1.4 \times 10^{-3} - 0.45 \times 10^{-3}$ (3.71-1.19 g/l), whereas the silty turbidity currents were characterized by concentrations of $0.25 \times 10^{-5} - 21.5 \times 10^{-5}$ (6-570 mg/l). In both cases, we observe extremely low concentrations (resembling those of low-density turbidity currents) that especially in the case of the silt turbidites appear to be almost unrealistic. This is probably due to: 1) the intense flow stratification of the turbidity currents, and 2) a significant underestimation of the flow velocities (Piper and Savoye, 1993; Hiscott, 1994; Mulder et al., 1997; Kneller and Buckee, 2000; Mulder and Alexander, 2001).

Table III-2. Results of the funneled turbidity current velocities and sediment concentrations, based on the two methods described in the paper.

Turbidite facies	Grain-diameter used from the grain population	Grain diameter (μm)	Velocity (cm/s)	Concentration (volume %)
S2	5 % (B=7)	206	414	$7-14 \times 10^{-2}$
S2	10 % (B=7)	184	331	$4.5-9 \times 10^{-2}$
S2	Mode (B=7)	149	216	$2-4 \times 10^{-2}$
S3	5% (B=30)	38-31	40-61	$0.5-3 \times 10^{-3}$
S3	10% (B=30))	31-24	27-40	$0.2-0.24 \times 10^{-3}$
S3	Mode (B=30)	17-20	12-16	$1-3.3 \times 10^{-3}$
M5b,c	5 % (B=30,)	62.5	162	$1.1-2.15 \times 10^{-2}$
M5b,c	10 % (B=30,)	44	81	$2.7-5.37 \times 10^{-3}$
M5b,c	Mode (B=30)	29	34	$5-10 \times 10^{-4}$
Turbidite facies	Structure	Modal diameter (μm)	Velocity (cm/s)	Concentration (volume %)
S2	Upper stage plane formations	149	90-126	$3.32-13 \times 10^{-3}$
S3	Ripple and/or upper stage plane formations	17-20	38.6-86 (or higher)	$6-0.61 \times 10^{-3}$
S3	Ripple formations	17-20	14-54	$0.08-2.4-10^{-3}$

The M5b,c mud turbidite facies are located on the overbank areas of Bryant Canyon. The flow velocities, based on the structural characteristics of the deposited sediments, have been corrected for the drag reduction of the flows (30-50 % reduction of U_*). The sediment concentrations of the turbidity currents estimated by assuming a canyon-wall height of 200-400 m.

Areas Subjected to Overflowing Processes

Sediment cores and high-resolution 3.5 kHz subbottom profiles indicate that the Bryant and Eastern Canyon areas have been subjected to intense overflowing and flow-stripping processes (Fig. III-15). The overbank deposits are characterized by a thickness exceeding 50 m (neither the sediment cores, nor the 3.5 kHz profiles were able to penetrate through these deposits). Hemipelagic sediments and bioturbation structures are negligible in these deposits, inferring the frequent occurrence of overflowing turbidity currents. The sedimentology of the overbank areas is expressed by alternations and successions of mud turbidite facies.

According to the spatial distribution and organization of the mud turbidite facies, three types of overflowing areas have been distinguished: 1) overflowing areas of high energy, 2) overflowing areas of medium to low energy, and 3) overflowing areas of low energy. High-energy overflowing areas are represented by the presence of all mud turbidite facies, with facies M5 and M4 being dominant. Medium- to low-energy, and low-energy areas are characterized by successions of M3, M2, M1, and M2/1, M1 (M1 facies are dominant) mud turbidite facies, respectively. One of the first observations from the spatial distribution of the mud turbidite facies is the gradational fining of the sediment, moving away from the canyons. This information reveals that the spillover flows were spread over the low gradients of the overbank areas, acquiring a strong depletive character. It is intriguing that the low-energy mud turbidite facies (M3 to M1, and especially M2/1 to M1) are the most dominant in the study area. This suggests that the funneled turbidity currents were sufficiently confined to the canyons, with only their upper most diluted parts (wash load) to be capable of overflowing the canyon walls. However, these very diluted spillover flows were able to travel for very long distances (exceeding 15-20 km), and dictate the sedimentology of the surrounding canyon areas.

High-energy mud turbidite facies M5 and M4 are exclusively observed at the first turning point of Bryant Canyon, on the middle/lower continental slope (Fig. III-15). This implies that the sudden intensification of the overbank flows was due to the flow-stripping of the turbidity currents, as they were forced to change their flowing direction. Flow-stripping of turbidity currents is a process that has been extensively discussed by Piper and Normark (1983), Piper and Savoye (1993), and Savoye et al. (1993). The narrow occurrence of the high energy mud turbidite facies indicates that these high-energy flows (flow regime 1 to 5) were rapidly

dissipated, resulting in the deposition of M5 and M4 facies only adjacent to the canyon. The absence of high-energy mud turbidite facies on the latter turning point of Bryant Canyon is interpreted by: 1) the reduction of the turbidity currents thickness and intensity, after their flow-stripping at the first turning point, and 2) a possibly higher canyon wall at the second turning point that would allow for the spilling-over of only the most diluted, upper parts of the funneled turbidity currents.

One of the most important observations of this study is the organization of the mud turbidite facies into: 1) sequences grading from high- to low-energy facies (waning sequences), and 2) sequences grading rapidly from low- to high-energy facies and then gradually to low-energy facies (waxing-waning sequences) (Fig. III-16). In order to interpret the development of these sequences, the over-flowing/flow-stripping processes of the channelized turbidity currents would have to be visualized first. Overflowing of turbidity currents occurs when their thickness exceeds the height of the canyon walls. When this condition is met, it would be expected that the sedimentology of the overbanking deposits would reveal the nature of their parental funneled turbidity currents (waning, steady, or waxing). However, internal waves on the upper surface of the channelized turbidity currents complicate the progression of their overflowing, which in this case resembles successive surges, resulting in the deposition of successive mud turbidite facies (sequences). Consequently, the individual mud turbidite facies express only momentarily the nature and evolution of their parental funneled turbidity currents, which can only be evaluated by the sedimentological character of the mud turbidite facies sequences.

Based on the above information, the two types of overbanking sequences infer the existence of two types of funneled turbidity currents. The first type is a typical surge-like turbidity current that results in the deposition of waning mud-turbidite facies sequences. The origin of these flows is most probably from sediment failures on the front of the Stage 6 Mississippi River Delta (Hampton, 1972; Fisher, 1983; Piper et al., 1999). The second type of channelized turbidity currents is dealing with a short waxing initial stage reaching a pinnacle, and then they enter gradually into a latter waning stage. This peculiar flow behavior is typical of turbidity currents generated directly from hyperpycnal river plumes (Kneller, 1995; Mulder et al., 1998a, 1998b; Kneller and Buckee, 2000; Mulder and Alexander, 2001).

Turbidity currents generated directly by hyperpycnal river plumes have been implied for the British Columbia rivers, the Var River, and the Huange River (Prior et al., 1986; Zeng et al., 1991; Piper and Savoye, 1993; Klauke et al, 2000; Migeon et al., 2001). Mulder and Syvitski

(1995) stated that due to the very low average suspended sediment concentration (~ 0.8 g/l) of the Mississippi River, it is not likely (not even during flood conditions) to exceed the critical concentration (~ 42.7 g/l), needed for the production of hyperpycnal turbidity flows. However, Parsons et al., (2001) concluded, through laboratory experiments, that hypopycnal river plumes as low as 1 g/l are able to produce hyperpycnal (bottom-riding) flows, through convective instabilities. The average concentration of the Mississippi River discharges is still lower than the limit of 1 g/l and probably was even lower during the dry glacial Stage 6. However, it is possible that the river sediment concentration was achieving periodically, during flood conditions, high enough values that could result in the production of hyperpycnal turbidity flows.

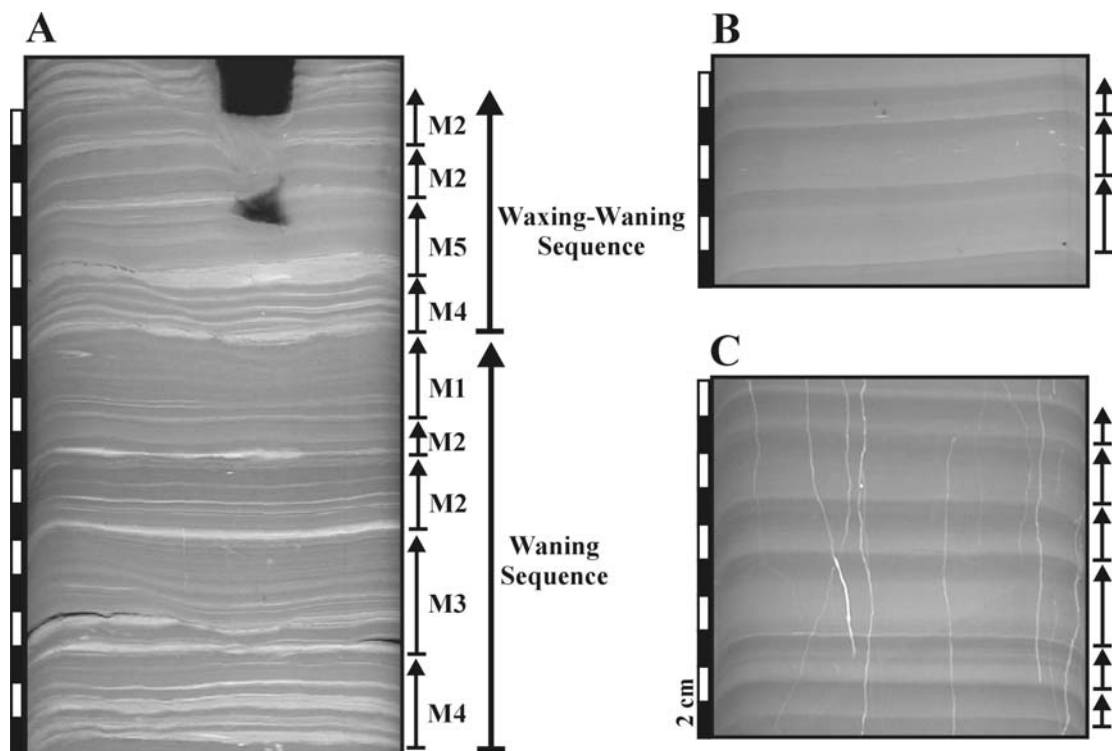


Fig. III-16. X-ray radiographs (negatives) of: 1) waning and waxing-waning coarse (high-energy) mud-rich turbidite facies sequences (A), and 2) waning (B) and waxing-waning (C) fine-grained (low-energy) mud turbidite facies sequences. The low-energy sequences consist entirely of successive M1 facies, where the relative intensity of their resultant flows is inferred by the thickness and grain-size (lighter shades indicate siltier sediments) of the units.

Flow Properties

Previous studies of spillover flows, from overbank deposits and mud wave fields of deep-sea fans, reveal that these features are characterized by velocities of 10-20 cm/s up to 100 cm/s, and have thickness of 100-800 m, and low suspended sediment concentrations of 26 to 2500 mg/l (Normark et al., 1980; Stow and Bowen, 1980; McHugh and Ryan, 2000; Nakajima and Satoh, 2000; Wynn et al., 2000; Gervais et al., 2001). It was discussed earlier in this paper that a complete mud turbidite sequence is developed by the passage of four successive flow regimes. However, the distinction of five overbanking mud turbidite facies reveals that spillover flows may consist of any waning spectrum of flow regimes. The determination of the velocity fields, under which each flow regime is developed, is of high importance since they can provide detailed information about the time and spatial evolution of the spillover flows (Fig. III-17).

Stage 1 flow regime occurs only when the flow velocity is high enough to sustain all of the sediment under suspension, and yet there is enough energy for the erosion and incorporation of seafloor sediments (Parker, 1982; Fukushima et al., 1985). Since no significant erosion is developed at the bases of the mud turbidite facies M5, it is concluded that the flows of this stage were close to an erosional-depositional equilibrium. A lower velocity limit of stage 1 could be in the range of 10-25 cm/s. These velocities have been estimated from laboratory experiments, and they represent values above which fine-grained sediments are not deposited (McCave and Swift, 1976; Stow and Bowen, 1980).

Stage 2 flow regime velocities can be estimated by two ways. The first is based on the sedimentary structures (microlaminations and ripples), observed in the basal silt zone of M5b facies, which infers velocity values of 14-86 cm/s (accounting for the drag reduction of the flows). The second estimation of the flow velocities is based on the application of equation 3, solved for the coarsest 5% of the grain population. Since the deposition from the spillover flows occurs due to loss of capacity, it is considered that the majority of the silt population was transported as suspended load ($B \approx 7$). Flow velocities according to this method range between 10 and 38 cm/s. It is observed that the velocity values of this stage are overlapping with those of the stage 1 flow regime. This is due to the fact that the domination of the erosional or depositional processes of the turbidity currents are not exclusively depended on their velocities, but also on their suspended sediment load capacities.

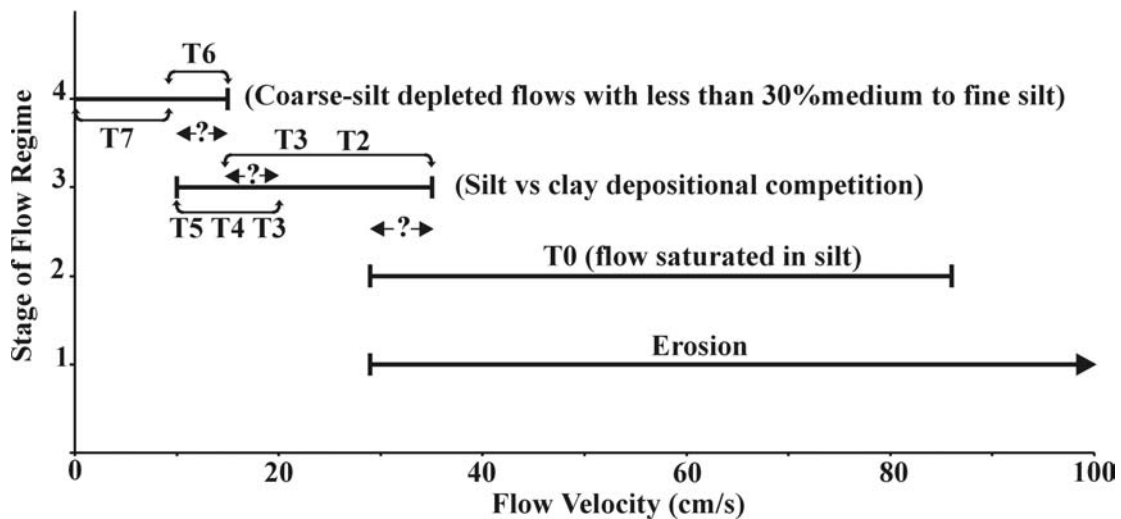


Fig. III-17. Diagram displaying the velocity fields of the four flow regime stages under which the mud turbidite facies were deposited. Stage 1 flow regime characterizes energetic flows that can retain their entire sediment load in suspension. Stage 2 flow regimes are characterized by fast running and rich in silt flows that allow for the deposition (loss of capacity) of the silt fraction only. Stage 3 is characterized by a vigorous silt vs clay depositional competition, leading to the development of the alternated silt and mud laminae of T2, T3, T4, and T5 divisions of Stow and Shanmugam (1980). The final stage 4 flow regime consists of two waning steps: 1) depleted in silt flows with velocities higher than 10 cm/s (flocculation processes are dominant and intensified leading to the deposition of graded mud, T6), and 2) highly decelerated, almost stationary, sediment clouds (deposition of massive mud, T7).

Stage 3 flow regimes are characterized by velocities, where the re-entrained cohesive sediments in the main flow (through the cyclic streak-bursting mechanism) are lesser than those settling in the boundary layer of the flow. Manning and Dyer (1999) and Dyer and Manning (1999) observed in laboratory experiments that there is a critical shear of 0.3 to 0.35 N/m^2 , below which the floc size is increased with increasing clay concentrations, and vice-versa for higher shear values. Similarly, they observed that the floc settling velocities were highest for the highest clay concentrations at low shear values ($< 0.25 \text{ N/m}^2$), and highest for the lowest clay concentrations at high shears ($> 0.25 \text{ N/m}^2$). They attributed the decrease of the floc size, at high shear and clay concentrations, to the higher collision rates of the flocs and their violent interactions that result in their breakage. Inversely, at low shear values the collisions between the flocs are gentler, leading to their further aggregation and development of higher order flocs with increasing clay concentrations. According to the findings of the above researchers, it would be acceptable to assume that these critical shear values may also represent

a boundary, above which the streak-bursting mechanism at the boundary layer overcomes the drag reduction effects of the cohesive sediments, and contributes to their substantial disaggregation and ejection back into the main flow. Consequently, these shear values (0.25-0.35 N/m² or 29-35 cm/s) may represent an upper threshold value for the development of stage 3 flow regime. In support of the above velocity values are the silt ripples observed in the silt laminae of facies 4 deposits (T2 division), which require velocities higher than 14-20 cm/s for their development.

It was mentioned previously that the grain-size distributions of the mud turbidites reveal a cross-point at 10-5.2 μm , interpreted as a critical diameter, below which sediment particles do not settle individually but only as aggregates. Velocities of 10-11.6 cm/s, under which sediment particles of the above critical diameter can be sustained in the flows, are estimated using the diagram of McCave and Swift (1976). Velocities below these threshold values would cause the deposition of the entire silt population, due to the incompetence of the flows. However, spillover flow deposition occurs because of the loss capacity, and consequently velocity values larger than these minimum threshold values are required for the gradational accumulation of silts and clays in the boundary layer, and their cyclic deposition (silt and mud laminae).

Sedimentological descriptions and grain-size analysis of stage 4 flow regime deposits (M1 facies) reveal that: 1) they are characterized by normal grading, 2) silt grains with a diameter larger than the critical (up to 31 μm) are still present but with the clay fraction to dominate (>70%), 3) the silt to clayey-silt laminae of the previous stage are replaced by slightly siltier silty-clay laminae, and 4) they are covered by a uniform silty-clay layer/laminae, which is slightly coarser. The first three observations indicate that stage 4 flow regimes are: 1) characterized by velocities close to the lower limit of stage 3 (justifying the presence of the silt grains and the siltier laminae), 2) highly depleted in the silt fraction allowing flocculation processes and deposition to dominate in the flows, and 3) gradually decelerating allowing the development of their normal grading (intensification of the deposition of aggregated sediments). An upper velocity boundary of this flow regime can be estimated from the presence of silt grains, with diameter up to 31 μm , which reveal flow velocities up to 15 cm/s (estimated using the diagram of McCave and Swift, 1976). The fourth observation infers the existence of a final depositional step, at which the flow becomes incompetent and massive deposition occurs from an almost stationary sediment cloud.

It is observed that the velocity fields of all flow regimes are overlapping and that there are no absolute velocity boundaries. This is ascribed to the dependence of the flow regimes not only on the velocities of the low-density turbidity currents, but also on their suspended sediment concentrations, silt to clay ratios, clay mineralogy, and suspended organic matter, which control the depositional rates, intensity of the flocculation processes, and drag reduction of the flows.

Conclusions

Erosional and mainly depositional processes of turbidity currents dictated the sedimentology of Oxygen Isotope Stage 6, in the Bryant Canyon area. The origin of the turbidity currents is either by sediment slope failures on the front of an ancestral Mississippi River Delta, or directly from hyperpycnal river plumes. Two sedimentological environments have been distinguished in the area: 1) intracanyon environments, and 2) overbanking environments that are pervasive along the canyons.

The suspended sediment load of the funneled turbidity currents consisted of sand-silt or silt, with substantial amounts of clay. Funneled turbidity currents were characterized by a uniform and waning flow character, with deposition to occur almost entirely from their diluted and slowly moving end members (S1 and M1 to M5 turbidite facies). However, main flow (head and body) turbidity current deposits (S2 and S3 turbidite facies) were also occurring episodically due to: 1) the reduction of their suspended sediment load capacity due to their intense flow-stripping at the turning points of the canyons, and 2) flow instabilities developed by morphological irregularities of the canyon floors. All stage 6 turbidity currents were probably highly stratified with the highest concentrations and velocities occurring along a narrow and highly erosional zone. The rest of the canyon floors were characterized by deposits similar to those of levee and overbank formations. Maximum velocities of the turbidity currents were in the range or higher than 38.6-414 cm/s.

Spillover processes of the channelized turbidity currents were dominant all along the canyons, and were significantly intensified on the turning points of the canyons by flow-stripping processes. These spillover flows were spread over the low inclinations of the canyon overbank areas, acquiring a strong depletive and waning character. Deposition of these flows was occurring gradually, due to loss of capacity, leading to the development of complete/middle-cut-out (high-energy: M5 and M4 facies), or base-cut-out (low-energy: M3, M2, and M1 facies) sequences of Stow and Shanmugam (1980). The great extent of the

overbank deposits around the canyon indicates that spillover flows were able to travel distances exceeding 15-20 km. It has been demonstrated that a complete mud turbidite sequence is deposited by the spectrum of four waning flow regimes. The development of each flow regime depends on the: 1) flow velocity, 2) suspended sediment concentration relative to the capacity of the flows, 3) silt to clay ratios and clay mineralogy of the suspended sediment load, and 4) organic matter concentration. The first two factors control the competition between the erosional and depositional processes of the turbidity currents, whereas the last two factors control the intensity of the flocculation processes, the drag reduction of the flow, and consequently the silt to clay depositional dominance. The first two flow regimes are characterized by velocities higher than 29-35 cm/s, whereas in the range of 29-86 cm/s there is an active competition whether erosion or deposition will dominate in the flow (Fig. III-17). The third flow regime represents a cyclic deposition of silt and mud laminae, due to the cyclic fluctuations of the shear in the boundary layer of the flow (11-35 cm/s). The final flow regime is characterized by mud (flocculation) dominated depositional flow conditions (< 15 cm/s), where graded mud layers are developed. This regime is followed by the massive deposition of an almost stationary sediment cloud.

Spillover flows are controlled by: 1) the nature of the funneled turbidity currents (thickness and intensity), and 2) the canyon/channel morphology (height and possible meandering). Internal waves on the upper surface of the funneled turbidity currents cause overflowing to occur in successive surges developing sequences of overbank mud turbidite facies, rather one discrete depositional unit. Consequently, each individual overbank mud turbidite facies represent only momentarily the nature of their parental channelized turbidity currents (waning, waxing, stable or a combination of them), which can only be inferred by the sedimentological character of their overflowing mud turbidite facies sequences.

CHAPTER IV

SLOPE INSTABILITY PROCESSES CAUSED BY SALT MOVEMENTS

Introduction

The destructive force of slope instability processes has been known from ancient times. Pausanias (2nd century AD, *Achaica*, Book 7 Κεφ, XXIV, 12) and Strabo (68 BC – 25 AD, *Geographica H'*, 7, 2, p. 384-385) were the first to describe the genesis and evolution of a large slump responsible for the destruction and submergence of the ancient town Eliki on the western Gulf of Corinth, Central Greece, in 373 BC. However, it is only during the last three to four decades that geologists realized the significance of sediment failures and mass transport on the geomorphological and sedimentological evolution of submarine environments. Prior et al. (1981, 1984) and Prior and Bornhold (1988) pointed out the importance of slope instability processes on the morphology and sedimentary processes of the British Columbia fjord delta fans, and according to their studies most failures occurred by liquefaction of delta front sediments due to excessive regional sedimentation. Similarly, Elverhøi et al. (1997), Dimakis et al. (2000), and Laberg and Vorren (2000) explained the downslope sediment propagation of the Norwegian-Barents Sea continental margins by extensive failure occurring in thick sequences of clay-rich glaciogenic sediments on the upper slope. Ferentinos et al. (1988), Papatheodorou and Ferentinos (1993, 1997), and Piper et al. (1985, 1999) pointed out the significance of earthquake-triggered sediment failures on the tectonic trench, Gulf of Corinth, and St. Pierre continental slope, Grand Banks.

The complex interaction of halokinetic and slope instability processes is the main factor controlling the geomorphological and sedimentological evolution of the intraslope basins of the northwest continental slope of the Gulf of Mexico. High-resolution seismic data, combined with long (up to 15 m) sediment cores from three basins in the Bryant Canyon area, northwest Gulf of Mexico (Fig. IV-1), are used to determine the interactions between halokinetic and slope instability processes, and their cooperative contribution in the morphology of the basins, and the spatial and time evolution of sediment failures in the area. A preliminary study of the slope stability of the Bryant Canyon area has been done by Tripsanas et al. (2003a).

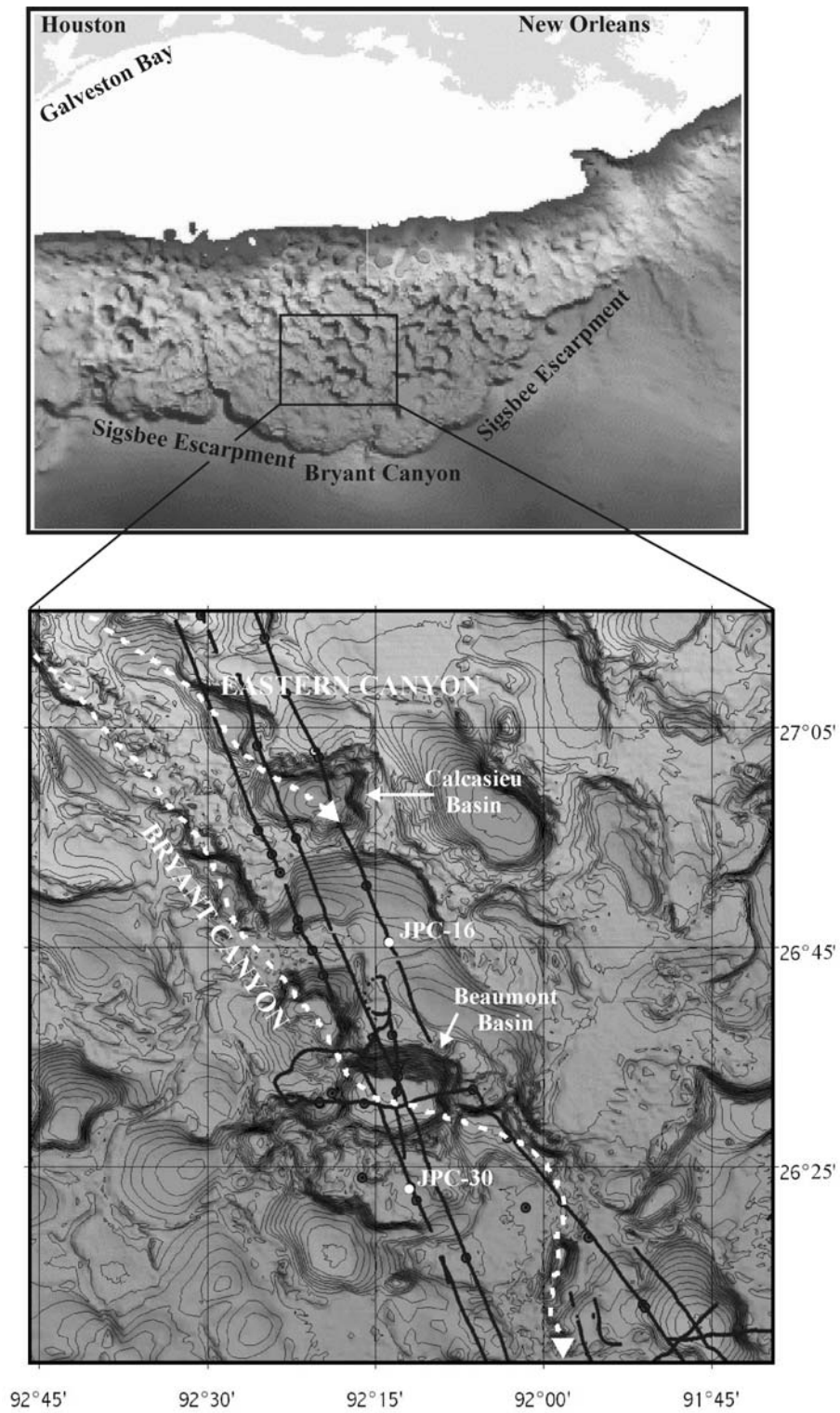


Fig. IV-1. Bathymetric/morphological map of Bryant Canyon area, focusing on the three studied intraslope-interlobal basins.

Geology of Bryant Canyon Area

Bryant Canyon is located on the northwest continental slope of the Gulf of Mexico, southwest of the present day Mississippi Delta (Fig. IV-1). Thick (up to 8 km) allochthonous salt masses, lying below Cenozoic sediments have resulted, through various halokinetic processes, in a very complex morphology. Numerous intraslope-interlobal and intraslope-supralobal basins with a relief in excess of 150 m, divided by sills and plateaus (representing shallow salt structures) are characteristic of the morphology of the area (Bryant et al., 1990; Lee, 1990; Lee et al., 1996). Intraslope-interlobal basins are usually of higher relief with steeper flanks and are formed by coalescing salt-lobes, whereas supralobal basins are subsiding basins on a salt sheet or nappe (Bouma, 1981; Bryant et al., 1990, 1991; Lee, 1990). The intralobal basins usually result from the diapiric blockage of inactive submarine canyon complexes (Bouma, 1982; Bouma et al., 1990; Bouma and Roberts, 1990; Saterfield and Behrens, 1990).

Bryant Canyon and Eastern Canyon systems are the primary erosional features in the investigated region (Fig. IV-1). Lee et al. (1996), and Twichell et al. (2000) have discussed extensively the formation and destruction of Bryant and Eastern canyon systems. Their formation initiated at the beginning of the glacial Oxygen Isotope Stage 6, by the development of an ancestral Mississippi River Delta at the shelf edge and/or upper continental slope. That led to the generation of numerous gravity flows, either by sediment failures of the delta front, or directly from hyperpycnal river plumes (Chapters II and III). In a first stage the gravity flows propagated downslope, developing a small erosional canyon on the upper continental slope, and were eventually confined in the most adjacent Stage 6 prevalent intraslope basins, which led to the formation of ponded intraslope-intrabasinal fan systems (channel-levee complexes and sheet sands). As soon as an intraslope basin was sufficiently infilled, the gravity flows were propagating to the next downslope intraslope basin, cutting through the structural saddles (sills/plateaus) between them, and leading to the development of a new ponded fan system. Repetitions of this infilling-bypassing process led to the formation of the peculiar Bryant and Eastern Canyon systems, which in the infilled intraslope basins had the form of well-developed channel-levee systems, and on the sills/plateaus separating the basins, had the form of typical V-shaped erosional canyons (Lee, 1990; Satterfield and Behrens, 1990; Twichell et al., 2000). The well-developed deepsea fan system at the mouth of Bryant Canyon

indicates that, at some point during Oxygen Isotope Stage 6, Bryant Canyon evolved into an unconfined river-sourced canyon system, acting as a conduit for Mississippi River sediments into the Sigsbee Abyssal Plain of Gulf of Mexico (Chapters II and III).

The existence of such erosional/depositional environments certainly disturbed the sensitive balance of the underlying salt masses, which, through differential sediment loading, tended to obliterate and transform the canyon morphology (uplifting on the erosional parts of the canyons, and collapsing underneath the infilled intraslope basins) (Lee, 1990; Lee et al., 1996; Twichell et al., 2000). However, coupled erosional-depositional processes of the gravity flows were balancing the salt movements during the Oxygen Isotope Stage 6. The destruction of Bryant and Eastern Canyons occurred after their abandonment, during the beginning of the interglacial Oxygen Isotope Stage 5 (94-125 ky B.P.), due to the confinement of most of the alluvial sediments on the wide continental shelf of the northwest Gulf of Mexico (Chapter II).

This paper is based on the study of three intraslope basins. Beaumont and Reveille Basins are located on the middle/lower slope, along the path of Bryant Canyon, whereas Calcasieu Basin is located at the terminal end of Eastern Canyon. There are two main reasons that led to the genesis of those basins: a) increased subsidence on the underlying salt nappe of the prominent infilled basins that the canyon systems used to prograde downslope, and b) the blockage of the canyons by salt diapirs after their abandonment.

Sediment Stratigraphy of Bryant Canyon Area

It was stated in Chapter II that the tranquil environments (sills and plateaus) of Bryant Canyon were characterized by continuous and undisturbed sedimentation during the last 125 ky. Six sedimentary units were recognized in the cores that were strongly correlated with Oxygen Isotope Stages 6 to 1, and display characteristic bulk density profiles (Fig. IV-2). The dating of the slump/gravity-flow deposits in the cores is based on the following six sedimentary units:

Unit A (Isotope Stage 1; up to 11.16 ky B.P.): Typical hemipelagic sediments.

Unit B (last deglaciation event, 11.16-18.17 ky B.P.): Dark greenish gray to greenish gray, partially bioturbated, organic-rich clay (34-48 cm thick) that is succeeded downwards by hemipelagic sediments (10-28 cm thick).

Unit C (Isotope Stage 2 and ending of Stage 3, 18.17-31.85 ky B.P.): Closely-spaced, normally-graded (0.2-5 cm thick) to mottled/lenticular (3-20 cm thick), clayey-silt to silty-clay layers,

interbedded in hemipelagic sediments. On the upper to middle/lower continental slope the silty layers are interpreted to originate from the gradational deposition of low-density, fine-grained turbidity currents, whereas on the middle and lower part of the lower continental slope by bottom-riding, low-density, fine-grained sediment flows driven by bottom currents.

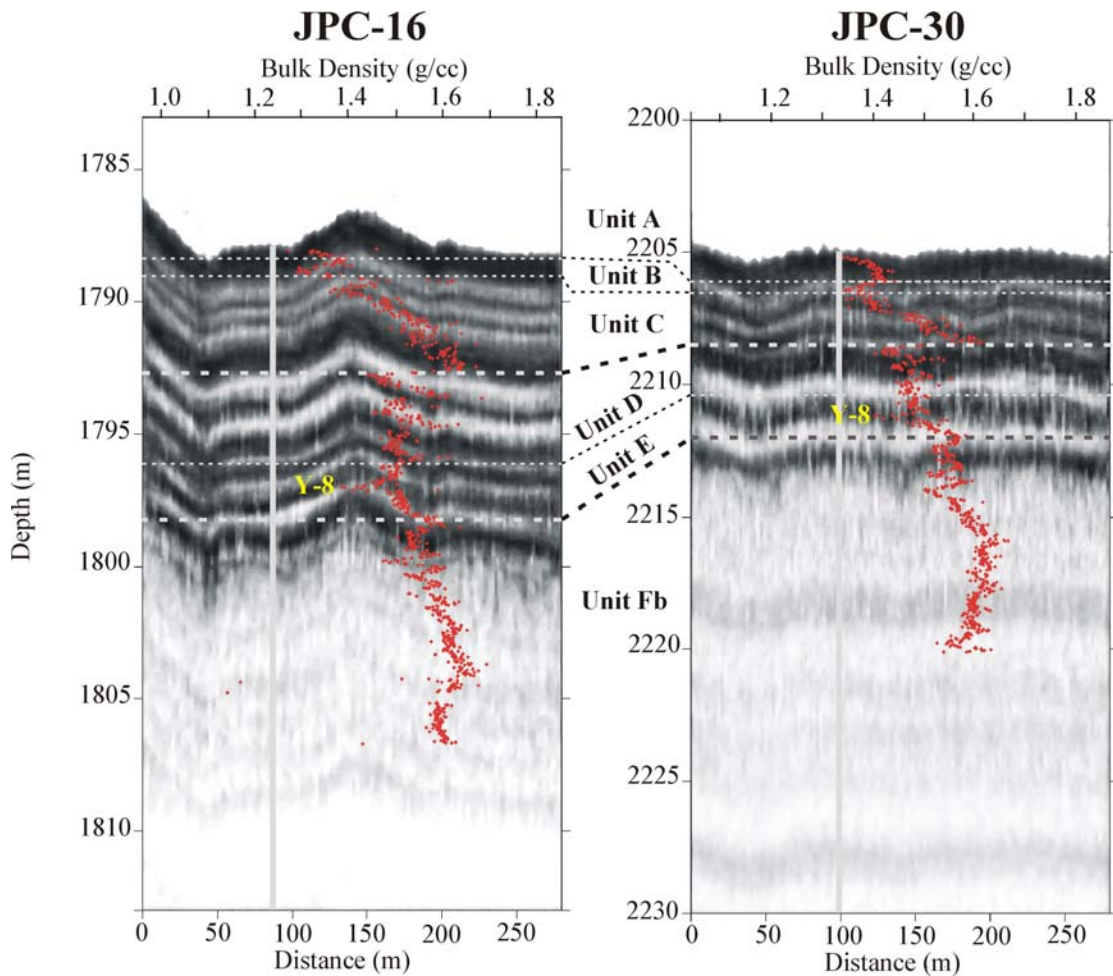


Fig. IV-2. Image displaying the bulk density profiles, and associated sedimentological units (Chapter II) of two typical sediment cores from the Bryant Canyon area, along with their corresponding 3.5 kHz subbottom profiles. The gray line indicates the location of the cores on the 3.5 kHz profiles. The locations of the cores are displayed in Figure IV-1. Y-8: Y-8 ash layer (84 ky B.P.).

Unit D (Isotope Stages 3 & 4, 31.85-71 ky B.P.): Hemipelagic sediments that are interbedded by a few isolated and irregularly-spaced, normally-graded (0.2-5 cm thick) to mottled (3-20 cm thick), clayey-silt to silty-clay layers. The interpretation of the silty layers of unit D is similar to the interpretation of the silty layers of unit C.

Unit E (Isotope Stage 5, 71-125 ky B.P.): Hemipelagic sediments, interbedded by the Y-8 ash layer, dated at 84 ky B.P.

Units F (Isotope Stage 6): Sand/mud thin-bedded (Fa) and fine-grained (Fb) turbidites, which are related to turbidity currents flowing through the Bryant and Eastern Canyon systems. The sandy deposits of unit Fa represent intracanyon deposits, whereas the mud turbidites of unit Fb overbank deposits.

Methods

Acoustic subbottom information from the three basins was collected during the R/V *Gyre* 1998 cruise, using the A&M Deep-tow system, equipped with a 3.5 kHz sub-bottom profiler and a 100 kHz side-scan sonar, towed thirty meters above the seafloor. Forty-eight long piston cores (up to 20 m long: JPC) were collected with the WHOI Jumbo Piston Corer, and sixty-two gravity (LGC) cores were retrieved from the Bryant Canyon area during a subsequent cruise in 1998 on the R/V *Knorr*. Bulk density and P-wave velocity profiles were derived from all cores, utilizing a GEOTEK Multi-Sensor Core Logger. Twelve JPC and three LGC cores are discussed in this paper. Four JPC-cores, presented in this study, were split lengthwise; one half was archived, while detailed optical descriptions at the millimeter-level scale and high-resolution photographs were obtained from the other half. X-ray radiographs were also taken over the entire length of the cores by producing 1-cm-thick sediment slabs. This was an attempt to find sedimentary structures not visible to the naked eye. The analysis of the remainder of the cores was mainly based on bulk density profiles. Additionally, descriptions of ten USGS cores were included in this study to fill gaps in the data of areas from where no JPC or LGC core was available (Twichell et al., 2000; Nelson, unpublished data).

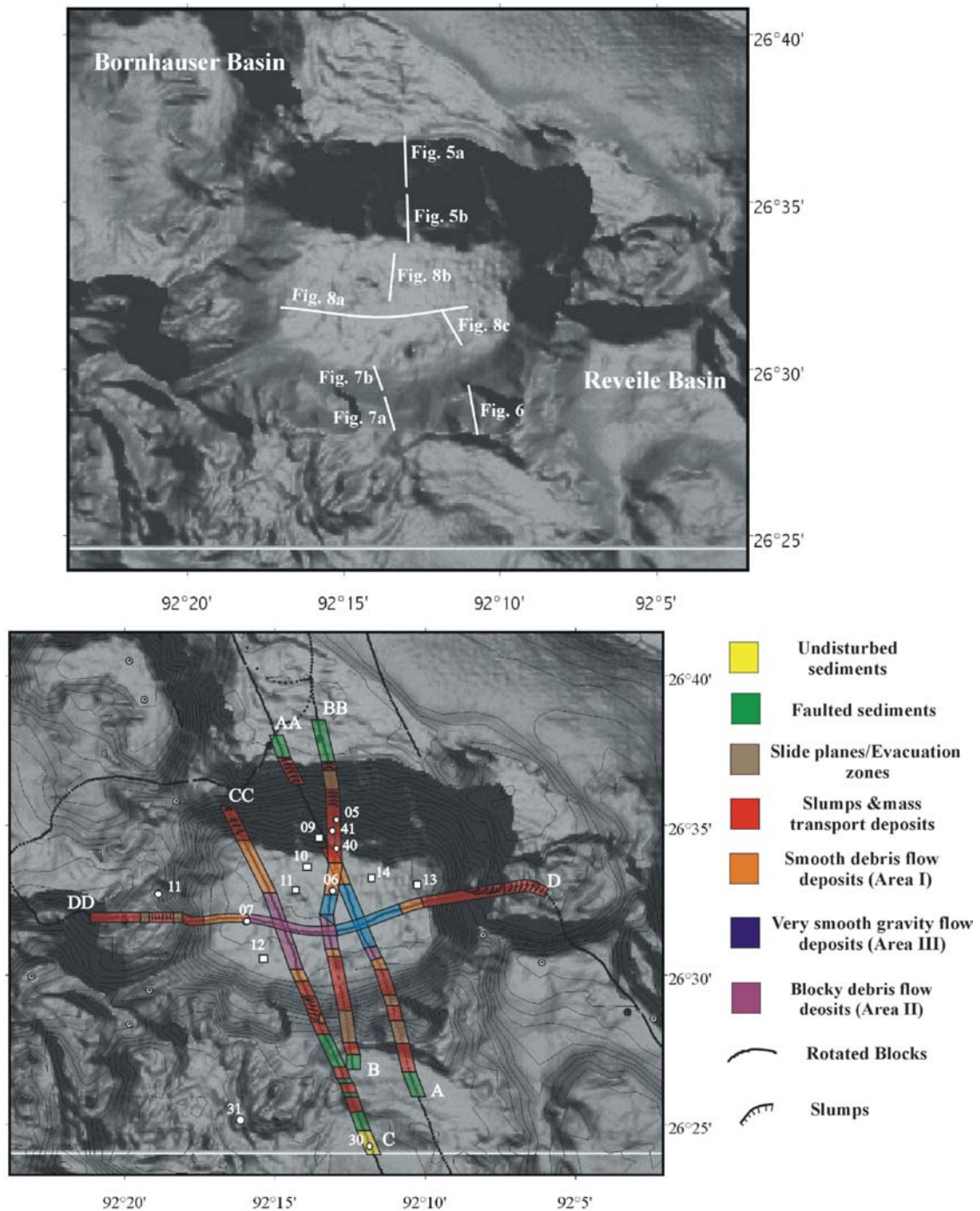


Fig. IV-3. Bathymetric and geomorphological maps of Beaumont Basin. The white lines indicate the locations of the 3.5 kHz profiles and side-scan sonar images that are displayed in the text. White circles and squares indicate the locations of the JPC and USGS sediment cores, respectively. The contours in the bottom image represent isobaths at 50 m intervals.

Beaumont Basin

Geomorphology

Beaumont Basin is located on the middle/lower continental slope of the northwest Gulf of Mexico, at a depth of about 2000 m (Fig. IV-1 and IV-3). It has a nearly square shape (16 km long and 18 km wide) and is characterized by a very high relief (600 up to 850 m) and steep flanks with gradients ranging between 4° and 14°. It communicates with Bornhauser and Reveille Basins through a 650 m and 550 m high sill, respectively. Both sills represent shallow salt structures (Lee, 1990; Lee et al., 1996). Bathymetric/morphological maps (Fig. IV-3) of Beaumont Basin reveal the presence of two slopes types: a) highly inclined slopes with very wide, elongated depressions of very low relief (< 30 m), and b) steep slopes that have been dissected by canyon-like to bowl-shaped elongated landslide troughs of high relief (greater than 100 m).

Uniform and highly inclined flanks (about 9°) are characteristic of the northern and northeastern flanks of the basin. Seismic data reveal (Fig. IV-4 and IV-5) that these areas have been extensively 'exfoliated' by partially overlapped sets of successive, widespread, adjacent retrogressive slumps/slides, that tend to evolve in discreet stratigraphic horizons (weak layers). The 'exfoliated' nature of the flanks, in combination with the presence of refailed sheet-like (15 to 20 m thick), and lens-like debris-flow deposits on the lower reaches and base of the flanks, indicates that the majority of sediment failures translated into debris flows that propagated onto the basin floor. Lineations on the lower flanks support the idea of gravity flows/mass transport material passing over the region.

Canyon-like landslide troughs are developed almost exclusively on the southern and western flanks of Beaumont Basin (Fig. IV-3 and IV-4). They are isolated, downslope narrowing and thinning features of high relief (50 to 200 m), and limited upslope by a well-developed headscarp (up to 200 m high and 1 to 3.5 km wide). Sub-bottom profiler data reveal that canyon-like troughs consist of several superimposed evacuation zones producing a step-like topography with the upper slide planes to cut deeper into the sediments and through lower slide planes/evacuation zones (Fig. IV-6). Such indicates that they originated as deep, channelized, retrogressive slumps that transformed into debris flows. Longitudinal lineations and local debris piles, that have been smoothed-over by a thin drape of hemipelagic sediments

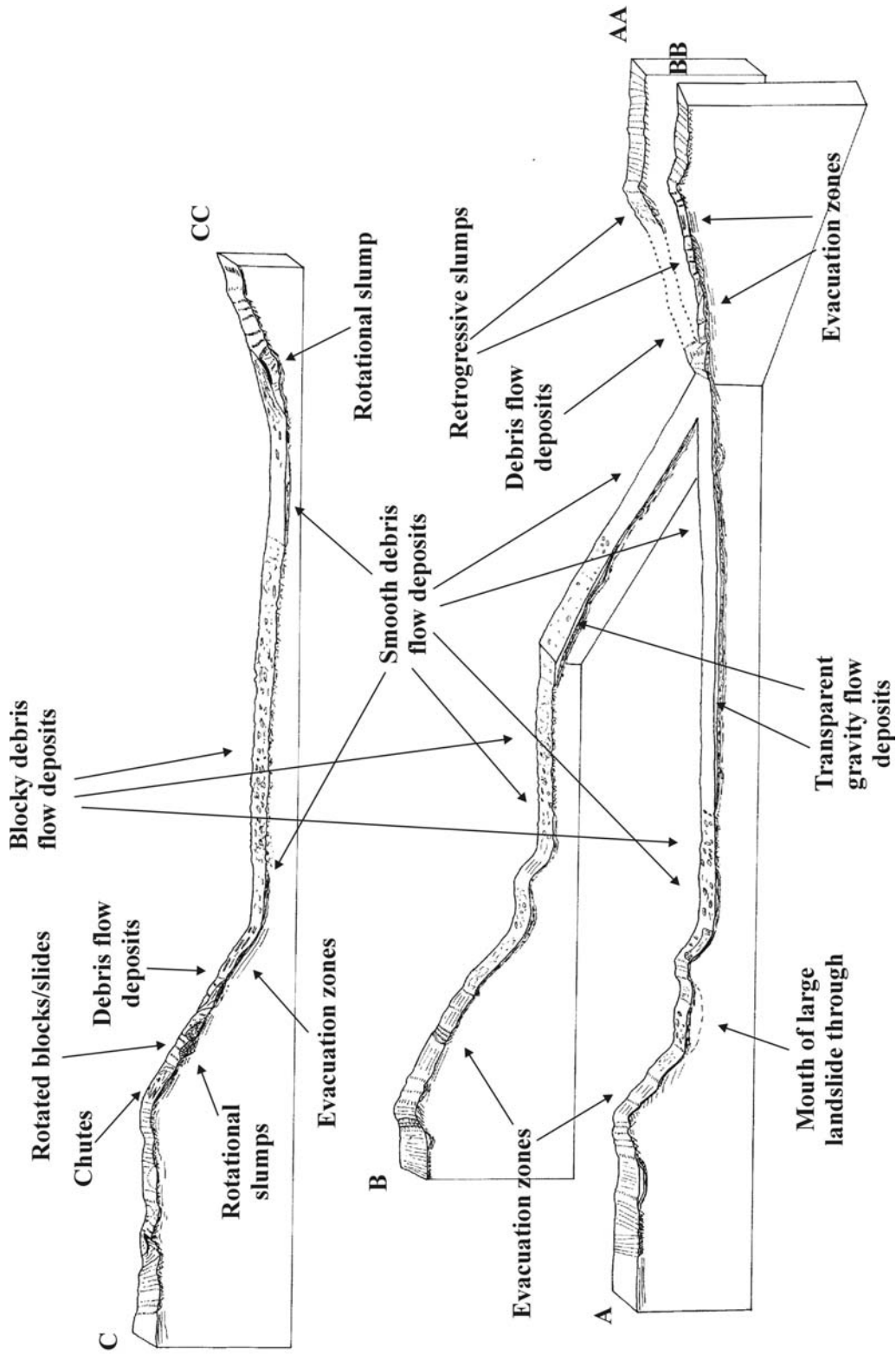


Fig. IV-4. Schematic illustration of three seismic lines from Beaumont Basin. The locations of the lines are shown in figure IV-3.

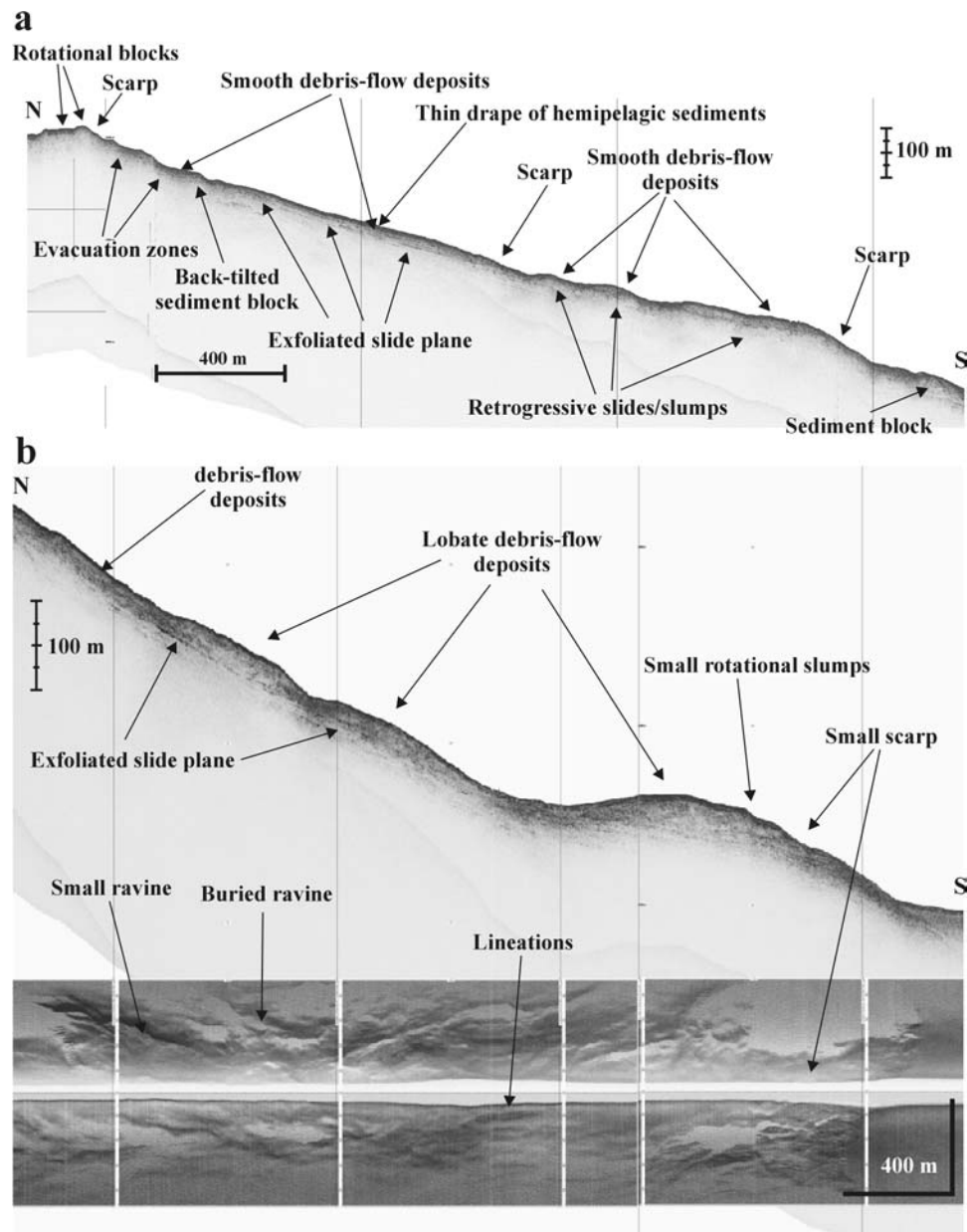


Fig. IV-5. Image displaying 3.5 kHz subbottom profiles and side-scan sonar images from the northern flank of Beaumont Basin. (a) Exfoliated slide plane on the upper flank that is covered by a thin drape of hemipelagic sediments and debris-flow deposits that are disturbed downslope by a younger set of retrogressive failures. (b) Exfoliated slide plane on the lower flank that is covered by sheet and lens-like debris-flow deposits. The lens-like debris-flow deposits of the lower flank tend to develop at the mouths of small ravines. The ravines are probably connected to small upslope liquefied-type failures that were initiated by either sudden loading of the sediments by passing over debris flows, or the accumulation of a thick series of failed sediment on the steep slopes. Note that both exfoliated slide planes are oriented parallel to the layering of the underlying sediments, and to the flank inclinations. That indicates that the failures developed on discrete and widespread stratigraphic horizons (weak layers), through which large slices of the flank collapsed. The locations of the survey lines are shown in Figure IV-3.

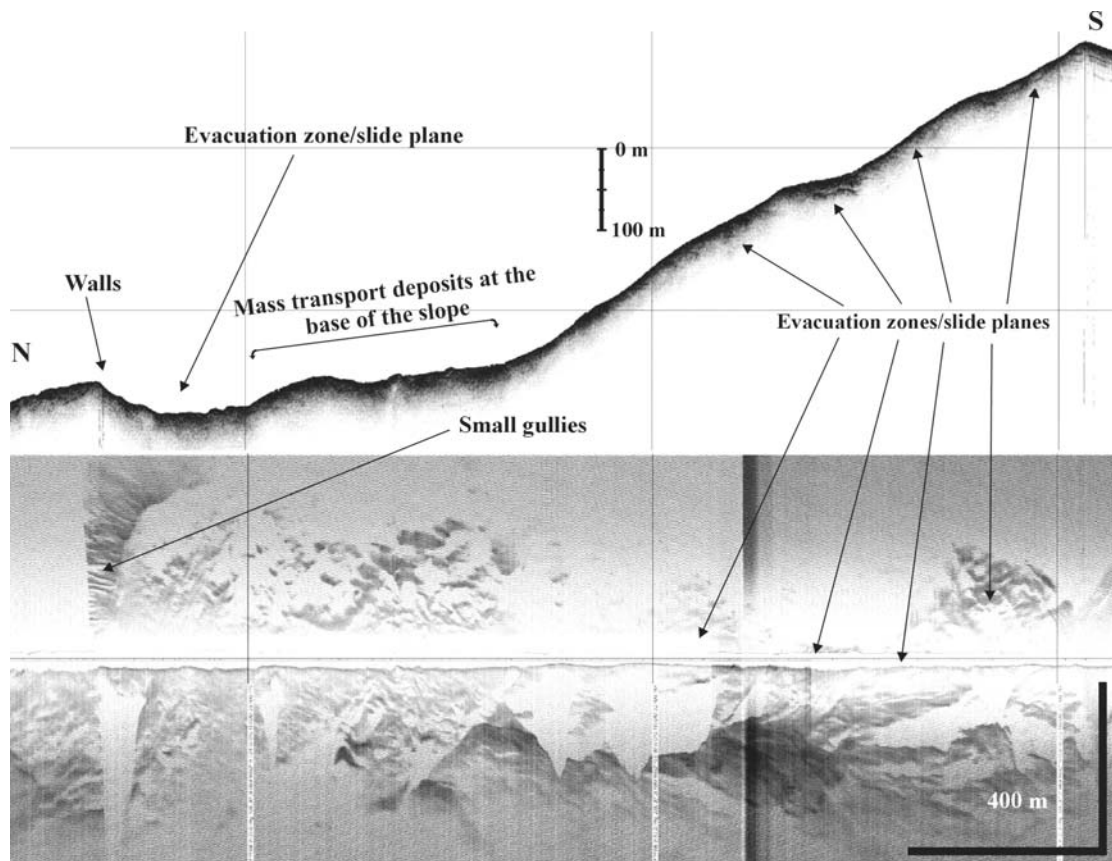


Fig. IV-6. Image displaying 3.5 kHz subbottom profile and side-scan sonar image of the complex geomorphology of the canyon-like landslide troughs. The seismic line crosses the foot of a large canyon-like landslide trough and moves upslope along the thalweg of a secondary canyon-like landslide trough. Note that the floor of the secondary landslide trough consists of successive evacuation zones, revealing that it has been resulted from the development of deep, channelized, retrogressive slumps. The secondary trough was probably created by the extensive erosion of gravity flows at the base of the walls of the larger trough. The absence of extensive mass-transport deposits in the canyon-like landslide troughs infers that the majority of the slumps translated into debris flows and were transported to the floor of Beaumont Basin. The location of the survey line is shown in Figure IV-3.

(about 3 m thick), characterize the evacuation zones. On the 3.5 kHz seismic profiles, the surface of the evacuation zones is represented by a sharp, prolonged echo with no further sound penetration, indicating the coarse and/or stiff nature of the canyon sediments.

The areas surrounding landslide troughs are characterized by steep slopes (14 to 18°), and bowl-shaped to elongated depressions of low relief (< 30 m). The upper parts of the flanks are characterized by groups of rotated blocks and rotational slumps/slides. The middle and lower flanks are replaced by successive, exfoliated slide planes that are covered by two types of

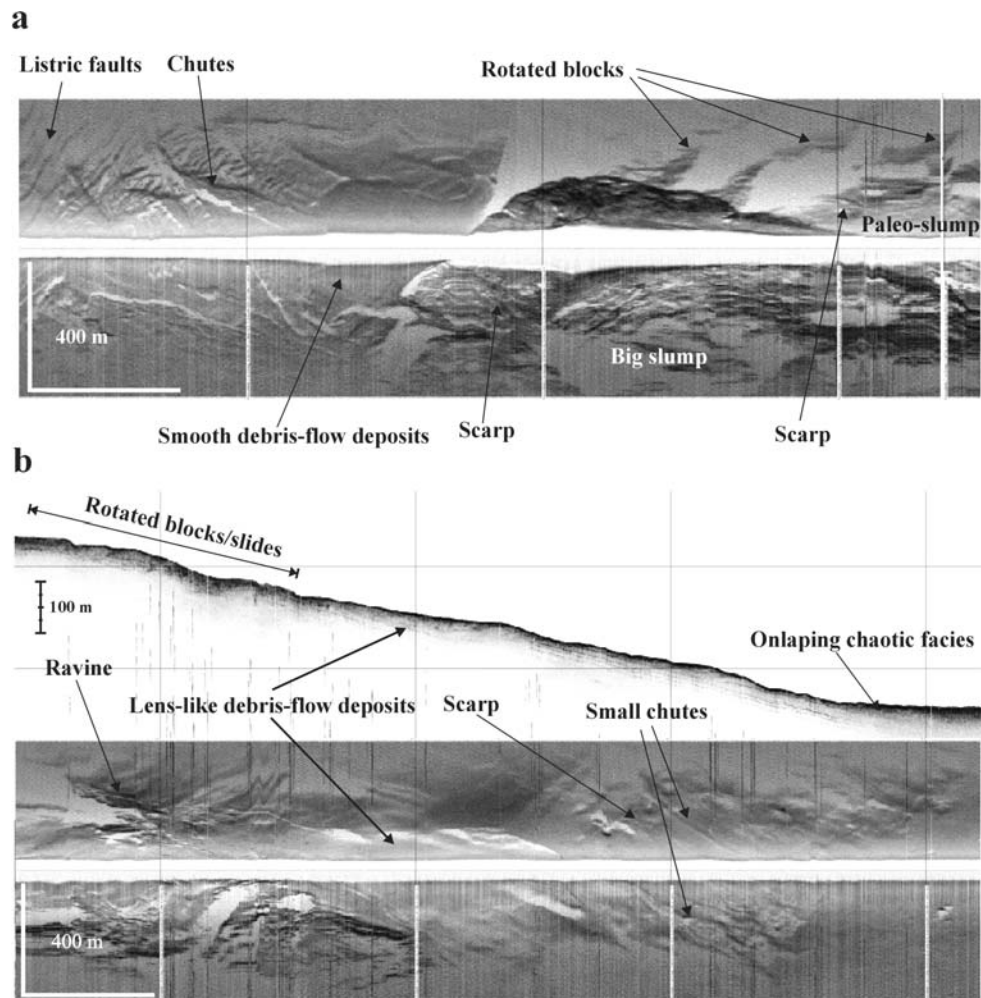


Fig. IV-7. Image displaying 3.5 kHz subbottom profile and side-scan sonar images from the (a) upper and (b) lower parts of the inter-trough areas on the southern flank of Beaumont Basin. Note how the younger big slump cuts through the older one (paleo-slump), and that the upper part of the southern flank (a) is characterized by rotated blocks and isolated slumps, compared to the exfoliated nature of the northern flank of Beaumont Basin (Figure IV-5). The locations of the survey lines are displayed in Figure IV-3.

debris-flow deposits: 1) the ones that had moved across flanks, and 2) well-preserved, lens-like debris-flow deposits developed at the mouths of topographic ravines (Fig. IV-4 and IV-7). The crests of the flanks grade from sharp-edged with rotational slumps to gradual with chutes connected upslope with shallow and small translational slumps. Isolated big slumps and retrogressive slumps are also common on those slopes and have resulted in the development of the bowl-shaped and elongated topographic depressions, respectively.

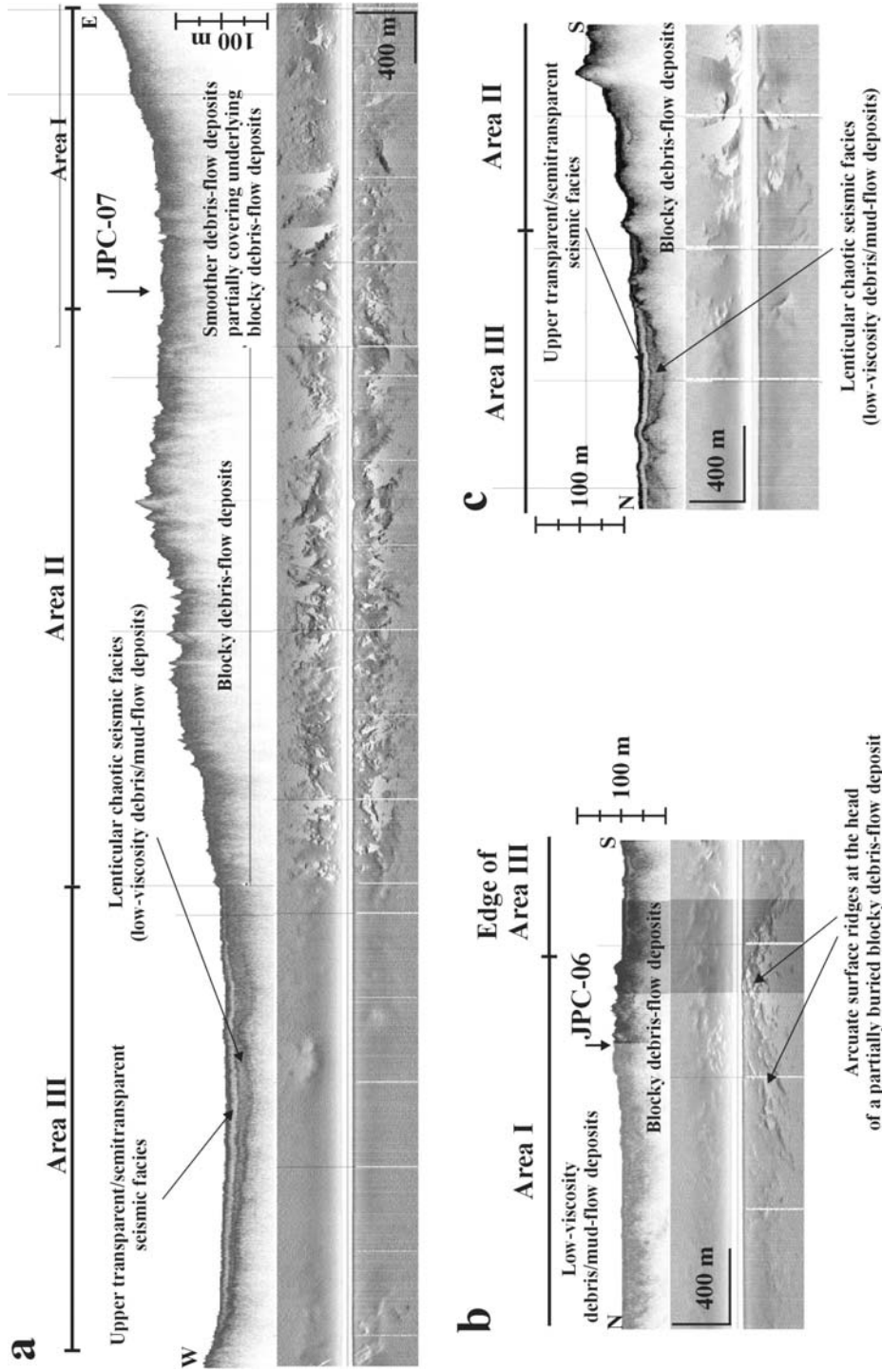


Fig. IV-8. Typical 3.5 kHz profiles and side-scan sonar images from the three geomorphological areas occurring on the floor of Beaumont Basin. The different acoustic character of area I in image (a) is due to the stiffer/coarser nature of smooth debris-flow deposits adjacent to the southwestern flanks that only result in the partial burial of the underlying blocky debris-flow deposits. Note how much thicker the smooth debris-flow deposits are adjacent to the northern flank of the basin (b) leading to the complete burial of the underlying blocky debris-flow deposits. For further explanation see text. The locations of the survey lines are displayed in Figure 3.

Three geomorphic areas are defined on the 3.5 kHz seismic profiles, side-scan sonar images and bathymetric/morphological maps (Fig. IV-3), they are:

Geomorphic Area I is located adjacent to the basin flanks and is characterized by smooth morphology that in places reveals a buried, hummocky paleo-topography (Figs. 3 and 4). In the 3.5 kHz seismic profiles Geomorphic Area I is represented by chaotic facies with prolonged to very prolonged surficial echoes overlying a strong and sharp, hummocky acoustic basement (Fig. IV-8a and IV-8b). The chaotic facies onlap the deposits at the foot of the flanks and the blocky deposits further onto the basin floor. The overlying chaotic facies are interpreted as younger, smooth deposits from low-viscosity debris/mud flows and gravity flows that spread over the basin floor adjacent to the flanks. The underlying hummocky surface resulted from amalgamated deposits of older blocky debris flows.

Basinward, the amalgamated blocky debris-flow deposits are exposed on the seafloor (Geomorphic Area II), indicating that the smooth debris/mud-flow deposits are limited to the basin flanks. Huge sediment blocks greater than 150 m in diameter and 25 m in thickness reveal the catastrophic nature of the blocky flows. Geomorphic Area II is located on the lobate southern and western parts of the basin floor and appears to be related to the canyon-like landslide troughs that are observed on the southern and western flanks of Beaumont Basin.

Geomorphic Area III is limited to the deeper parts of the basin floor and is characterized by a very smooth and flat morphology that only at its margins reveals partly buried blocky topography. Two layers/seismic facies represent this area on the 3.5 kHz sub-bottom profiles (Fig. IV-8): 1) a deeper lenticular chaotic layer, and 2) an upper transparent/semi-transparent layer with a typical thickness of 6 to 9 m that drapes the entirety of Area III and thins towards its edges. Both units onlap the surrounding blocky debris-flow deposits, indicating their younger age. The lower chaotic facies was mainly deposited in the depressions of an underlying hummocky topography and is characterized by flat to concave upper surfaces that become convex at their margins. This indicates that this facies resulted from deposition of fluid debris/mud flows similar to those in Area I. The overlying transparent layer may represent ponded deposits by highly fluid (low-viscosity) mud flows, and/or ponded mud turbidites (Blanpied and Stanley, 1981; Stanley, 1981; Behrens, 1984). However, the draping character and great extent of the upper transparent layer weakens the argument for deposition by low-viscosity mud flows. The ponded mud turbidites have been deposited by low-density turbidity currents, the origin of which is from: a) the overriding turbulent clouds of debris flows, and/or

b) the depositional segregation of large turbidity currents initiated on the outer shelf/upper continental slope (due to the basin-sill morphology the coarsest material of the turbidity currents is deposited in the intraslope basins of the upper continental slope) (Hampton, 1972; Hart et al., 1992; Mohring, 1998, 1999; Piper et al., 1999) (Chapters II and V).

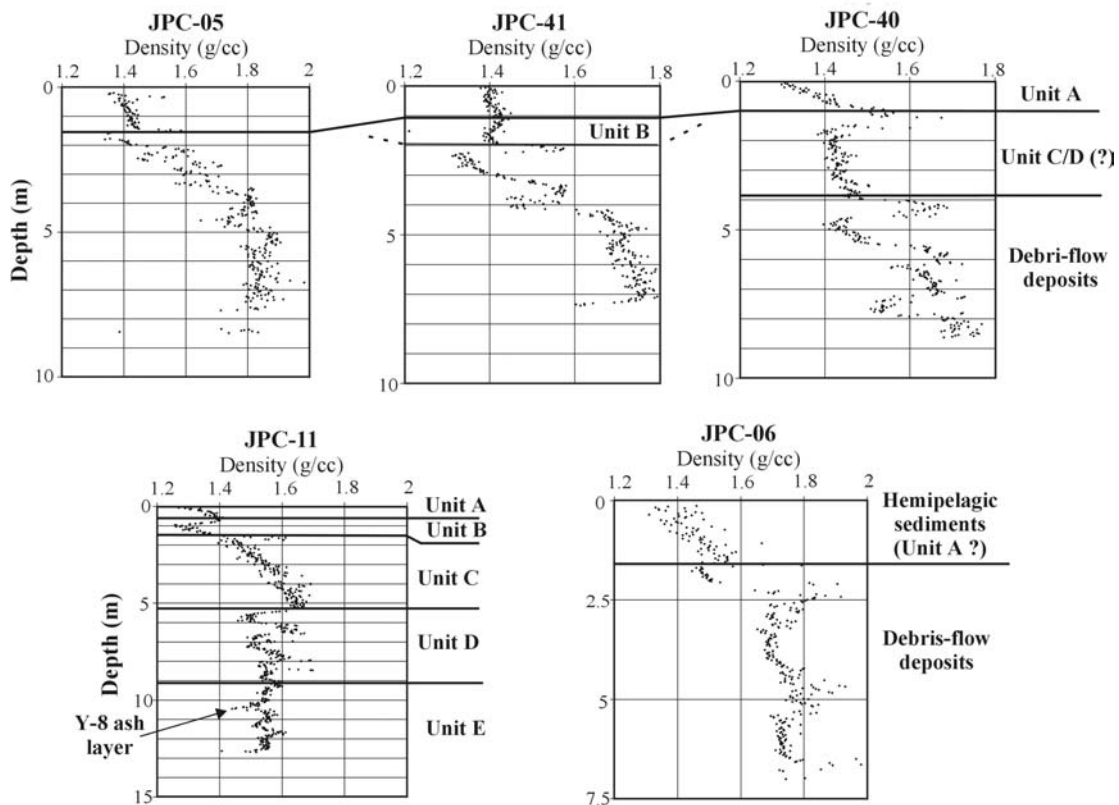


Fig. IV-9. Bulk density profiles and associated sedimentological units (Chapter II) of five Jumbo Piston cores (JPC) from Beaumont Basin.

Core Descriptions

Three JPC cores and one USGS core were collected on the lower part of the northern flanks of the Beaumont Basin (Figs. IV-3 and IV-9). Core JPC-05 was collected from debris-flow deposits that have been partially removed by more recent slumping events, whereas JPC-41 and JPC-40 came from an area of lobate debris-flow deposits. All three JPC cores consist of

debris-flow deposits that have been blanketed by a 1.5-4-m-thick drape of hemipelagic sediments. The debris-flow deposits are overlain on an exfoliated area/slide plane characterized by prolonged, semi-transparent, continuous reflectors interpreted as Oxygen Isotope Stage 6 overbank/overflow deposits from the Bryant Canyon system (silt/mud couplets or laminated mud with small variances in the silt percentage). Hemipelagic sediments overlying laminated muds of core USGS-09 support the above interpretation.

Sediment core JPC-11 was retrieved from a canyon-like landslide trough on the western flank of Beaumont Basin. Based on the sedimentary units that have been described from the Bryant Canyon area (Chapter II), the core represents continuous deposits of Oxygen Isotope Stage 1 (Holocene) to Stage 5 (Fig. IV-9), indicating that the major slumping in this specific area occurred at the beginning or previous to Oxygen Isotope Stage 5 (about 135ky B.P.).

Four cores were retrieved from Geomorphic Area I (Fig. IV-3). Core JPC-06 consists of debris flow deposits blanketed by a thin (2-m-thick) drape of hemipelagic sediments (Fig. IV-9). Cores USGS-10, USGS-11, and USGS-14 are similarly characterized by debris-flow deposits that have been covered by a thin drape (1 to 5 m) of hemipelagic sediments, interbedded by thin-bedded sand to mud turbidites in the lower and middle sections. Turbidites are interpreted to be deposits of overriding turbulent clouds that originated from upslope-deposited mass transports. The presence of laminated muds in the lower 1 m of core USGS-11, covered by a thin debris-flow deposit, probably represents the relatively undisturbed structure of an underlying sediment block.

Geomorphic Area II consists of blocky debris-flow deposits that adjacent to the southern and western flanks (area I) are partially covered by stiff/coarse deposits of smaller, younger smooth gravity flows. JPC-07 core (Figs. IV-3 and IV-10), located at the border of Area I and II, has been described in millimeter-scale and X-ray radiographs have been taken over its entire length to determine all the sedimentary units. The upper 34 cm of the core consists of thin-bedded turbidites (related to upslope-limited failures), overlying a massive muddy-sand layer, where the sand is mainly of biogenic (carbonate) origin. Below 34 cm, four successive debris-flow deposits (three mud-clast dominated and one mud matrix dominated) are observed in the core, which become stiffer, thicker and contain larger clasts/boulders (cm to decimeters in diameter) with depth. Cores USGS-12 and USGS-13, from the southern and eastern floor of Beaumont Basin, respectively, are similar in sedimentology to core JPC-07. The only exceptions are that

they are covered by a thin drapage of hemipelagic sediment (about 1-m-thick). However, no turbidites were observed in sediment core USGS-13.

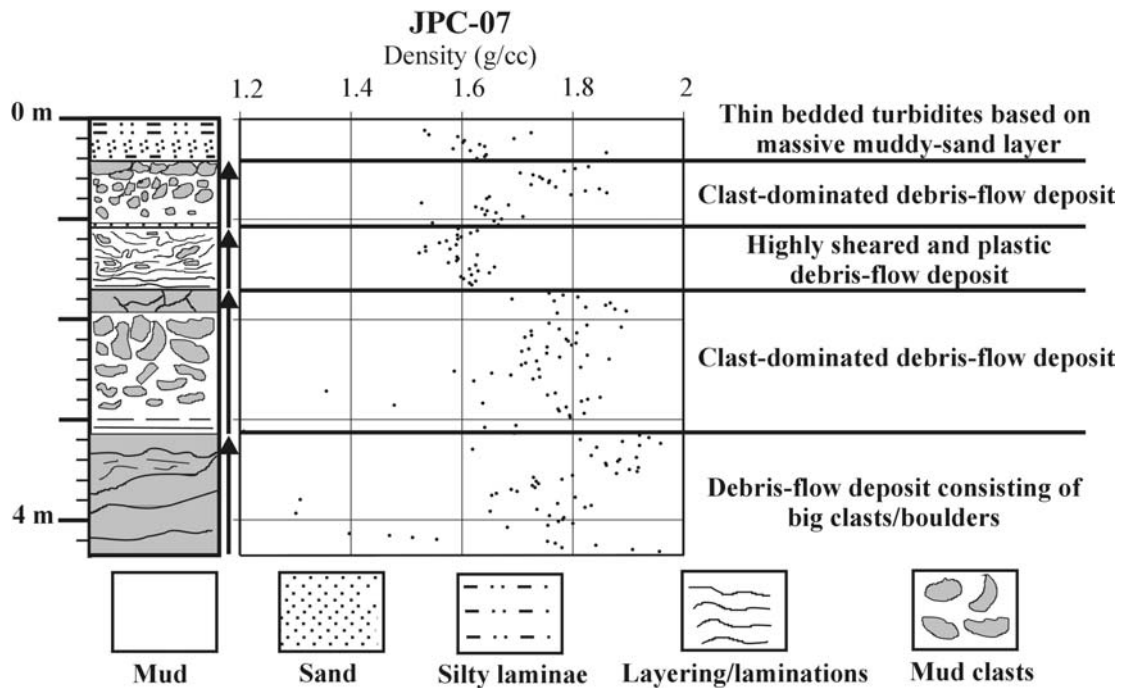


Fig. IV-10. Sedimentological descriptions and bulk density profiles of sediment core JPC-07.

Reveille Basin

Geomorphology

Reveille Basin is located on the lower continental slope along the path of Bryant Canyon (Figs. IV-1 and IV-11). It is characterized by a highly irregular topography, high relief (about 400 m) and has the shape of an arrow pointing to the northwest. The southern part of the basin resembles a step-like canyon and consists of two terrace-like areas with gradients less than 2° , bounded by highly inclined walls (6° to 10°). The terraces appear to extend into the eastern walls of the basin, which are much steeper (7° to 18°) than the western flank (8° to 9°). The northern flank has the highest gradients (15° to 18°) and is characterized at its crest/upper

region by a terrace-like feature most likely caused by extensive retrogressive slumping. In the north, the basin communicates with Beaumont Basin by a narrow sill, while an 11 km sill separates it from Iberia Basin in the south. Along the northeastern and southwestern flanks two very well-developed canyon-like landslide troughs are visible (2 to 3 km wide, with a relief of up to 250 m) that connect the basin with topographic depressions on the northeastern and southwestern plateaus.

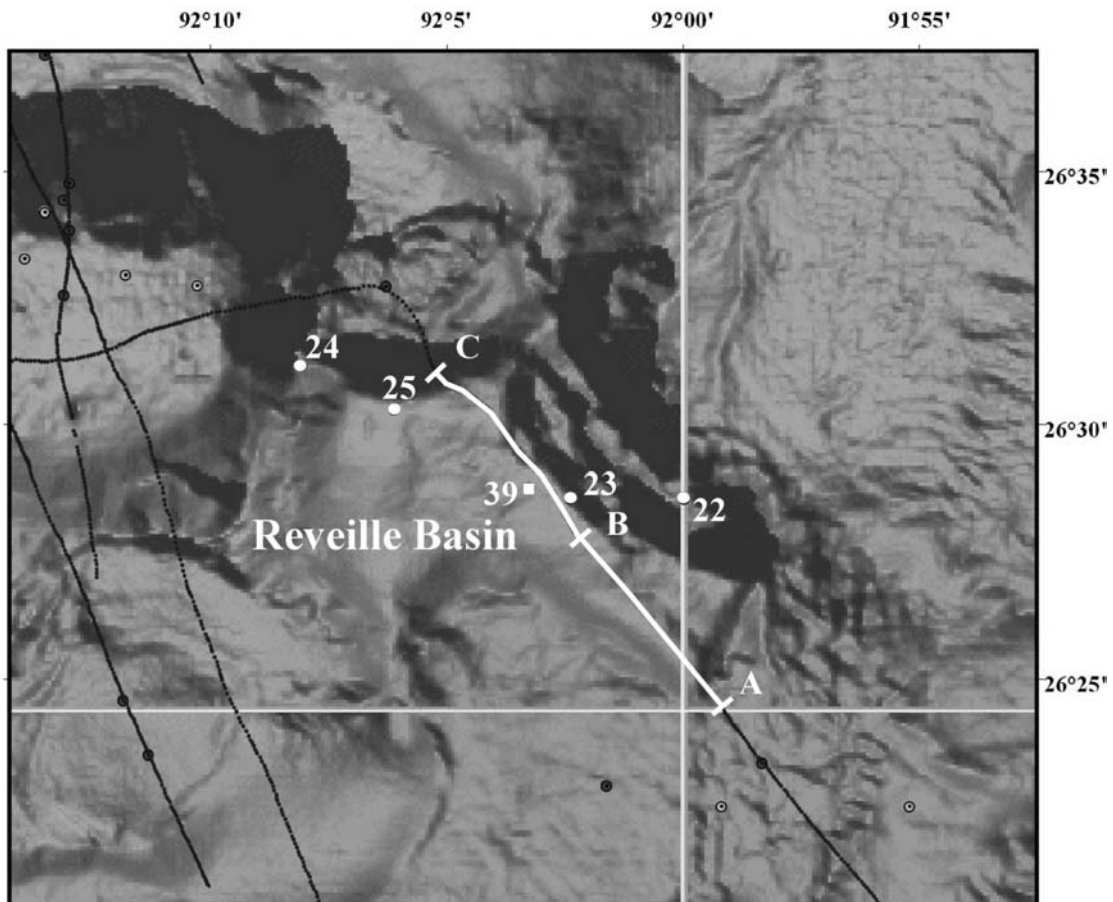


Fig. IV-11. Morphological map of Reveille Basin displaying core locations (circles: USGS-cores; squares: JPC-cores) and deep-tow line.

Seismic data in Reveille Basin are limited to only one deep-tow transect, running along its main axis (SE-NW) (Fig. IV-11). Two terraces are present in the southeastern part of the basin,

that step down to the north onto the basin-floor. The upper terrace is bounded in the southwest by a head-scarp (about 80 m high) with slump deposits at its foot (Fig. IV-12). Smooth, chaotic layers, interpreted as debris/mud-flow deposits, blanket the southern and central parts of the upper terrace, whereas at its northern reaches the sediments become thinner and well stratified. The stratified sediments of the northern part of the upper terrace are interpreted as: 1) hemipelagic sediments, 2) turbidites that resulted from the overriding turbulent clouds and/or transformation of mass transports/debris flows initiated on the southern part of the terrace (Hampton, 1972; Fisher, 1983; Hart et al., 1992; Mohrig et al., 1998, 1999), and 3) a combination of the above. A strong acoustic reflector is observed where sound penetration was sufficiently deep (Fig. IV-12) and probably represents coarse intra-canyon deposits of Oxygen Isotope Stage 6.

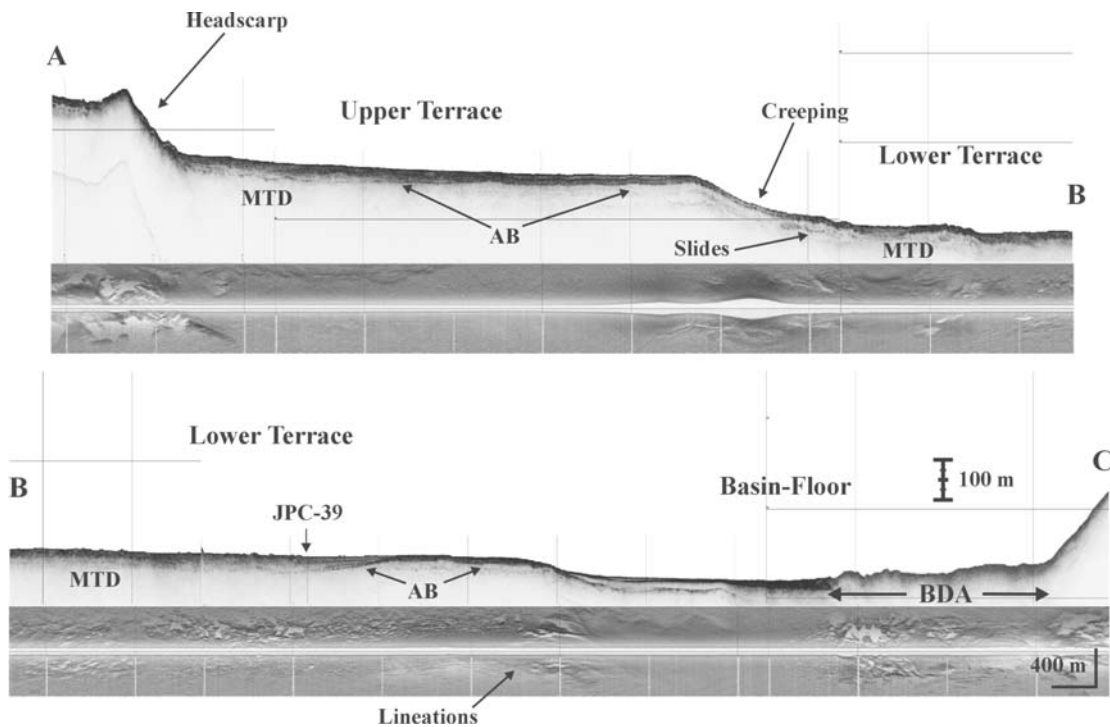


Fig. IV-12. Image showing 3.5 kHz profile and side-scan sonar imagery across Reveille Basin. Note how smooth gravity-flow deposits have covered blocky mass-transport (debris flow) deposits on the terraces, and how they become thinner and well-stratified moving towards their northern (right) limits. The location of the seismic line is displayed in Figure IV-11. MTD: Mass-Transport Deposits; AB: Acoustic Basement (limit of sound penetration); BDA: Blocky Debris Apron.

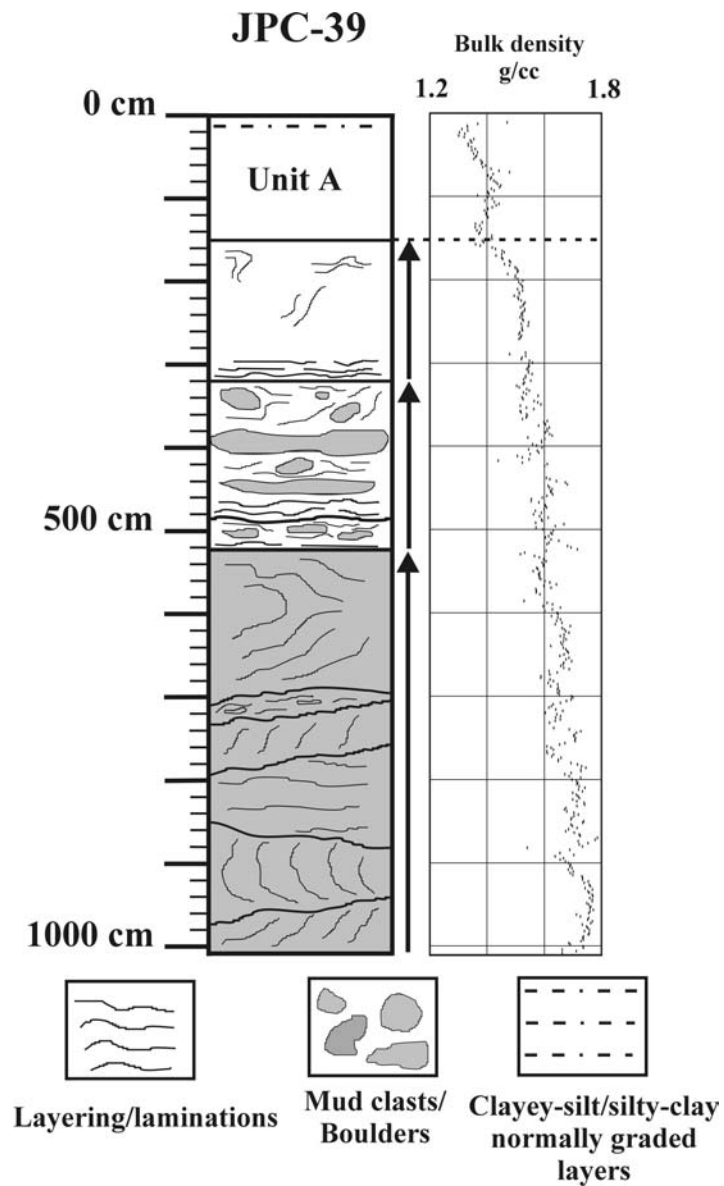


Fig. IV-13. Sedimentological descriptions and bulk density profile of sediment core JPC-39 located on Reveille Basin. Note how the deposits grade downward from hemipelagic sediments to mud-flow to debris-flow to slump deposits.

The lower terrace is bounded in the north by a gently inclined step (about 4°) that appears to be relatively stable, with only a few possible small rotational slides at its foot (Fig. IV-12). The wavy morphology/shape of the upper 10 m of sediment indicates possible sediment creep. The smoothed, hummocky topography of the lower terrace, in combination with the chaotic

character of the sediments on the 3.5 kHz subbottom profiles indicate that this area is covered by blocky mass-transport deposits, that are blanketed by more fluid, post-generated mud/debris-flow deposits. Adjacent to the northern boundary of the terrace the mass-transport deposits thin and become stratified, whereas an acoustic background similar to that of the upper terrace emerges in the seismic sections. Buried, linear depressions are observed close to and at the crest of the lower step (Fig. IV-12), and are interpreted as erosional structures of overflowing gravity flows.

The basin floor is made up of various types of deposits due to the presence of multiple sediment sources. The southern half of the floor is composed of lenticular, transparent to semi-transparent seismic units with a convex to concave upper surface, overlying hummocky topography, interpreted as mud/debris-flow deposits. Adjacent to the northern flank of the basin, a hummocky apron of blocky debris-flow deposits develops. The fact that it onlaps onto the southern transparent facies and has a rough, blocky topography, has lead us to conclude that it is of a younger age than the southern transparent/semitransparent deposits. The deepest part of the basin floor is draped by flat-topped lenticular seismic facies with discontinuous, subparallel, prolonged, reflectors. Sediment cores of this area reveal that the lenticular drape consists of alternating hemipelagic sediments, turbidites, and thin debris/mud-flow deposits.

Finally, the deep-tow transect on the northern flanks of the basin revealed its highly exfoliated nature and clearly showed the presence of successive evacuation zones resulting from intense, retrogressive slumps that transformed into debris flows. On the crest of the flanks the failures have penetrated deep into the plateau creating an amphitheatre-shaped, terrace-like geomorphologic feature (Fig. IV-11).

Core Descriptions

Four USGS and one JPC core were collected in Reveille Basin. Core JPC-39 and USGS-23 are located on the lower terrace of the southeastern part of the basin (Figs. IV-11 and IV-12). Both cores consist of mud/debris-flow deposits (Fig. IV-13) blanketed by a thin drape (160 cm) of hemipelagic sediments that in JPC-39 are interbedded by a silty lamina (mud turbidite) at 8 cm. Core USGS-22, located on the upper terrace on the steep ESE flank of the basin, consists of debris flow deposits draped by a 220 cm thick layer of hemipelagic sediments. Cores USGS-24 and 25 were retrieved from the sill and basin floor, respectively. Both cores consist of debris flow deposits (chaotic mud and silt with mud clasts), and sand/silt turbidites interbedded with

hemipelagic sediments that are covered by a very thin drape (about 10 cm) of Holocene hemipelagic sediment. In core USGS-25 (basin floor), the gravity-flow deposits are thinner (20 to 50 cm) with more abundant turbidites and hemipelagic sediments.

Calcasieu Basin

Geomorphology

Calcasieu Basin is located (Figs. IV-1 and IV-14) at the terminus of the confined Eastern Canyon system on the upper Texas-Louisiana continental slope at a depth of about 1500 m, and is characterized by a very high relief (up to 700 m) and highly variable gradients (6° to 14°). The flanks of Calcasieu Basin have been strongly affected by slope instability processes that created various geomorphic features ranging from slump complexes to amphitheater-shaped terraces, to large canyon-like landslide troughs with well-developed depositional lobes at the base of the flanks (Fig. IV-14).

The western and northeastern flanks of Calcasieu Basin are characterized by numerous, large, superimposed bowl-shaped depressions (evacuation zones) that resulted from successive adjacent rotational slumps/flows (Cf. Mulder and Cochonat, 1996) up to 3 km wide and 150 m high, creating the amphitheater-shaped and terraced morphology (Figs. IV-14 and IV-15). This morphology is more pronounced on the upper flanks, where the amphitheater-like features appear to extend and propagate backwards into the plateaus through a series of retrogressive slumps (Fig. IV-16). The floor of the amphitheater-shaped zones on the upper part of the flanks is partially covered by large sediment blocks (lag deposits) that in turn are covered by successive debris-flow deposits, which probably resulted from the latest retrogressive failures on the heads of the amphitheater-shaped zones. Younger failures (small slumps and debris flows), developed in the blanketing deposits, are very common and contribute to the complex morphology of the area (Fig. IV-17). The absence of thick mass-transport deposits in these zones (relative to the volume of the evacuated areas) indicates that most of the slumps translated into debris flows and traveled downslope onto the basin floor. Extensive hummocky aprons/lobes of blocky debris-flow deposits at the foot of the flanks support this interpretation (Figs. IV-14 and IV-18). Younger, smooth debris/mud-flow deposits appear to have been deposited around the hummocky lobes of the blocky debris-flow deposits.

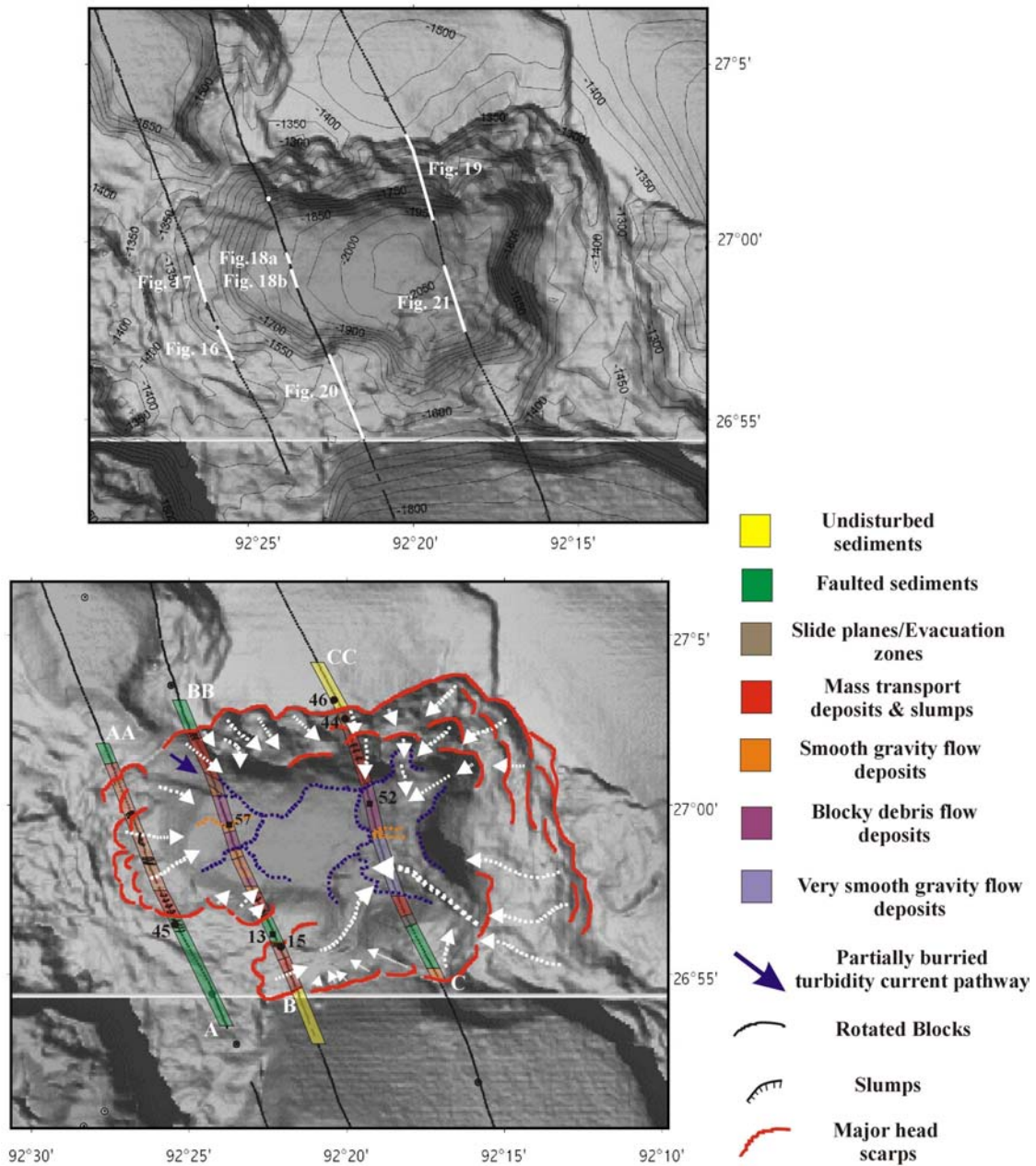


Fig. IV-14. Bathymetric and geomorphological maps of Calcasieu Basin. The white lines indicate the locations of the seismic lines displayed in the text. The black circles and squares indicate the locations of the JPC and LGC sediment cores, respectively. The white arrows display the direction of the mass transports. The black lines represent the location of the survey lines. The isobaths on the top image are in meters.

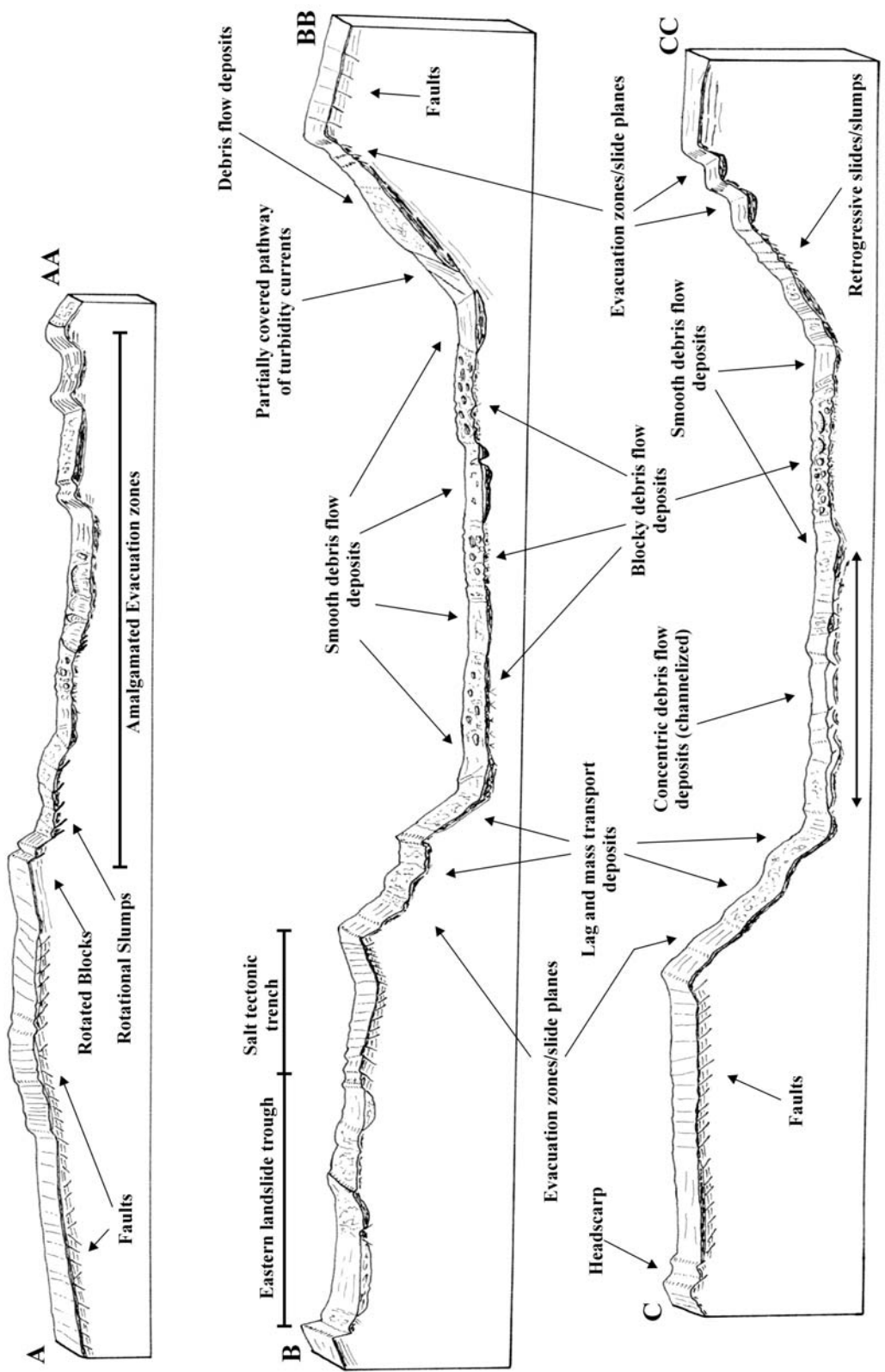


Fig. IV-15. Schematic illustrations of the three seismic lines crossing Calcasieu Basin. Line locations are displayed in Figure IV-14.

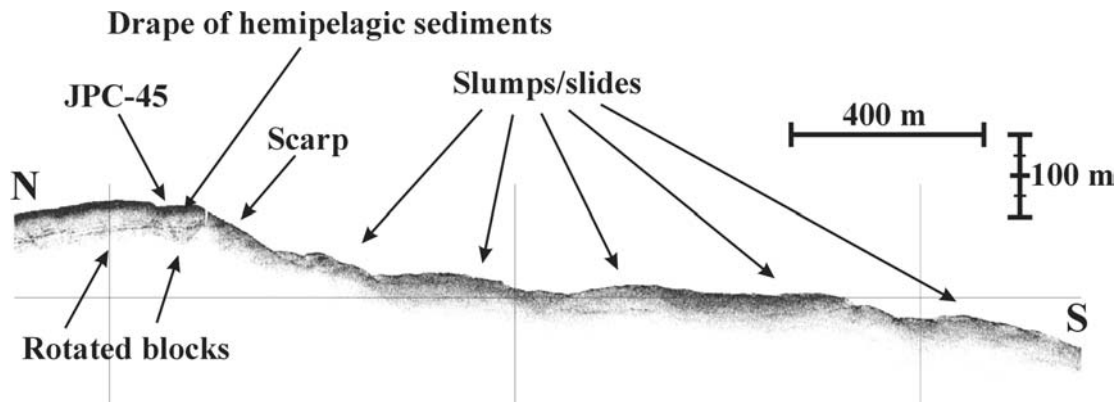


Fig. IV-16. Image showing a 3.5 kHz subbottom profile from the western flanks of Calcasieu Basin. Head-scarp with several rotational slides/slumps developed at its foot, indicating the strong retrogressive character of the sediment failures. Note that on the slumped area, the hemipelagic drape is not observed (absent or very thin) revealing the young age of the failures. The location of the seismic line is displayed in Figure IV-14.

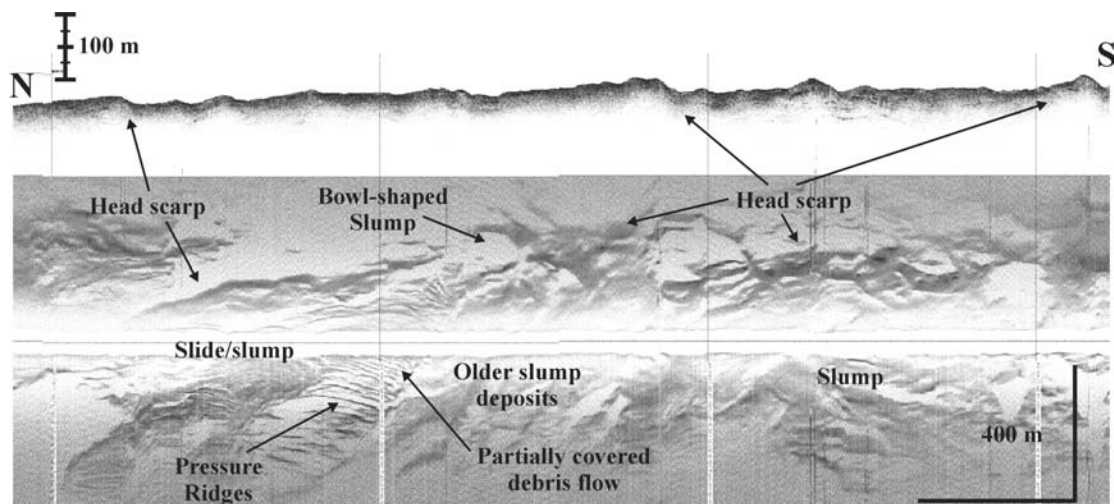


Fig. IV-17. Image showing 3.5 kHz subbottom profiles and side-scan sonar image from the western flanks of Calcasieu Basin. Evacuation zones of the amphitheatre-shaped terrace on the upper western flank that have been covered by sediment blocks and successive, refailed, debris-flow deposits. Note that all the failures are limited to the debris-flow blanket, revealing their post-generated nature. The location of the seismic line is displayed in Figure IV-14.

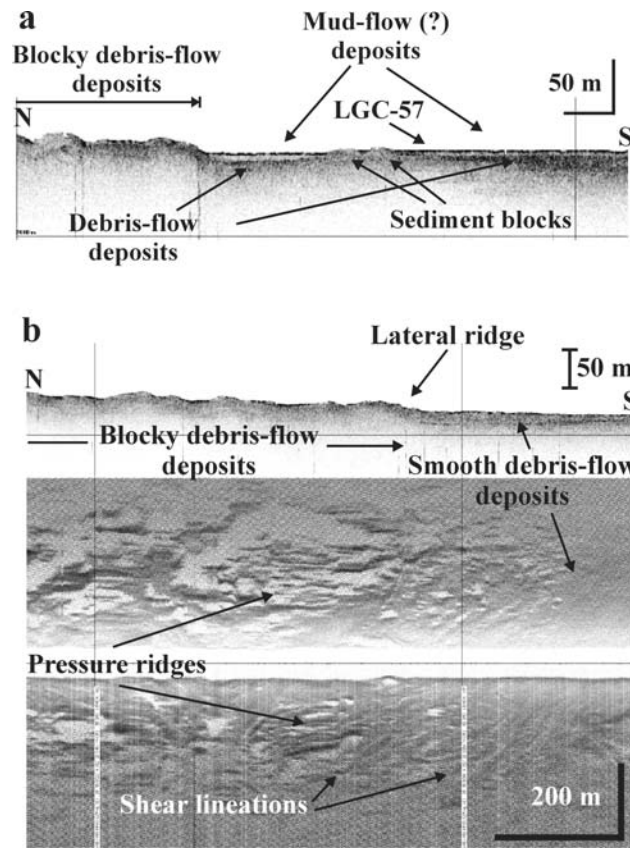


Fig. IV-18. Image showing 3.5 kHz profiles and side-scan sonar image from the apron at the foot of the western flank of Calcasieu Basin. Note how the smooth debris/mud-flow deposits are partially overlying and surrounding the blocky debris-flow deposits. Pressure ridges behind the sediment blocks and their presence only at the edges of the smooth debris-flow deposits in image (b) reveal that probably deposited as out-runner blocks of the blocky debris flows and then covered/surrounded or joined the flow of the younger smooth debris flows. The locations of the seismic lines are displayed in Figure IV-14.

The northern flank of Calcasieu Basin is characterized by multiple superimposed bowl-shaped to elongated landslide evacuation zones of high-relief with highly variable slope inclinations in the upper reaches (4° to 8°), and steep slopes (8° to 15°) of lesser relief in the lower reaches, producing a step-like morphology. A seismic line across the northern flank clearly illustrates evacuations zones of two retrograde rotational slumps, up to 110-m-thick, on the upper flank, whereas the middle and lower flank is characterized by uniform gradient and the development of a younger sequence of shallow (about 30 m) retrograde slides that evolved downslope into a well-developed slump (Fig. IV-19). The shallow retrogressive failures of the middle and lower flank consist of packages of chaotic facies (debris-flow deposits) overlain by

a thin, stratified drape of hemipelagic sediment. This information reveals the recent age of the secondary, shallow failures that developed on lag/debris-flow deposits of the flank. The large evacuation zones on the upper and middle flank probably resulted from deep, successive, and adjacent, retrogressive slumps/flows (Cf. Mulder and Cochonat, 1996) that led to the collapse of the initially very steep slope. However, no extensive blocky debris-flow deposits are visible at the foot of the northern flank. This is probably due to their burial by smoother gravity-flow deposits and hemipelagic sediments.

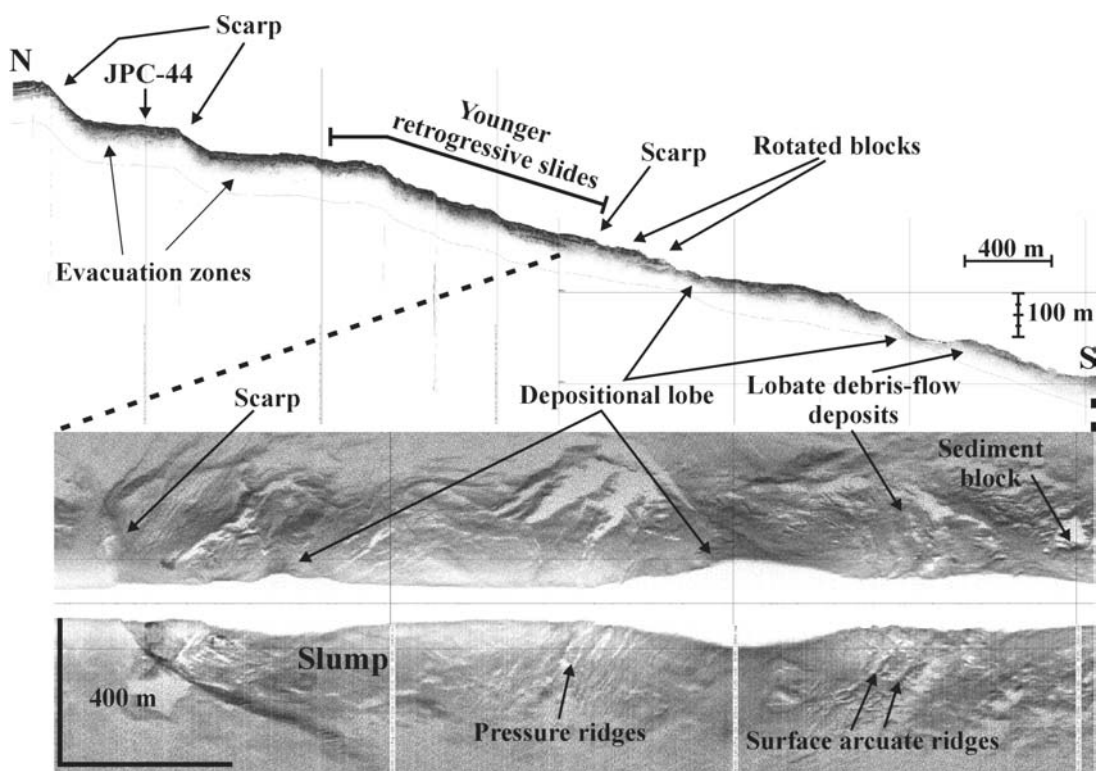


Fig. IV-19. Image showing a 3.5 kHz profile and side-scan sonar imagery from the northern flank of Calcasieu Basin. Note how the older evacuation zones penetrate (retrograde) into the plateau, and the development of a younger set of retrogressive slides that have occurred at the head of a large slump on the lower flank. The lobate debris-flow deposits in front of the slump probably represent a detachment of the foot of the slump from the main body, supporting a possible hydroplaning of the failing mass (Mohring et al., 1998, 1999). The location of the seismic line is displayed in Figure IV-14.

The south and southwest flanks of Calcasieu Basin are dissected by two large, canyon-like, landslide troughs accompanied by well-developed depositional lobes extending from their mouths at the foot of the flanks (Fig. IV-14). The floor of the eastern trough, , is represented by successive evacuation zones created by retrogressive rotational slumps/flows. On the plateau, the trough is replaced by an amphitheatre-shaped landslide terrace. The western canyon-like trough has a unique character, its middle-lower section following the general slope inclination and its upper part turning west into the sill, where its geometry is mainly determined by the orientation of an antithetic listric fault system on the southern sill (Figs. IV-14, and IV-15). In Figure IV-20, the development of two antithetic listric-fault systems due to uplifted salt diapirs is apparent, leading to the development of two grabens. The northern graben includes stratified sediments characterized by prolonged, parallel, semi-transparent and continuous echoes (fine-grained turbidites/laminated mud) covered by a 10-m-thick drape of hemipelagic sediments disturbed by listric growth faults. In contrast, the southern graben has been incorporated into the western landslide trough by the retrogression of numerous deep retrogressive slumps that transformed into debris flows. The graben boundaries are characterized by fault-like scarps and back-tilted rotated blocks, whereas its floor is partially covered by re-failed slump deposits and sediment blocks. Around the slumped masses and large sediment blocks, channel-like depressions/pathways develop. On the 3.5 kHz seismic profiles, the channel-like depressions are characterized by chaotic layers with prolonged, discontinuous, interbedded reflectors blanketed by a thin (10-m-thick to absent) drape of continuous, parallel, prolonged reflectors. Based on the descriptions of JPC-15, the chaotic underlying facies represent thin debris-flow deposits, whereas the overlying blanket is hemipelagic sediments that are intensively interbedded with thin-bedded silt turbidites. The silt turbidites resulted from overriding turbidity currents from debris flows and/or the total transformation of debris flows into turbidity currents (Hampton, 1972; Fisher, 1983; Piper et al., 1985, 1999; Hart et al., 1992; Mohring et al., 1998, 1999). The presence of turbidites up to the top of the core indicates that sediment failures are still occurring in this area, and that probably the western trough is still acting as a conduit for mass transport to the floor of Calcasieu Basin. However, it must be mentioned that the infilling of the channel-like areas indicates the abatement of slope failures during the Holocene, possibly due to a deceleration of the uplift of the surrounding salt diapirs.

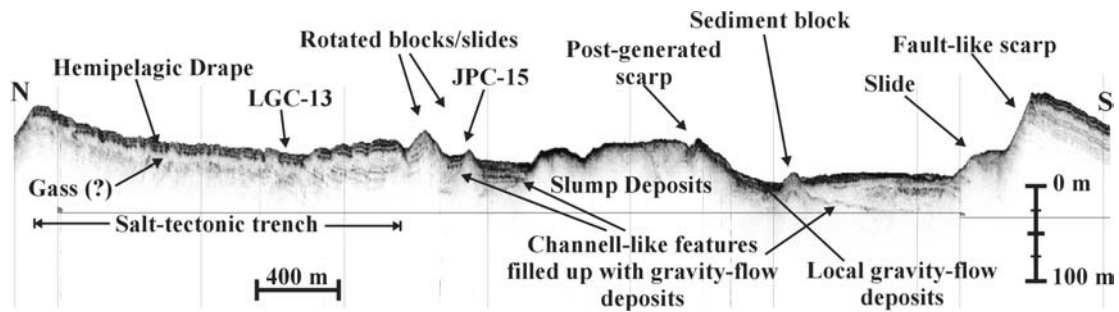


Fig. IV-20. Image displaying 3.5 kHz profile of the southern ridge, Calcasieu Basin. The location of the seismic line is shown in Figure IV-14.

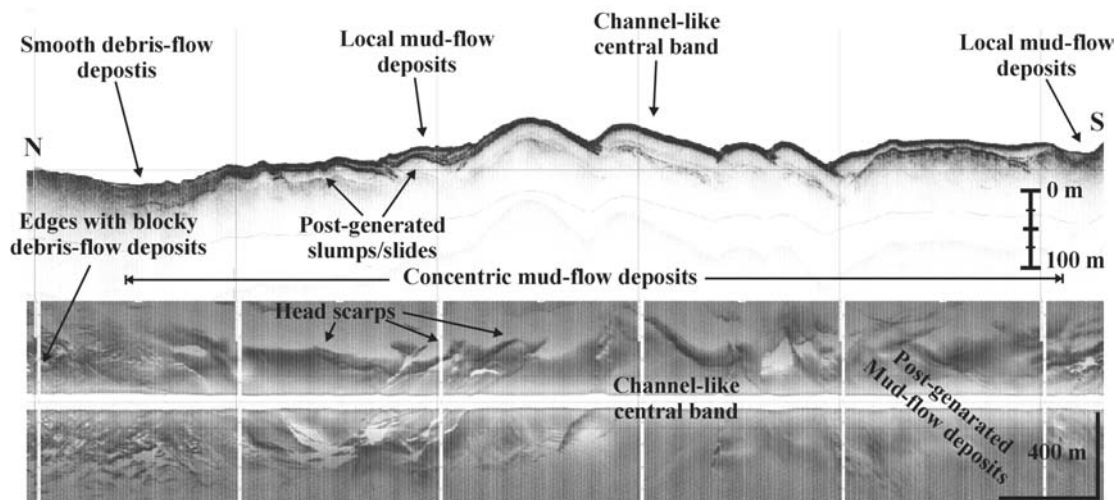


Fig. IV-21. Image showing 3.5 kHz profile and side-scan sonar imagery of the concentric mud flow deposits at the southeast floor of the basin. Note the re-failures at the edges of the mud flow deposits and gradual “freezing” of the flow towards the center (channel). The location of the seismic line is displayed in Figure IV-14.

As mentioned previously, the canyon-like landslide troughs of the south-southwestern flanks are replaced at the basin floor by two depositional lobes. Based on the geomorphological map of Calcasieu Basin (Fig. IV-14), the depositional lobes subscribe a lobate, fan-like shape with the eastern lobe partially overlapping the western lobe. The eastern trough is characterized by a well-developed, channel-like feature that extends to the middle part of its respective depositional lobe (Fig. IV-14). The 3.5 kHz seismic profile and side-scan sonar image in Figure IV-21, running across the foot of the eastern lobe, reveal that the eastern lobe consists of

amalgamated debris-flow deposits covered by a thick transparent layer. That layer exceeds 25 m in thickness and thins at its edges, and probably represents large, smooth, mud-flow deposits. Upon closer inspection, these deposits blanket the entire eastern lobe and generally mimic the underlying topography and reveal a concentric pattern in deposition. They consist of bands ranging from broad and flat at the edges with small, local re-failures (small slides, and local debris/mud-flow deposits), to convex, thicker and relatively undisturbed bands towards the center. The deposits of the central band are the thickest and tend to coincide geographically with the location of the channel-like feature of the eastern canyon-like trough (Figs. IV-14, IV-15, and IV-21). All are blanketed by a 5- to 10-m-thick drape of high amplitude, parallel, prolonged, and continuous reflectors that probably represent turbidites fed by the western canyon-like landslide trough. The stratified drape is disturbed in the north by younger debris-flow deposits that occurred in the junction area between the depositional lobe of the eastern trough and the slope apron of the northeastern amphitheater-shaped flanks. Based on the overlying pattern of the northern slope apron and on its rough blocky morphology (Figs. IV-14, IV-15, and IV-21), we conclude that it is probably younger than the depositional lobe of the eastern trough.

Four possible explanations are considered for the deposition of the seismically transparent mud-flow deposits on the lobe of the western trough. The first is that they are the result of a single mud-flow event that initially spread out radially, creating widespread, outer, lateral margins, and later, through a concentric solidification of the flow, developed lateral convex bands, leading to the final solidification of the central channel-like band. This model would imply the existence of several flow pulses within the same mud-flow event becoming 'channelized' in and through the deposits of the previous pulses (Iverson, 1997; Major, 1997; Huang and Garcia, 1999; Major and Iverson, 1999; Sohn, 2000). Similar flow patterns have been assumed to occur in the Saharan debris flow (Masson et. al., 1993). The second explanation implies the gradual deposition of several mud flows that through time evolved from unconfined to confined by building several low- to high-relief terraces/lateral margins (Major and Iverson, 1999). The third interpretation is that these deposits simply represent mud-flow deposits (single or multiple events) that mimic the general underlying morphology (Masson et al., 1993). Finally, a fourth interpretation combines elements of all of the above-listed interpretations.

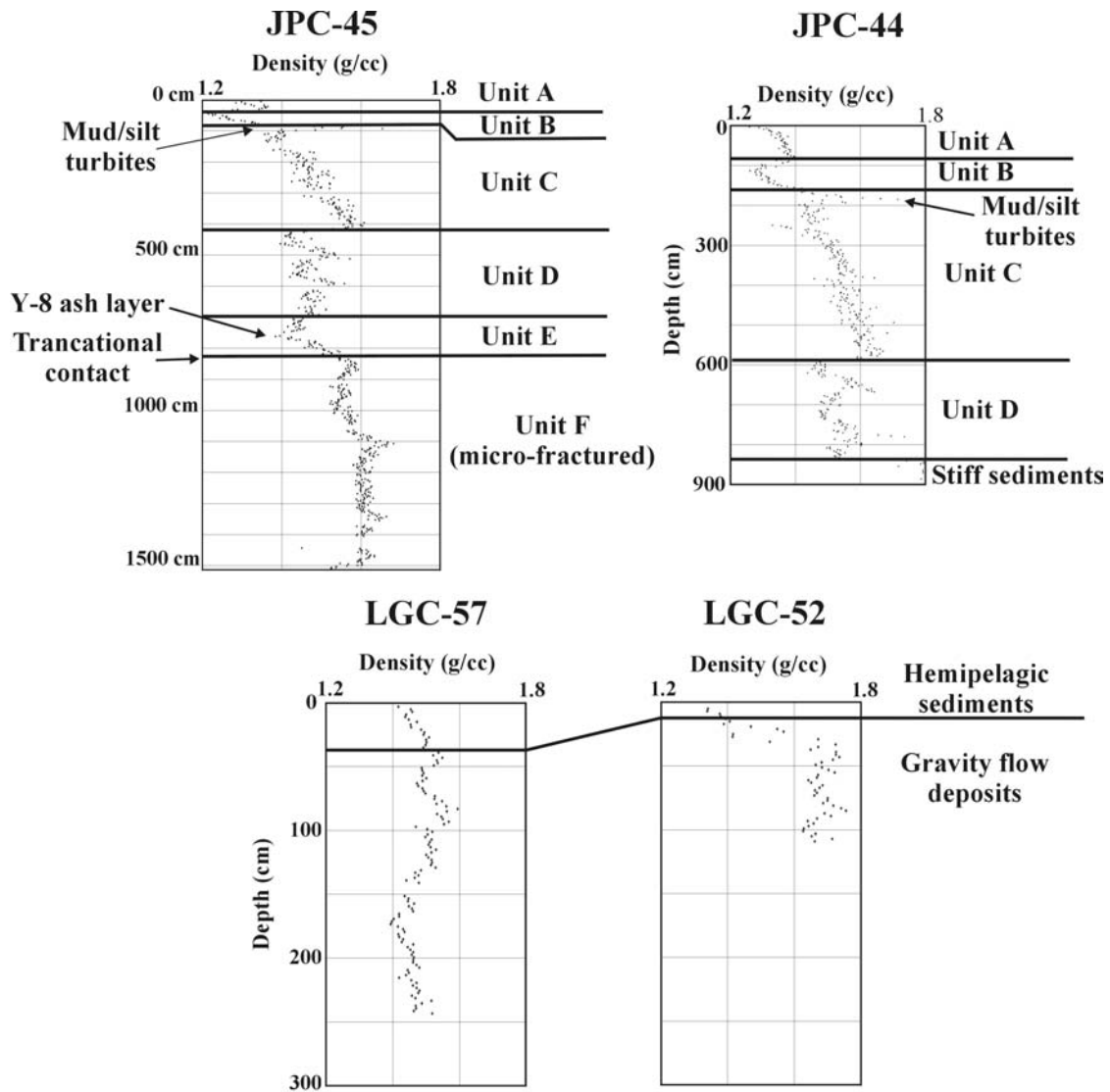


Fig. IV-22. Bulk density profiles and associated sedimentological units (Chapter II) of four sediment cores from Calcasieu Basin.

Core Descriptions

Three gravity (LGC) cores and four JPC cores, located in and around Calcasieu Basin (Fig. IV-14), are discussed in this chapter to identify and define the nature and approximate age of sediment failures. Cores JPC-45 and JPC-15 were split and studied in great detail, whereas the sedimentological interpretation of the other cores is mainly based on their bulk-density profiles.

Core JPC-45 is located at the top of a rotated block at the head of the amphitheater-shaped western flank (Fig. IV-16) and is characterized by a pattern of continuous sedimentation similar to the cores from the tranquil environments. The only exception is the fault-like contact between the hemipelagic sediments of Stage 5 (unit E) and the mud turbidites of Stage 6 (unit F), with a few mud-fragments floating in the overlying hemipelagic sediment (Fig. IV-22). This surface probably represents a failure plane created at the end of Stage 6 or the beginning of Stage 5. However, the failure surface just above the rotated block, penetrating into the most recent sediments and the absence of a drape of hemipelagic sediments (deposits of Stage 5 to 1) on the downslope slumped sediments, indicate that sediment failures developed up to the present time in this area (Figs. IV-14 and IV-16).

Cores LGC-57 and LGC-52, located on the slope aprons of the west and northeast amphitheater-shaped basin flank, consist almost entirely of gravity-flow deposits covered by a thin blanket (15-35 cm) of hemipelagic sediment (based on bulk-density profiles). This indicates that sediment failures of reduced size and frequency occurred at least up to the early/middle Holocene (Figs. IV-14, IV-18, and IV-22).

Core JPC-44 came from an old evacuation zone in a small terrace on the upper part of the northern flank (Figs. 14, 19, and 22). The upper 8.36 m of the core is characterized by continuous hemipelagic sediment (units A, B, C, and D) that overlay high bulk-density (probably gravity-flow deposits) sediments (Fig. IV-22), indicating that the sediment failures that developed the evacuation zones on this small terrace occurred at some point prior to, or at the beginning of Stage 4.

Core JPC-15 is located at the edge of the western canyon-like landslide trough on the south ridge of Calcasieu Basin (Figs. IV-14, IV-20, and IV-23). Its upper 80 cm is characterized by thin-bedded silt turbidites interbedded in hemipelagic sediment that downcore is succeeded between 80-142 cm depth by mud turbidites. Below 142 cm, various mass-transport deposits (thin carpets of debris-flow to debris-flow/slump deposits) developed that overlay mottled and ghost-layered, highly micro-fractured, hemipelagic sediment representing units C and/or D. The presence of gravity-flow deposits up to the top of the core suggests that the trough may still be active, even though the sediment failures should be of smaller extent when compared to the older, massive debris-flow/slump deposits. The micro-fractured hemipelagic sediment in the lower 4.5 m of the core represents the structure and sedimentology of an underlying rotated

block, indicating that the upslope propagation and evolution of the canyon-like trough reached that point at some time during the last glacial episode (Stage 2 or 3).

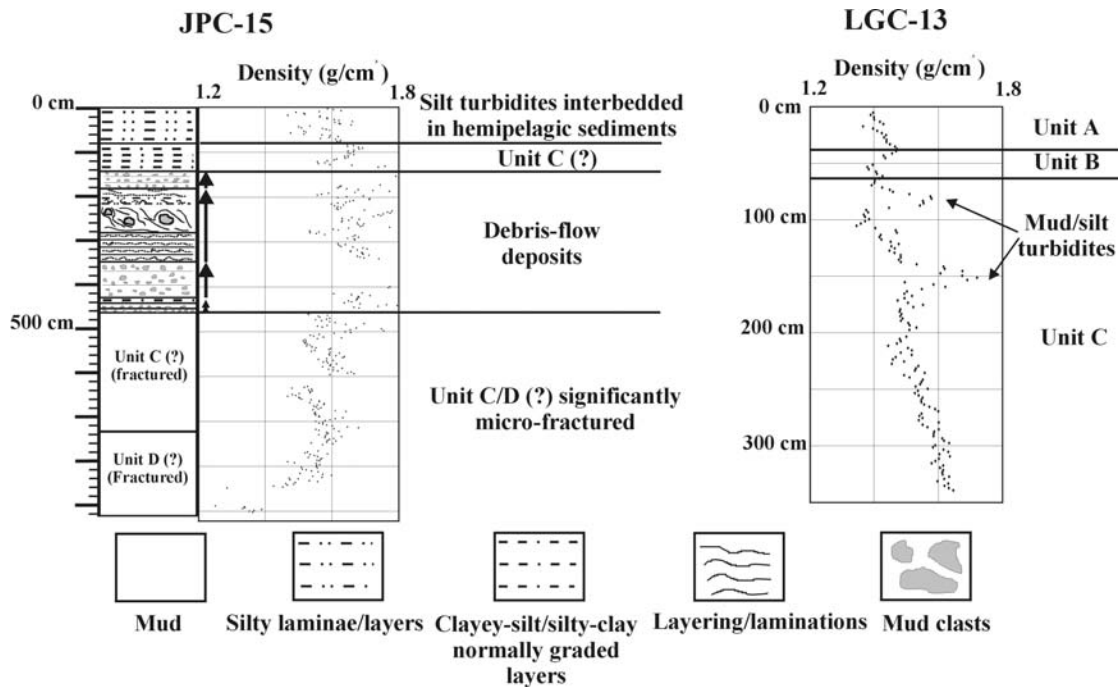


Fig. IV-23. Sedimentological descriptions and bulk density profiles of sediment cores JPC-15, and LGC-13.

Finally, core LGC-13, located on the salt-tectonic graben north of the landslide trough, described above, consists of units A, B and C that in the intervals 0.75-0.9 m and 1.4-1.6 m are interbedded with silty turbidites (Figs. IV-14, IV-20, and IV-23). Based on the 3.5 kHz seismic profiles, the area is characterized by a continuous drape and that the principal sediment disturbance occurred through the action of the antithetic listric faults formed by the underlying uplifted salt diapir; no sediment failure is observed to occur in this area.

Discussion

Basin Flanks

Lee (1990) and Twichell et al. (2000) argued that the collapsing of the basin flanks occurred at the beginning of interglacial Oxygen Isotope Stage 5 (94-125 ky B.P.), right after the abandonment of the Bryant and Eastern Canyon systems (Chapter II). However, sediment cores reveal that most failures occurred during the last glacial episode (Stages 2, 3, and 4), with a pause during the late half of Oxygen Isotope Stage 5. The contradiction in the two observations is most probably answered by the development of two episodes of highly active halokinetic processes. The first episode occurred during the early interglacial Stage 5, and led to the deformation of the Bryant and Eastern canyon systems by salt adjustment to the erosional/depositional canyon environments. The second episode of halokinetic processes took place during the last glacial episode due to differential loading caused by the extensive deposition of clastic sediments on the upper continental slope and outer shelf of the Gulf of Mexico (Lee, 1990; Lee et al., 1996). The extensive terraces observed in Reveille Basin and the early Stage 5 age of failures found in cores JPC-11 and JPC-45 support the occurrence of two halokinetic episodes.

The occurrence of two salt tectonic episodes in this area should make us cautious about structural interpretation in the basins, since its present morphology reflects the activities of both episodes, with the latest assumed to be dominant. The main cause of slope instabilities is the 'over-steepening' of the basin flanks by the subsidence of the basins themselves and the concomitant uplift of the surrounding salt diapirs (Lee et al., 1996; Twichell et al., 2000; Tripsanas et al, 2003). Consequently, the extensive slump complexes observed on the flanks of basins are developed in order for the flanks to achieve a critical inclination, through excavation by sediment failures, under which their remaining sediment on the basin flanks would be stable (Crozier, 1984; Keney, 1984; Allen, 1985; Iverson et al., 1997). According to the morphological appearance of the basin flanks, three general types of slopes are distinguished.

Slope type 1 has highly inclined flanks with indistinct morphological features of low relief and is mainly observed on the northern and northeastern flanks of Beaumont Basin. Acoustic data reveal that these areas are characterized by the development of retrogressive slump complexes up to and, in some cases, exceeding 50 m in depth through which large slices of the

basin flanks collapsed. The exfoliated nature of the flanks and the absence of extensive mass-transport deposits indicate that most of the failures were converted into debris flows (Hampton, 1972; Iverson and LaHusen, 1989; Iverson et al., 1997); some of these deposits can still be seen at the base of the flanks.

Slope type 2 is characterized by highly inclined flanks of a bimodal nature represented by multiple bowl-shaped to elongated landslide depressions of high relief with highly variable gradients, producing a step-like morphology on their upper parts, and steep inclinations with morphological features of low relief on their lower parts. In some cases the slump complexes on the upper flanks are observed to extend significantly into the plateaus, developing characteristic amphitheater-shaped terraces on the upper flanks. The high-relief morphologic landslide features on the upper reaches of the flanks and the on the plateaus propagation of the sediment failures are best developed along topographic bulges (related to uplifting salt diapirs), developed on the rims of the flanks. The western, northern and eastern flanks of Calcasieu Basin, and the northern and northeastern flanks of Reveille Basin belong in this category.

Slope type 3 has relatively steep slopes dissected by large canyon-like landslide troughs. Acoustic information reveals that canyon-like landslide troughs developed by retrogressive, channelized, rotational slumps that converted to debris flows (Hampton, 1972; Iverson and LaHusen, 1989; Iverson et al., 1997), developing lobes/aprons of debris flow deposits at the foot of the flanks. The inter-trough areas are characterized by relatively steep flanks with shallow failures (rotated blocks and slides) and a few isolated rotational slumps developing bowl-shaped and elongated depressions of low relief. This slope category preferentially develops on the southern flanks of Beaumont and Calcasieu Basins. Canyon-like landslide troughs are also observed on the southwestern and northeastern flanks of Reveille Basin, but the absence of detailed information from the area does not make it possible to determine if they represent features dating prior to, or after the abandonment of Bryant Canyon. Landslide troughs are best developed in Calcasieu Basin, where they have regressed significantly into the southern sill and southeast plateau. Inversely, on the southern flanks of Beaumont Basin, canyon-like landslide troughs are mainly expressed on the middle and upper reaches with limited regression of failures on the plateau. In most cases, canyon-like troughs appear to be connected upslope on the plateau with topographic bulges related to uplift of the underlying salt diapirs (Figs. IV-3, IV-11, and IV-14).

The preferential development of type 1 and 2 slopes on the northern flanks of the basins, and type 3 slopes on the southern flanks of the basins attracts our curiosity, as to what conditions and processes led to that result. A possible answer to this issue points to the development of different halokinetic processes on the northern and southern flanks. Previous studies revealed that the northern slopes of the basins are usually characterized by shallow, almost exposed, uplifted salt diapirs, whereas on the southern slopes salt diapirs appear to be uplifted further south of the basin boundaries (Lee, 1990; Lee et al., 1996). These salt structures most probably developed during the second halokinetic episode, when thick sediment deposits on the upper slope pushed the underlying salt diapirs seaward (Lee, 1990). Seaward moving/uplifting diapirs resulted in significant over-steepening of the northern flanks, leading to the development of extensive and widespread slump complexes (slope types 1 and 2) (Fig. IV-24). Inversely, the southward propagation of the salt diapirs would have caused limited disturbance to the inclination of the southern flanks, mainly local bulges on the plateaus and crests of the flanks. The formation of the bulges on the plateaus/crests by the uplift of salt diapirs would have caused the development of locally unstable conditions in the sediments of the middle/upper southern flanks of the basins that in turn would have initiated the development of the canyon-like troughs (slope type 3) (Fig. IV-24). The complicated nature of the eastern and western flanks of the basins are interpreted as effects of the salt diapirs that tend to over-steepen the flanks by expanding themselves towards the topographic depressions and uplift the adjacent plateaus.

The morphological structures of type 1 and 2 slopes indicate that their development occurred in two stages (Fig. IV-24). Initially, the increased gradients of the flanks (due to the seaward mobilization of the salt masses) led to significantly increased shear stresses, and subsequently resulted in the development of deep (up to, or even exceeding 100 m in thickness) rotational retrogressive slump/slide complexes. The evacuation zones of such failures are observed on the middle and upper parts of the flanks of Calcasieu Basin (high-relief landslide depressions) (Fig. IV-19). The passage of the mass-transports, of the first generation failures, over the flanks, and their deposition at the foot and lower parts of the flanks, led to the sudden increase of the overburden pressure of the underlying sediments of the flanks. That, in combination with the alternating sand/silt and mud layers/laminae, of which the flank sediments (canyon sediments) consist, resulted in the escalation of the pore-fluid pressures in the non-cohesive layers (silt/sand) of the sediments, with the impermeable mud layers acting as seals and sustaining

them under undrained conditions. Thus leading to the significant reduction of the shear strength of those ‘weak layers’, and the development of a second generation of retrogressive translational slump/slide complexes (30 to 50 m thick); through such failures, large slices of the flanks collapsed (Keney, 1984; Prior and Coleman, 1984; Allen, 1985; Papatheodorou and Ferentinos, 1993, 1997). Parallel to the slopes exfoliated slide planes and retrogressive slumps/slides, produced by second generation failures, are observed on type 1 and the lower parts of type 2 basin flanks (Figs. IV-5 and IV-19).

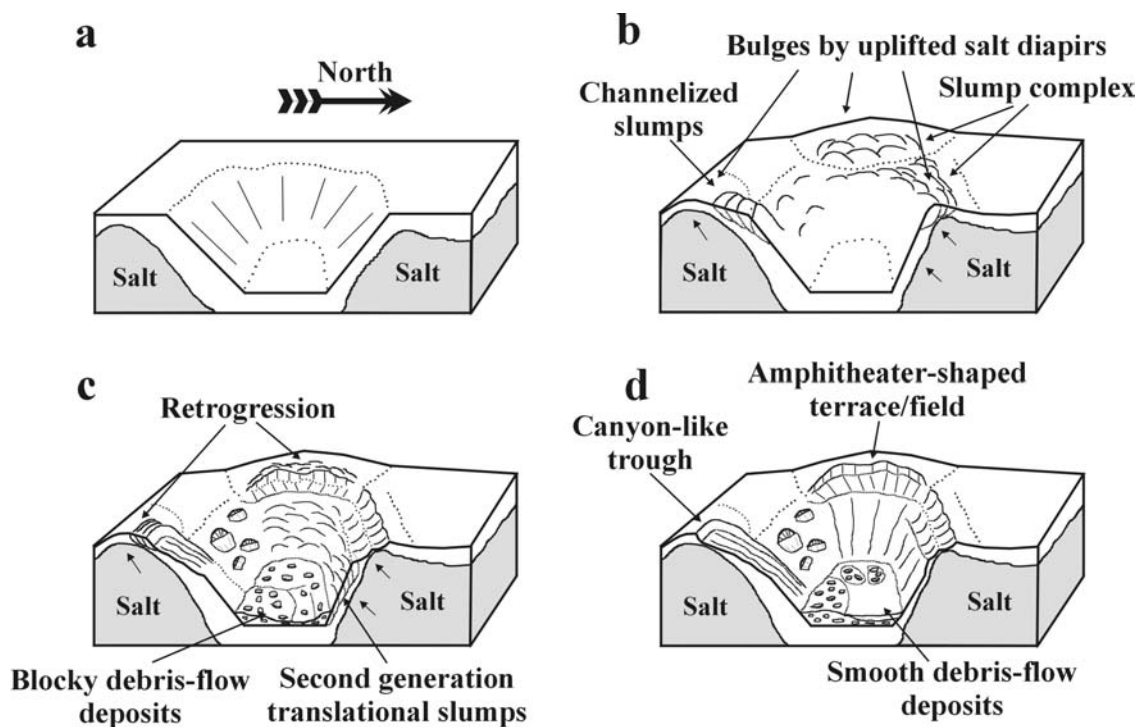


Fig. IV-24. Cartoon of the evolution of the basins during the second episode of high salt-tectonic activity. (a) Basin morphology at the beginning of the last glacial episode. (b) The seaward mobilization of the salt masses leads to the large increase of the flanks' gradients contributing to the development of deep rotational slump complexes (note that the inclinations of the southern flanks are only locally increased by isolated bulges developed by the uplifting of salt diapirs). (c) Deposition of mass-transport deposits at the foot and lower parts of flanks leads, through the increased pore-fluid pressures and reduced shear strength of the underlying sediments, to the development of successive sets of retrogressive translational slumps/slides. (d) Present morphology of the intraslope basins which, during the Holocene, achieved stability due to the deceleration of the salt masses mobility. Note that the majority of the failures has translated into debris flows, resulting in the latest infilling of the basin floors (modified from Tripsanas et al., 2003a).

A two-stage model is also proposed for the evolution of the canyon-like landslide troughs. In the first stage, elongated landslide troughs of high relief are formed by the development of large, isolated, rotational, retrogressive, channelized slumps translated into debris flows. Those slumps were probably related to slope over-steepening caused by the uplift of the underlying salt diapirs. The landslide troughs on the southern flanks of Beaumont Basin represent troughs of this first stage. In a later, second stage, the troughs extend further into the plateaus by a series of retrograde failures. The translation of those failures into debris flows and turbidity currents led to the excavation and downslope evolution of canyon-like troughs (Hampton, 1972; Fisher, 1983; Piper et al., 1999). Prior and Doyle (1985), and Klaus and Taylor (1991) reported similar features on the New Jersey continental slope and Aoga Shima Canyon, respectively. In both cases, the observed features are assumed to have been initiated by retrogressive slumps that evolved by means of density currents and progressive evolution into their present morphology.

Basin Floors

Lee et al. (1996) and Twichell et al. (2000) observed in deep seismic profiles that extensive and very thick mass-transport deposits are present on the floors of the basins and are related to the collapse of the flanks during the two episodes of high salt-tectonic activity. As are the prevailing geomorphological features on the flanks, the mass-transport deposits on the floors of the basins, recorded in the 3.5kHz seismic profiles and sediment cores, are mainly related to slope instabilities of the second halokinetic episode. Three categories of mass-transport deposits have been recognized in this study on the floors of the basins: 1) blocky debris-flow deposits, 2) smooth debris/mud-flow deposits, and 3) sand- to mud-rich turbidites.

Blocky debris-flow deposits are the most pervasive sedimentary units in the basins, producing extensive aprons/lobes adjacent to the flanks characterized by amphitheater-shaped fields/terraces and immature canyon-like landslide troughs. Blocky debris-flow deposits are interpreted to have been resulted from the translation of the large landslides/slumps (coulomb-type failures) that produced the high-relief features on the basin flanks. Throughout the remainder of the basin floors, blocky debris-flow deposits are observed to be partially to totally blanketed by smooth debris/mud-flow deposits. The more fluid nature of the smooth debris/mud-deposits, combined with the absence of sediment rafts in their masses, indicate that resulted from more readily liquefied slumping sediment masses, originating most probably

from the second generation failures. The greater thickness of the smooth debris/mud-flow deposits adjacent to type 1 and 2 slopes, where second generation failures are best developed, supports the above theory.

Iverson et al. (1997) stated that landslides mobilize to form debris flows by three processes: 1) widespread Coulomb failure within a sloping sediment mass, b) partial or complete liquefaction of the mass by high pore-fluid pressures, and c) conversion of landslide translational energy to internal vibrational energy. The third process is considered of minor importance, in the formation of the debris flows, observed in our study area, because of the fine-grained nature of the sediments (clay and silt mainly) (Sohn, 2000). In addition, Iverson and LaHusen (1989) stated that dynamic pore-pressure fluctuations that accompany shearing on discrete failure surfaces can propagate diffusively from their source and change the effective stress to enhance the potential for liquefaction (Iverson et al., 1997). The above information concludes that, since both generations of failures occurred in similar sediments, liquefaction of the slumped sediment masses of the first generation coulomb-type failures, could have also been a very important deformational factor during their downslope transportation. However, the very different structure of the blocky debris-flow deposits reveals that, at some critical point, the mobilization of their sediment masses reached an equilibrium, where large sediment blocks were rafted passively on highly deformed chaotic sediment mixtures, with no further deformation (Prior et al., 1984; Prior and Coleman, 1984; Nemeč, 1990; Masson et al., 1993). This is probably due to: 1) the deeper character (exceeding 100 m) of the first generation failures that would have involved deeper and higher consolidated sediment sections of higher deformation resistance, and 2) the more gradational translation, of the first generation slumping sediment masses, into debris flows.

The youngest basin deposits are represented by hemipelagic sediments interbedded with a few sandy to muddy turbidites that downcore become more abundant and which are almost absent at core tops. Most of the turbidites originated by the development of local isolated failures on the flanks of the basins (Hart et al., 1992; Mohring et al., 1998, 1999). The presence of the hemipelagic sediments, interbedded with turbidites on the tops of the cores, reveals that, after the last glacial episode, the flanks of the basins tended to achieve stability. This switch is also recorded in the spatial and temporal distribution of the different types of gravity-flow deposits over the floors of the various basins. The debris-flow deposits gradually retreat and become limited to the flanks of the basins and deposition of their overridden turbidity currents

and hemipelagic sediments gradually prevail on the floors of the basins. In addition, the general absence of turbidites in the upper part of the hemipelagic sediment sections reveals that the basins are now relatively stable. However, the presence of gravity-flow deposits (mainly thin-bedded turbidites) on the top of a few sediment cores reveals that slope failures are still occurring in the basins but are of a local, infrequent, and isolated character (see core descriptions).

Additional study should be dedicated to the depositional lobes of the canyon-like landslide troughs of Calcasieu Basin. They are characterized by a fan-like and lobate shape large debris/mud-flow deposits. The more fluid and smooth (muddy) character of the upper, younger debris/mud-flow deposits is probably due to the larger distances traveled, and/or by a reworking/filtering of previously failed sediment on the low-gradient of the upper flank (Hampton, 1972; Fisher, 1983; Iverson, 1997; Iverson et al., 1997). One of the most interesting features is the presence of a channel/chute on the eastern landslide trough. It extends from the upper eastern trough down to the middle part of the depositional lobe and it is believed that in the trough the channel is an erosional feature. Significant erosion of the seafloor by debris flows lead to the formation of channels/chutes, as has been reported and documented in many studies (Prior and Bornhold, 1988, 1990; Nemec, 1990; Lee et al., 1999). However, there is no high-resolution seismic information from the eastern trough to support the above interpretation. Seismic data reveal that the possible erosional character of the channel/chute in the trough becomes strongly depositional on the lobe. This information indicates the channelized character of the waning debris flows on the basin's floor. The channelization of the debris/mud flows was probably caused by the building of extensive and successive lateral margins through successive surges/flows, and led to the further propagation of the flows into the basin (Major, 1996; Iverson; 1997).

CHAPTER V

UNIFORM MUD DEPOSITS (UNIFITES)

Introduction

Sedimentary processes operating in small, perched intraslope basins have been a focus of research mainly because of their importance as potential petroleum reservoirs. Two very important processes that occur in these basins are: a) the development of slope instabilities on their flanks, and b) the depositional segregation of turbidity currents initiated on the outer shelf/upper continental slope (Blanpied and Stanley, 1981; Bouma, 1982; Lee, 1990; Bryant et al., 1991; Twichell et al., 2000). Slope instabilities are strongly related to the tectonic setting of the basinal areas and external environmental factors (e.g., storms, tsunamis) (Blanpied and Stanley, 1981; Mutti et al., 1984; Ferentinos et al., 1988; Cita et al., 1996). The segregation of turbidity currents results from the entrapment of the coarsest load in intraslope basins on the upper part of the continental slope, and the downslope bypassing of their finer-grained load as low-density turbidity currents. This process has resulted in the development of intraslope-intrabasinal sand systems/fans, and extensive uniform mud deposits (unifites) (Blanpied and Stanley, 1981; Bouma, 1981, 1982; Lee, 1990; Satterfield and Behrens, 1990).

Unifites are extraordinarily homogeneous fine muds characterized by the total absence of sedimentary structures under visual observations. Although they most commonly occur in small perched intraslope basins, they have also been observed on the abyssal plains of deep-water basins (Damuth, 1977; Stanley, 1981; Blanpied and Stanley, 1981; Behrens, 1984; Cita and Aloisi, 2000). Unifites have been reported from the Eastern Mediterranean, Western Equatorial Atlantic, and Northwest Gulf of Mexico. They demonstrate a subtle textural fining upward through the units, with basal components being siltier and faintly to well-laminated (or even characterized by a basal, normally-graded, sandy layer where the sand fraction is comprised almost entirely of biogenic material) (Damuth, 1977; Blanpied and Stanley, 1981; Behrens, 1984; Cita et al., 1996). Blanpied and Stanley (1981) distinguished two types of unifites: FL (faintly laminated), and U (uniform-completely structureless). In seismic profiles, unifites are identified as acoustically transparent units that occupy flat basin plains and are characterized by a flat to slightly concave upper surface.

Similar depositional units, called “Homogenites”, have been reported to be interbedded in Holocene sediments in the Eastern Mediterranean. Although they share similar characteristics with “unifites”, they differ in that they originate by slope instability processes (large turbidity currents) related to the passage of an enormous tsunami wave initiated by the catastrophic eruption of the volcanic island Thera (Santorini) at 3500 yr. B.P. (Cita et al., 1984, 1996; Cita and Aloisi, 2000).

Behrens (1984) reported the common presence of unifites in the intraslope basins of the upper and middle continental slope of the Gulf of Mexico. This paper focuses on a unifite sequence from Hedberg Basin, located on the mid-continental slope, south of Louisiana in the northern Gulf of Mexico (Fig. V-1). It provides insight into the depositional processes of this unit, and its possible relationship and interaction with the local intrabasinal slope instability processes.

Geology of the Area

Salt diapirism has resulted in the hummocky topography of the northwest continental slope of Gulf of Mexico (Fig. V-1). The diapirs originate from the Middle and Upper Jurassic Luann Salt, which is overlain by thick Cretaceous and Cenozoic sediments. Halokinetic processes have resulted in a topography that consists of uplifts caused by salt domes, ridges, and sheets with intervening salt withdrawal basins. Bryant et al. (1990) identified the presence of over 90 intraslope basins in the Northwest Gulf of Mexico with a relief in excess of 150 m. Based on their particular characteristics, they are divided into intraslope-interlobal and intraslope-supralobal basins, the former usually being related to the diapiric blockage of a previous submarine canyon complex. Intraslope-interlobal basins are usually of higher relief with steeper flanks, and formed by coalescing salt-lobes, whereas supralobal basins are subsiding basins on a salt sheet or nappe, resembling depressions that originate by pressing a pebble into soft clay (Bouma, 1981, 1982; Bouma et al., 1990; Bryant et al., 1990, 1991; Lee, 1990).

Hedberg Basin borders both the terminal end of the confined Eastern Canyon System (Calcasieu Basin) to the north and the unconfined Bryant Canyon System to the west (Fig. V-1). Both canyon systems are considered to have been active during Oxygen Isotope Stage 6 and were deformed by halokinetic processes immediately after their abandonment at the beginning

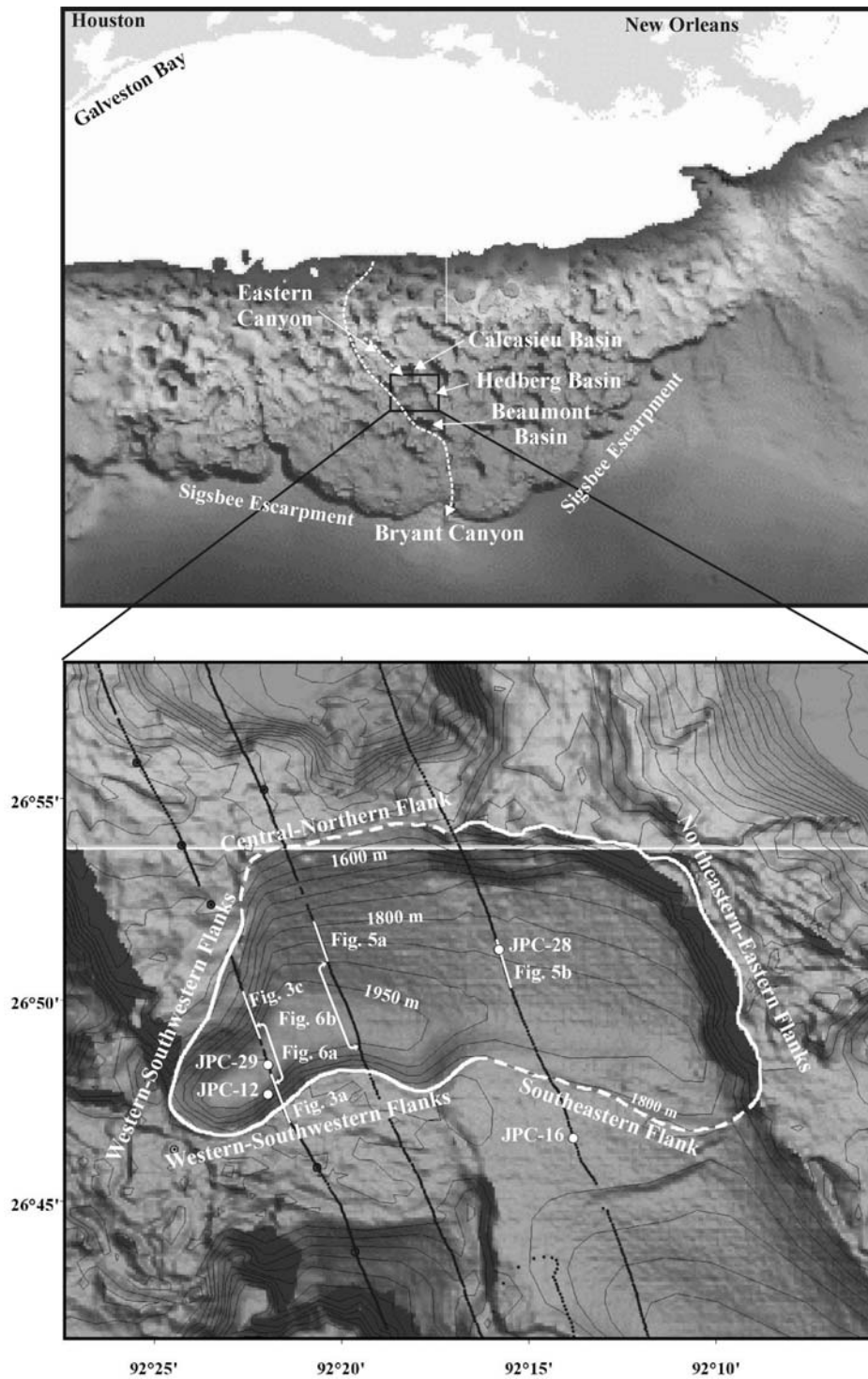


Fig. V-1. Morphologic map of the northwest Gulf of Mexico (upper image) and Hedberg Basin (lower image), showing core locations and seismic lines. The pathways of Bryant and Eastern Canyons are adopted from Lee et al. (1996) and Twitchell et al. (2000).

of interglacial Stage 5 (Lee, 1990; Lee et al., 1996; Twichell et al., 2000) (Chapter II). It was discussed in Chapter IV that the morphology of the canyons has been influenced and modified mainly by two episodes of intense salt-tectonic activity. The first and most severe episode occurred during the early Oxygen Isotope Stage 5 by salt adjustments to the abandoned erosional/depositional environments of the canyons. These processes led to the dissection and transformation of the canyon systems into several sills and basins along their axis (Lee et al., 1996; Twichell et al., 2000). Turbidity currents and gravity flows of the last glacial episode were trapped in the intraslope basins of the upper continental slope, where they deposited the majority of their sediment load. The second pulse of salt tectonics occurred during the last glacial episode (Stages 4, 3, and 2), and is assumed to have been caused by extensive deposition of terrigenous sediments on the outer shelf and upper continental slope, which mobilized the underlying salt masses and sent them seaward (Lee, 1990; Lee et al., 1996) (Chapter IV).

Hedberg Basin combines features of both supralobal and interlobal basins. Seismic profiles reveal that Hedberg Basin represents the northern section of a larger basin that has been divided into two parts by the development of a “horst” formed by the withdrawal of the underlying salt masses (Figure 20 in Lee, 1990). The deep sediment section of the basin (4.5 sec two-way travel-time), in combination with the thicker low-amplitude (low-stand) facies, present in the lower part of the seismic profile, probably indicates that a sediment-channeling canyon system passed through this area prior to the genesis of the Bryant and Eastern Canyon Systems.

Sediment Stratigraphy of Bryant Canyon Area

It was discussed in Chapter II that the tranquil environments (sills and plateaus) of Bryant Canyon are characterized by continuous and undisturbed sedimentation during the last 125 ky. Seven sedimentary units were recognized in the cores. These units are strongly correlated with Oxygen Isotope Stages 6 to 1 and display characteristic bulk density profiles (Fig. V-2a). The dating of the slump and gravity-flow deposits in the cores is based on these seven sedimentary units.

The sedimentology of the seven units, beginning with the youngest, is as follows:

Unit A (Isotope Stage 1, present to 11.16 ky B.P.): Typical hemipelagic sediments

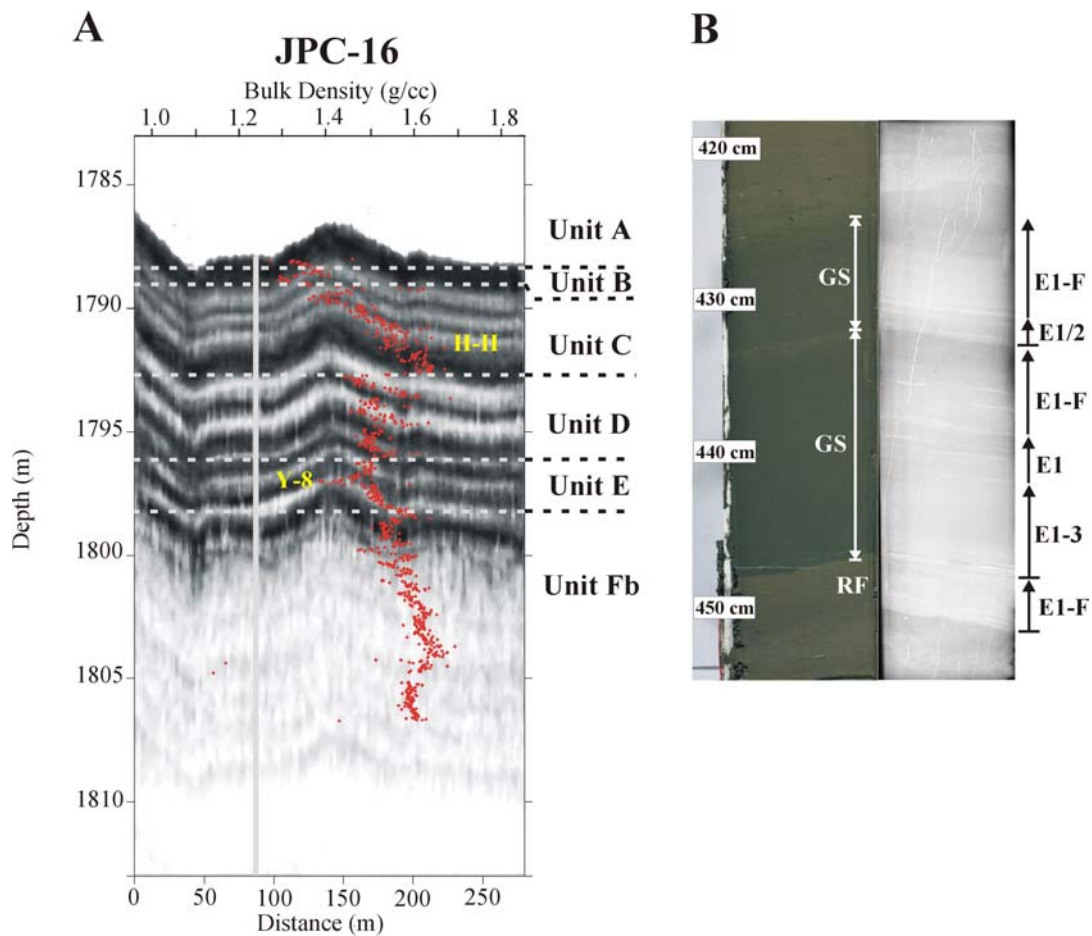


Fig. V-2. A) bulk-density profile, associated sedimentological units, and corresponding 3.5 kHz subbottom profile of a typical sediment core located south-southwest of Hedberg Basin, and B) photograph and X-ray radiograph of chronostratigraphic horizon II (H-II). Horizon II consists of two greenish gray series of successive mud turbidites (GS), and a reddish, basal mud turbidite (RF). Note that, in the greenish gray series, hemipelagic sediments and bioturbation structures occur only on the upper turbidite whereas the rest are characterized by a top-cut-out nature with sharp but not erosional contacts. This implies that each greenish gray series of successive turbidites resulted from a single, pulsating (showing internal surges), low-density turbidity current, and not of multiple and discrete low-density turbidity currents. E1 (laminated mud), E2 (graded mud), E3 (ungraded mud), and F (hemipelagic sediments) represent the three subdivisions of Bouma's T_c division, according to Piper (1978). The gray line indicates the location of the core in the 3.5 kHz subbottom profile. The location of core JPC-16 is shown in Figure V-1. Y-8 = Y-8 ash layer (84 ky B.P.).

Unit B (last deglaciation event, 11.16-18.17 ky B.P.): Dark greenish gray to greenish gray, partially bioturbated, organic-rich clay (34-48 cm thick) that is succeeded downwards by hemipelagic sediments (10-28 cm thick). The organic-rich clay zone was named as chronostratigraphic horizon I in Chapter II.

Unit C (Isotope Stage 2 and ending of Stage 3, 18.17-31.85 ky B.P.): Closely-spaced, normally-graded (0.2-5 cm thick) to mottled/lenticular (3-20 cm thick), clayey-silt/silty-clay layers, interbedded in hemipelagic sediments. On the upper to middle continental slope the silty layers are interpreted to originate from the gradational deposition of low-density, muddy turbidity currents, whereas on the middle and lower part of the lower continental slope they result from bottom-riding, low-density, muddy sediment flows driven by bottom currents. An interesting feature that it was observed and discussed in Chapter II is the presence of a distinct zone of siltier and successive mud turbidites (Fig. V-2b). This zone is named chronostratigraphic horizon II. It can be traced in all cores from the upper to middle continental slope. The thickness of horizon II ranges from 9 to 59 cm, revealing a strong downslope fining and thinning trend. Horizon II is dated to have been deposited between 28.6 and 29 ky B.P., and it is interpreted to have been formed from the deposition of three discrete low-density turbidity currents, of which the last two consisted of multiple internal surges (Chapter II). The origin of these three low-density turbidity currents is assumed to be from the flow transformation of a series of massive sediment failures on the shelf edge/upper continental slope at the end of a major melt water event.

Unit D (Isotope Stage 3 & 4, 31.85-71 ky B.P.): Hemipelagic sediments that are interbedded by a few isolated and irregularly spaced normally-graded (0.2-5 cm thick) to mottled/lenticular (3-20 cm thick) clayey-silt/silty-clay layers. The interpretation of the silty layers of unit D is similar to the interpretation of the silty layers of unit C.

Unit E (Isotope Stage 5, 71-125 ky B.P.): Hemipelagic sediments, containing the Y-8 ash layer, dated at 84 ky B.P.

Units F (Isotope Stage 6): Sand/mud thin-bedded (Fa) and fine-grained (Fb) turbidites, which are related to turbidity currents flowing through the Bryant and Eastern Canyon systems. The sandy deposits of unit Fa represent intracanyon deposits, whereas the fine-grained turbidites of unit Fb are overbank deposits.

Data and Methods

High-resolution acoustic subbottom data were collected during a 1998 cruise on R/V *Gyre*, using the Texas A&M Deep-Tow System equipped with a 3.5 kHz subbottom profiler, and a 100 kHz side-scan sonar, towed thirty meters above the seafloor.

Forty-eight Jumbo piston cores (JPC), up to 20 m long, were acquired from the Bryant Canyon area during a cruise in 1998 on the R/V *Knorr*, using the WHOI Jumbo Piston Corer. Bulk-density and P-wave velocity profiles were derived from all cores with a GEOTEK Multi-Sensor core logger. Three long sediment cores from Hedberg Basin form the focus of this study. Sediment cores JPC-28 and JPC-29 were split in half; one half was archived, and detailed optical descriptions at the millimeter scale, and high-resolution photographs were obtained from the other half. X-ray radiographs were taken from 1-cm-thick sediment slabs of the whole length of the cores to determine sedimentary structures not visible to the naked eye. The analysis of core JPC-12 was mainly based on its bulk-density profile.

Geomorphology, Sedimentology, and Seismic Interpretation

Hedberg Basin is an E-W elongated basin with relief ranging from 200 to 400 m (Fig. V-1). It is characterized by a multimodal geomorphology and highly variable gradients ranging from 13° to less than 2°. Five geomorphologic provinces were identified inside the basin: a) the western-southwestern flanks, b) the central-northern flank, c) the northeastern-eastern flank, d) the southeastern flank, and e) the basin floor (area below the isobath of 1950 m). Different geomorphologic characteristics and sedimentological processes characterize each one of these provinces.

The western part of the basin is the deepest, and is surrounded by shallow uplifted salt diapirs and highly inclined flanks (9° to 11°). Fig. V-3a reveals that the southwestern flank is characterized by the presence of a large, spoon-like evacuation zone on the upper and middle flank that is cut by shallow (15-25 m thick) retrogressive slides/slumps. The large evacuation zone is interpreted to originate from the development of a deep first generation slump complex (exceeding 50 m), which probably accounts for the narrow slope apron (blocky mass-transport deposits) at the foot of the flank. The shallow retrogressive sediment failures are interpreted as younger, second generation sediment failures. Core JPC-12 revealed that the second generation of failures was active until almost the end of the last glacial maximum, whereas during the Holocene no failures have been observed (Fig. V-4). The deep basinward burial of the blocky mass-transport deposits, in combination with a superimposed layer of undisturbed Oxygen Isotope Stage 5 hemipelagic sediments, observed in core JPC-29 (Figs. V-4 and V-6a), indicates that the first generation of sediment failures probably occurred during the first episode of high salt-tectonic activity. In contrast to the early onset of deformation in the west,

the eastern part of the southwestern flank has been affected only by the latest generation of sediment failures.

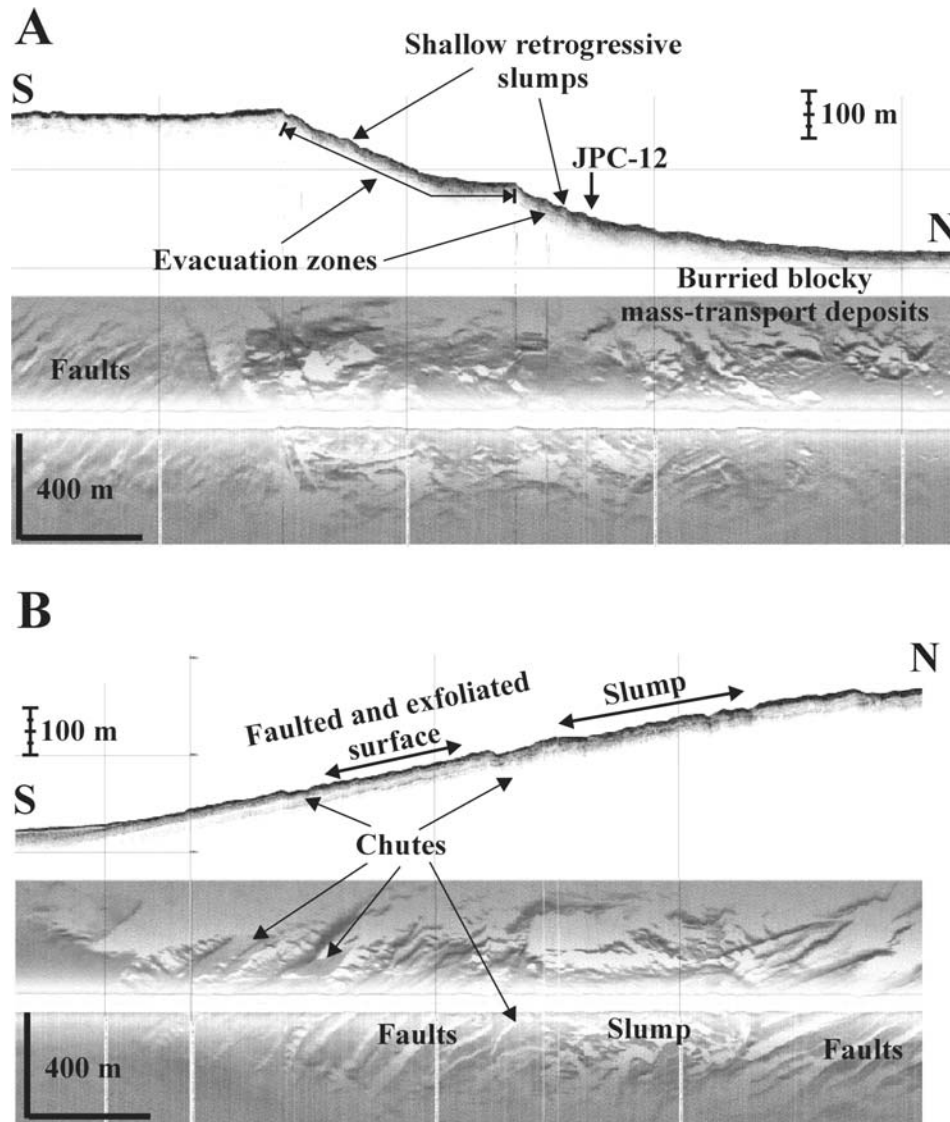


Fig. V-3. 3.5 kHz profiles and side-scan sonar images from the western-southwestern flanks of Hedberg Basin. A: two generations of sediment failures have influenced the morphology of the slope. The first generation was the most severe and resulted in the development of large evacuation zones on the basin flanks and a narrow slope apron (blocky mass-transport deposits) at the foot of the flank. The second generation of sediment failures is expressed by shallow retrogressive slumps, which are superimposed on the first generation failures; B: the complex geomorphology of the northwestern basin flank, characterized by dissection resulting from faults, chutes, and slumps. Locations of the profiles are shown in Figure V-1.

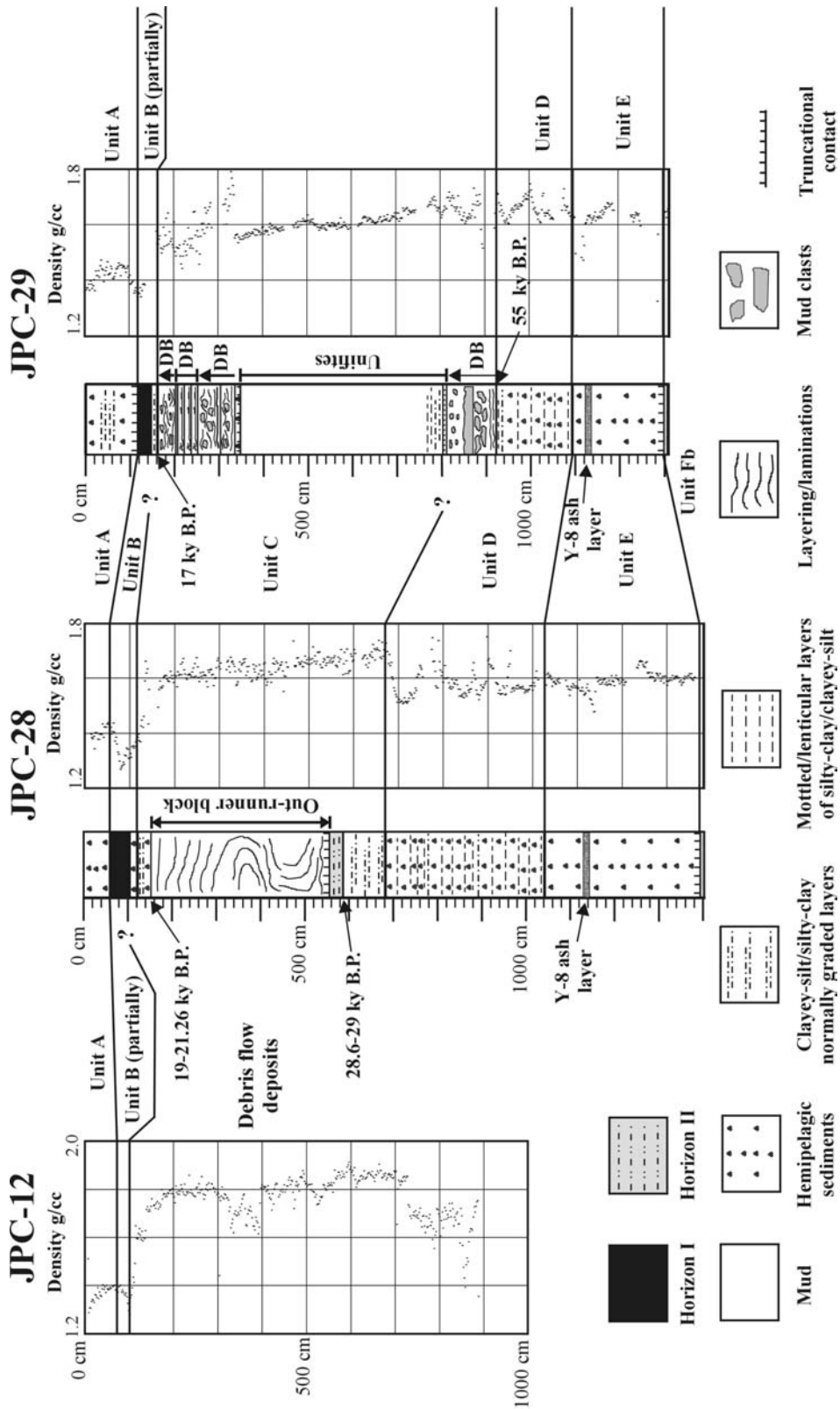


Fig. V-4. Sedimentological descriptions and bulk density profiles of three Jumbo Piston cores from Hedberg Basin. The dates, in cores JPC-28 and JPC-29, have been estimated using the sediment stratigraphy of Bryant Canyon area and sedimentation rates given in Chapter II. Locations of the cores are shown in Figure V-1. DB = debris flow deposits.

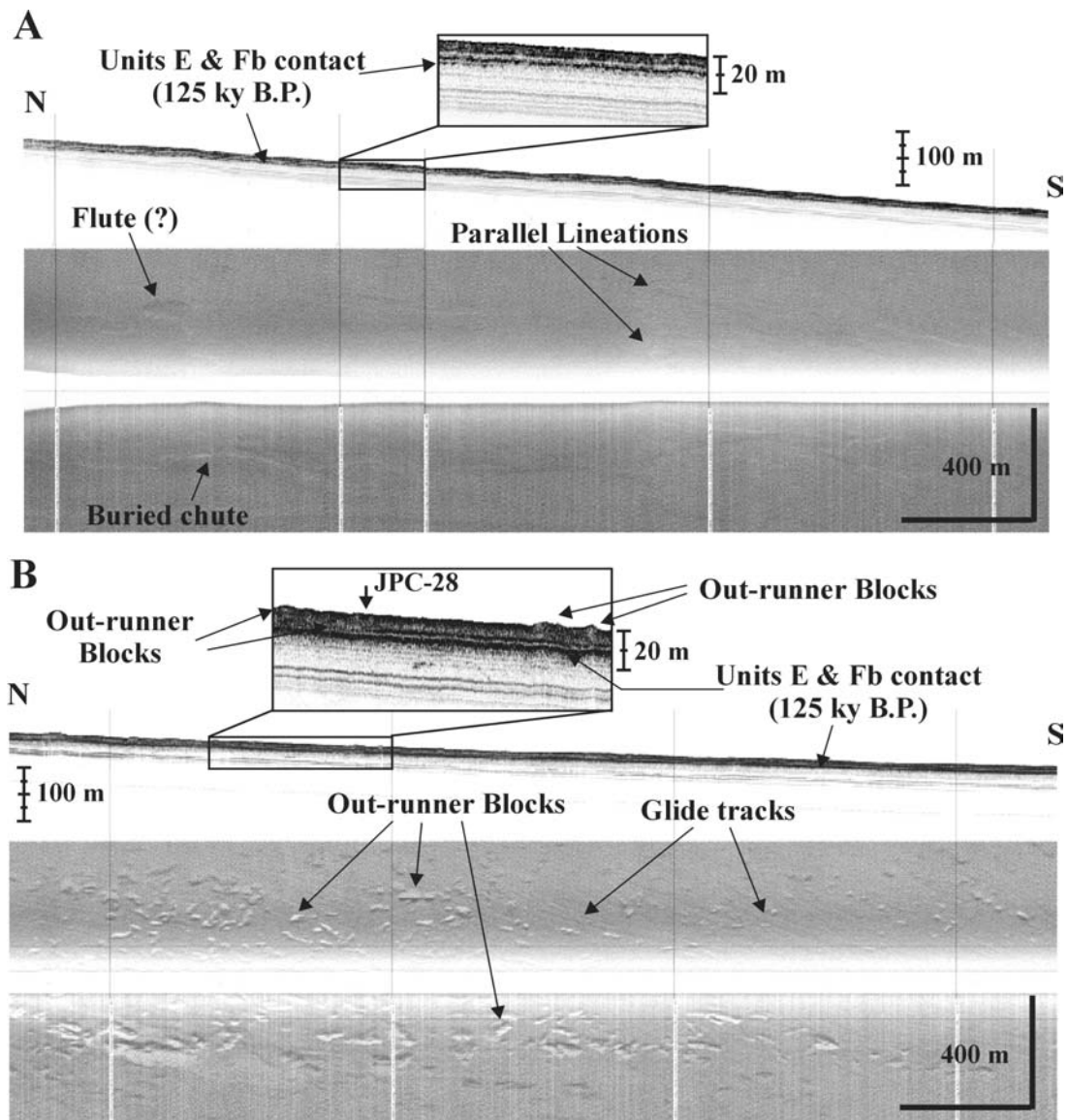


Fig. V-5. 3.5 kHz profiles and side-scan sonar images from the (A) central-northern flanks of Hedberg Basin displaying buried (smoothed) parallel lineations and possible flute marks, revealing the passage of debris flows and turbidity currents, and (B) eastern flanks of Hedberg Basin characterized by abundant sediment blocks and their glide tracks. Locations of the profiles are shown in Figure V-1.

The northern flank of the western basin is characterized by a considerably different geomorphology as compared to the southwestern flank. Seismic profiles (Fig. V-3b) reveal that the northern flanks are dissected by numerous of ESE-WSW oriented faults with a NNE dip, indicating intense salt activity. A few isolated slumps (20-25 m thick), and chutes parallel to

the direction of the faults are visible on the slope. The chutes probably were created by shallow retrogressive slumps. However, due to limited acoustic data coverage, it is not certain whether those characteristics are representative of the entire northern flank or represent only a transition towards the tranquil environment of the central-northern flank.

The central-northern flank of the basin contains low angle slopes (4.5° to 2.5°), the steepest being on the upper part (Fig. V-1). A 3.5 kHz seismic profile from the area indicates a continuous sedimentation pattern for the last 135 ky. However, side-scan sonar images reveal that small skin failures, buried by hemipelagic sediments, developed on the upper flank, whereas on the middle to lower flank the buried remnants of chutes and lineations (and possibly flute marks) suggest the passing of debris flows and/or turbidity currents (Fig. 5a).

The eastern part of the basin consists of steep slopes (12° to 13°) that rapidly pass downslope into a gently inclined slope (1° to 2°) (Fig. V-1). Abundant, buried glide tracks and out-runner sediment blocks, detached from the front of large slumps on the steep eastern upper flank, are visible in the side-scan sonar images and 3.5 kHz seismic profiles (Fig. V-5b). Core JPC-28 (Fig. V-4), located on the gently inclined middle/lower eastern flank of the basin, is characterized by a continuous and undisturbed sediment section that covers the last 125 ky. The only exception to the undisturbed section occurs in the interval between 156-559 cm that consists of disturbed and convoluted sediments that may represent an out-runner sediment block. Its location in sediment deposits of the last glacial maximum (Unit C) reveals that the development of large sediment failures on the steep upper part of the eastern flank occurred during this period.

The eastern part of the southern boundary of Hedberg Basin passes over a steep “step” 25 to 50 m high (Fig. V-2). This step coincides with a large normal growth-fault (about 2.5 seconds two-way travel-time deep) that borders the northern side of a horst separating Hedberg Basin from a southward trending morphological depression (Figure 20 in Lee, 1990).

The basin floor is located on the western-central part of Hedberg Basin (Fig. V-1). The western-central and eastern part of the floor is of a different sedimentological character due to the diverse nature of the surrounding basin flanks (Fig. V-2 and V-6). Thick mass-transport deposits, resulting from the collapsed flanks of the western part of Hedberg Basin, characterize the western-central floor with chaotic acoustic facies exceeding the penetration of the 3.5 kHz sub-bottom profiler (>50 m). In the upper section of the mass-transport deposits, a transparent lenticular layer (up to 10 m thick), with an overall flat upper surface drapes the basin floor and

fills topographic depressions (Fig. V-6a). Core JPC-29 revealed that this transparent layer consists of a homogeneous, structureless mud zone (unifite), which deposited at some point between 55 and 17 ky B.P. (Fig. V-4).

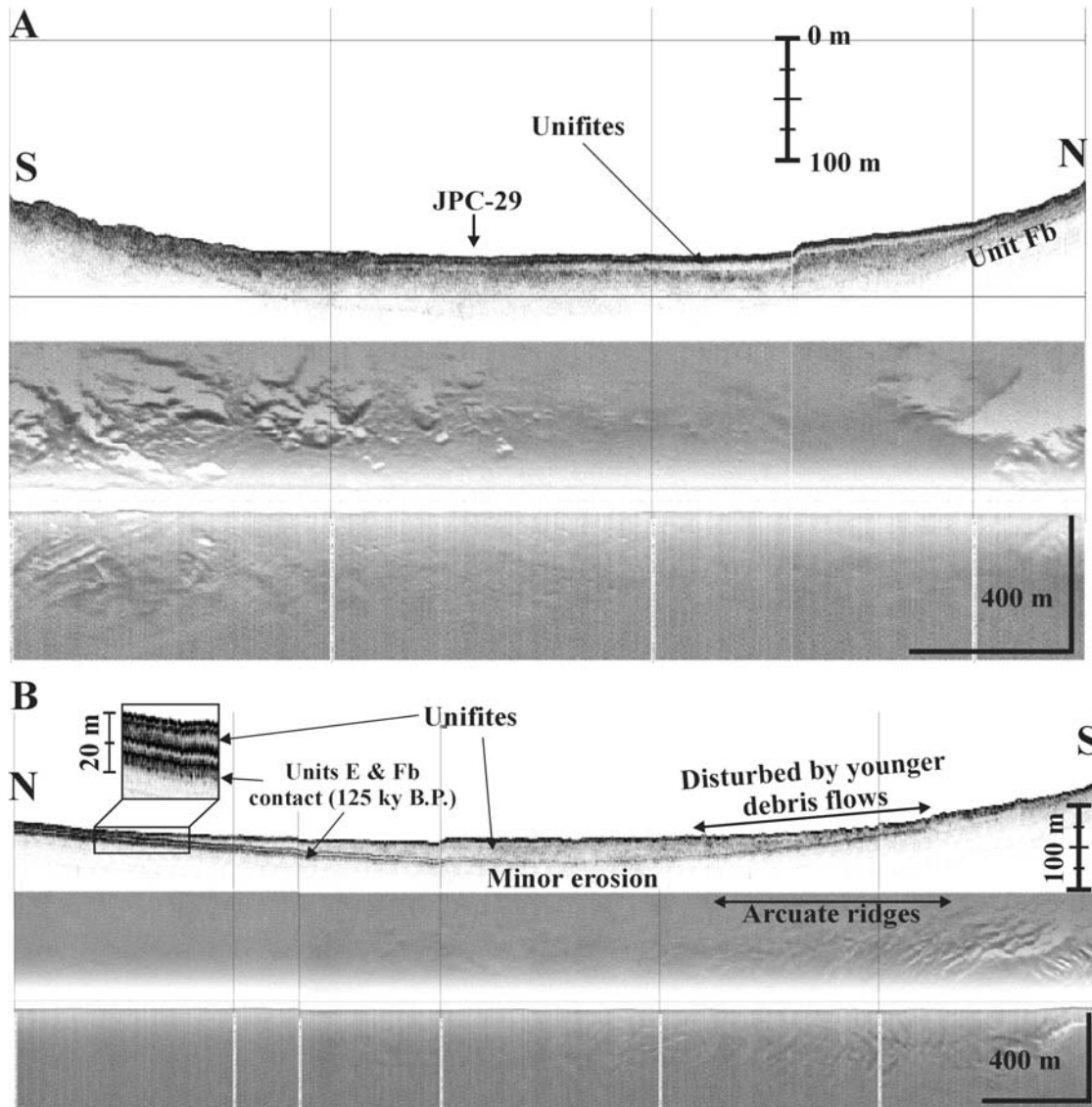


Fig. V-6. 3.5 kHz profiles and side-scan sonar images of the floor of Hedberg Basin. Note how the unifites are disturbed on their southern reaches by younger debris flows in the right part of both profiles. Locations of the profiles are shown in Figure V-1.

The eastern part of the basin floor is characterized by the presence of an interbedded, lenticular, transparent layer (up to 25 m thick) that thins towards the edges of the floor, in

relatively undisturbed sediments with minor erosion at the base of the transparent layer (Fig. V-6b). Based on observations of the western basin floor, the transparent layer is interpreted to represent the eastern extension of the unifite observed in core JPC-29. At the southern boundary of the eastern floor, the unifite is disturbed by younger debris-flow deposits. The unifite and the debris-flow deposits are capped by a 3 to 4 m thick zone, which is characterized by a strong, semi-prolonged surficial and subbottom reflector (compare with Figure V-2). This zone probably represents sediments of Units A, B, and C (partially). This indicates that the deposition of the unifite and the debris flows occurred between 18 and 31.9 ky B.P. (depositional time interval of unit C).

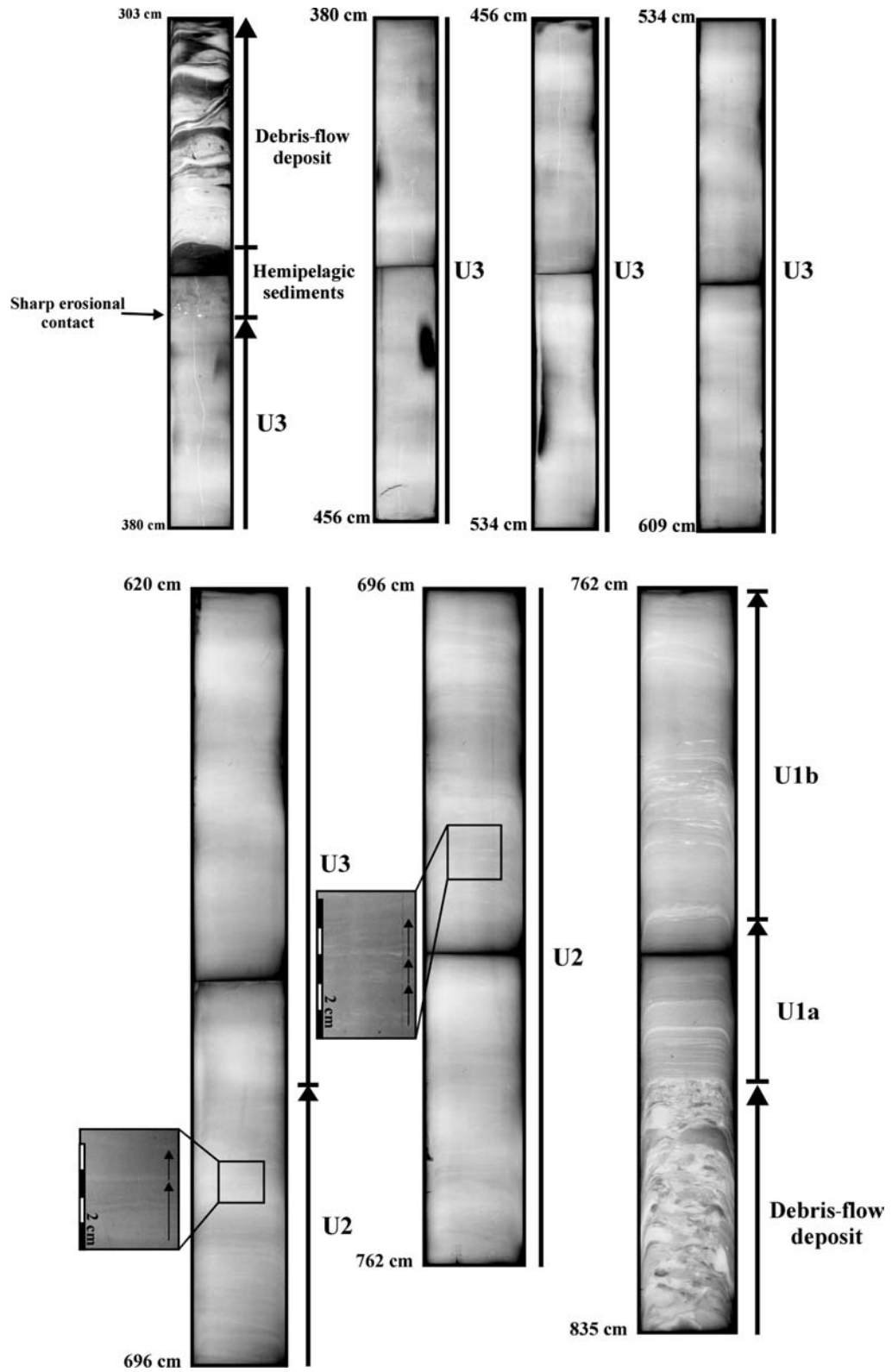
Unifites

Structureless mud deposits (unifite) occupy the floor of Hedberg Basin with a maximum thickness in the central-eastern (deepest) part and thinning towards the edges (Figs. V-2, V-3, and V-6). Behrens (1984) reported that unifites from intraslope basins in the northwest Gulf of Mexico consist of clayey mud, generally with less than 0.25 % sand and a mean grain size of 10 phi.

Core JPC-29 is located adjacent to the southwest edge of the unifite. The unifite thickness is 462 cm, and it is interbedded in debris-flow deposits that occurred between 17 and 55 ky B.P. X-ray radiographs and visual descriptions reveal that this unifite consists of three divisions (Fig. V-7). This is in contradiction with the original meaning of the term “unifite”, which has value only for the third upper division. However, in order to preserve the relation of these mud deposits with those of previous studies, the term “unifite” will remain in use in this paper.

The lower division (U1: 811-762 cm) is represented by two sequences of sandy-mud/mud layers that fine upwards (Fig. V-7). The sand fraction is entirely of biogenic origin (foraminifera). The lower sequence (U1a: 811-795 cm) consists of five normally-graded sandy-mud layers with sharp silty bases, and an upper mud layer characterized by a sharp base and basal silty laminae. The lower two sandy-mud layers are distinctly laminated, whereas in the upper three layers the laminations become indistinct or absent. The overlying sequence (U1b: 795-762 cm) consists of 11 normally-graded mud layers, characterized by silty bases, which grade from thick silty basal layers/laminae, with ripple laminations in the lower mud units, to discontinuous/wispy silty basal laminae in the upper mud units.

Fig. V-7. X-ray radiographs displaying the entire unifite sequence, which is observed in core JPC-29. The gap in the interval 609-620 cm is due to sampling for consolidation tests. The black intervals in the image represent the contacts of successive X-ray radiographs. Note how the unifite grades from: a) well-developed, laminated, sandy-mud (sand is entirely of biogenic origin) and mud, normally-graded layers with fading upwards silty laminae, organized in two fining upwards sequences (U1a and U1b), to b) faint, normally-graded mud layers (left enlarged image), which occasionally are characterized by faint, wispy, silty laminae (right enlarged image) (U2), to c) uniform mud with faint siltier (lighter) and more clayey (darker) bands (U3). The arrows in the enlarged sections indicate individual mud units. The grading from well-developed, laminated, normally-graded mud layers in U1 division to uniform mud deposits in U3 division indicates that, during the deposition of the unifite, there was a gradual suppression of the tractional forces and domination of suspension deposition. The absence of any bioturbation structures and hemipelagic sediments at the top of the mud layers indicates that the unifite resulted from the deposition of successive flow events occurring in a single, fine-grained sediment flow, and not of multiple and independent, fine-grained sediment flows. In addition, note the sharp and erosional top of the unifites, which indicates that part of the unifites either slumped away or was eroded by the passage of a sediment flow.



The sediments of the second division (U2: 762-668 cm) consist of uniform, structureless mud under visual observations. However, X-ray radiographs reveal that this interval is characterized by subtle, normally-graded, ghost layers/units (typically 2-10 cm thick) with sharp bases (Fig. V-7). Occasionally, a few upwards-fading silty, discontinuous/wispy laminae are observed in some of the ghost mud units.

The upper division (U3: 668-349 cm) is represented by uniform structureless mud deposits. However, subtle, lighter (slightly siltier) and darker (slightly more clayey) bands (5-20 cm thick), with gradational boundaries are observed in the X-ray radiographs (Fig. V-7). Occasionally, a few isolated, faint, wispy, silty laminae are observed in some of the siltier bands. These silty laminae are only apparent in the original data.

Neither hemipelagic sediments, nor bioturbation structures are observed to occur within the unifite sequence described above.

Discussion and Conclusions

Sedimentological investigations reveal that the U1 and U2 divisions of core JPC-29 consist of fine-grained turbidites. Piper (1978) proposed three subdivisions of Bouma's T_e division from top to bottom (Stow and Piper, 1984):

F: Hemipelagic sediments,

E3: Ungraded mud,

E2: Graded mud,

E1: Laminated mud,

D: Laminated sand and silt.

This nomenclature will be utilized for the convenience and simplification of our discussion.

The mud turbidites of the lower U1 division grade from complete or top-cut out (E1-E2-E3 to E1) units at the lower parts of the U1a and U1b sequences to base-cut out (E2-E3) units at their upper part; revealing that they were deposited by two successive waning sequences of flow events, the first being the most intense. Base-cut out (E2-E3) mud turbidites in the U2 division, and the uniform structure of the U3 division indicate the gradual suppression of the tractional forces and the dominance of suspension sedimentation through time. It was stated earlier that, in some cases, the normally-graded ghost layers of division U2 and the slightly siltier bands of division U3 are characterized by a few wispy, silty laminae. The wispy, silty laminae infer that, although suspension sedimentation was dominant during the deposition of

division U2 and U3, it was interrupted episodically by short intervals of tractional sedimentation, which probably resulted from flow intensification episodes. The above discussion, combined with the total absence of hemipelagic sediments and bioturbation structures at the top of all of the mud units (which make up the unifite sequence), indicate that the flow events, which resulted in the deposition of the unifite in Hedberg Basin, did not occur as discrete, low-density turbidity currents, but probably as successive surges occurring in a single low-density turbidity current.

However, it is unclear whether the origin of the pulsating (showing internal surges), low-density turbidity current is through the flow transformation of intrabasinal debris flows or through the depositional segregation of a large, pulsating turbidity current initiated at the shelf edge or upper continental slope (Hampton, 1972; Blanpied and Stanley, 1981; Cita et al., 1996; Piper et al., 1999). The correlation of unifites to intrabasinal slope instability processes is considered improbable for two reasons. The first is the presence of the slope aprons at the foot of the basin flanks, consisting entirely of slump and debris-flow deposits. This indicates that no extensive flow transformation occurred on these sediment failures. Extra support for this conclusion is provided by the absence of mud clasts in the mud units, which would be an indication for flow transformation of intrabasinal debris flows into turbidity currents. The second reason is that even if the unifite would have been deposited by the overridden turbulent clouds of intrabasinal debris flows, it would require the majority of the intrabasinal sediment failures to have occurred almost simultaneously to account for their large thickness (up to 25 m), and complete absence of interbedded hemipelagic sediments and bioturbation structures. Such is rather difficult to accept.

Consequently, the most reasonable explanation for the origin of the pulsating, low-density turbidity current, which resulted in the deposition of the unifite in Hedberg Basin, is through the depositional segregation of a large, pulsating turbidity current produced on the shelf edge or upper continental slope. The presence of parallel lineations on the central-northern flank of Hedberg Basin, suggesting the passage of possible turbidity currents, provides extra support for this hypothesis. It was stated earlier that horizon II (28.6-29 ky B.P.) has been deposited from three discrete low-density turbidity currents, of which the last two consisted of multiple internal surges. It is very possible that unifites resulted from one of these two low-density, pulsating turbidity currents. Although deposits of many more low-density turbidity currents have been recorded in the sediments of the last glacial episode, none of them is characterized

by a pulsating nature to be able to result in the deposition of the unifite observed in core JPC-29.

To summarize, three are the main conclusions of the above discussion: a) the unifite in Hedberg Basin has been formed from the deposition of a pulsating (showing internal surges), low-density turbidity current (dated at 28.6-29 ky B.P.), b) the mud units, which consist the unifite, are organized in finning upwards sequences (this is most apparent in U1 division), and c) during the deposition of the unifite, there is a gradual suppression of the tractional forces and a gradual domination of suspension deposition. According to the above information, a three stage depositional model is proposed for the unifite that has been recorded in Hedberg Basin:

Stage 1: During this stage the lower U1 division was deposited. It has been proposed by many researchers that when a turbidity current is trapped in an enclosed basin, it bounces on the flanks of the basin and generates a waning series of reflected flows (Pickering and Hiscott, 1985; Muck and Underwood, 1990; Kneller et al., 1991; Edwards et al., 1994; Haughton, 1994). A similar scenario can also be envisaged for the successive surges of the pulsating, low-density turbidity current that led to the deposition of the unifite in Hedberg Basin. The two sequences in division U1 probably represent deposits from the first two introduced surges of a pulsating low-density turbidity current in Hedberg Basin. The morphology of Hedberg Basin indicates that these surges would have been deflected to the west and restricted to the basin floor. The upward-fining mud turbidite units in the sequences are interpreted as successive depositional units of reflected flows (moving hydraulic jumps that transport mass) generated by the rebound of the surges against the basin walls. Stow and Bowen (1980) stated that low-density turbidity currents are characterized by low concentrations (2500 mg l^{-1}), velocities of $10\text{-}20 \text{ cm s}^{-1}$, and thickness ranging from 200 to 800 m (sometimes exceeding 1000 m). This indicates that low-density turbidity currents/surges do not deposit all of their suspended sediments in one intraslope basin, but, due to their large thickness, are able to override the sills between two adjacent intraslope basins and continue to propagate downslope. This interpretation is supported by the presence of horizon II further downslope of Hedberg Basin.

Stage 2: The successive and almost continuous introduction of sediment clouds into Hedberg Basin, and settling of sediments from the suspended load, would be expected to lead to the gradual development of a stratification interface separating a lower layer of higher sediment concentration from an upper layer of lower sediment concentration. The high-density stratified layer would sustain its sediment load under suspension by the turbulence of the waning

reflected flows, resembling to internal waves at this point, and the transmission of turbulent energy by surges introduced later. The existence of such a density interface would have: a) forced the subsequent surges to ride this interface, b) suppressed the transmission of the applied shear stress, and c) led to the domination of suspension deposition. Division U2 is believed to have been deposited by suspension sedimentation during the development of the stratification interface. The wispy, silty laminae, observed in some of the subtle, normally-graded mud units (E2-E3), indicate that short period tractional deposition of settled silty material was still occurring. This is probably due to the hydraulic perturbations produced by later introduced surges and/or by the penetration of their lower siltier and denser part into the still weak and still forming intrabasinal stratified layer. The remaining, subtle normally-graded mud units, characterized by the absence of silty laminae, represent suspension deposits of weaker flow events, and most probably of the depletive reflected flows.

Stage 3: During this last stage the stratification interface is fully developed, constituting suspension sedimentation as the major depositional process, and suppressing the traction forces and turbulence of the overriding flows. The U3 division is assumed to have been deposited during this stage. The faint, slightly siltier, layers/bands are explained by the partial settling of the coarsest load of the overriding surges and reflected flows through the stratified layer. Sudden intensification of the vague bedding in U3 division is interpreted as the influence of subsequently introduced surges.

Studies on continental shelves have revealed that river plumes can lead to the development of a high-concentration lower layer (fluid mud) that, due to its own gravity and/or shear stresses applied by tidal currents and wave activities, can be mobilized seaward as a gravity flow (Cacchione et al., 1995; Ogston et al., 2000; Wright et al., 2001). Similarly, it has been speculated that, as a low-density turbidity current decelerates, sediment settling and the damping of turbulence may lead to flow stratification and the formation of a slow-moving, hyper-concentrated flow ($50-100 \text{ kg m}^{-3}$) that may solidify as an ungraded mud layer (McCave and Jones, 1988; Stow et al., 1996). Fluid muds and muddy debris flows are characterized by a homogeneous undifferentiated structure, with particles in contact throughout the slurry, prohibiting suspension sedimentation (Krone, 1993; Winterwerp, 2002). In addition, muddy debris-flow deposits are characterized by a uniform to chaotic internal structure (Tripsanas et al., 2003b). However, even the most uniform U3 division displays a very faint, ghost layering with, occasionally, a few, isolated, wispy laminae resulting from suspension sedimentation,

with weak and very short intervals of traction sedimentation. This structure of the unifite in Hedberg Basin indicates that the concentration of the lower stratified layer probably never exceeded the fluid mud limit (10 g l^{-1}) and sedimentation was more on a continuous basis than a sudden event.

Independent of whether a fluid mud layer was developed or not, the above depositional model appears to apply for the deposition of unifites. In addition, it can also explain the widespread deposition of unifites in the intraslope basins of the upper and middle continental slope of the northwest Gulf of Mexico (Behrens, 1984). The low-density turbidity currents are not confined to one intraslope basin, but due to their large thickness and the development of the stratification interfaces, deposit only part of their suspended load while propagating downslope, depositing their sediment load in a series of successive downslope intraslope basins (Chapter II). The presence of a transparent draping layer that occupies the deepest part of the floor of Beaumont Basin, similar to unifites, supports this model (Chapter IV). However, no sediment cores have been retrieved from that area to confirm their interpretation as unifites.

It was stated earlier that the mud units, which make up the unifite of Hedberg Basin, represent deposits from successive surges of a pulsating, low-density turbidity current and their respective reflected flows. Accordingly, it is safe to assume that the depositional time of two successive mud units is the time that is required for a flow event to move from the location of core JPC-29 to the western flank of Hedberg Basin, being reflected and move towards the central-northern flank of the basin, and again being reflected and come back to the core JPC-29 location. This distance (L) is estimated to be about 25 km. Consequently, the depositional time (T) of the unifite can be estimated by the equation:

$$T = NL/2U$$

Where, N= the number of mud units observed in the unifite (U1: 17 units, U2: 23 units, U3: 24 units), and U= the velocity of the flows (10 to 20 cm/s, according to Stow and Bowen, 1980). Solving this equation, it is assessed that the unifite of Hedberg Basin deposited within 47-92 days. This depositional time clearly indicates that the pulsating, low-density turbidity current, which resulted in the deposition of the unifite, was also of very long duration.

Although the pulsating nature of a long-lasting turbidity current is necessary for the deposition of the unifite observed in Hedberg Basin, it is not considered to be a requirement for the deposition of unifites in general. A simple turbidity current of long duration could also lead to the development of unifites, since the production of the density interface is not dependent on

the pulsating nature of the turbidity currents, but on the almost continuous supply of a sediment cloud in the intraslope basins. In this case, due to the behavior of the sediment flow as a single long-lasting surge, it would be expected: a) divisions U1 and U2 to be indistinguishable from each other and expressed by a single fining upwards sequence of successive fine-grained turbidites (successive waning and depletive reflections of the head of the flow against the basin walls), and b) division U3 to be characterized by a very uniform appearance (no perturbations by later introduced surges).

CHAPTER VI

CONCLUSIONS

Sedimentological History

This study reveals that the sedimentological history of Bryant Canyon area is very complex, and that for each time period it was mainly dependant on: 1) the sea-level stand, 2) the climatic conditions and magnitude of the river discharges, 3) location of the main river/delta discharges, and 4) the morphology of Bryant Canyon area.

Bryant and Eastern channel/canyon systems were the main morphological areas, during Oxygen Isotope Stage 6, into which gravity flows were transporting and depositing Mississippi River derived sediments across the shelf and continental slope toward the deep abyssal plain of the Gulf of Mexico. The origin of turbidity currents in the area was either from the flow transformation of sediment failures (surge-like turbidity currents), or directly from hyperpycnal river plumes (hyperpycnal turbidity flows). The sediment load of both types of turbidity currents was fine sand-silt or silt with substantial amounts of clay-sized material.

Oxygen Isotope Stage 6 overbank deposits are more than 50 m thick and 15 km wide, and reveal that overflowing processes of the funneled turbidity currents were very frequent and dominant. Five facies (M1-5) of overbank deposits were recognized. The facies consist of complete/middle-cut-out to base-cut-out Stow and Shanmugam's mud turbidite sequences. Sedimentological data show that a complete sequence results from the succession of five flow regimes, occurring in a waning and depletive low-density, mud-rich turbidity current. The development of each flow regime depends on the: 1) flow velocity, 2) suspended sediment concentration relative to the capacity of the flows, 3) silt to clay ratios of the suspended sediment load, 4) clay mineralogy, and 5) organic matter concentration. The first two factors control erosional versus depositional processes of the turbidity currents, whereas the last three factors control the intensity of the flocculation processes, the drag reduction of the flow, and consequently the silt/clay depositional competition.

Spillover flows are controlled by the nature of their parental, funneled turbidity currents (thickness and intensity), and the canyon/channel morphology (height and meandering). Internal waves on the upper surface of the funneled turbidity currents cause the overflowing to

occur in successive surges, developing sequences of mud turbidite facies, rather than discrete depositional units.

The existence of erosional/depositional environments of Bryant and Eastern Canyon systems certainly disturbed the stability of the underlying salt masses, which, through differential loading, tended to obliterate and restore the seafloor morphology on the erosional parts of the canyons (uplifted salt diapirs), and to retreat and collapse on the canyons depocenters (salt withdrawal). However, coupled erosional-depositional processes of the gravity flows were able to balance the salt movements during the active low-level stand (Stage 6) of the canyon systems (eroding the uplifted sections of the canyons, and depositing in the collapsing sections).

During the high sea-level stand of Oxygen Isotope Stage 5, the majority of river-sourced sediments were trapped on the widespread continental shelf of the northwest Gulf of Mexico. That prohibited the generation of turbidity currents on the shelf margin and/or upper continental slope, causing the abandonment of Bryant and Eastern Canyons. It was during the first 30 ky of Stage 5 that both canyons transformed by halokinetic processes into a series of basins and sills along their axis.

The low sea-level stand of the Last Glacial Episode (Stages 2, 3, and 4) was characterized by the eastward switch of the major discharges of the Mississippi River. However, river discharges, even though significantly reduced, were still occurring on the continental shelf updip of Bryant Canyon area. Two sedimentological provinces coexisted in Bryant Canyon area during this time interval. The first was extended from the upper to middle/lower continental slope, and it was supplied with sediments from the continental shelf, through low-density (mud) turbidity currents. The low-density turbidity currents originated from the depositional segregation of large turbidity currents, generated on the shelf margin and/or upper slope, by depositing their coarsest material in the intraslope basins of the upper continental slope. The second province was located on the middle and lower part of the lower continental slope, and was supplied with sediments from low-density, fine-grained, bottom-riding sediment clouds driven by westward flowing bottom currents. The sediment clouds originated from the piracy of Mississippi Canyon and Fan turbidity currents from bottom currents.

Five discrete sedimentological time periods occurred during the Last Glacial Episode:

1. The first period occurred during Oxygen Isotope Stages 4 and 3 (71-31.85 ky. B.P.). The sea-level stand of this period was ranging between – 70 m (during Stage 4) and –20 to –40

m (during Stage 3), and consequently, it never reached the shelf edge (- 120 m). This led to the confinement of the majority of the river-sourced sediments on the continental shelf, whereas the seaward sediment transportation was succeeded by the generation of infrequent turbidity currents related to either sediment failures, or exceptionally large river discharges (flooding episodes). Two melt water events, centered at 36 and 52 ky B.P., occurred during this first period, and they were characterized by the frequent initiation of turbidity currents.

2. The second period was developed at the end of Oxygen Isotope Stage 3 (31.85-28.57 ky B.P.). It represents a major melt-water pulse, which moved large amounts of sediments on the outer continental shelf and upper continental slope, resulting in the initiation of numerous sediment failures and gravity flows.
3. The third period occurred from 28.57 to 21.26 ky B.P. (Stage 2). During this period, the sea level dropped to the shelf edge (-120 m), which led to the development of shelf margin deltas, which contributed to the development of numerous sediment failures and turbidity currents.
4. The fourth period represents the latest part of the Last Glacial Maximum (21.26-18.17 ky B.P.), and it is characterized by hemipelagic sedimentation (except for two series of turbidity currents occurring at 19 ky, and 19.9–21.6 ky B.P.) on the continental slope, indicating the development of colder and arid climatic conditions. This arid period is probably related to the Heinrich Event H2.
5. The fifth and last period represents the last deglaciation event (18.17-11.16 ky B.P.). It is characterized by the occurrence of a melt water pulse occurred at 16.10-11.16 ky B.P., which was interrupted at 15.18-14.61 ky B.P. by an arid period that probably corresponds to the Heinrich Event H1. During this melt-water pulse, the bottom waters of the northwest Gulf of Mexico became partially anoxic due to: 1) the development of a low salinity surficial layer on the water column, and 2) the vast amounts of organic matter introduced in the ocean environment through the highly increased river discharges of this time interval, and 3) the highly increased primary production caused by the introduction of ample nutrients in the euphotic zone through the highly increased river discharges of this time interval.

At about 12-11 ky B.P., the North America melt-water discharges switched from the Mississippi River to St. Lawrence Seaway, leading to the significant reduction of the

Mississippi River discharges. This led to the restriction of the river-sourced sediments on the continental shelf, and the domination of hemipelagic sedimentation of the continental slope, which continue to dominate up to the present time.

Slope Stability

Halokinetic and slope instability processes have sculpted numerous morphological features on the flanks of the intraslope basins in the Bryant Canyon area. Two episodes of increased salt-tectonic activity are defined: a) the first acted at the beginning of interglacial oxygen isotope stage 5 as salt adjusted to the abandoned environments of the Bryant and Eastern Canyon systems, and b) the second one occurred during the last glacial period and is characterized by the seaward propagation of salt diapirs.

Most present day basin structures resulted from the latest episode of increased salt-tectonic activity. Three types of slopes are recognized in the intraslope basins: I) highly inclined slopes with morphologic features of low relief, II) highly inclined slopes with morphologic features of high relief, and III) highly inclined slopes dissected by canyon-like landslide troughs of very high relief. The first two slope types occur mainly on the over-steepened northern flanks of the intraslope basins. They have been formed by the development of widespread sediment failures, through which large slices of the flanks collapsed. The triggering mechanism for the sediment failures was the oversteepening of the slopes during the seaward mobilization of the underlying allocthonous salt masses. The third slope type occurs on the southern flanks of the intraslope basins. The canyon-like landslide troughs on this slope type are due to the development of local channelized slope instabilities related to locally increased slope gradients. The locally increased gradients of the slopes have been caused by the formation of small salt diapir bulges on the plateaus.

The majority of the sediment failures in the intraslope basins transformed into debris flows and led to the most recent phase of infilling of the basin floors by numerous and various mass-transport deposits. Blocky debris-flow deposits are the most pervasive, originating from enormous Coulomb-type failures. They are covered/surrounded by younger, smooth gravity-flow deposits, originating by a second generation of more readily liquefied sediment failures, and reworking of the mass-transport deposits rested on the flanks.

Unifites

Structureless mud deposits (unifites) are a common depositional phenomenon in the intraslope basins of the continental slope of the northwest Gulf of Mexico. High-resolution acoustic data and long sediment cores from Hedberg Basin (middle slope) were used to provide a better insight into the origin of these enigmatic depositional units. The unifite, occurring in Hedberg Basin, is structureless under visual observations, but X-ray radiographs reveal that it consists of three divisions: a) "U1-division", representing waning sequences of fine-grained (mud) turbidites, b) "U2-division", characterized by faint, normally-graded mud layers with occasionally wispy, silty interlaminae, and c) "U3-division", characterized by a very uniform appearance with no obvious sedimentological structures other than a faint banding of slightly siltier and slightly more clayey layers.

Acoustic data reveal that there is no connection between intrabasinal sediment failures and the unifite. It is suggested that the unifite has resulted from the deposition of a long-lasting (1.5 to 3 months), pulsating (showing internal surges), fine-grained turbidity current (dated at 28.6-29 ky B.P.) that originated from the flow transformation of a series of massive sediment failures on the shelf edge and/or upper continental slope. The fine-grained nature of the turbidity current is probably due to the depositional segregation of the flow by depositing its coarsest material on intraslope basins in more proximal locations. It is proposed that the uniform texture of the unifite is attributed to the development of a stratification interface (lower stratified layer) generated by the successive and almost continuous introduction of turbulent sediment clouds in Hedberg Basin. The lowest two unifite divisions are considered to have been developed prior to and during the development of the stratified layer.

REFERENCES

- Allen, J.R.L., 1985. Principles of physical sedimentology. George Allen & Unwin, London, 774 pp.
- Allen, J.R.L., 1991. The Bouma division and the possible duration of turbidity currents. *Journal of Sedimentary Petrology*, 61, 291-295.
- Anastasakis, G.C., Stanley, D.J., 1984. Sapropels and organic-rich variants in the Mediterranean: sequence development and classification. In: Stow, D.A.V., Piper, D.J.W. (Eds.), *Fine Grained Sediments: Deep-Water Processes and Facies*. Geological Society Special Publication 15, pp. 497-510.
- Baas, J.H., Van Dam, R.L., Storms, J.E.A., 2000. Duration of deposition from decelerating high-density turbidity currents. *Sedimentary Geology*, 136, 71-88.
- Babonneau, N., Savoye, B., Cremer, M., Klein, B., 2002. Morphology and architecture of the present canyon and channel system of the Zaire deep-sea fan. *Marine and Petroleum Geology*, 19, 445-467.
- Bahk, J.J., Chough, S.K., Han, S.J., 2000. Origins of paleoceanographic significance of laminated muds from the Ulleung Basin, East Sea (Sea of Japan). *Marine Geology* 162, 459-477.
- Behrens E.W., 1984. Unifite muds in intraslope basins, Northwest Gulf of Mexico. *Geo-Marine Letters*, 4, 227-233.
- Best, J.L., Leeder, M.R., 1993. Drag reduction in turbulent muddy seawater flows and some sedimentary consequences. *Sedimentology* 40, 1129-1137.
- Blanpied C., Stanley, D.J., 1981. Uniform mud (Unifite) deposition in Hellenic Trench Eastern Mediterranean. *Smithsonian Contribution to the Marine Sciences*, 13, 40p.
- Boessenkool, K.P., Brinkhuis, H., Schönfeld, J., Targarona, J., 2001. North Atlantic sea-surface temperature changes and the climate of western Iberia during the last deglaciation; a marine palynological approach. *Global and Planetary Change* 30, 33-39.
- Bornhold, B.D., Ren, P., Prior, D.B., 1994. High-frequency turbidity currents in British Columbia fjords. *Geo-Marine Letters* 14, 238-243.
- Bouma A.H., 1981. Depositional sequences in clastic continental slope deposits, Gulf of Mexico. *Geo-Marine Letters* 1, 115-121.

- Bouma A.H., 1982. Intraslope basins in northwest Gulf of Mexico, a key to ancient submarine canyons and fans, In: Watkins, J. S., and Drake, C. L., (Eds.), Studies in continental margin geology, AAPG Memoir 34, pp. 567-581.
- Bouma, A.H., 2000. Fine-grained, mud-rich turbidite systems: model and comparison with coarse-grained, sand-rich systems. In: Bouma, A.H., and Stone, C.G., (Eds.), Fine-grained turbidite systems, AAPG Memoir 72/SEPM Special Publication, 68, 9-20.
- Bouma, A.H., 2001. Fine-grained submarine fans as possible recorders of long- and short-term climatic changes. *Global and Planetary Change*, 28, 85-91.
- Bouma, A.H., Coleman, J.M., 1985. Mississippi Fan: Leg 96 program and principal results. In: Bouma, A.H., Barnes, N.E., Normark, W.R. (Eds.), *Submarine Fans and Related Sequences*. Springer-Verlag, New York, pp. 247-252.
- Bouma, A.H., Sterling, C.E., Coleman, J.M., 1985. Mississippi Fan, Gulf of Mexico. In: Bouma, A.H., Barnes, N.E., Normark, W.R. (Eds.), *Submarine Fans and Related Sequences*. Springer-Verlag, New York, pp. 143-150.
- Bouma A.H., Roberts, H.H., Coleman, J.M., 1990. Acoustical and geological characteristics of near-surface sediments, upper continental slope of Northern Gulf of Mexico. *Geo-Marine Letters*, 10, 200-208.
- Bouma A.H., Roberts, H.H., 1990. Northern Gulf of Mexico continental slope: *Geo-Marine Letters* 10, 177-181.
- Bowen, A.J., Normark, W.R., Piper, D.J.W., 1984. Modelling of turbidity currents on Navy Submarine Fan, California Continental Borderland. *Sedimentology*, 31, 169-185.
- Bryant, W.R., Bryant, J.R., Feeley, M.R., Simmons, G.R., 1990. Physiographic and bathymetric characteristics of the continental slope, Northwest Gulf of Mexico. *Geo-Marine Letters* 10, 182-199.
- Bryant W.R., Simmons, G.R., Grim, P., 1991. The morphology and evolution of basins in the continental slope, Northwest Gulf of Mexico. *GCAGS Transactions*, 41, pp. 73-82.
- Cacchione D.A., Drake, D.E., Kayen, R.W., Stenberg, R.W., Kineke, G.C., Tate, G.B., 1995. Measurements in the boundary layer on the Amazon subaqueous delta. *Marine Geology*, 125, 235-257.
- Camoin, G.F., Ebrein, Ph., Eisenhauer, A., Bard, E., Faure, G., 2001. A 300000-yr coral reef record of sea level changes, Mururoa atoll (Tuamotu archipelago, French Polynesia). *Palaeoceanography, Palaeoclimatology, Palaeoecology* 175, 325-341.

- Cita M.B., Camerlenghi, A., Kastens, K.A., McCoy, F.W., 1984. New findings of Bronze Age homogenites in the Ionian Sea: geodynamic implications for the Mediterranean. *Marine Geology*, 55, 47-62.
- Cita M.B., Camerlenghi, A., Rimoldi, B., 1996. Deep-sea tsunami deposits in the eastern Mediterranean: new evidence and depositional models. *Sedimentary Geology*, 104, 155-173.
- Cita M.B., Aloisi, G., 2000. Deep-sea tsunami deposits triggered by the explosion of Santorini (3500y BP), eastern Mediterranean. *Sedimentary Geology*, 135, 181-203.
- Coleman, J.M., Prior D.B., Lindsay, J.F., 1983. Deltaic influences on shelf edge instability processes. In: Stanley D.J., Moore G.T. (Eds.), *The Shelf Break, Critical Interface on Continental Margins*. Society of Economic Paleontologists and Mineralogists Special Publication 33, pp. 121-137.
- Crozier M.J., 1984. Field assessment of slope instability. In: Brudsen, D., and Prior, D.B., (Eds.), *Slope instability*. New York, John Wiley & Sons, pp. 103-142.
- Damuth, J.E., 1977. Late Quaternary sedimentation in the western equatorial Atlantic. *Geological Society of America Bulletin*, 88, 695-710.
- Dimakis P., Elverhøi, A., Høeg, K., Solheim, A., Harbitz, C., Laberg, J.S., Voren, T.O., Marr, J., 2000. Submarine slope stability on high-latitude glaciated Svalbard-Barents Sea margin. *Marine Geology*, 162, 303-316.
- Dyer, K.R., Manning, A.J., 1999. Observation of the size, settling velocity and effective density of flocs, and their fractal dimensions. *Journal of Sea Research*, 41, 87-95.
- Edwards D.A., Leeder, M.R., Best, J.L., Pantin, H.M., 1994. On experimental reflected density currents and the interpretation of certain turbidites. *Sedimentology*, 41, 437-461.
- Elverhøi A., Norem, H., Andersen, E.S., Dowdeswell, J.A., Fossen, I., Halfidason, H., Kenyon, N.H., Laberg, J.S., King, E.L., Sejrup, H.P., Solheim, A., Vorren, T.O., 1997. On the origin and flow behavior of submarine slides on deep-sea fans along the Norwegian-Barents Sea continental margin. *Geo-Marine Letters*, 17, 119-125.
- Fairbanks, R.G., 1989. 17,000-year glacio-eustatic sea level record: influence of glacial melting rates on the Younger Dryas event and deep-ocean circulation. *Nature* 342, 637-642.
- Ferentinos, G., Collins, M.B., Pattiarachi, C.B., Taylor, P.G., 1985. Mechanisms of sediment transport and dispersion in a tectonically active submarine valley/canyon system: Zakynthos Straits, NW Hellenic Trench. *Marine Geology* 65, 243-269.

- Ferentinos G., Papatheodorou, G., Collins, M.B., 1988. Sediment transport processes on an active submarine fault escarpment, Gulf of Corinth, Greece. *Marine Geology*, 83, 43-61.
- Fisher, R.V., 1983. Flow transformation in sediment gravity flows. *Geology*, 11, 273-274.
- Fukushima, Y., Parker, G., Pantin, H.M., 1985. Prediction of ignitive turbidity currents in Scripps Submarine Canyon. *Marine Geology*, 67, 55-81.
- Gardner, W.D., 1989. Baltimore Canyon as a modern conduit of sediment to the deep sea. *Deep-Sea Research* 36, 323-385.
- Geraga, M., Tsaila-Minopolis, St., Ioakim, Chr., Papatheodorou, G., Ferentinos, G., 2000. Evaluation of paleoenvironmental changes during the last 18,000 years in the Myrtoon Basin, SW Aegean Sea. *Palaeoceanography, Palaeoclimatology, Palaeoecology* 156, 1-17.
- Gervais, A., Mulder, T., Savoye, B., Migeon, S., Cremer, M., 2001. Recent processes of Levee formation on the Zaire deep-sea fan. *Earth and Planetary Sciences*, 332, 371-378.
- Hagen, R.A., Bergersen, D.D., Moberly, R., Coulbourn, W.T., 1994. Morphology of a large meandering submarine canyon system on the Peru-Chile forearc. *Marine Geology*, 119, 7-38.
- Hagen, R.A., Vergara, H., Naar, D.F., 1996. Morphology of San Antonio submarine canyon on the central Chile forearc. *Marine Geology*, 129, 197-205.
- Hampton M.A., 1972. The role of subaqueous debris flow in generating turbidity currents. *Journal of Sedimentary Petrology* 42, 775-793.
- Hart B.S., Prior, D.B., Barrie, J.V., Currie, R.G., Luternauer, J.L., 1992. A river mouth submarine channel and failure complex, Fraser Delta, Canada. *Sedimentary Geology*, 81, 73-87.
- Haughton, P.D.W., 1994. Deposits of deflected and ponded turbidity currents, Sorbas Basin, southwest Spain. *Journal of sedimentary Research*, A64, 2, 233-246.
- Hill, P.R., 1984. Facies and sequence analysis of Nova Scotian Slope muds: turbidite vs 'hemipelagic' deposition. In: Stow, D.A.V., Piper, D.J.W. (Eds.), *Fine Grained Sediments: Deep-Water Processes and Facies*. Geological Society Special Publication 15, pp. 311-318.
- Hiscott, R.N., 1994. Loss of capacity, not competence, as the fundamental process governing deposition from turbidity currents. *Journal of Sedimentary Research*, A64, 209-219.
- Huang X., García, M.H., 1999. Modeling of non-hydroplaning mudflows on continental slopes. *Marine Geology*, 154, 131-142.
- Iverson R.M., 1997. The physics of debris flows. *Reviews of Geophysics*, 35, 245-296.

- Iverson R.M., LaHusen, R.G., 1989. Dynamic pore-pressure fluctuations in rapidly shearing granular materials. *Science*, 246, 796-799.
- Iverson R.M., Reid, M.E., LaHusen, R.G., 1997. Debris-flow mobilization from landslides. *Annual Review of Earth Planetary Sciences*, 25, 58-138.
- Keney C., 1984. Properties and behaviors of soils relevant to slope instability, In: Brudsen, D., and Prior, D.B., (Eds.), *Slope Instability*, New York, John Wiley & Sons, pp. 27-65.
- Klaucke, I., Savoye, B., Cochonat. P., 2000. Patterns and processes of sediment on the continental slope off Nice, SE France. *Marine Geology* 162, 405-422.
- Klaus A., Taylor, B., 1991. Submarine canyon development in the Izu-Bonin Forearc: a SeaMARC II and seismic survey of Aoga Shima Canyon. *Marine Geophysical Researches*, 13, 131-152.
- Kneller, B., 1995. Beyond the turbidite paradigm: physical models for the deposition of turbidites and their implications for reservoir prediction. In: Hartley, A.J., and Prosser, D.J., (Eds.), *Characterization of Deep Marine Clastic Systems*, Geological Society Special Publication, 94, 31-49.
- Kneller B., Edwards, D., McCaffrey, W., Moore, R., 1991. Oblique reflection of turbidity currents. *Geology*, 14, 250-252.
- Kneller, B.C., Braney, M.J., 1995. Sustained high-density turbidity currents and the deposition of thick massive beds. *Sedimentology*, 42, 607-616.
- Kneller, B.C., Buckee, C., 2000. The structure and fluid mechanics of turbidity currents: a review of some recent studies and their geological implications. *Sedimentology*, 47 (Suppl. 1), 62-94.
- Kolla, V., Perlmutter, M.A., 1993. Timing of Turbidite sedimentation on the Mississippi Fan. *American Association of Petroleum Geologists Bulletin* 77, 1129-1141.
- Komar, P.C., 1969. The channelized flow of turbidity currents with application to Monterey deep-sea fan channel. *Journal of Geophysical Research*, 78, 4544-4558
- Komar, P.C., 1977. Computer simulation of turbidity current flow and the study of deep-sea channels and fan sedimentation. In: Goldberg, E.D., McCave, I.N., O'Brien, J., and Steele, J.H., (Eds.), *The Sea*, 6, 603-621.
- Komar, P.D., 1985. The hydraulic interpretation of turbidites from their grain size and sedimentary structures. *Sedimentology*, 32, 395-407.

- Krone, R.B., 1993. Sedimentation revisited, In: Metha, A.J., (Ed.), Nearshore and Estuarine Cohesive Sediment Transport. Washington, D.C., American Geophysical Union, pp. 108-125. (Coastal and Estuarine Studies, v. 42).
- Laberg J.S., Vorren, T.O., 2000. Flow behavior of the submarine glacial debris flows of the Bear Island Trough Mouth Fan, western Barrents Sea. *Sedimentology*, 47, 1105-1117.
- Lea, D.W., Martin, P.A., Pak, D.K., Spero, H.J., 2002. Reconstructing a 350 ky history of sea level using planktonic Mg/Ca and Oxygen isotope records from a Cocos Ridge core. *Quaternary Science Reviews* 21, 283-293.
- Lee G.H., 1990. Salt tectonics and seismic stratigraphy of the Keathley canyon area and vicinity, Northwestern Gulf of Mexico. Unpublished Ph.D. Dissertation, Texas A&M University, Texas.
- Lee G.H., Watkins, J.S., Bryant, W.R., 1996. Bryant Canyon Fan System: an unconfined, large river-sourced system in the Northwest Gulf of Mexico. *American Association of Petroleum Geologists Bulletin* 80, 340-358.
- Lee S.H., Chough, S.K., Back, G.C., Kim, Y.B., Sung, B.S., 1999. Gradual downslope change in high-resolution acoustic characters and geometry of large-scale submarine debris lobes in Ulleung Basin, East Sea (Sea of Japan), Korea. *Geo-Marine Letters*, 19, 254-261.
- Lewis, K.B., 1994. The 1500-km-long Hikurangi Channel: trench-axis channel that escapes its trench, crosses a plateau, and feeds a fan drift. *Geo-Marine Letters* 14, 19-28.
- Li, M.Z., Gust, G., 2000. Boundary layer dynamics and drag reduction in flows of high cohesive sediment suspensions. *Sedimentology*, 47, 71-86.
- Major J.J., 1997. Depositional processes in large-scale debris-flow experiments. *Journal of Geology*, 105, 345-366.
- Major J.J., Iverson, R.M., 1999. Debris-flow deposition: Effects of pore-fluid pressure and friction concentrated at flow margins. *GSA Bulletin*, 111, 10, 1424-1434.
- Manning, A.J., Dyer, K.R., 1999. A laboratory examination of flocculation characteristics with regard to turbulent shearing. *Marine Geology*, 160, 147-170.
- Martinson, D.G., Pisias, N.G., Hays, J.D., Imbrie, J., Moore, T.C., Shackleton, N.J., 1987. Age dating and orbital theory of the ice ages: development of a high-resolution 0 to 300,000-year chronostratigraphy. *Quaternary Research* 27, 1-29.

- Massé, L., Faugères, J.C., Hrovatin, V., 1998. The interplay between turbidity and contour current processes on the Columbia Channel Fan Drift, Southern Brazil Basin. *Sedimentary Geology* 115, 111-132.
- Masson D.G., Hugget, Q.J., Brunsten, D., 1993. The surface texture of the Saharan debris flow deposit and some speculations on submarine debris flow processes. *Sedimentology*, 40, 583-598.
- McCave, I.N. and Swift, S.A., 1976. A physical model for the rate of deposition of fine-grained sediments in the deep sea. *Geological Society of America Bulletin* 87, 541-546.
- McCave I.N., Jones, K.P.N., 1988. Deposition of ungraded muds from high-density non-turbulent turbidity currents. *Nature*, 333, 250-252.
- McCave, I.N., Carter, L., 1997. Recent sedimentation beneath the Deep Western Boundary Current off northern New Zealand. *Deep-Sea Research* 44, 1203-1237.
- McHugh C.M.G., Ryan, W.B.F., 2000. Sedimentary features associated with channel overbank flow: examples from the Monterey Fan. *Marine Geology*, 163, 199-215.
- Middleton, G.V., 1993. Sediment deposition from turbidity currents. *Annual Review of Earth and Planetary Sciences*, 21, 89-114.
- Migeon, S., Savoye, B., Zanella, E., Mulder, T., Faugères, J.-C., Weber, O., 2001. Detail seismic-reflection and sedimentary study of turbidite sediment waves on the Var Sedimentary Ridge (SE France): significance for sediment transport and deposition and for the mechanisms of sediment-wave construction. *Marine and Petroleum Geology*, 18, 179-208.
- Mohring D., Whipple, K.X., Hondzo, M., Ellis, C., Parker, G., 1998 Hydroplaning of subaqueous debris flows. *GSA Bulletin*, 110, 3, 387-394.
- Mohring D., Elverhøi, A., Parker, G., 1999. Experiments on the relative mobility of muddy subaqueous and subaerial debris flows and their capacity to remobilize antecedent deposits. *Marine Geology*, 154, 117-129.
- Morton, R.A., Price, W.A., 1987. Late Quaternary sea-level fluctuations and sedimentary phases of the Texas coastal plain and shelf. In: Nummedal, D., Pilkey, O.H., Howard, J.D. (Eds.), *Sea-Level Fluctuations and Coastal Evolution*. Society of Economic Paleontologists and Mineralogists Special Publication 41, Tulsa, Oklahoma, pp. 181-198.
- Muck M.T., Underwood, M.B., 1990. Upslope flow of turbidity currents: A comparison among field observations, theory, and laboratory models. *Geology*, 18, 54-57.

- Mulder, T., Syvitski, J.P.M., 1995. Turbidity currents generated at river mouths during exceptional discharges to the world oceans. *Journal of Geology* 103, 285-299.
- Mulder T., Cochonat, P., 1996. Classification of offshore mass movements. *Journal of Sedimentary Research*, 66, 1, 43-57.
- Mulder, T., Savoye, B., Syvitski, J.P.M., 1997. Numerical modelling of a mid-sized gravity flow: the 1979 Nice turbidity current (dynamics, processes, sediment budget and seafloor impact). *Sedimentology*, 44, 305-326.
- Mulder, T., Savoye, B., Piper, D.J.W., Syvitski, J.P.M., 1998a. The Var submarine sedimentary system: understanding Holocene sediment delivery processes and their importance to the geological record. In: Stoker, M.S., Evans, D., Cramp, A. (Eds.), *Geological processes on Continental Margins: Sedimentation, Mass-Wasting and Stability*. Geological Society Special Publications 129, London, pp. 145-166.
- Mulder, T., Syvitski, J.P.M., Skene, K.I., 1998b. Modeling of erosion and deposition by turbidity currents generated at river mouths. *Journal of Sedimentary Research*, 68, 124-137.
- Mulder T., Alexander, J., 2001. The physical character of subaqueous sedimentary density flows and their deposits. *Sedimentology*, 48, 269-299.
- Mutti E., Lucchi, F.R., Seguret, M., Zanzucchi, G., 1984. Seismoturbidites: A new group of resedimented deposits. *Marine Geology*, 55, 103-116.
- Nakajima, T., Satoh, M., 2001. The formation of large mudwaves by turbidity currents on the levees of the Toyama deep-sea channel, Japan Sea. *Sedimentology*, 48, 435-463.
- Nemec W., 1990. Aspects of sediment movement on steep delta slopes. In: *Coarse-Grained Deltas*, London, Blackwell Scientific Publications, International Association of Sedimentologists Special Publication, 10, 29-73.
- Normark, W.R., Hess, G.R., Stow, D.A.V., Bowen, A.J., 1980. Sediment waves on the Monterey fan levee: a preliminary physical interpretation. *Marine Geology* 37, 1-18.
- Normark, W.R., Piper, D.J.W., Hiscott, R.N., 1998. Sea level controls on the textural characteristics and depositional architecture of the Hueneme and associated submarine fan systems, Santa Monica Basin, California. *Sedimentology*, 45, 53-70.
- Ó Cofaigh, C., Dowdeswell, J.A., 2001. Laminated sediments in glacial marine environments: diagnostic criteria for their interpretation. *Quaternary Science Review* 20, 1411-1436.

- Ogston A.S., Cacchione, D.A., Sternberg, R.W., Kineke, G.C., 2000. Observations of storm and river flood-driven sediment transport on the northern California continental shelf. *Continental Shelf Research*, 20, 2141-2162.
- Papatheodorou G., Ferentinos, G., 1993. Sedimentation processes and basin-filling depositional architecture in an active asymmetric graben: Srava graben, Gulf of Corinth, Greece. *Basin Research*, 5, 235-253.
- Papatheodorou G., Ferentinos, G., 1996. Submarine and coastal sediment failure triggered by the 1995, $M_s=6.1$ R Aegion earthquake, Gulf of Corinth, Greece. *Marine Geology*, 137, 287-304.
- Parker, G., 1982. Conditions for the ignition of catastrophic erosive turbidity currents. *Marine Geology*, 46, 307-327.
- Parsons J.D., Bush J.W.M., Syvitsiki, J.P.M., 2001. Hyperpycnal plume formation from riverine outflows with small sediment concentrations. *Sedimentology*, 48, 465-478.
- Pérez-Folgado, M., Sierro, F.J., Flores, J.A., Cacho, I., Grimalt, J.O., Zahn, R., Shakleton, N., 2002. Western Mediterranean planktonic foraminifera events and millennial climatic variability during the last 70 kyr. *Marine Micropaleontology* 907, 1-22.
- Pickering K.T., Hiscott, R.N., 1985. Contained (reflected) turbidity currents from the Middle Ordovician Cloridorme Formation, Quebec, Canada: an alternative to the antidune hypothesis. *Sedimentology*, 32, 373-394.
- Piper D.J.W., 1978. Turbidite muds and silts on deep-sea fans and abyssal plains. In: Stanley, D.J., and Kelling, G. (Eds.), *Sedimentation in Submarine Canyons, Fans and Trenches*, Dowden, Hutchinson & Ross, Stroudsburg, PA. pp. 163-176.
- Piper, D.J.W., Normark, W.R., 1983. Turbidite depositional patterns and flow characteristics, navy Submarine fan, California Borderland. *Sedimentology*, 30, 681-694.
- Piper D.J.W., Shor, A.N., Farre, J.A., O'Connell, S., Jacobi, R., 1985. Sediment slides and turbidity currents on the Laurentian Fan: side-scan sonar investigations near the epicenter of the 1929 Grand Banks earthquake. *Geology*, 13, 538-541.
- Piper, D.J.W., Savoye, B., 1993. Processes of late Quaternary turbidity current flow and deposition on the Var deep-sea fan, north-west Mediterranean Sea. *Sedimentology*, 40, 557-582.
- Piper, D.J.W., Skene, K.I., 1998. Latest Pleistocene ice-rafting events on the Scotian Margin (eastern Canada) and their relationship to Heinrich events. *Paleoceanography* 13, 205-214.

- Piper D.J.W., Cochonat, P., Morrison, M.L., 1999. The sequence of events around the epicenter of the 1929 Grand Banks earthquake: initiation of debris flows and turbidity current inferred from side-scan sonar. *Sedimentology* 46, 79-97.
- Pratson, L.F., Ryan, W.B.F., Mountain G.S., Twichell, D.C., 1994. Submarine canyon initiation by downslope-eroding sediment flows: Evidence in late Cenozoic strata on the New Jersey continental slope. *Geological Society of America Bulletin*, 106, 395-412.
- Prior D.B., Wiseman, W.M.J., Gilbert, R., 1981. Submarine slope processes on a fan delta, Howe Sound, British Columbia. *Geo-Marine Letters*, 1, 85-90.
- Prior D., Bornhold, B., Johns, M., 1984. Depositional characteristics of a submarine debris flow. *Journal of Geology* 92, 707-727.
- Prior D.B., Coleman, J.M., 1984. Submarine slope instability, In: Brudsen D., Prior, D.B., (Eds.), *Slope Instability*, New York, John Wiley & Sons, pp. 419-455.
- Prior D.B., Doyle, E.H., 1985. Intra-slope canyon morphology and its modification by rockfall processes, U.S. Atlantic Continental Margin. *Marine Geology*, 67, 177-196.
- Prior D.B., Yang, Z.-S., Bornhold, B.D., Keller, G.H., Lin, Z.H., Wiseman, Jr., W.J., Wright, L.D., Lin, T.C., 1986. The subaqueous delta of the modern Huange (Yellow River). *Geo-Marine Letters*, 6, 67-75.
- Prior D.B., Bornhold, B.D., 1988. Submarine morphology and processes of fjord fan deltas and related high-gradient systems: modern examples from British Columbia, In: Nemeč, W., Steel, R.J., (Eds.), *Fan deltas: sedimentology and tectonic settings*: London, Blackie and Son, pp. 125-143.
- Prior D.B., Bornhold, B.D., 1990. The underwater development of Holocene fan deltas, In: Colella, A., and Prior, D.B. (Eds.), *Coarse-Grained Deltas*, Special Publications of the International Association of Sedimentologists, London, Blackwell Scientific Publications, 10, pp. 75-90.
- Puig, P., Ogston, A.S., Mullenbach, B.L., Nittrouer, C.A., Sternberg, R.W., 2003. Shelf-to-Canyon sediment-transport processes on the Eel continental margin (northern California). *Marine Geology* 193, 129-149.
- Rabek, K., Ledbetter, M.T., Williams, D.F., 1985. Tephrochronology of the western Gulf of Mexico for the last 185,000 years. *Quaternary Research* 23, 403-416.

- Rashid, H., Hesse, R., Piper, D.J.W., 2003. Origin of unusually thick Heinrich layers in ice-proximal regions of the northwest Labrador Sea. *Earth and Planetary Science Letters* 6547, 1-18.
- Rasmussen, S., Lykke-Andersen, H., Kuijpers, A., Troelstra, S.R., 2003. Post-Miocene sedimentation at the continental rise of Southeast Greenland: the interplay between turbidity and contour currents. *Marine Geology* 196, 37-52.
- Ren, P., Bornhold, B.D., Prior, D.B., 1996. Seafloor morphology and sedimentary processes, Knight Inlet, British Columbia. *Sedimentary Geology*, 103, 201-228.
- Reynolds, S., 1987. A recent current event, Hueneme Fan, California: reconstruction of flow properties. *Sedimentology*, 34, 129-137.
- Rohling, E.J., 1994. Review and new aspects concerning the formation of eastern Mediterranean sapropels. *Marine Geology* 122, 1-28.
- Satterfield W.M., Behrens, E.W., 1990. A late Quaternary canyon/channel system, Northwest Gulf of Mexico continental slope. *Marine Geology* 92, 51-67.
- Savoie, B., Piper, D.J.W., Droz, L., 1993. Plio-Pleistocene evolution of the Var deep-sea fan off the French Riviera. *Marine and Petroleum Geology*, 10, 550-571.
- Shakleton, N., Opdyke, N., 1973. Oxygen isotope and paleomagnetic stratigraphy of equatorial Pacific core V28-238: oxygen isotope temperatures and ice volumes on a 10^5 year and 10^6 year scale. *Quaternary Research* 3, 39-55.
- Sohn, Y.K., 2000. Coarse-grained debris-flow deposits in the Miocene fan deltas, SE Korea: a scaling analysis. *Sedimentary Geology*, 130, 45-64.
- Stanley D.J., 1981. Unifites: structureless muds of gravity-flow origin in the Mediterranean basins. *Geo-Marine Letters*, 1, 77-83.
- Stanley D.J., 1983. Parallel laminated deep-sea muds and coupled gravity flow-hemipelagic settling in the Mediterranean. *Smithsonian Contributions to the Marine Sciences* 19, 19 pp.
- Stow, D.A.V., Bowen, A.J., 1980. A physical model for the transport and sorting of fine-grained sediment by turbidity currents. *Sedimentology* 27, 31-46.
- Stow, D.A.V., Shanmugam, G., 1980. Sequence of structures in fine-grained turbidities: comparison of recent deep-sea and ancient flysch sediments. *Sedimentary Geology* 25, 23-42.
- Stow, D.A.V., Alam, M., Piper, D.J.W., 1984. Sedimentology of the Halifax Formation, Nova Scotia: Lower Paleozoic fine-grained turbidites. In: Stow, D.A.V., and Piper, D.J.W. (Eds.),

- Fine-Grained Sediments: Deep-Water Processes and Facies, Geological Society Special Publication, 15, 127-144.
- Stow, D.A.V., Piper, D.J.W., 1984. Deep-water fine-grained sediments: facies models. In: Stow, D.A.V., Piper, D.J.W. (Eds.), *Fine-Grained Sediments: Deep-Water Processes and Facies*, Geological Society Special Publication, 15, pp. 611-646.
- Stow D.A.V., Reading, H.G., Collinson, J.D., 1996. Sedimentary environments: processes, facies and stratigraphy. In: Reading, H.G. (Ed.), *Deep seas*, Third Edition, Blackwell Science, Oxford, pp. 395-453.
- Stow, D.A.V., Mayall, M., 2000. Deep-water sedimentary systems: new models for the 21st century. *Marine and Petroleum Geology*, 17, 125-135.
- Stuiver, M., Reimer, P., 1993. Extended ¹⁴C database and revised CALIB radiocarbon calibration program. *Radiocarbon* 40, 215-230.
- Stuiver, M., Reimer, P., Bard, E., Beck, J., Burr, G., Hughen, K., Kromer, B., McCormac, F., v.d. Plicht, J., Spurk, M., 1998. INTCAL98 Radiocarbon age calibration 24,000-0 cal BP. *Radiocarbon* 40, 1041-1083.
- Suter, J.R., Berryhill, Jr., H.L., 1985. Late Quaternary shelf-Margin deltas, northwest Gulf of Mexico. *American Association of Petroleum Geologists Bulletin* 69, 77-91.
- Suter, J.R., Berryhill, H.L., Penland, S., 1987. Late Quaternary sea-level fluctuations and depositional sequences, southwest Louisiana continental shelf. In: Nummedal, D., Pilkey, O.H., Howard, J.D. (Eds.), *Sea-Level Fluctuations and Coastal Evolution*. Society of Economic Paleontologists and Mineralogists Special Publication 41, Tulsa, Oklahoma, pp. 199-219.
- Tripsanas E.K., Bryant, W.R., Prior, D.B., Phaneuf, B.A., 2003a. Interplay Between salt activities and slope instabilities, Bryant Canyon area, northwest Gulf of Mexico, In: Locat, J., Mienert, J. (Eds.), *Submarine Mass Movements and their Consequences*, Kluwer Academic Publishers, Dordrecht, pp. 307-316.
- Tripsanas E.K., Bryant, W.R., Prior, D.B., Phaneuf, B.A., 2003b. Structural characteristics of cohesive gravity-flow deposits, and a sedimentological approach on their flow mechanisms, In: Locat, J., Mienert, J. (Eds.), *Submarine Mass Movements and their Consequences*, Kluwer Academic Publishers, Dordrecht, pp. 129-136.
- Twichell, D.C., Nelson, C.H., Damuth, J.E., Pratson, L.F., 2000. Distribution and late-stage development of a turbidite pathway on the Louisiana continental slope. 20th Annual

- GCSSEPM Foundation Research Conference 2000-Deep-water Reservoirs of the World, CD-Rom, 45 pp.
- Weaver, P.P.E., Wynn, R.B., Kenyon, N.H., Evans, J., 2000. Continental margin sedimentation, with special reference to the north-east Atlantic margin. *Sedimentology* 47, 239-256.
- Wilson, P.A., Roberts, H.H., 1995. Density cascading: off-shelf sediment transport, evidence and implications, Bahama banks. *Journal of Sedimentary Research* A65, 45-56.
- Winterwerp, J.C., 2002. On the flocculation and settling velocity of estuarine mud. *Continental Shelf Research*, 9, 1339-1360.
- Wonham, J.P., Jayr, S., Mougamba, R., Chuilon, P., 2000. 3D sedimentary evolution of a canyon fill (Lower Miocene-age) from the Mandorove Formation, offshore Gabron. *Marine and Petroleum Geology*, 17, 175-197.
- Wright, L.D., Friedrichs, C.T., Kim, S.C., Scully, M.E., 2001. Effects of ambient currents and waves on gravity-driven sediment transport on continental shelves. *Marine Geology* 175, 25-45.
- Wynn, R.B., Masson, D.G., Stow, D.A.V., Weaver, P.P.E., 2000. Turbidity current sediment waves on the submarine slopes of the western Canary Islands. *Marine Geology*, 163, 185-198.
- Zaragosi, S., Eynaud, F., Pujol, C., Auffret, G.A., Turon, J.-L., Garlan, T., 2001. Initiation of the European deglaciation as recorded in the northwestern Bay of Biscay slope environments (Meriadzek Terrace and Trevelyan Escarpment): a multi-proxy approach. *Earth and Planetary science Letters* 188, 493-507.
- Zeng, J., Lowe, D.R., Prior, D.B., Wiseman, Jr., W.J., Bornhold, B.D., 1991. Flow properties of turbidity currents in Bute Inlet, British Columbia. *Sedimentology*, 38, 975-996.

VITA

Efthymios Tripsanas

Date of Birth: August 4, 1973

Mailing Address: Department of Oceanography, Texas A&M University,
College Station, Texas 77843.

Telephone (979) 693-8582 (home).
(979) 845-2153 (work).

Education: B.S., University of Patras, Greece (Geology),
December 1996.
Ph.D., Texas A&M University (Oceanography),
December 2003.

Experience: 03/2001 to 12/2002 and 06/2003 to 12/2003 – Graduate Research
Assistant, Department of Oceanography, Texas A&M University,
College Station, Texas.

01/2003 to 06/2003 – Teaching Assistant, Department of
Oceanography, Texas A&M University,
College Station, Texas.

01/1997 to 12/1997 – Research Assistant, Department of Geology,
University of Patras,
Patras, Greece.

08/1994 to 09/1994 – Geologist (Summer Internship), Delphoi-
Distomon A.M.E. (Parent Company of Pechiney),
Distomon, Greece.